https://doi.org/10.15388/vu.thesis.885
https://orcid.org/0000-0002-4826-9856

VILNIUS UNIVERSITY

Kamilė Mikalauskaitė

The Role of Environmental Factors in Protein Amyloid Aggregation

DOCTORAL DISSERTATION

Technological Sciences,
Chemical Engineering (T 005)

VILNIUS 2026

The dissertation was prepared between 2021 and 2025 at Vilnius university. The research was supported by Research Council of Lithuania, Lithuanian Academy of Sciences.

Academic Supervisor – Dr. Vytautas Smirnovas (Vilnius University, Technological Sciences, Chemical Engineering, T 005).

This doctoral dissertation will be defended in a public meeting of the Dissertation Defence Panel:

Chairman – Prof. Dr. Rolandas Meškys (Vilnius University, Technological Sciences, Chemical Engineering, T 005).
Members:
Dr. Lina Baranauskienė (Vilniaus University, Technological Sciences, Chemical Engineering, T 005),
Dr. Rima Budvytytė (Vilniaus University, Natural Sciences, Biochemistry, N 004),
Prof. dr. Per Hammarström (Linköping University, Sweden, Technological Sciences, Chemical Engineering, T 005),
Dr. Rebecca Sternke-Hoffmann (Institute of Paul Scherrer, Switzerland, Natural Sciences, Biochemistry, N 004).

The dissertation shall be defended at a public meeting of the Dissertation Defence Panel at 10:00 on 29 January 2026 in Room R401 of the Life Sciences Center.

Address: Saulėtekio av. 7, Room R401, Vilnius, Lithuania
Tel. +370 641 38704; e-mail: kamile.mikalauskaite@gmc.vu.lt

The text of this dissertation can be accessed at the library of Vilnius University, as well as on the website of Vilnius University:
www.vu.lt/lt/naujienos/ivykiu-kalendorius

https://doi.org/10.15388/vu.thesis.885
https://orcid.org/0000-0002-4826-9856

VILNIAUS UNIVERSITETAS

Kamilė Mikalauskaitė

Aplinkos sąlygų poveikis baltymų amiloidinei agregacijai

DAKTARO DISERTACIJA

Technologijos mokslai,
Chemijos inžinerija (T 005)

VILNIUS 2026

Disertacija rengta 2021–2025 metais Vilniaus universitete.
Mokslinius tyrimus rėmė Lietuvos mokslo taryba, Lietuvos mokslų akademija.

Mokslinis vadovas – dr. Vytautas Smirnovas (Vilniaus universitetas, Technologijos mokslai, Chemijos inžinerija, T005).

Gynimo taryba:
Pirmininkas – prof. dr. Rolandas Meškys (Vilniaus universitetas, technologijos mokslai, chemijos inžinerija, T005)
Nariai:
dr. Lina Baranauskienė (Vilniaus universitetas, technologijos mokslai, chemijos inžinerija, T005),
dr. Rima Budvytytė (Vilniaus universitetas, gamtos mokslai, biochemija, N004),
prof. dr. Per Hammarström (Linčiopingo universitetas, Švedija, technologijos mokslai, chemijos inžinerija, T005),
dr. Rebecca Sternke-Hoffmann (Paul Scherrer institutas, Šveicarija, gamtos mokslai, biochemija, N004).

Disertacija ginama viešame Gynimo tarybos posėdyje 2026 m. sausio mėn. 29 d. 10:00 val. Gyvybės mokslų centre, R401 auditorijoje. Adresas: Saulėtekio al. 7, R401 auditorija, Vilnius, Lietuva, tel. +370 641 38704; el. paštas kamile.mikalauskaite@gmc.vu.lt

Disertaciją galima peržiūrėti Vilniaus universiteto bibliotekoje ir Vilniaus universiteto interneto svetainėje adresu: *https://www.vu.lt/naujienos/ivykiu-kalendorius*

CONTENTS/TURINYS

ACKNOWLEDGEMENTS

I would like to thank all the people who contributed to my journey towards dissertation defense during my PhD studies.

First of all, I would like to thank my PhD supervisor dr. Vytautas Smirnovas, who accepted, a completely inexperienced student, who has never seen work in a laboratory, into his group during bachelor studies and gave me the opportunity to get to know the field of Amyloid research. I am grateful for the faith, support, help and transfer of endless knowledge throughout my studies while trying to piece together the complex puzzle of amyloid aggregation.

I would like to sincerely thank my colleagues at Amyloid Research Sector, especially dr. Mantas Žiaunys, who helped me overcome even the most difficult stages, achieving new heights in scientific research. I would like to thank dr. Andrius Sakalauskas, dr. Darius Šulskis, Rūta Sniečkutė and other laboratory friends who created an atmosphere at work and outside of it that encouraged me to try something new, never give up, motivating me to move on and explore new areas.

I am very grateful to my colleagues from the Faculty of Chemistry and Geosciences, especially dr. Ieva Žutautė and dr. Indrė Misiūnaitė, for their collaboration in conducting aggregation studies with imidazothiazine derivatives, which have resulted in a joint publication.

For financial support, I would like to thank Vilnius University, the Research Council of Lithuania, and COST Action CA21160 - Non-globular proteins in the era of Machine Learning (ML4NGP)

Finally, I would like to thank my family and friends who supported me throughout my studies.

ABBREVIATIONS

Asyn – alpha-synuclein

Ac – acetic acid

AFM – atomic force microscopy

ALS – amyotrophic lateral sclerosis

ANS – 1-anilinonaphthalene-8-sulfonate

APTES – (3-Aminopropyl)triethoxysilane

CD – circular dichroism spectroscopy

CR – Congo red

DLS – dynamic light scattering

EEM – excitation-emission matrices

FDA – food and drug administration

FTIR – Fourier-transform infrared spectroscopy

GuHCl – guanidine hydrochloride

GuSCN – guanidine thiocyanate

GPI – glycosylphosphatidylinositol

IPTG – Isopropyl β-D-1-thiogalactopyranoside

LB – Luria Bertani broth

LDH – lactate dehydrogenase

MRP-8 – migration inhibitory factor-related protein-8

MRP-14 – migration inhibitory factor-related protein-14

MTT – 3-(4,5-dimethylthiazol-2-yl)-2,5-diphenyltetrazolium bromide

PrP – prion protein

sHsp – small heat shock protein

SOD-1 – superoxide dismutase-1

TEM – transmission electron microscopy

ThT – thioflavin-T

INTRODUCTION

The first cases of amyloidosis caused by the aggregation of amyloidogenic proteins were observed as early as the 17th century. Currently, protein aggregation in the form of amyloid fibrils is associated with various neurodegenerative disorders, such as Alzheimer's, Parkinson's or prion diseases, and as many as 42 amyloid disease-related proteins have been identified in mammals.

Amyloidogenic proteins and peptides differ from each other in both size and amino acid sequences, but under certain conditions all of them have a tendency to alter their conformation, forming similar aggregates. Aggregation is associated with the increase of the amount of specific beta-sheet structures. The resulting fibrils are insoluble and partially resistant to proteases. Despite the fact that research in this area has been conducted for many years, only a few disease-modifying drugs or treatments have been approved. Currently, many unanswered questions remain about the mechanism of protein aggregation in diseases the factors affecting this process. Nowadays, protein aggregation studies are widely performed all over the world. However, a wide range of experimental conditions are chosen for *in vitro* aggregation studies of the same proteins, and they often differ among the many laboratories studying amyloids.

One of the most interesting aspects of amyloid aggregation is the occurrence of fibril polymorphism. Numerous studies show that the same protein can form structurally or morphologically distinct amyloid fibrils, which also differ in their self-replication rates, stability, affinity for fluorescent dyes or other small molecule compounds, as well as their toxicity to cells. This variability of aggregates can depend on various environmental factors, such as solution pH, ionic strength, etc. However, some studies have shown that some proteins can form aggregates with different conformations even under identical conditions. Such fibril variability is not only characteristic of protein aggregation *in vitro*, but is also observed in diseases, where distinct types of amyloid assemblies cause different disease phenotypes.

Therefore, the aim of this work was to determine how the aggregation process of various amyloidogenic proteins (kinetics, structure and morphology of the resulting aggregates) can be affected by environmental factors, which are among the most common variables in aggregation studies *in vitro*, and to identify the condition-structure dependence of aggregates.

Aim

To understand the influence of various environmental factors on the amyloid aggregation process.

Objectives

1. Analyze the impact of the protein folding state on lysozyme amyloid aggregation.
2. Investigate the influence of various solution conditions on the process of insulin aggregation.
3. Evaluate the effects of small-molecule compounds on alpha-synuclein amyloid aggregation.
4. Assess the impact of protein–protein cross-interactions on prion protein aggregation in the presence of superoxide dismutase-1 and S100A9.

SCIENTIFIC NOVELTY

Amyloid aggregation has been an actively researched field for several decades, leading to advances in our understanding of protein fibril formation mechanisms and their role in multiple widespread disorders. During these studies, a peculiar phenomenon was observed, where the same protein could misfold and assemble into multiple structurally distinct aggregate types. However, a clear correlation between the fibril characteristics and factors that influence them have yet to be fully understood.

In this work, it was observed that even minor alterations in various environmental factors, such as temperature, ionic strength or pH, can significantly alter both the aggregation mechanism, as well as the resulting protein fibril structure and morphology. Interestingly, this effect of environmental factors appeared to be a generic feature of amyloids, as all of the proteins used in this study displayed a condition-structure relationship. These findings have several important implications in the fields of amyloid disorders, as well as functional nanomaterials.

In the case of amyloid diseases, these results demonstrate that the conclusions drawn from mechanistic research of protein aggregation or the search for potential anti-amyloid compounds may be heavily impacted by the selected test conditions. In this work, it was shown that the aggregation conditions can influence fibril stability, self-replication potential, bound-dye signal intensity and their cytotoxicity. All aforementioned parameters are widely used as criteria to interpret the results of amyloidogenic protein aggregation assays, which may explain the disparity between *in vivo* and *in vitro* studies, as well as diverging reports from different research groups.

Additionally, amyloid fibrils have begun to be recognized as potential nanomaterials for hydrogel formation, tissue engineering and bioscaffold assembly. The results of this work highlight the possibility of generating a large variety of different length, width and stability fibrils from multiple amyloidogenic proteins. By altering the environmental conditions, it is possible to modulate the level of fibril self-assembly into tightly packed clusters, web-like structures or laterally associated filaments. Taking into consideration all results of this study, it is likely that the condition-structure relationship can be applied to shape the majority of amyloidogenic proteins and used to create a large variety of functional structures.

DEFENDING STATEMENTS

1. Lysozyme amyloid aggregation is influenced by the protein's folding state. Protein unfolding promotes resulting fibril structural variability.
2. Elevated environmental temperature causes alpha-synuclein fibril restructurization to a single distinct conformation.
3. Insulin amyloid aggregation is highly sensitive to solution components, pH and ionic strength. Insulin aggregation in phosphate and HCl solution conditions results in formation of the same type of fibrils, while acetic acid promotes distinct aggregate isoform stabilization.
4. Alpha-synuclein amyloid aggregation is modulated by imidazothiazine derivatives, which inhibit the reaction and induce the formation of distinct fibril isoforms.
5. Cross-interactions with S100A9 and superoxide dismutase-1 modulate prion protein amyloid aggregation by inhibiting its kinetics and reducing the structural polymorphism of the resulting fibrils.

LITERATURE OVERVIEW

History of amyloids

The timeline of recorded amyloid-related diseases dates back to the 17th century. It is believed that the first source describing cases of amyloidosis was a book published in 1639 by the doctor and dramatist N. Fonteyn. In this work, the author described autopsies in which unusual deposits were found in organs[1,2]. However, the term “amyloid” itself was created only in 1838 by the German botanist M. Schleiden, when he noticed similar deposits composed of starch in plant cells[3]. For this reason, the meaning of the term is “starch-like” and is derived of the Latin word “amylum” and the Greek word “amylon”[4,5]. In the case of humans, the term amyloid was used later in 1854 by the German pathologist Rudolf Virchow. During an autopsy, he found protein deposits in organs that could be stained with iodine and mistakenly considered them to be composed of starch[4]. Just 5 years later, Friedreich and Kekule proved that these aggregates were different from starch or cellulose because they were similar to proteins[6].

Despite these reports of peculiar, starch-like deposits and their possible role in disease, the first widespread amyloidosis described in detail was Scrapie[7,8]. The name of this disorder came from the unusual behavior of disease-affected sheep scraping their skin against their enclosure's posts and fences[7]. The cause of this disease remained elusive until 1967, when Griffith hypothesized that it could be a specific protein[9,10]. Until then, it was believed that this disease was caused by parasites, bacteria or viruses[9,11]. However, 15 years after the "protein only" hypothesis declaration, Prusiner and colleagues proved it and the infectious particles were indeed protein aggregates, which they later named as prions[9,12].

After it was observed that these aggregates could be stained with iodine, further efforts were made to find alternative methods for their detection and analysis[4]. In 1922, Bennhold observed that amyloids could also bind Congo red, a dye previously used for cloth staining and as a pH-indicator[13]. For a long time, this dye was used as a standard to diagnose amyloidosis. Since amyloids from different afflictions were able to bind the same dye, it was assumed that they might have structural similarities[14]. This hypothesis was confirmed in 1959 by Cohen and Calkins using electron microscopy. They observed that aggregate samples obtained from various tissues or organs were composed of filaments or fibrils[15]. Almost 10 years later, researchers analyzed the aggregate secondary structure using X-ray diffraction and observed that amyloid fibrils have a cross beta-sheet structure[16]. This term arose from analyzing the diffraction pattern of amyloid fibrils, which consists of two diffraction signals perpendicular to each other. There is one intense meridional reflection,

corresponding to the spacing between β-strands aligned perpendicular to the fibril axis, and another broader equatorial reflection - corresponding to the distance between stacked β-sheets running parallel to the fibril axis[17,18]. Moreover, in 1971, Glenner, Benditt and colleagues were the first scientists who determined the sequences of two amyloid aggregate forming proteins - immunoglobulin light chain and amyloid-A[19,20]. In 1982, Prusiner and colleagues noted that amyloid aggregates exhibit resistance to proteases and some fibrils are insoluble in denaturing agents[21].

Although many studies of amyloid aggregates have been carried out over the past years to identify various aspects of this process, several significant discoveries have been made. A review by Chiti and Dobson published in 2006 suggested that the aggregation processes of different amyloid proteins have a common mechanism[22]. Three years after these scientists' insights, in 2009 Knowles and colleagues proposed a theoretical description of this process, which consists of nucleation, elongation and secondary nucleation/fragmentation stages[23]. Another important development in the study of amyloid fibrils was the use of cryo-electron microscopy for high-resolution structure determination since 2010. This methodology provided significant insights into the structural differences between fibrils formed in humans and *in vitro*[24,25]. Although cryo-EM has been used in the study of amyloid fibrils for more than 10 years, it is only recently that its usefulness has grown significantly. The application of this method allows to determine the 3D structures of fibrils at the atomic level, their structural polymorphism, and provide useful insights in the development of potential drugs[26,27].

Last decade, it was observed that some proteins associated with amyloidoses tend to form protein droplets during liquid-liquid phase separation and this process may be related to their aggregation[28]. Recent studies suggest that the formation of amyloid protein biocondensates may be a crucial step and may induce the nucleation and further aggregation process[29]. These findings may help scientists to answer more questions about the onset of amyloid diseases. Even though many different factors that promote or inhibit the aggregation process and methods for detecting aggregates have been identified, only a few effective drugs or treatments have been found. In 2019 Tafamidis, a drug for the treatment of transthyretin-related cardiomyopathy and in 2021 Aducanumab, a monoclonal antibody for the treatment of Alzheimer's disease, were approved by the FDA[30–32].

The small molecule compound Tafamidis acts as a transthyretin stabilizer. It interacts with the T4 binding site of the transthyretin tetramer, thereby inhibiting the dissociation of the tetramer and thus preventing further aggregation process[33]. Unlike the previously mentioned drug, the monoclonal

antibody aducanumab targets amyloid beta in its aggregated form, particularly its 3 - 7 amino acid residue region[34]. Unfortunately, the production of the latter was stopped in 2024 due to a number of dangerous side-effects. Other similar, but more effective in reducing cognitive decline monoclonal antibodies, such as Lecanemab (2023), Donanemab (2024) have been approved[35–37]. The targets of these monoclonal antibodies are soluble amyloid beta protofibrils and N-terminally truncated pyroglutamate-modified amyloid beta peptide at position 3, respectively[38]. Lecanemab neutralizes and removes early aggregates, while donanemab cleares plaques by recognizing the toxic aggregated form of amyloid beta[39].

Amyloidosis

In recent years, amyloidogenic proteins and their aggregation process have attracted the attention of many scientists. Currently, 42 amyloid proteins have been identified, whose aggregation is associated with various human amyloidoses[40].Amyloidosis is a group of diseases caused by protein conformational changes and their subsequent aggregation. During this process, insoluble fibrillar structures are formed, which accumulate and damage cells[41]. The formation of these amyloid plaques ultimately disrupts the functioning of various organs[8]. Amyloidoses are classified according to several aspects. One of them is the localization of the aggregates. These diseases can be localized (aggregates accumulate in only one organ or area of the body) or systemic (aggregates spread to several organs or tissues)[42]. Another distinction is the principle of the onset of the disease. These disorders can be sporadic (arising from random gene mutations or other unknown factors), iatrogenic (developing due to infection through contaminated surfaces, blood transfusion, organ transplantation) or hereditary (gene mutations that determine the disease onset are passed to subsequent generations)[42]. Finally, amyloidoses can be classified according to the protein whose aggregation is related to the development of the disease[41]. These diseases also differ in their rate of progression and age of onset[42]. Some amyloidosis are rapidly progressive and fatal (Creutzfeldt-Jacob disease), while others appear predominantly at an older age (Alzheimer's disease)[43]. There are also disorders that do not cause any fatal consequences and people can survive for many years (Injection-localized amyloidosis)[44]. Most of these diseases are currently incurable and the available treatment modalities usually only slow down the disorder progression or reduce their symptoms[45]. Some examples of amyloid proteins associated with various human diseases are listed in Table 1[40].

Table 1. Examples of amyloidogenic proteins/peptides, number of their amino acid residues and associated diseases[40].

Peptide/ protein	Number of residues	Systemic/ localized	Acquired/ hereditary	Disease
Amyloid beta	40 or 42	L	A, H	Alzheimer's disease, Inclusion body myositis
Alpha-synuclein	140	L	A	Parkinson's disease
Beta-2-microglobulin	101	S	A, H	Dialysis-related amyloidosis
Insulin	51	L	A	Injection site amyloidosis
Lysozyme	129	S	H	Lysozyme systemic amyloidosis
Prion protein	208	L	A, H	Spongiform encephalopathies (Creutzfeldt-Jacob disease)
Tau	352-441	L	A	Alzheimer's disease, Fronto-temporal dementia
Transthyretin	127	S	A, H	Senile systemic amyloidosis

Aggregation mechanism

To function properly, synthesized polypeptide chains must acquire a certain native structure. Folding itself is a complex, stochastic process, during which intermediate forms can be assembled, which are less stable than the correct native state[46]. However, in some cases, the protein misfolds into aggregation-prone conformation and begins to self-associate into oligomeric intermediates, forming an aggregation nucleus and ultimately amyloid fibrils that is more stable than its native state[47]. Amyloid aggregation follows a nucleation-dependent polymerization mechanism, where a misfolding event precedes all further assembly phases[47]. The overall process consists of several stages, including nucleation, elongation and secondary processes (Fig. 1)[22,47].

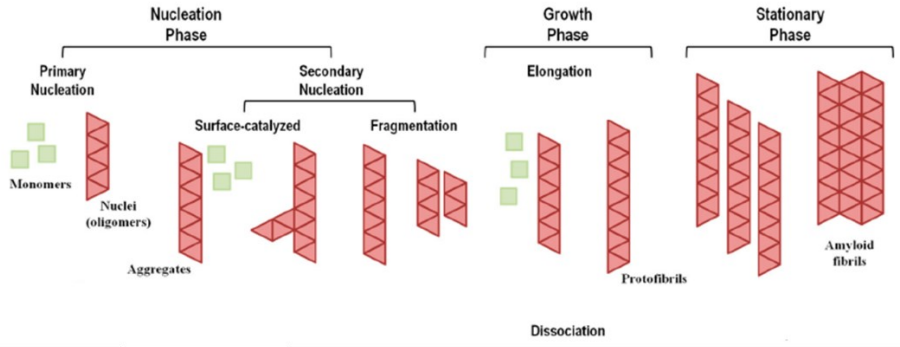

Figure 1. Representative general model for amyloid fibril formation by nucleation-dependent mechanism[48].

In the case of spontaneous aggregation, the reaction begins with primary nucleation, where conformational changes of the native monomeric protein are accompanied by oligomerization, forming a nucleus to which further monomer incorporation can take place[49]. This is the rate-limiting stage of the entire process, since conformational changes in the native protein structure are thermodynamically unfavorable reactions[50]. However, the resulting aggregation nucleus is usually stable enough to prevent disassembly into its native arrangement. These protein conformational changes can be initiated by random mutations, post-translational modifications, cellular stress or protein quality control dysfunction[51,52]. In order to accelerate this process during *in vitro* studies, proteins are destabilized by increasing temperature, changing the pH of the solution or using denaturants[53]. Nucleation can also be accelerated by promoting interactions between protein molecules (increasing protein concentration), changing the ionic strength of the solution or using agitation[53]. However, studies show that in some cases, increasing protein concentration can also slow down the aggregation process itself, as off-pathway native-like oligomeric protein structure can be formed or self-stabilization can occur[54]. The initial nucleus often acts as a structural template, determining how the rest of the fibril assembles. Aggregate polymorphism refers to the phenomenon where the same protein can form multiple distinct aggregate structures (fibril strains), under different or even identical conditions[55].

The formation of stable critical size aggregation nuclei is followed by the elongation phase. During it, native monomeric protein molecules bind to the formed nucleus, and adopt its conformational template[50]. This process is typically several orders of magnitude faster than primary nucleation[56]. Elongation occurs at fibril ends in either semi- or bi-directional paths[48]. The fibril strains can replicate themselves, maintaining their physical and structural properties and transferring this “conformational memory” to the neighboring monomer[14,57]. This feature of fibrils can be used to initiate protein

amyloid formation without the rate-limiting nucleation step by adding preformed fibrils into monomer solution. It is usually called seeded-aggregation, or just seeding and is a probable mechanism of proteinaceous infectivity[58,59].

The rapid elongation phase is usually accompanied by additional processes - fibril fragmentation and fibril surface-mediated nucleation (often referred to as secondary nucleation)[47]. During the reaction, when the resulting fibrils reach a critical length, they tend to break, thus creating more ends to which new monomer molecules can bind. This process significantly increases the rate of aggregation[12]. In order to stimulate the fragmentation process *in vitro*, various modes of agitation are often used (shaking, glass beads, disruption by ultrasound)[60]. Another secondary process is surface-mediated nucleation. In this step the surface of fibrils acts as a catalyst for the formation of new aggregation nuclei[61]. Monomeric proteins bind to the hydrophobic surface of fibrils, change their conformation and form nuclei, which then separate from the fibril and serve as an additional aggregation center[62].

Aggregation monitoring

There are several ways to track the aggregation process *in vitro*. First dye used in the studies of amyloid protein aggregation was Congo red. It was invented in 1884 by the German chemist P. Bottiger[63]. However, the discovery of this dye was accidental, because Bottiger sought to create a new pH indicator, but synthesized a dye that binds to textile fibers[13]. Despite the history of its discovery, the German doctor Bennhold was the first person who used Congo red in 1922 to diagnose amyloidosis[13]. This dye has a hydrophobic center, which consists of two phenyl rings, as well as terminal molecule regions, which contain sulfonic acid and amino groups (Fig. 2A)[64]. When this dye binds to amyloid aggregates, a shift in the absorbance peak from 490 nm to 512 nm is observed and a new peak appears at 540 nm[65]. In addition, an increase in the optical anisotropy of the aggregates (apple green birefringence) is visible in polarized light (Fig. 2 B)[66]. However, the use of this dye has decreased due to non-specificity, as it also binds to other proteins, such as collagen and elastin[67].

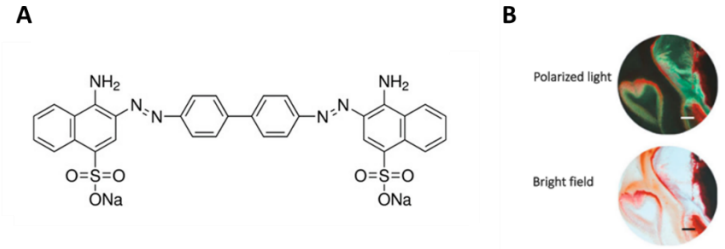

Figure 2. Molecular structure of Congo Red (A)[68] and example of amyloids stained by it (B)[53].

One of the most commonly used dyes for amyloid aggregation tracking is thioflavin-T, which is quite specific for amyloid aggregates and usually does not interact with proteins in their native, partially or fully unfolded form[69]. In 1959 Vassar and Culling were the first researchers who announced the possibility of using this dye for aggregation analysis[70]. Thioflavin-T consists of a dimethylated benzothiazole ring connected to a dimethylamino benzyl ring through a single bond (Fig. 3). In aqueous solutions, both rings rotate freely. This rotational movement is immobilized in the beta-sheet grooves of the forming aggregates. In this way, an increase in the fluorescence quantum yield is visible[49].

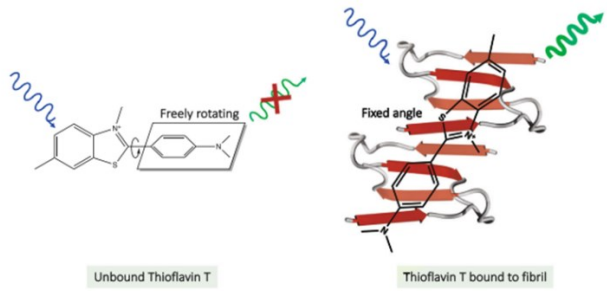

Figure 3. The principle of thioflavin-T (ThT) fluorescence enhancement via rotational immobilization[53].

When following the spontaneous aggregation process, a sigmoid-shaped change in fluorescence intensity is typically observed (Fig. 4 red)[49]. During seeded aggregation, when preformed aggregates are present in the reaction mixture, the lag phase is significantly shortened and aggregation usually is described as an exponential kinetic curve (Fig. 4 blue)[53]. However, studies show that in some cases of spontaneous protein aggregation, a different shape of the fluorescence intensity curve is possible. There are cases of double sigmoidal kinetics, in which it is believed that intermediate ThT-positive aggregates are formed[71]. Another possible case is a continuous increase in

fluorescence intensity, in which neither a clear lag nor a plateau phase is visible[72].

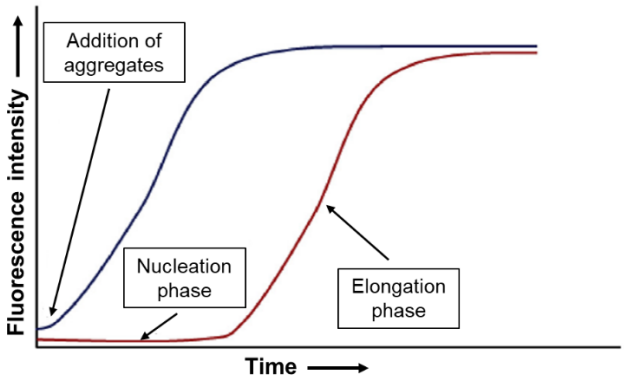

Figure 4. Graph showing fibril formation via nucleation-dependent manner (red curve) or seeding (blue curve)[50].

Despite the fact that ThT has been widely used in amyloid aggregation studies for many years, scientists are always striving to develop a new, more effective dye to monitor the protein aggregation process. A new dye, YAT2150 (Fig. 5), was recently introduced, which, according to research results, has high affinity and selectivity for amyloid aggregates. It can be used both for *in vitro* studies and for analyzing cell cultures[45]. Examples of other newer dyes are luminescent conjugated oligothiophene dyes (LCOs), marketed under the trade name Amytracker, and NIAD-4 (Fig. 5), which was developed for optical amyloid-β imaging and is able to cross the blood-brain barrier[73–76]. However, these and the previously mentioned dyes are specific for formed fibrillar aggregates and are unable to detect early soluble oligomeric forms. Studies show that in some cases, dyes such as aminonaphthalene 2-cyanoacrylate-spiropyran (AN-SP) and triazole-containing boron-dipyrromethene (taBODIPY) (Fig. 5) are able to interact with early-stage amyloid-beta aggregates[77].

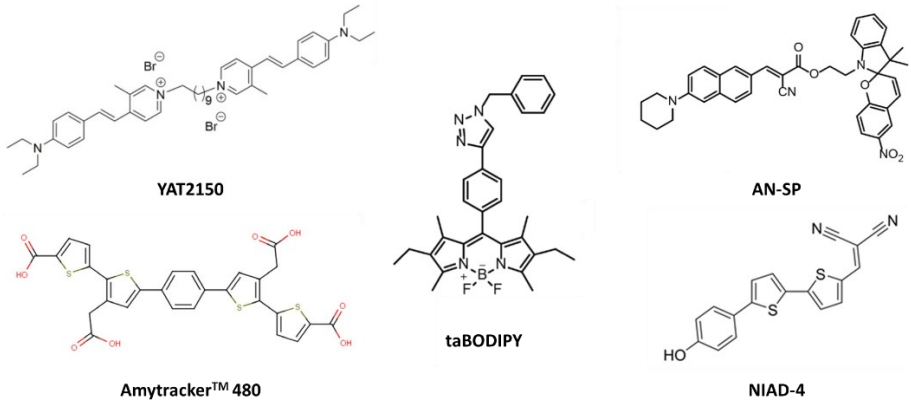

Figure 5. Molecular structures of YAT2150[78], Amytracker™480[73], taBODIPY[77], AN-SP[77], NIAD-4[79].

Fibril structure and morphology

One of the main and primary structural features of amyloid fibrils is their predominantly beta-sheet structure, where intermolecular beta sheets perpendicular to the fibril axis are formed[18]. Since the amount of these secondary structure elements changes during protein misfolding and aggregation, various methods are used to track these alterations, including CD, FTIR and Raman spectroscopies[53]. Although the beta-sheet structure is characteristic for different protein amyloid fibrils, its length and distribution vary depending on the protein[48]. Beta-sheets can form several types of quaternary structures, which are found in amyloid fibrils (Fig. 4).

One example of such structures is the beta-sandwich, where two beta-sheets are arranged face to face and are often separated by a loop hinge region (Fig. 6 A)[80]. Studies show that a further arrangement of such motifs is possible, called a superpleated beta-sheet structure. In this case, several beta-sheets form a stack aligned in one direction (Fig. 6 C)[81]. Another way of beta-sheet organization in amyloid fibrils is the beta-solenoid. In this structure, the polypeptide chain forms a fibril layer or rung, which turns around through the loop and further forms the second layer (Fig. 6 B)[80]. Other studies demonstrate hetero-amyloid or hetero fibrils, which are composed of two different types of beta-sheets[48]. However, in this case, an unusual ladder-shaped stack is formed, which is stabilized by hydrogen bonds and hydrophobic packing[48]. This type of different variability in the distribution of secondary structure motifs demonstrates the phenomenon of amyloid aggregate polymorphism[55].

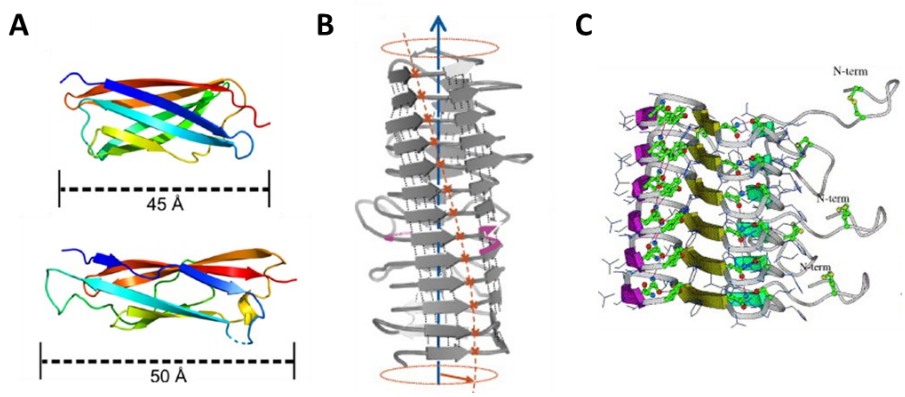

Figure 6. Examples of beta-sandwich (A)[82], beta-solenoid (B)[80] and superpleated beta-sheet (C)[81] structures found in amyloid fibrils.

Mature fibrils have a periodic structure that depends on the protofilament twisting in relation to one another[83]. Since protofilaments can form different 3D structures, depending on how they pack together, aggregates with different morphological structures are formed (examples of different fibril morphology is shown in Fig. 7)[48]. These distinct fibril morphologies can be divided according to the degree of fibril twisting, their diameter, weight per length or the number of protofilaments that create the fibril[48,84]. In some cases, aggregates also tend to associate laterally or form large clusters[53]. In order to distinguish morphologically different isoforms, atomic force, cryo-electron or transmission electron microscopy techniques are often used[85–87]. Aggregate polymorphism is also observed in cases of neurodegenerative disorders, which can influence the type and progression of the disease[88]. *In vitro* studies show that the formation of amyloid aggregates with different structures or morphologies may depend on multiple environmental factors[83]. In some cases, even identical conditions have yielded a mixture of structurally distinct fibrils[89]. These data indicate that amyloid aggregate polymorphism may be a key factor responsible for the variety of neurodegenerative disorders, as well as one of the main hindrances in elucidating the mechanisms of fibril formation.

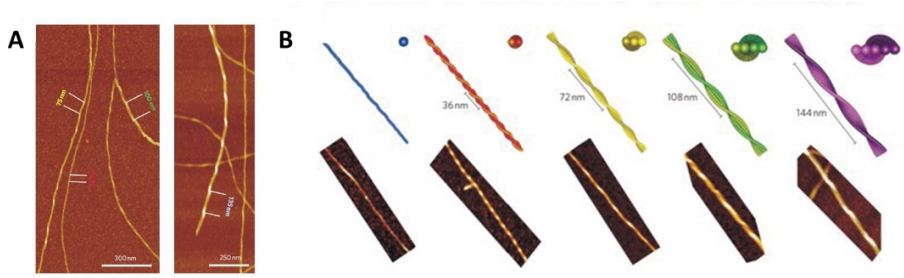

Figure 7. AFM images (A) and corresponding models (B) of β-lactoglobulin fibrils with different periods[90].

Fibril stability

In aggregation studies, environmental conditions that destabilize the protein are often used to promote misfolding and fibril formation. Therefore, higher temperatures, high salt concentrations and denaturants are used. These conditions also affect the stability of already formed amyloid fibrils[91]. This is one of several parameters that are used in studies to identify different types of aggregates. The stability of fibrils often depends on several structural parameters. One of them is the cross-beta structural motif, which, depending on the number of hydrogen bonds formed, is one of the most important factors stabilizing the fibril structure[92]. This motif is also responsible for the aggregate partial resistance to proteases[18]. Another factor contributing to the stability of fibrils is the increase in Van der Waals interactions and the reduced exposure to solvents[93].

Although *in vivo* studies of aggregate stability are not possible, this property provides many insights into the fibrils which are isolated from patients. During a fibril denaturation assay with aggregates from a patient with prion disease, a correlation was observed between fibril stability and the length of the incubation periods of prion diseases[94]. The results showed that prions that were detected in cases with a short incubation period were less stable under denaturing conditions[95]. Similar structure-stability correlations were observed for a number of other amyloid proteins *in vitro*, such as insulin, lysozyme, indicating that this parameter can be used to distinguish between different amyloid fibril strains[96].

Amyloidogenic proteins used in this work

Insulin

Insulin is a hormone that is primarily responsible for regulating blood sugar levels, as well as carbohydrate, protein, and fat metabolism in the body[97]. This hormone is secreted into the bloodstream by the Langerhans islet beta cells in the pancreas. Before secretion, insulin is stored in an inactive form – a

hexamer consisting of three dimer pairs bound to two Zn^{2+} ions[98]. In the bloodstream, the hexamer breaks down into dimers and then into monomers. The monomeric form of insulin is the active molecule that performs its function in the body[99]. Insulin consists of two chains, the secondary structure of which, in its native state, is dominated by alpha-helices. The two chains consist of 21 and 30 amino acids, which are connected by two disulfide bridges[100]. In 1921, scientists from Canada - F. Banting, C. Best, J. Macleod, J. Collip - successfully isolated insulin from the blood and demonstrated its function in the body[101]. In 1969, D. C. Hodgkin determined the crystal structure of this protein and was later awarded the Nobel Prize in Chemistry[98].

However, under certain conditions, this globular protein tends to change its native conformation and form amyloid fibrils. The analysis of its aggregation process was prompted by the observation of insoluble aggregates around its injection site in the case of people with type I and type II diabetes[102]. This disorder was named non-lethal local injection amyloidosis[44]. In 1940, Waugh was the first scientist who described the stages involved in this protein's aggregation and the resulting fibrils[103]. Despite the wide range of environmental conditions used for *in vitro* insulin aggregation studies, it is usually carried out at low or neutral pH and at elevated temperatures. Agitation is also often used to accelerate the process[104]. Due to its low price and simple aggregation protocol, this protein is often used as a model of amyloid fibril formation studies. Since it is known that insulin aggregation is characterized by fibril polymorphism, and these studies are usually performed at low pH, with different major solution components, this particular protein was chosen to analyze the complex effect of three environmental factors - pH, ionic strength, and the major solution chemical component - on the aggregation process (Publication 4).

Lysozyme

Lysozyme is a globular protein that acts as an enzyme in the body. In 1922, A. Fleming was the first who isolated lysozyme from human nasal mucosa and determined its antibacterial function[105]. This protein is found not only in the mucosa, but also in saliva, tears and blood serum[105]. Lysozyme hydrolyzes the β-1,4 glycosidic bond between N-acetylmuramic acid and N-acetylglucosamine in the peptidoglycan cell wall of gram-negative bacteria, thereby disrupting their integrity[106]. During research, it was observed that a mutation in the gene encoding lysozyme and its aggregation cause hereditary systemic lysozyme amyloidosis[107]. As this disease progresses, the accumulation of lysozyme aggregates damages various organs and causes their dysfunction[108].

Hen egg-white lysozyme, which was used in this work, consists of a single polypeptide chain comprised of 129 amino acids[109]. The crystal structure of it was first determined in 1965[106]. This protein is divided into two domains (alpha and beta), which are connected by four disulfide bridges. These domains differ in their secondary structure - the alpha region is composed of four alpha-helices, and the beta - is dominated by antiparallel beta sheets[110]. Since the lysozyme from hen egg white is an ortholog of human protein variants associated with amyloidosis, it has a similar sequence, and the production of this protein is relatively cheap, it is often used for aggregation studies *in vitro*. Research shows that this protein tends to easily form fibrils at low pH or elevated temperatures[106,110]. Other factors, which also enhance its amyloid aggregation, include: the addition of denaturants or organic solvents, as well as intensive sample agitation[111]. Given that lysozyme aggregation is characterized by polymorphism of the formed fibrils, and that the melting point of the native protein is highly dependent on the solution pH, lysozyme was chosen to analyze the influence of the initial protein folding state at different pH conditions on the structural and morphological variability of the formed aggregates (Publications 1 and 2).

Prion protein

Cellular prion proteins are membrane glycoproteins that bind to the lipid bilayer using a glycosylphosphatidylinositol anchor[112]. Prion proteins are synthesized and undergo post-translational modifications, such as removal of signal sequences, attachment of a GPI anchor, formation of disulfide bridges or N-terminal glycosylation[113]. The largest amounts of this protein are synthesized specifically in the central nervous system, but are also found in other organs[114]. Native prion proteins are believed to be involved in the management of oxidative stress, modulation of signaling pathways and ion binding processes[115]. Mammalian prion proteins are composed of approximately 250 amino acids, with signal sequences at the C- and N-terminals. The native prion protein consists of two regions: an N-terminal unstructured region and a C-terminal globular domain. The N-terminal protein end is also divided into two hydrophilic regions and one octapeptide repeat domain[116–118].

Conformational changes of prion proteins to their infectious forms are associated with neurodegenerative diseases called transmissible spongiform encephalopathies. Examples of such disorders include Creutzfeldt-Jacob disease, Gersmann-Straussler-Scheinker syndrome, fatal familial insomnia and Kuru disease[114]. Prions were the first identified proteins that were acting as a template and initiating further conformational changes of the native protein molecules[119]. Due to its stability, *in vitro* aggregation studies require high concentrations of denaturing agents, such as guanidine hydrochloride,

urea, as well as elevated temperatures and intensive sample agitation[120]. It has also been shown that fibrils formed under such conditions *in vitro* have a relatively lower amount of beta-sheets in their structure compared to those isolated from infected mammalian tissues, which greatly reduces their infectivity[120]. Under identical conditions prion proteins are highly prone to form structurally distinct aggregates that differ not only in the amount of secondary structure elements, but also in morphological parameters[121]. This conformational variability and the protein's high susceptibility to environmental factors was the main reason it was chosen for cross-interaction studies in this work (Publications 6 and 7).

The amino acid sequences of human and mouse prion proteins are more than 90% homologous[122]. In addition, both proteins have a similar secondary structure[123,124]. However, the differences between the human and mouse prion protein sequences (18 amino acids) determine the emergence of a species barrier[125,126]. Studies show that the core of mouse prion protein aggregates consists of the amino acid sequence 89-230. This sequence remains stable after protease digestion[127]. For these reasons, this fragment of mouse prion protein is often used during *in vitro* studies.

Alpha-synuclein

Alpha-synuclein is a protein, consisting of 140 amino acid residues[57]. It belongs to the synuclein protein family, which is found in vertebrates[128]. This protein was first discovered in 1988 by the French scientist Maroteaux, who studied the nuclei and synaptic vesicles of fish cholinergic neurons[57]. Because of its localization, this protein's name was composed of - "syn" - from the word synapse and "nuclein" – nucleus[129]. In later years, alpha-synuclein became the subject of numerous studies where it was shown to be a major component of Lewy bodies and neurites – the markers of Parkinson's disease or dementia with Lewy bodies[130].

Predominantly, Asyn is synthesized in the brain, but in smaller quantities it can also be found in other organs[131]. The N-terminal end of the protein contains a conserved amino acid sequence. This is followed by a hydrophobic central domain known as non-amyloid component, which tends to form β-sheets during aggregation. The flexible C-terminal end of the protein is dominated by negatively charged amino acid residues and proline[132]. After translation, the most common post-translational modification of synuclein in disease-related cases is phosphorylation[133]. Although the exact physiological function of alpha-synuclein is not clear, it is believed that this protein is responsible for the movement of synaptic vesicles in the synaptic cleft[134,135].

Alpha-synuclein is an intrinsically disordered protein, but when incubated for longer periods of time under physiological conditions, it tends to aggregate into amyloid fibrils[136]. Studies show that alpha-synuclein forms structurally different fibril strains based on the environmental conditions and additives used during the process[137,138]. It has also been observed that this protein is able to form distinct aggregates under identical experimental conditions[128]. For this reason, alpha-synuclein was chosen in this work to investigate how fibrillar structures are influenced by changes in environmental conditions or the addition of potential inhibitor molecules (Publications 3 and 5).

S100A9

S100 are a family of calcium-binding proteins found only in mammals[139]. In 1965, B. W. Moore first purified these proteins from bovine brains and named them S100 due to their solubility in 100% saturated ammonium sulfate solution at neutral pH[140]. Currently, 25 members of the S100 protein family have been identified[141]. They are involved in various extracellular and intracellular regulatory processes, such as apoptosis, differentiation, proliferation, calcium homeostasis[140]. One of the most studied members of this family, S100A9, is a pro-inflammatory protein also known as calgranulin B or migration inhibitory factor-related protein 14 (MRP-14). This protein is mainly produced by neutrophils and, to a lesser extent, by neurons and microglia[142]. The secondary structure of S100A9 is characterized by a long unstructured C-terminus and four alpha helices, which form two helix-loop-helix motifs, also known as EF-hands. The ends of these motifs are associated with hydrophobic protein regions and two calcium ions bind to the EF-hands[143]. Upon binding of calcium ions conformational changes are initiated, exposing the protein hydrophobic regions to the solution, thereby facilitating the interaction of S100A9 with other proteins in the body[139]. *In vivo*, S100A9 is most often found as a heterodimer with S100A8 (calgranulin A or MRP-8). Although homodimers of these proteins are also discovered in smaller quantities, they are less stable than heterodimers[72].

In vitro, S100A9 is able to aggregate and form amyloid fibrils under physiological conditions, without calcium ions in the reaction[142]. This leads to the loss of its signaling function and the resulting fibrils possess cytotoxic properties. Studies show that S100A9 aggregation depends on the concentration of calcium ions, where a higher concentration can completely suppress its fibrilization[139]. When analyzing atomic force microscopy images of the formed S100A9 protein fibrils, it is seen that this protein often forms worm-like aggregates[142]. It has also been observed that during interactions with other proteins, S100A9 can modulate their aggregation propensity and redirect their fibril formation pathway[144,145]. For this reason, S100A9 was

chosen to investigate its cross-interaction with the previously mentioned prion protein fragment (Publication 7).

Superoxide dismutase-1

Superoxide dismutase-1 (SOD1) is a highly conserved metalloenzyme found in the cytosol, outer membrane and intermembrane space of mitochondria[146]. SOD1 is one of the most commonly found proteins in cells, accounting for 1–2% of total protein count. It is involved in the scavenging of superoxide radicals, which are released by mitochondria as byproducts of redox reactions[147]. The enzyme converts these radicals into hydrogen peroxide and oxygen, which is one of the main protein functions in the body. In addition, SOD1 is believed to work as an RNA-binding protein or transcription factor activator[148]. SOD1 is a 32 kDa homodimer, which is synthesized in various mammalian tissues. The highest levels of SOD1 are found in the central nervous system and liver[146]. Monomers of this protein contain one zinc and one copper ion, as well as an intermolecular disulfide bond that stabilizes the homodimer structure, in addition to the subunits being held together by hydrogen bonds and hydrophobic interactions[147].

Misfolding and aggregation of SOD1 are associated with the development of amyotrophic lateral sclerosis (ALS). ALS is a life-threatening neurodegenerative disorder in which motor neurons die, leading to muscle atrophy, paralysis and ultimately respiratory failure[149]. Most cases of ALS are spontaneous and only about 10% are inherited. SOD1 was the first identified gene, whose mutations were associated with the development of ALS[150]. Studies have shown that ALS is characterized by more than 200 different mutations that destabilize the homodimeric protein structure and thus promote aggregation[151]. The protein is modified after translation, thereby affecting its folding and ability to bind metal ions. Post-translational modifications of SOD1 can also alter its localization in the cell and its function[148]. Mutations in the SOD1 gene are also known to result in SOD1 variants with higher tendencies for aggregation[150]. However, studies have shown that not all post-translational modifications are associated with the development of ALS[148]. Despite mutations, SOD1 aggregation can be induced by removing metal ions that stabilize the protein homodimeric structure or by breaking the disulfide bridge. Vigorous mixing of samples is also used to accelerate this process[147]. During studies with SOD1, it was observed that it can alter the process of other amyloidogenic protein aggregate formation. For this reason, similarly to S100A9, it was chosen to investigate its cross-interaction with the previously mentioned prion protein fragment (Publication 6).

Environmental factors

Temperature and agitation

Temperature is one of the most frequently changed factors in protein aggregation studies. Modulation of this experimental condition itself affects the aggregation process in several aspects - by altering the kinetic parameters and the structure of the resulting aggregates. Increasing the temperature is usually used to accelerate this process. In the case of kinetics, higher temperature accelerates the nucleation process (the lag time is shortened), because a larger part of the protein molecules are in a partially or fully unfolded state, which promotes conformational changes and the formation of aggregation nuclei, as well as an increased molecular motion promotes monomer interactions and nucleation[14]. However, sometimes the effect of lower temperature on proteins and their aggregation is also observed, called cold denaturation or cold-unfolding, which promotes the nucleation process and further protein aggregation[152].

Temperature also affects the subsequent aggregation stage - elongation. At higher temperatures, the movement of molecules accelerates, more collisions and hydrophobic interactions in solution occur, so the reaction rate increases[46]. However, temperature affects not only primary processes, but also secondary ones, such as fragmentation[60]. In addition to affecting the kinetic parameters of aggregation, temperature can also alter the structure of the resulting fibrils. Literature analysis reveals that at higher temperatures, greater variability in the structures of the formed fibrils can be observed[89]. Moreover, fibrils formed under different temperature can vary in their stability, cell toxicity, seeding efficiency, morphology or number of protofilaments[46].

Despite the common use of higher temperature in studies to accelerate the aggregation process, the publications frequently describe the enhanced kinetics (lag time, rate constant) without providing the precise mechanistic cause. However, it is important to understand how subtle shift in the initial protein folding equilibrium predetermines subsequent fibril variability. Discovering the influence of this parameter on aggregate polymorphism could provide important insights into the appearance of distinct disease phenotypes (e.g., in prionopathies), differences in aggregate toxicity, and the spread of aggregates in disease. For this reason, part of my work was dedicated to determining the relationship between the initial protein folding state at the start of the reaction and the polymorphism of the resulting aggregates. The link between these two parameters was identified by taking into account the melting point of lysozyme, while also changing secondary environmental factor - the solution pH (Publications 1 and 2).

Another important aspect where literature does not provide sufficient insight concerns the effect of temperature on already formed aggregates. Often, studies identify structurally different aggregate strains, which are compared not only according to their structural and morphological parameters, but also by their stability against denaturants or resistance to proteolysis, but the effect of temperature on the structural integrity of fibrils remains unknown. Despite the possibilities of identifying different strains, many unanswered questions remain in this area, particularly concerning the dynamic stability of aggregates. For this reason, part of my work was committed to analyzing how incubation at higher temperatures affects different alpha-synuclein pre-formed aggregate strains (Publication 3). In this way, the study provided important information for understanding the possible propagation and pathology of fibril strains *in vivo* during inflammation events.

Another environmental factor - agitation of samples, in addition to temperature is often used to accelerate and promote the process of protein aggregation during *in vitro* studies. There are several methods of agitation, which include rotating, shaking, stirring and vortexing[14]. Aggregation-inducing factors that arise from various forms of agitation include: additional liquid-surface or liquid-air interfaces (protein misfolding at interfaces), sample mixing (higher molecule collision frequency and fibril fragmentation)[46].

pH and ionic strength

Another factor that varies during *in vitro* aggregation studies is the pH of the solution. Since proteins are very sensitive to changes in pH, this parameter affects both the aggregation kinetics and the structure of the resulting fibrils. First of all, in terms of its influence on the aggregation kinetic parameters, this environmental factor can promote or slow down the aggregation process[46]. Aggregation can be promoted by the following pH-dependent factors: changes in the protein charge (closer to the pI value, proteins interact more easily, nucleation and elongation stages are accelerated), decrease in stability (hydrogen or non-covalent bonds are broken, exposure of hydrophobic regions to solvent increases, thus promoting conformational changes)[14]. However, aggregation can also be inhibited by altering the pH further away from the protein pI, thus increasing its net charge. This slows down the aggregation process (nucleation, elongation) due to increased electrostatic repulsion between more charged protein molecules[153]. In addition to affecting kinetic parameters, the structure of the resulting fibrils may depend on the pH at which the aggregation process took place. Studies show that in some cases, the solution's pH affects the structural variability of aggregates [154]. In case of some proteins, fibrils formed at lower pH are thinner, more fragmented and less stable than those formed at neutral pH[155].

Solution ionic strength can affect the electrostatic interactions between protein molecules. Therefore, when analyzing the aggregation process, it is important to evaluate this factor as well. The change in ionic strength itself can affect the kinetic parameters of aggregation and the resulting fibril structure. The main factor influencing this process is the protein net charge[46]. Higher ionic strength reduces the electrostatic repulsion between similarly charged protein molecules, reduces protein stability and enhances hydrophobic interactions by diminishing the solvation of nonpolar residues, which accelerates the aggregation process[14]. However, anions and cations affect protein aggregation differently by binding or screening the protein molecules. This effect is largely dependent on the pH[156]. Furthermore, the ability of anions to affect aggregation varies with the electroselectivity and polarizability of the protein[46]. As in the previously discussed case, ionic strength can also affect the structural and morphological parameters of the resulting fibrils. Studies show that fibrils formed at higher ionic strength, the are more straight and rigid[157]. Ionic strength can also affect stability, cytotoxicity and seeding ability of the resulting fibrils[14].

The influence of pH and ionic strength on protein amyloid aggregation is well-described. Literature shows that the effects of these two environmental factors are strongly dependent on each other. However, the main problem in studies remains that these parameters are usually evaluated separately, and their overall synergistic effect is not determined. For this reason, part of my work was aimed at analyzing how small changes in pH, ionic strength or the solution's main chemical component can affect the structural and morphological variability of the resulting insulin aggregates (Publication 4).

Other proteins

Other proteins, whether specific interactors, chaperones or random bystanders, can dramatically alter the aggregation kinetics. Some of these proteins — molecular chaperones, such as Hsp70, Hsp90, small heat shock (sHsp) — bind to misfolded proteins or aggregation prone regions[158,159]. By interacting, they can slow down or stop the nucleation or elongation stages. These proteins act mainly by stabilizing the monomers or by disaggregating already formed oligomeric forms[160]. Some proteins can also interact with each other to slow down the fibrillization process. For example, previous studies have shown that alpha-synuclein aggregation is slowed down by the presence of the S100A9 protein, which interacts with its N-terminus[144]. In another case, reports have demonstrated that the interaction between amyloid-beta and alpha-synuclein promotes the formation of soluble but toxic beta-sheet rich hetero-oligomers. This stabilization of oligomeric form slowed down the further process of amyloid-beta fibrillization[161,162]. However, in some cases, other proteins or their aggregates can act as a surface and promote the surface-initiated

nucleation, thereby accelerating the aggregation of this protein. One example of such interaction is between amyloid-beta and prion protein. *In vitro* studies have shown that amyloid-beta induces prion protein aggregation even at submicromolar concentrations[163]. Such cross-interactions are also detected *in vivo*. One reported example has shown that the fibrillar form of amyloid-beta accelerated tau aggregation process *in vivo*[164]. In addition, other macromolecules can act as a molecular crowding agent, which leads to the formation of high-concentration protein droplets and thus promote the aggregation[165]. All of these interactions can also affect the structural and morphological parameters of the resulting fibrils, leading to new types or stabilizing a certain strain.

While numerous studies focus on identifying molecules that modulate aggregation kinetics, the research generally focuses on simplified identifications of inhibition by seeking compounds that slow down the aggregation process (e.g., increasing half-time). This approach disregards a crucial mechanistic detail - the inhibitor's effect on the structural properties of the resulting aggregate. For this reason, a large part of my work was devoted to determining how small molecule compounds (imidaziothiazine derivatives) or proteins involved in the aggregation reaction, in their native or fibril form, can affect not only the aggregation kinetics, but also the structural or morphological parameters of the formed aggregates, as well as the variability of the resulting fibrils strain (Publications 5, 6 and 7).

METHOD OVERVIEW

Protein purification

In order to perform aggregation studies, it was necessary to first purify the various recombinant proteins. All proteins used in this work were either purchased from commercial companies (human recombinant insulin, hen-egg white lysozyme) or synthesized in *E. coli* BL21 (DE3) cells (mouse prion protein fragment 89-230, human alpha-synuclein, human SOD1, human S100A9). First, the cells were transformed using heat shock and grown in autoinduction ZYM-5052 or LB medium, induced by IPTG. Since the prion protein and S100A9 contained a histidine tag, these proteins were purified using immobilized nickel ion affinity chromatography and eluted from the sorbent using buffers containing imidazole[72,166]. Other proteins (SOD1 and alpha-synuclein) were purified using a combination of ion exchange and size-exclusion chromatographies[167,168]. After purification steps, in some cases proteins (alpha-synuclein, SOD1) were lyophilized and stored at -20°C. Before use, the protein powder was dissolved in the buffer solution required for the study. Alternatively, the proteins (MoPrP 89-230, S100A9) were exchanged into the storage buffer solution, concentrated and frozen at -20°C. This method was used in all publications included in the dissertation.

Induction of fibrillization

To induce folded protein aggregation, the protein's native structure must first be destabilized. This can be achieved by various methods. For instance, increasing the temperature can lead to partial or complete protein unfolding, depending on its melting point[169,170]. Similarly, a change in pH can destabilize the protein by altering the charge distribution on its surface, which disrupts electrostatic interactions. This effect depends on the protein's isoelectric point (pI) and amino acid exposure to the solvent[14]. Chemical denaturants, such as guanidine hydrochloride (GuHCl) and thiocyanate (GuSCN) or urea, are also commonly used to destabilize proteins[171]. Other methods include inducing oxidative stress, using high salt concentrations, or exposing the protein to metal ions, which can promote aggregation[6].

However, many amyloidogenic proteins require specific conditions for their aggregation. Studies show that in the case of insulin, aggregation is often carried out at low pH[172]. For lysozyme and prion proteins, neutral pH values are commonly used, but denaturing agents are necessary to facilitate misfolding. In addition, the aggregation process of these proteins can be accelerated by employing higher temperatures[121,173]. Alpha-synuclein and S100A9, in contrast to the previously mentioned proteins, are able to aggregate spontaneously at physiological pH and temperature without

denaturants[72,137]. Finally, various forms of agitation can also be used to promote and accelerate the aggregation process. For most protein amyloid assemblies, it fragments the formed fibrils, thereby creating additional ends for monomer incorporation[14]. This method was used in all publications included in the dissertation.

Aggregation tracking

The fluorescent dye thioflavin-T (ThT) is one of the most commonly used tools for monitoring the amyloid aggregation process[174]. The concentrations of the dye used in aggregation assays varies depending on the protein concentration involved in the reaction (10-100 μM). However, one drawback of this method is that the dye becomes hydroxylated at the benzothiazole ring during prolonged incubation at neutral or alkaline pH and elevated temperatures, which diminishes its fluorescence potential[175]. The maximum ThT fluorescence is typically achieved by excitation at a wavelength of 440 - 450 nm, with the maximum emission measured at 480 - 490 nm[70]. During aggregation, a change in fluorescence intensity is observed, which correlates with the number of dye-binding structures. This method was used in all publications included in the dissertation.

Another dye 1-anilinonaphthalene-8-sulfonate (ANS) is often used not only to monitor the aggregation process, but also in protein melting assays. This molecule interacts with the hydrophobic regions of the protein, thus causing a blue-shift in its fluorescence spectra and an increase in fluorescence intensity[176,177]. In addition to these commonly used molecules, the aggregation process can also be monitored by tracking changes in sample optical density [178]. This method was used in publications 1, 2 and 7.

Kinetic analysis

The aggregation curves (monitored using ThT assay), is usually analyzed by comparing three main factors – lag time, half-time, apparent rate constant. To determine them, data fitting is first required. In the case of spontaneous aggregation, which is usually characterized by sigmoidal curves, a Boltzmann sigmoidal equation is often used. As for seeded aggregation, defined by an exponential curve, linear fitting is used between the 40 and 60 % total fluorescence intensity points and the half-time is interpolated. The Boltzmann equation sigmoidal fit example with calculation of kinetic parameters is shown in Figure 8. Alternatively, the reaction kinetics can be fit with a variety of different amyloid aggregation models, which provide reaction rate constants for each step, such as the widely used online tool – AmyloFit[179]. This method was used in all publications included in the dissertation.

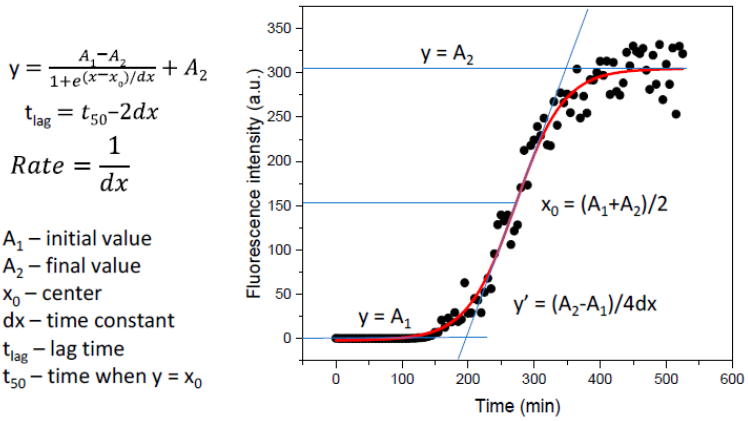

Figure 8. The Boltzmann equation sigmoidal fit example with calculation of aggregation kinetic parameters (lag time, apparent rate constant, half-time)[89].

Fourier-transform infrared spectroscopy (FTIR)

One commonly applied method to assess the structural differences of the formed aggregates is Fourier-transform infrared spectroscopy (FTIR). This technique allows to determine the aggregate secondary structure, regardless of the protein's physical form, such as protein solutions, films, crystals, hydrogels, etc.[180]. This methodology is based on specific absorbance spectral positions related to the vibration of the protein peptide bonds[181]. When analyzing the secondary structure of aggregates, the main focus is on the amide I region (1700-1600 cm^{-1}). In this region, the spectra have characteristic maxima positions related to various secondary structure elements, such as alpha-helices, beta-sheets, random-coil, turns and loops[182]. The FTIR spectra band positions in D_2O corresponding to different secondary structure elements are shown in Table 2.

Table 2. FTIR spectra band position in D_2O corresponding to different secondary structure elements. Adapted from[180].

Secondary structure elements	**Band position in D_2O**
α-helix	1660-1642 cm^{-1}
Parallel β-sheet	1694-1672 cm^{-1}; 1638-1615 cm^{-1}
Antiparallel β-sheet	1694-1672 cm^{-1}
β-turn	1691-1653 cm^{-1}
Random coil	1654-1639 cm^{-1}

Before scanning the protein FTIR spectra, the samples are usually exchanged into deuterium oxide in order to avoid water-related signals and to obtain a good quality spectrum. When analyzing the obtained data, the spectra are first processed by subtracting deuterium oxide and water vapor spectra. Afterwards, the spectra are baseline corrected and normalized to the same Amide I/I' band area. This procedure is important when comparing the differences in structural elements between the samples, as it is not influenced by different protein concentrations in the samples (example of fibril FTIR spectrum and its second derivative is shown in Fig. 9). In order to quantify the distribution of alpha-helices, beta-sheets and other secondary structures, the FTIR spectra are deconvoluted into separate peaks. The peak positions are chosen based on the spectra second derivative minima positions. This method was used in all publications included in the dissertation.

Figure 9. Example of insulin fibril FTIR spectrum and its second derivative. Adapted from[138].

Circular dichroism spectroscopy (CD)

Another method for determining the structure of proteins is circular dichroism spectroscopy. During this analysis, changes in the protein's secondary and tertiary structure, the dynamics of folding/unfolding and binding characteristics are assessed[50,183]. The principle of this methodology is based on the differential absorption of circularly polarized light. Molecules absorb left- or right-handed circularly polarized light, depending on the chiral center of the molecule or the 3D structure that forms the chiral environment[46,184]. The advantage of this method is that information about the protein's structure is obtained in a relatively short time and using a low concentration of it in solutions that correspond to experimental conditions[184]. When studying conformational changes in amyloid proteins, CD signals are analyzed in the far UV wavelength region (240-190 nm range)[183]. Characteristic CD spectra of different secondary structure elements are shown in Fig. 10. This method was used in publication 3.

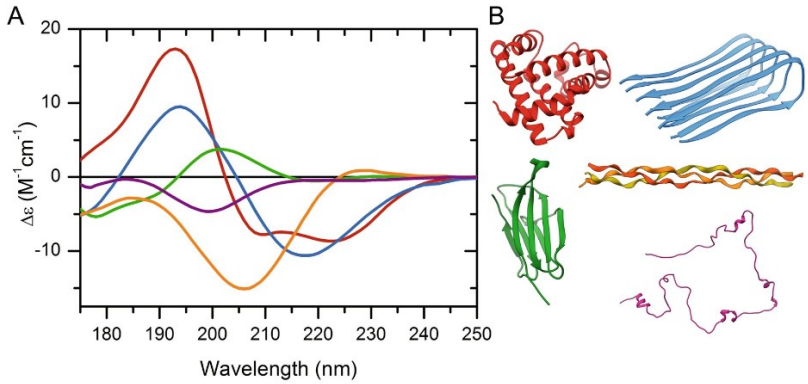

Figure 10. Characteristic CD spectra (A) of different secondary structure elements (B). Figure shows secondary structures such as α-helix (red), parallel β-sheet (blue), antiparallel β-sheet (green), polyproline-helix (orange) and disordered chain (purple)[185].

Atomic force microscopy (AFM)

AFM is often used to assess the morphology of fibrils, by creating 3D maps of surfaces covered with aggregates at nanometer resolution[53]. This is achieved by determining the sample position with respect to the needle, recording the height of the probe and converting this data into a three-dimensional image, usually displayed as a color scheme showing the height differences[50]. In this way, it is possible to assess the morphological parameters of the formed fibrils that have covered the mica surface, such as height, width and periodicity[86]. In addition, it is possible to see whether the sample contains a mixture of fibrils or amorphous aggregates. This method also allows to assess whether the formed fibrils tend to associate laterally, into large clusters or remain separate (example of fibril AFM image and corresponding cross-sectional height distributions are shown in Fig. 11). In certain cases, fibrils do not always adhere to the mica surface due to their charge. In this event, the mica surface is first treated with (3-aminopropyl)triethoxysilane (APTES) to improve adhesion before sample application. This method was used in publication 1-4, 6 and 7.

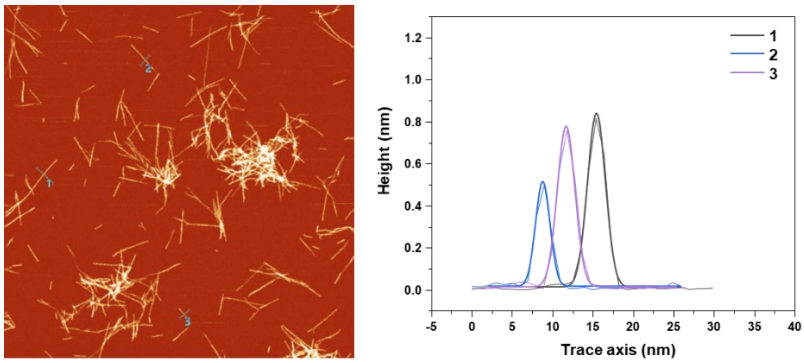

Figure 11. Example of fibril AFM image and corresponding cross-sectional height.

Transmission electron microscopy (TEM)

Another way to assess the morphology of the formed aggregates is by using TEM. This method is an excellent tool that allows high-resolution visualization of the formed aggregates at the nanometer scale[87]. TEM is based on the passage of a high-energy electron beam through the sample. Since some of the electrons interact with the sample, and the other part passes through the thin surface, an image is obtained in which the aggregates are reconstructed using contrast[53]. This technique allows to determine the size, shape and distribution of the formed aggregates, but unlike AFM, it does not allow to assess height and topographic information. When preparing the sample for TEM analysis, it is applied to a carbon-formvar coated grid. In order to obtain good contrast and well-preserved morphology, the sample is negatively stained using metal salts, such as uranyl acetate or phosphotungstic acid. These materials coat the aggregates and form a layer of radiation-stable and electron-dense material[87]. An advantage of this technique compared to AFM is the simultaneous capture of a larger area, which allows the determination of the formed aggregate homogeneity. This method was used in publication 5.

Fluorescence and absorbance

To assess the variability of the formed aggregates, bound-dye excitation-emission matrices can be measured[186,187]. Since the excitation and emission positions at which the fluorescence maximum is observed may vary depending on the dye binding mode and the corresponding structurally distinct aggregate strain, this method allows to separate samples that may differ in their structure [187]. In order to determine the maximum positions, the fluorescence intensity is first scanned at a range of excitation wavelengths with a fixed emission wavelength and vice versa. A 3D map of fluorescence intensity is obtained (Fig. 12 A). The map is then corrected for the first and second inner filters effects, which can arise from light reabsorbance by the sample. After this

correction, it is possible to calculate the positions at which the fluorescence maximum is observed for each sample (Fig. 12 B). This method was used in publications 1, 2 and 3.

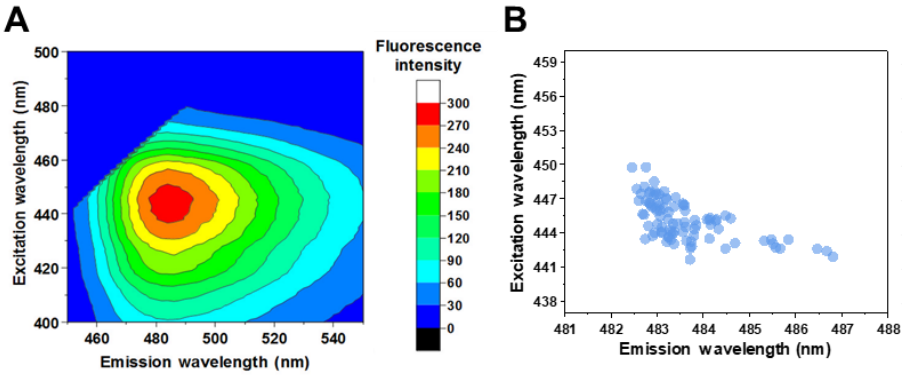

Figure 12. Example of excitation-emission matrices (A) [89] and fibril EEM maximum position distribution under identical conditions (B) [187].

Dye binding can also be assessed using absorbance spectroscopy. By scanning the absorbance spectra of samples with fibrils and their supernatants, it is possible to calculate the concentration of the bound dye[186]. Additionally, shifts of the absorbance spectra maximum positions can indicate different dye binding modes[188]. This method was used in publications 2, 3 and 4.

Fibril stability under denaturing conditions

Another characteristic that can help identify distinct fibril strains is their stability under denaturing conditions. For this purpose, protein aggregates are mixed with a range of different denaturant concentrations, where all the resulting samples have identical initial aggregate concentrations. The samples are then incubated, and their optical densities are measured (Fig. 13). Typically, the optical density of the samples decreases in a sigmoidal shape as a function of denaturant concentration. This data can then be fit using a Boltzmann sigmoidal equation. The denaturant concentration value, at which half of the aggregates are dissociated, and the other half are stable, is considered as the stability midpoint[91]. According to this parameter, it is possible to compare different aggregate samples and determine if the formed structures are more or less resistant to denaturation. This method was used in publications 2, 4, 6 and 7.

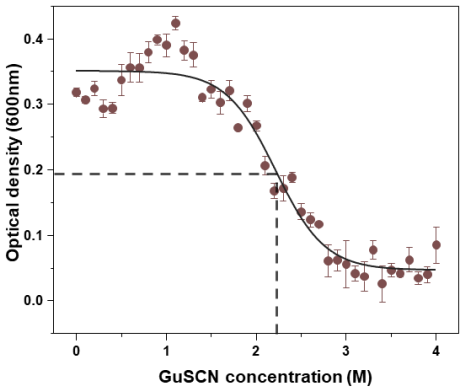

Figure 13. Optical density dependence on GuSCN concentration. The dotted line represents the GuSCN concentration at which half of the aggregates have dissociated.

Cell toxicity

Another property analyzed in aggregate studies is their toxicity to cells. Two methods are most often used for this. One of them is the MTT assay. This test establishes mitochondrial activity and is applicable to determining the number of viable cells. This methodology is based on a color change, which can be assessed using absorbance spectroscopy, which reflects the number of viable cells[189]. During the test, cells are incubated with yellow 3-(4,5-dimethylthiazol-2-yl)-2,5-diphenyltetrazolium bromide (MTT), which is converted by active mitochondrial succinate dehydrogenase to a blue-violet product - formazan[190]. Although this method is often used to determine toxicity, it also has its drawbacks. Cell viability is ascertained indirectly during the study and is recalculated by taking into account the activity of mitochondrial enzymes and cell metabolism. For this reason, it is necessary to assess whether the experimental conditions do not change the metabolic process and cell proliferation[189].

Another method used is the LDH release assay. Similar to the previously mentioned MTT assay, it is also based on determining the secreted product using absorbance spectroscopy. However, this technique helps to determine cell death based on the loss of its membrane integrity[191]. During cell damage, lactate dehydrogenase is released into the medium. It converts lactate to pyruvate, which interacts with iodonitrotetrazolium chloride, thus forming formazan. The amount of formazan formed during this study is directly related to cell viability[192]. These methods can also be applied to examine the cytotoxicity of any potential anti-amyloid compounds. All toxicity studies in this work were performed using

SH-SY5Y neuroblastoma cells. All cell toxicity assays were conducted by R. Sniečkutė. This method was used in publications 5 and 7.

Dynamic light scattering (DLS)

One of the most commonly used techniques to determine particle size (hydrodynamic radius or diameter) on the nanometer scale is dynamic light scattering spectroscopy. This is a relatively fast method that does not require complex sample preparation. The only important aspect of the sample is low particle concentration[193]. When a beam of monochromatic light encounters macromolecules in solution, the light is scattered in all directions, depending on the size and shape of the molecules. This scattering intensity is measured by a detector and a digital autocorrelator is used to determine how quickly the intensity of the light scattering fluctuates[194]. Since the intensity fluctuations occur due to the Brownian motion of macromolecules in solution, analyzing the obtained data allows us to determine the diffusion coefficient, which is related to the hydrodynamic size of the molecule[195]. Using this method, not only the particle size is estimated in the case of a homogeneous population, but also their polydispersity, which is presented as a standard deviation[194]. When analyzing proteins, this method is often used to evaluate the degree of protein oligomerization and aggregation. However, when using this method for particle size determination, it is necessary to take into account experimental conditions, such as temperature or solvent viscosity, as these parameters can affect the movement of molecules and the determined size. This method was used in publication 4.

RESULT OVERVIEW

Publication 1

Lysozyme Amyloid Fibril Structural Variability Dependence on Initial Protein Folding State

Aim of the study – to determine the influence of temperature and lysozyme folding state on the polymorphism of its amyloid fibrils.

Results – according to the lysozyme melting point in the presence of 2M GuHCl (PBS pH 7.4), 4 temperature values were selected for further studies - when most of the protein molecules were either mostly folded or unfolded (50°C, 65°C) and intermediate temperatures (55°C, 60°C) with mixtures of both protein forms.

When analyzing the kinetic parameters of lysozyme aggregation, it was observed that with an increase in temperature, the lag times became shorter and the apparent rate constants - higher. The lag time dependence on temperature had a point of discontinuity at 57°C, corresponding to the melting temperature of lysozyme in the presence of the denaturant. For the apparent rate constant, this point appeared slightly below the lysozyme melting temperature - 55°C.

To determine the structural variability of the resulting fibrils, EEMs were scanned and analyzed. This study showed that at temperatures lower than the protein melting temperature, the maximum ThT intensity excitation and emission positions were similar and concentrated in one region. However, at higher temperatures, a significantly larger scatter of positions was observed with an additional cluster appearance under 65°C conditions.

FTIR spectra of the samples were also determined. When the majority of lysozyme was in its folded state, the sample FTIR spectra were very similar. However, higher temperatures resulted in the appearance of different shape FTIR spectra and higher structural variability. In total, 3 types of aggregates were identified, where lower temperature assemblies had the highest relative amount of beta-sheet structures. AFM analysis revealed that Type 1 fibrils were long and not prone to self-association, Type 2 were predominantly short and assembled into networks, Type 3 were mostly short aggregates, which formed large amorphous clusters.

Conclusions – lysozyme unfolding promotes greater variability of fibril secondary structures, which are characterized by different morphologies.

Publication 2

Investigating lysozyme amyloid fibril formation and structural variability dependence on its initial folding state under different pH conditions

Aim of the study – to determine the influence of solution pH and the initial lysozyme folding state on the aggregation process and variability of the resulting fibrils.

Results – during the previous study, it was observed that temperature and the folding state of lysozyme alter its aggregation process. Since pH can also influence the protein's stability, the aggregation of lysozyme was investigated under a range of different pH conditions (2.0-7.0). Similar to the previous study, a thermal stability assay was employed to determine the melting point of lysozyme under each condition. Lysozyme aggregation was then carried out under each pH using temperatures that cause the initial protein to be either in its folded or unfolded state.

To assess the influence of these factors on the aggregation process, kinetic parameters such as lag time and apparent rate constant were first determined. In all cases, the change in temperature (and, accordingly, initial protein folding state) had a statistically significant influence on both kinetic parameters. However, the effect of protein folding state on lag time depended on the solution pH value, while its influence on the apparent rate constant remained similar under the entire pH range.

Next, to assess the influence of these two factors on the structural parameters of the formed fibrils, the sample FTIR spectra were scanned and analyzed. The results showed that FTIR spectra variability depended on both temperature and pH. The spectra became more diverse when lysozyme aggregated at temperatures above its melting point and at fringe pH values (2.0 and 7.0). When analyzing the FTIR spectra of the samples, 6 different fibril types were identified, and their distribution depended on both pH and the initial protein state. Based on AFM analysis of the samples, apart from the amorphous aggregates, the morphologies of fibrils from all samples were similar. However, the different aggregate types possessed distinct stabilities against denaturation, as well as ThT-binding properties.

Conclusions – the kinetics of lysozyme aggregation and the structural variability of the resulting fibrils depend on the solution pH, as well as the temperature and initial folding state of the protein. The lowest structural variability was observed at pH 5 and pH 6, with the formation of one type of aggregate structure, regardless of protein folding.

Publication 3

Rapid restructurization of conformationally-distinct alpha-synuclein amyloid fibrils at an elevated temperature

Aim of the study – to determine whether pre-formed alpha-synuclein fibrils remain structurally stable when incubated at a higher temperature than they were formed.

Results – to assess elevated temperature effect on fibrils, 96 samples of alpha-synuclein were aggregated and analyzed. For initial strain separation, sample excitation-emission matrix maximum intensity positions were used. 8 samples with different EEM positions were isolated, reseeded and analyzed using FTIR spectroscopy. Based on the obtained FTIR spectra, 4 types of fibrils were identified, which were further used to study the effect of elevated temperatures. For this, fibril samples with distinct secondary structures were kept at room temperature (control) or 60°C for 24/48 h.

When analyzing the changes in FTIR spectra, it was observed that all four fibril samples were altered by incubation at an elevated temperature. After incubation, all four sample spectra overlapped perfectly, indicating that a single fibril type was stabilized. To clarify whether these spectral changes were related to alpha-synuclein restructurization or other potential factors (fibril lateral association, formation of amorphous structures), the incubated samples were reseeded at their initial preparation temperature. This analysis revealed that the incubated fibril secondary structure remained stable during reseeding and the replicated aggregates did not return to their original conformation.

Finally, UV/Vis spectra showed no significant absorbance changes during incubation, indicating that alpha-synuclein restructurization did not affect the number of bound ThT molecules. However, there was a notable change in the sample EEM maximum positions, which varied mostly during the first 4 hours and then gradually moved to a similar point. These results indicated that alpha-synuclein fibril restructurization at elevated temperatures likely occurs over a short period of time.

Conclusions – restructurization of alpha-synuclein fibrils at elevated temperatures is a rapid process that results in changes to the fibril secondary structure by stabilizing a single secondary structure. However, this process does not have a notable effect on the morphology or ThT-binding capacity of the aggregates.

Publication 4

Study of Insulin Aggregation and Fibril Structure under Different Environmental Conditions

Aim of the study – to determine the influence of solution components, pH and ionic strength on insulin aggregation and the resulting fibril structure.

Results – different pH and ionic strength reaction solutions were prepared by using sodium phosphate, acetic acid or hydrochloric acid as the main solution component. Then, insulin was dissolved in this range of distinct reaction mixtures and its aggregation kinetics were monitored. The majority of kinetic curves pertained standard nucleation, exponential growth and plateau phases. In some cases, however, either double-sigmoidal or curves with a slowly increasing intensity after the exponential phase were observed.

In the case of the sodium phosphate solution, all ionic strength conditions resulted in a similar dependence of lag time on solution pH. Lower pH conditions led to short lag times and higher pH conditions resulted in significantly longer lag phases, especially under higher ionic strength conditions. Under Ac conditions, increasing ionic strength led to substantial reductions in the lag phase. Oppositely, ionic strength had almost no effect on insulin aggregation under HCl conditions. The aggregation reaction apparent rate constants did not follow a clear trend under most of the tested conditions.

The resulting samples were then analyzed using FTIR spectroscopy. In the case of phosphate solution, three types of secondary structures were identified. Acetic acid conditions resulted in two additional secondary structures. One of them formed in the lower ionic strength condition, while the other was present in higher NaCl concentration solutions. Interestingly, the HCl reaction solutions promoted the formation of the same three types of insulin fibrils, which were detected in the phosphate buffered solution. The different secondary structure samples were further analyzed using AFM. In the case of phosphate solution, three types of fibril distributions were observed – 1) networks of long intertwined, 2) laterally associated or 3) few visible individual short fibrils. For acetic acid aggregates, their length and cross-interactions depended on the NaCl concentration. In the case of HCl, the formed fibrils had similar morphological tendencies to those in phosphate solutions.

Conclusions – insulin aggregation is highly sensitive to a range of environmental factors. Insulin aggregation under phosphate and HCl solution conditions resulted in fibrils with similar secondary structure and morphology, while Ac conditions resulted in distinct type of aggregates.

Publication 5

Imidazo[2,1-b][1,3]tiazine derivatives as potential modulators of alpha-synuclein amyloid aggregation

Aim of the study – to determine the potential of imidazothiazine derivatives in modulating alpha-synuclein aggregation.

Results – for this, 21 small molecule compounds were chosen. When analyzing how they influence the relative aggregation half-time, it was observed that many of the chosen compounds (10 out of 21) had no effect on this parameter when compared to the control samples. However, the effect of 11 compounds was statistically significant in altering the aggregation kinetics of alpha-synuclein. Most of them (10) were characterized by an aggregation inhibition effect, with some resulting in a 3 times higher aggregation half-time value. In addition to neutral and aggregation-inhibiting compounds, an aggregation-promoting effect was also observed in one case.

To assess the effect of these compounds on fibril structural characteristics, multiple technical repeat samples for each condition were examined using FTIR spectroscopy. In total, 7 distinct types of spectra were identified among all the samples. The control repeats were characterized by 3 different spectra. The greatest variability of structures was observed in the case of compound 5d, where 5 different types of spectra were identified. The least variation of structures was noticed in the cases of compounds 2c, 2e and 2j, where only one FTIR spectra type was observed. Interestingly, there also appeared to be a correlation between the inhibitory effect of the compounds and the resulting fibril type. It was observed that in the case of aggregation-inhibiting compounds, the variability of fibril structures decreased.

In addition to changes in secondary structures, morphological differences between fibril types were also analysed using TEM. In the case of fibril types I, II, III and VI, a clear aggregate tendency to associate into large clusters was observed. In addition to large clusters, short fibrils were also visible in the type II samples. For type VII, small amounts of short fibrils were observed, but a considerable number of small amorphous aggregates and oligomeric derivatives were also detected.

Conclusions – small molecular weight imidazothiazine derivatives possess the ability to inhibit alpha-synuclein amyloid aggregation and also redirect the reaction, resulting in fibrils with distinct secondary structures and morphologies.

Publication 6

Superoxide dismutase-1 alters the rate of prion protein fragment 89-230 aggregation and resulting fibril formation

Aim of the study – to determine whether superoxide dismutase-1 alters the aggregation process of prion protein, as well as the variability of the resulting aggregates.

Results – to assess how native superoxide dismutase-1 can affect prion protein aggregation when they are present together in solution, experimental conditions were selected which promote PrP fibril formation. When analyzing the kinetic parameters of this process, it was detected that higher SOD1 concentrations resulted in longer lag times and lower apparent rate constants of prion protein aggregation. In addition, it was observed that higher SOD1 concentrations yielded samples with lower bound-ThT fluorescence intensities, which indicates the possibility of different aggregate type formation.

Because of this it was important to determine the possible influence of the interaction not only on the kinetic parameters, but also on the structural properties of the resulting aggregates. The resulting prion protein aggregate samples were analyzed using FTIR spectroscopy. Based on the FTIR spectra, it was possible to identify four groups of aggregates, characterized by a different distribution of secondary structure elements. It was observed that when prion proteins were aggregated in the absence of SOD1, three types of spectra were detected. When 25 μM SOD1 was present in the reaction solution, a different variety of FTIR spectra were observed. Interestingly, at even higher concentrations of SOD1, the variability of structures disappeared, and all spectra could be attributed to one group. This type of aggregate was observed under all conditions, however, under lower SOD1 concentrations it comprised only a small fraction of samples.

Morphological analysis of the samples using AFM revealed that all types of aggregates had a tendency to assemble into large clusters, however, the fibrils differed from each other in their morphological parameters, such as cross-sectional height and width.

Conclusions – superoxide dismutase-1 not only inhibits the processes of prion protein nucleation but also affects the conformation of the resulting aggregates in a concentration-dependent manner, leading to the formation of a single type of aggregates.

Publication 7

S100A9 inhibits and redirects prion protein 89-230 fragment amyloid aggregation

Aim of the study – to determine the influence of the pro-inflammatory S100A9 protein on the aggregation of a mouse prion protein.

Results – to assess the influence of S100A9 on the aggregation of mouse prion protein, it was first necessary to select suitable experimental conditions. An environment was required, which would facilitate rapid prion protein aggregation, slow down S100A9 aggregation and maintain the stability of preformed S100A9 fibrils. During the optimization procedure, it was determined that the prion protein aggregated sufficiently quickly in the presence of 1.4 M – 3.0 M GuHCl. The S100A9 fibrils remained stable up to 1.5 M GuHCl and S100A9 aggregated slower under 1.5 M GuHCl conditions. Therefore, this concentration of denaturant was chosen for all further assays.

Prion protein aggregation was analyzed in the presence of different concentrations (0-50 μM) of non-aggregated S100A9 or its pre-formed fibrils. In the case of non-aggregated S100A9, the lag time of PrP aggregation increased as a function of S100A9 concentration. Conversely, S100A9 fibrils had no significant effect on the lag phase. When the experiment was repeated with the addition of preformed PrP fibrils (seeded aggregation), both forms of S100A9 inhibited their growth

The influence of S100A9 on the secondary structure of prion protein aggregates was analyzed using FTIR spectroscopy. FTIR spectra showed that low concentrations of S100A9 (both non-aggregated and fibrils) did not radically change the structure of PrP fibrils and only caused a slight shift in the main peak position. However, the influence of 50 μM of both S100A9 forms was much greater, promoting the formation of a different type of PrP fibrils. A similar effect was observed during the seeded aggregation experiment, suggesting that the presence of any form of S100A9 can stabilize a certain PrP fibril type.

Conclusions – both fibrillar and non-aggregated forms of S100A9 affect the aggregation process of the prion protein fragment by altering the resulting fibril secondary structure and stabilizing a specific aggregate type. In addition, non-aggregated S100A9 inhibits PrP nucleation.

DISCUSSION

Role of temperature and protein folding state in amyloid aggregation

During *in vitro* aggregation studies, temperature is often changed to accelerate the fibril formation process, which typically occurs very slowly under physiological conditions. However, such alterations in conditions are often made without considering their implication on the reaction mechanism. In some cases, even small differences in temperature can result in significant deviations of aggregation kinetics and fibril types[196,197].

The first aspect of temperature that we must consider is the change in the protein's folding state. The initial folding state can significantly affect the aggregation kinetic parameters, both in spontaneous and seeded reactions. It was observed in this work when studying lysozyme aggregation at four different temperatures, which pertained distinct protein folding state equilibria. During our study with lysozyme, it was observed that the unfolding of protein molecules promoted the formation of amyloid nuclei, as well as the apparent rate constant. Similar results were observed in a study by Andlinger et al., with human myeloma antibody light chain aggregation at elevated temperatures. During that research, it was observed that protein unfolding accelerates the aggregation process, and both unfolding and aggregation processes are strongly kinetically coupled[198]. Additionally, Simmons et al. showed that full unfolding (encompassing both head and tail regions) drastically increased the growth rate of myofibrillar protein aggregates[199]. It is not surprising that increasing the temperature affects the kinetic parameters of aggregation, because in many cases this is exactly what is sought. However, usually the factor that is not considered is whether such temperature alterations will also affect the structure of the resulting fibrils.

When studying the dependence of lysozyme aggregation on the protein folding equilibrium, a shift in the structure of aggregates was observed. Analysis of the results showed that the fibril-like structure, which formed at lower temperatures, contained more beta-sheets than the aggregate strains generated under higher temperature conditions. Similarly, the work by Cao et al. demonstrated the importance of lysozyme's folding state in dictating the structure of fibrils formed during aggregation. The authors demonstrated that complete or partial protein unfolding can lead to the formation of two distinct fibril types (reversible/irreversible), characterized by differing proportions of parallel and anti-parallel beta sheets[200]. However, the aggregate types in our research were not strictly confined to specific conditions, as certain structural variants formed at more than one temperature. Interestingly, there were also distinct fibril types observed among technical repeats of the same temperature

conditions, which displayed different FTIR spectra peak maxima positions. Previous reports have shown a similar phenomenon when analyzing prion protein aggregation, suggesting that such structural variability under identical conditions may be a generic trait of amyloid aggregates[89]. These results show that when lysozyme is folded, it forms one dominant fibril strain, alongside a small amount of other structures, while protein unfolding can lead to significantly greater structural variability and up to 3 different fibril strains.

In previous studies, it was observed that the binding mode of thioflavin-T and its fluorescence quantum yield may depend on the structural parameters of amyloid aggregates[187]. Such effect was also detected in the case of lysozyme. Since the structure of the formed aggregates depended on the initial protein folding state, the low temperature condition aggregates possessed a 10-fold larger bound-ThT fluorescence intensity when compared to their higher temperature counterparts. In addition, the fluorescence maximum positions of excitation emission matrices were also different. This lower fluorescence intensity could be due to the reduced amount of beta sheets in higher temperature condition fibrils, which was determined during analysis of FTIR spectra. However, the change in fluorescence intensity is not always directly related to the beta-sheet content of the fibril structure. An example of such a phenomenon was presented by Cao et al., where analysis of ThT binding sites revealed that distinct strains of alpha-synuclein fibrils exhibited varying ThT fluorescence intensities, despite having similar β-sheet content[200]. This difference in our study could also be explained by the formation of a large amount of other non-amyloid structures in the samples, observed in AFM images. This may be attributed to ThT's specificity for amyloid aggregates, with its interaction with globular proteins or amorphous aggregates often considered negligible compared to its affinity for amyloid fibrils[201].

Finally, the initial protein folding state also affected the self-replication of the aggregates. In the case of lysozyme, it was observed that the low-temperature strain was able to successfully replicate its structure and form long fibrils even under elevated temperatures. However, a different picture was observed in the case of high-temperature strains. These aggregates were able to successfully replicate themselves under the initial fibril formation conditions, but not when in the presence of fully folded lysozyme at lower temperatures. This effect could be explained by fibril ends ability to bind only partially or fully unfolded protein molecules. Previously presented studies also have shown that higher temperatures and protein unfolding promote the elongation process[166,202]. The previously mentioned high content of non-amyloid structures in the lysozyme samples may also have contributed to the poor level of self-replication. This is supported by previously presented evidence that amorphous aggregates represent an end-state, incapable of self-replication[203].

As previously noted, conformational dynamics play an important role in the aggregation process of lysozyme, as well as other amyloidogenic proteins. Therefore, it is very important to determine the relationship between the protein folding state and the structure and morphology of the resulting fibrils. It can significantly change not only the aggregation kinetics, but also the variability of the resulting structures, dye binding and self-replication properties.

These results showed that temperature variations at the beginning and during aggregation can affect the equilibrium of the protein state and thus alter the entire process. However, this parameter is also very important for already formed structures. Previous reports have shown that reduced environmental temperature can destabilize the formed amorphous aggregates or fibrils[204,205]. On the contrary, high temperature can, in some cases, affect the maturation of fibrils. Under physiological conditions this process is very slow and, in some cases, can take several days or even months[206]. Studies by Bocharova et al. indicate that high temperatures can induce a rearrangement of prion protein fibrils, leading to their annealing and the formation of a larger, proteinase K-resistant core[207].

In this work, the maturation phenomenon was studied using four structurally distinct alpha-synuclein fibril samples. When the temperature was raised to 60°C, the restructurization of different alpha-synuclein strains occurred quickly, with significant shifts in the secondary structure being detected within 24 hours. Based on changes in ThT intensity and EEM maximum fluorescence positions as a criterion for structural transition, the majority of restructurization occurred within the first 4 hours of incubation. Interestingly, all four different types of fibrils rearranged into one common strain during incubation. These fibrils were able to replicate their structure at 37°C after incubation at a higher temperature, as were the initial aggregate samples. Analysis of the sample CD spectra over time showed that the amount of beta-sheets did not significantly increase, but the existing structural elements rearranged. This could be explained by the possible metastability of fibrils formed at 37°C. The existence of these strains at lower temperatures is facilitated only by the high energy barrier that must be overcome for the aggregates to transition into a more stable form. Another study investigated the metastability of hen egg white lysozyme's oligomeric form through variations in salt and protein concentrations. The authors elucidated the mechanisms of two types of amyloid fibril formation and demonstrated how alterations in these conditions can drive the oligomer's transition to a more stable state [208]. This hypothesis is also supported by the fact that in our research the FTIR spectra of the aggregates incubated and those initially produced at 60°C were similar. These results further confirm that the effect of temperature

is very important not only for the initial aggregation reaction, but also for the stability of preformed aggregates.

pH and folding state correlation

Protein stability is a pH-dependent parameter, and these macromolecules are often very sensitive to even small changes in pH. This parameter affects the net charge of the protein, which can, in turn, influence further fibril formation [209]. For this reason, it was important to assess how this parameter can influence their amyloid aggregation. When lysozyme was in its folded state, all tested pH conditions yielded highly stochastic lag time values. In its unfolded state, amyloid aggregation proceeded with significantly shorter lag phases (approximately 3 – 4 times lower average lag times) except for pH 3. Under this specific condition, both the lag time values, as well as the relative difference between folded and unfolded reaction lag time values were considerably higher. Interestingly, the ratio of apparent rate constants remained similar under all pH conditions, which shows that pH 3 has a significant impact on the initial protein misfolding and nucleation, but not on the elongation of fibrils. This effect could be explained by lysozyme's deviation from the two-state model under these specific conditions[210]. Empirical application of this model showed that the difference between T_m and T_{onset} (temperature at which protein begins to aggregate) is larger precisely under acidic conditions (pH 2 and 3) compared to others. In addition, this means that our choice of using 5°C above or below the melting temperature for this study may lead to a different distribution of folded/unfolded lysozyme equilibrium between neutral and acidic environments. However, this did not explain why the lag time ratio was only high in the case of pH 3.0 and not pH 2.0. Further analysis of the samples revealed that under pH 3.0, there was a large concentration difference of aggregated lysozyme between lower and higher temperature conditions. This suggested that the observed phenomenon at pH 3.0 may be related to not just differences between T_m and T_{onset}, but also the condition-specific equilibrium between native and aggregated states of the protein.

The combination of pH and temperature can affect not only the aggregation kinetics, but also the structure and morphology of the resulting fibrils. During this study with lysozyme, a large variability of structures was found depending on the solution's pH, as well as its folding state. The influence of pH on fibril polymorphism extends to other proteins as well. For instance, alterations in the solution's pH within the physiological range of 5.8–7.4 were found to induce distinct fibril structures and varying levels of structural heterogeneity in alpha-synuclein[211]. A similar case has also been described for the amyloid-beta core fragment, where changes in pH and temperature affect peptide oligomerization and the structure and morphology of the ultimately formed

fibrils [212]. Although the morphological parameters in our work did not differ significantly in most cases, one aggregate sample type was characterized by short fibrils and a large amount of amorphous assemblies. This type was specific to only pH 7.0 conditions and only above the protein's melting temperature. These specific conditions were also where the highest variability of FTIR spectra was detected among all samples, likely owing to the presence of the amorphous structures. These results are also consistent with our previous observations, where lysozyme aggregation in PBS at pH 7.4 and above the melting temperature resulted in assemblies with a lower amount of beta-sheets.

Regardless of pH and temperature, one type of lysozyme aggregates appeared to be dominant among all conditions. At pH 5 and pH 6, this strain was the only one which formed, regardless of the protein's folding state. It was characterized by the highest relative stability under denaturing conditions and had only one type of beta-sheet hydrogen bonds in its structure. Similar results were observed in study by Ziaunys et al. on alpha-synuclein, where fibril variability depended on the ionic strength of the solution and protein concentration. During that study, it was observed that under certain conditions, one fibril strain was stabilized[137]. Taking all these observations into consideration, the acidic pH or pH 7.4 conditions, which are most often used in lysozyme aggregation studies, are characterized by high structural variability of aggregates and may lead to false conclusions. In contrast, pH 6 conditions offered the lowest stochasticity in both kinetic, as well as structural data and resulted in a single, highly stable strain of fibrils.

Insulin aggregation dependence on reaction conditions

Often, during insulin aggregation studies, the reaction is carried out under acidic conditions, while disregarding the exact pH or ionic strength of the solution. In many cases, reaction mechanisms or potential anti-amyloid compounds are screened and directly compared between research groups without accounting for the aforementioned parameters. Previously discussed studies show that these environmental factors can have a huge impact on the protein aggregation process, affecting not only kinetic parameters, but also the structure or other properties of the resulting fibrils[154,213]. Therefore, it was important to carefully analyze how each combination of conditions affect the insulin aggregation process. To achieve it, in this work insulin amyloid formation was examined using a range of pH values (1.0 – 3.0), different ionic strength solutions (100 mM – 500 mM), as well as three solution components (acetic acid, hydrochloric acid and sodium phosphate).

First of all, before analyzing the condition influence on the insulin aggregation process, it was important to evaluate how reaction solution variations affected

the oligomeric state of the protein. Previously published studies have shown that this protein is able to exist in various oligomeric forms depending on the solution's pH and ionic strength [214]. In this work, the influence of ionic strength on the oligomeric state followed a similar trend between all tested conditions, regardless of pH or chemical components present in the reaction solution. Another important aspect was the chemical components in the reaction solution. In the case of hydrochloric acid, insulin hydrodynamic diameter differed between all ionic strength conditions, while in acetic acid the same ionic strength values resulted in very small hydrodynamic diameter variations. In a previous study of lysozyme aggregation by Zazeri et al., which analyzed the effect of high concentrations of organic solvents on aggregation mechanism, a possible role for the oligomerization process was also observed[215].

Next, insulin aggregation was carried out under all of the aforementioned conditions to evaluate their influence on the amyloid formation kinetics. At low pH conditions in sodium phosphate solutions, the reaction kinetic parameters were similar among all ionic strength conditions. However, the highest tested pH conditions (2.5 – 3.0) resulted in a drastic increase in the process lag time. Such results may be related to the previously discussed insulin oligomeric state and solubility. Under these conditions, the solubility of insulin was low, and the determined hydrodynamic diameter was large, which could explain the slow nucleation process. However, in the case of hydrochloric acid, the highest ionic strength conditions yielded a comparatively high insulin hydrodynamic diameter, while no pronounced effect on the lag time was observed. This may indicate that the oligomeric state of insulin is only one component in determining its amyloid aggregation propensity. The influence of the oligomeric state is also supported by previous studies. It has been observed that in some cases, the dissociation of an amyloidogenic precursor from an oligomeric state is the rate-limiting reaction and occurs slower than nucleation[216].

During this examination, a peculiar phenomenon was observed. Under certain conditions, depending on the pH or ionic strength, the change in bound-ThT signal intensity did not follow the usual sigmoid-shaped kinetics. Instead, either double-sigmoidal kinetics or an endlessly increasing fluorescence intensity was detected. When analyzing the obtained results, it was identified that these curves only appeared under a few specific conditions. In cases of low pH, constantly increasing fluorescence curves were observed more often, while double sigmoidal ones were found under intermediate pH and low ionic strength conditions. The double sigmoidal kinetics were previously described in literature as the result of ThT positive intermediates, while the constantly

increasing fluorescence may be related to fibril maturation or cluster formation[71,206,217].

While it was possible to detect certain trends when analyzing the kinetic data under various conditions, matters were far more complicated when comparing the aggregate secondary structures. A large level of FTIR spectra variability was observed among all conditions and there was no clear condition-dependent trend. In contrast, when analyzing the morphology of the aggregates, certain condition-dependent trends could be seen. Under low pH and ionic strength, long, intertwined structures of relatively low cross-sectional height were detected with AFM. Higher ionic strength and pH favored the formation of short fibrils and many amorphous aggregates. Acetic acid conditions at high NaCl concentrations produced the largest structures, which consisted of many long filaments connected laterally. The size of all these fibril structures was also directly related to their stability under denaturing conditions. The same effect of ionic strength on the lateral association of insulin fibrils in acetic acid was also observed in another study, where this effect was believed to arise from the oligomeric state of insulin[218].

Alpha-synuclein aggregation inhibition by imidazothiazine derivatives

Currently, scientists are still facing many challenges in finding drugs to treat various neurodegenerative disorders associated with amyloid protein aggregation. Often, the goal is to synthesize a small molecule compound that could cross the blood-brain barrier and stop the protein aggregation process. Despite a number of compounds often showing inhibitory potential in the initial stages of screening for aggregation inhibitors, only a few are approved in the later phases. Therefore, it is important to determine what causes these failures. When analyzing insulin aggregation under the conditions of different chemical compounds, it was observed that this factor changes not only the kinetic parameters of aggregation, but also determines the differences in the secondary structure and morphology of the resulting fibrils. For this reason, the next goal was to find out whether potentially inhibitory small molecule compounds can change the alpha-synuclein aggregation process.

When analyzing the aggregation inhibition-compound structure relationship, it was observed that the thiazine ring played the most important role in this process. Compounds lacking this structural element did not alter either the aggregation half-time or the fluorescence intensity endpoint compared to controls. In addition to their inhibitory efficacy, in most cases alpha-synuclein samples exhibited increased fluorescence intensity, although the compounds themselves did not fluoresce in this excitation-emission region. This effect could be explained in two ways – either the compound shifted the equilibrium

between aggregated and native alpha-synuclein in the direction of fibril formation, or aggregates with different ThT binding modes were formed during aggregation[134,137,219]. Previous studies have shown that inhibitors can alter the alpha-synuclein aggregation process by forming different types of fibrils[138].

This possibility was further confirmed by analyzing the FTIR spectra of the formed aggregates. In the case of control samples, three types of spectra were distinguished. Such polymorphism of alpha-synuclein aggregates was previously observed under similar conditions by Toleikis et al[220]. In our work, when alpha-synuclein was aggregated together with imidazothiazine derivatives, four additional FTIR spectra were determined. Interestingly, in the cases of compounds that increased the aggregation half-time and/or fluorescence intensity, aggregates with four types FTIR spectra uncharacteristic of the control samples were most often formed. Such results demonstrate a possible correlation between the compound inhibitory efficiency, the type of formed secondary structures and the ThT binding properties.

Although these compounds exhibit strong anti-amyloid activity, it is important to consider their cytotoxicity. In the MTT assay, it was observed that all selected compounds statistically significantly reduced the viability of SH-SY5Y neuroblastoma cells in the absence of Asyn fibrils. However, when analyzing cell viability in the presence of the compound in the sample together with alpha-synuclein fibrils, it was observed that in some cases the toxicity to the cells was reduced. Such results indicate a possible dual benefit - the compound inhibits alpha-synuclein aggregation and at the same time reduces the harmful effects of the formed fibrils. Similar results were observed in the study by Seidler et al. When tau protein fibrils were incubated with the small molecule compound EGCG, their cytotoxicity was reduced compared to control[221]. However, the results of our study highlight that when developing new potential anti-amyloid compounds, it is crucial to consider not only how they inhibit protein amyloid aggregation, but also how they affect the aggregation mechanism, and potentially impact cells *in vivo*.

Protein-protein cross-interaction

Amyloid protein aggregation under physiological conditions occurs in an environment full of various macromolecules, including other proteins. Often, mechanistic *in vitro* aggregation studies are performed using only one type of amyloid protein and do not consider how other molecules could affect this process. Previous reports have shown that multiple distinct amyloidogenic proteins can be found within amyloid plaques, as well as affect each other's

aggregation kinetics[163,222]. This makes it important to further study how protein-protein interactions can influence the amyloid fibril formation process.

First, these interactions can affect the kinetics of aggregation. This was also observed in this work. When prion proteins were aggregated in the presence of SOD1, the nucleation process was inhibited and the reaction lag time increased. A similar effect was previously observed *in vivo* - when SOD1 deficiency accelerated prion protein aggregation[223]. The effect on the kinetics of PrP aggregation was also dependent on the concentration of SOD1. It was determined that at equimolar concentrations, only the lag time was increased, but higher concentrations of this protein also lowered the stochasticity of the results and reduced the apparent rate constant. These differences could be explained by the possible interaction of SOD1 with prion proteins during the nucleation phase, which affects the secondary structure and morphology of the formed fibrils. However, this effect is not characteristic of all protein cross-interactions. In another study by Honda et al., it was observed that the peptide amyloid-beta accelerates the amyloid aggregation of prion proteins at submicromolar concentrations. This accelerating effect of amyloid-beta was also seen in its interactions with lysozyme and insulin[163].

In this work we also observed the same impact on the nucleation process, when the interaction between prion proteins and S100A9 was analyzed. The native form of S100A9 was capable of inhibiting prion protein nucleation, while its aggregated form had no notable effect on this process. These results support the hypothesis that other amyloidogenic proteins can disrupt the PrP nucleation process by interacting with its monomeric or prefibrillar forms. On the other hand, S100A9 fibrils were able to enhance the apparent rate constant of prion protein aggregation. This is likely due to the hydrophobic surface of S100A9 fibrils, which act as a catalyst for surface-mediated secondary nucleation[224]. Interestingly, the self-replication of prion protein fibrils also depended on whether S100A9 was involved in the preparation of the initial PrP samples or only during reseeding. This shows that this cross-interaction promotes the formation of only certain PrP nuclei, which can replicate efficiently only in the presence of the S100A9 protein.

Since it is known that S100A9 can spontaneously aggregate under physiological conditions, it is possible that the aggregation of this protein is at least partially associated with the development of prion diseases[225,226]. These two proteins are found together in the cerebral cortex and cerebrospinal fluid, which makes it possible that S100A9 has a two-fold effect, based on its own state[225–227]. The native form of S100A9 inhibits the formation of prion protein nuclei, while its aggregated state serves as a surface for prion protein nucleation.

Another important aspect of cross-interaction is the effect on the fibril structure. Since the participation of another protein in its native or aggregated form strongly affects the aggregation mechanism, it usually also leads to a structural change of the resulting fibrils. In this study of PrP and SOD1 cross-interaction, an impact on the variability of PrP amyloid structures was detected. When SOD1 was not involved in the reaction, FTIR analysis revealed that the prion protein formed three different types of fibrils. In the case of an equimolar SOD1 concentration, the distribution of aggregates changed and a new conformation appeared. When the concentration of SOD1 was further increased, the conformational variability disappeared and most of the FTIR spectra were identical. A similar cross-interaction effect on the stabilization of one type of aggregate was also observed in a study by Toleikis et al. when analyzing the interaction of S100A9 with alpha-synuclein[220].

If we assume that the strain of PrP fibrils depends on the conformation of the initial nuclei, this would mean that the process of the nuclei formation is directly affected due to the possible interaction of these two proteins. It is probable that SOD1 disrupts the formation of certain PrP nuclei formation, thereby shifting the reaction towards a specific PrP conformation. This process may also be associated with a delayed lag phase, where SOD1 merely prolongs the time for nucleation of any conformation, thus creating an opportunity for strains that require a longer time period to form and become the dominant type. Interestingly, identical concentrations of SOD1 and S100A9 did not promote the formation of the same strain of PrP fibrils according to FTIR analysis. This suggests that the presence of different proteins can have distinct effects on the amyloid aggregation process, similar to other environmental factors. Such results confirm that when conducting protein aggregation studies, it is very important to consider other macromolecule participation in this reaction in order to get as close as possible to the processes occurring under physiological conditions.

CONCLUSIONS

1. Lysozyme unfolding accelerates both the nucleation and apparent rate constant of aggregation. Below its melting temperature, lysozyme forms beta-sheet rich fibrils prone to lateral association.
2. The structural variability of lysozyme aggregates is dependent on both pH and the dominant protein folding states during aggregation. The lowest variability was observed under pH 5 and 6 conditions, regardless of the protein's folding state.
3. Incubation of structurally diverse alpha-synuclein aggregates at elevated temperatures leads to a strain restructurization process, resulting in an identical secondary structure.
4. Insulin aggregation exhibits peculiar trends influenced by pH, ionic strength, and the solution's main chemical component, with kinetics sometimes displaying irregular shapes (double sigmoid, no-plateau) and both secondary structure and morphology being highly environment-dependent.
5. Imidazothiazine derivatives influence both the aggregation half-time and the structural variability of formed aggregates. Notably, a correlation was identified between a compound's inhibitory effect and the type of fibrils formed.
6. Protein-protein cross-interaction, specifically with SOD1 or S100A9, can inhibit prion protein nucleation, though S100A9 fibrils can also serve as a surface for prion protein surface-initiated nucleation. In both cases, cross-interaction stabilized a single aggregate strain.

Taken together, these studies of various environmental factors on different amyloidogenic proteins highlight the complex nature of their condition-structure relationship.

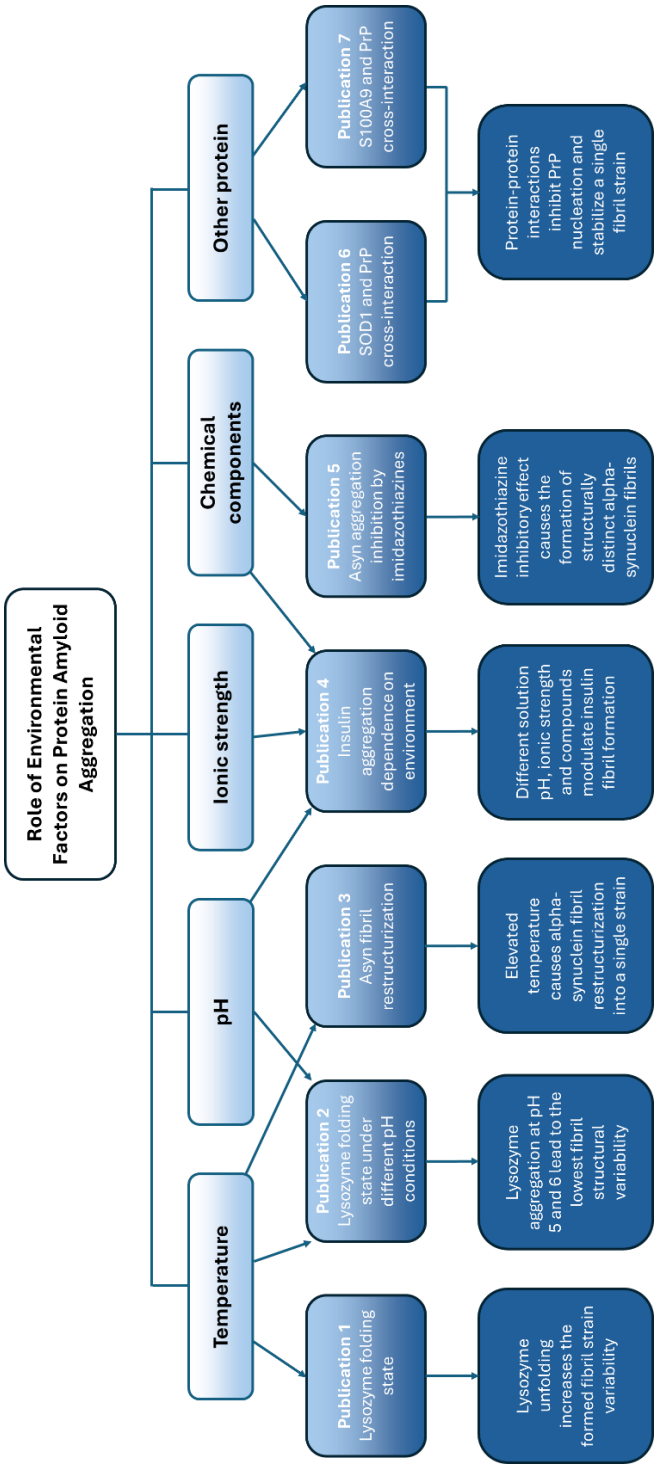

Figure 14. A diagram summarizing the results of the thesis and the main findings.

ĮVADAS

Pirmieji amiloidozių, kurias sukelia baltymų agregacija, atvejai buvo pastebėti dar XVII amžiuje. Šiuo metu baltymų agregacija amiloidinių fibrilių forma yra siejama su įvairiais neurodegeneraciniais sutrikimais, tokiais kaip Alzheimerio, Parkinsono ar prioninės ligos.

Amiloidogeniniai baltymai ir peptidai tarpusavyje skiriasi tiek dydžiu, tiek aminorūgščių sekomis, tačiau visi jie pasižymi polinkiu tam tikromis sąlygomis pakeisti savo konformaciją ir sudaryti amiloidines fibriles. Šių struktūrinių pokyčių metu žymiai padidėja beta-klosčių kiekis. Tokiu būdu susidariusios fibrilės yra netirpios ir dalinai atsparios proteazėms. Nepaisant ilgalaikių ir intensyvių tyrimų šioje srityje, yra atrasti tik keli ligą-modifikuojantys vaistai ar gydymo būdai. Šiuo metu vis dar išlieka daug neatsakytų klausimų apie patį baltymų agregacijos mechanizmą ligų atvejais ir kokie faktoriai gali paveikti šį procesą. Dėl šios priežasties baltymų agregacijos tyrimai yra plačiai atliekami visame pasaulyje. Vis dėlto atliekant tų pačių baltymų agregacijos *in vitro* tyrimus yra pasirenkama plati eksperimentinių sąlygų įvairovė, kuri neretai skiriasi tarp amiloidus tiriančių laboratorijų.

Vienas įdomiausių aspektų, būdingų amiloidinei agregacijai, yra polimorfizmas. Tyrimai rodo, kad tas pats baltymas gali sudaryti struktūriškai ar morfologiškai skirtingas amiloidines fibriles, kurios taip pat gali skirtis savo savireplikacijos greičiais, stabilumu, fluorescencinių dažų ar kitų mažamolekulinių junginių afiniškumu, bei toksiškumu ląstelėms. Būtent šis susidariusių agregatų variabilumas gali priklausyti nuo įvairių aplinkos faktorių, tokių kaip tirpalo pH, joninė jėga ir pan. Tačiau ankstesnių tyrimų rezultatai rodo, kad kai kurie baltymai geba suformuoti skirtingų konformacijų agregatus net ir identiškomis sąlygomis. Toks fibrilių variabilumas yra būdingas ne tik baltymų agregacijai *in vitro*, tačiau yra pastebimas ir ligų atvejais, kuomet skirtingų tipų agregatai sukelia skirtingą ligos fenotipą.

Todėl šiame darbe buvo siekiama nustatyti kaip įvairių amilodogeninių baltymų agregacijos procesą (kinetikos, susidarančių agregatų struktūros ir morfologijos, parametrus) gali paveikti dažniausiai tyrimuose *in vitro* kintantys aplinkos faktoriai ir identifikuoti sąlygų-agregatų struktūros priklausomybę.

Tikslas

Nustatyti įvairių aplinkos faktorių įtaką baltymų agregacijos procesui.

Uždaviniai

1. Nustatyti pradinės baltymo susilankstymo būsenos įtaką lizocimo agregacijos procesui.
2. Identifikuoti įvairių tirpalo sąlygų poveikį insulino agregacijai.
3. Įvertinti mažamolekulinių junginių efektą alfa-sinukleino agregacijai.
4. Įvertinti baltymo-baltymo sąveikos įtaką prioninio baltymo agregacijai sąveikaujant su S100A9 ir superoksido dismutaze-1.

GINAMIEJI TEIGINIAI

1. Lizocimo amiloidinę agregaciją veikia pradinė baltymo susilankstymo būsena. Baltymo išsilankstymas skatina susidariusių fibrilių struktūrinį variabilumą.
2. Padidėjusi aplinkos temperatūra sukelia alfa-sinukleino fibrilių restruktūrizaciją į vieną konformaciją.
3. Insulino amiloidinė agregacija yra labai jautri tirpalo komponentams, pH ir joninei jėgai. Insulino agregacija fosfato ir HCl tirpalo sąlygomis lemia to paties tipo fibrilių susidarymą, o acto rūgšties sąlygos skatina skirtingų agregatų izoformų stabilizavimą.
4. Alfa-sinukleino amiloidinę agregaciją moduliuoja imidazotiazino dariniai, kurie slopina reakciją ir skatina skirtingos fibrilių izoformos susidarymą.
5. Tarpusavio sąveika su S100A9 ir superoksido dismutaze-1 moduliuoja prioninio baltymo amiloidinę agregaciją, slopindama kinetiką ir mažindama susidariusių fibrilių struktūrinį polimorfizmą.

LITERATŪROS APŽVALGA

Amiloidų istorija

Amiloidinių baltymų ir jų sukeliamų ligų atradimo istorija siekia net XVII amžių. Manoma, kad pirmasis šaltinis, kuriame buvo aprašyti amiloidozių atvejai, buvo gydytojo ir dramaturgo N. Fonteyn 1639 metais išleista knyga. Joje autorius aprašė autopsijos atvejus, kurių metu organuose aptiko neįprastų sankaupų[1,2]. Vis dėlto pats terminas „amiloidas“ buvo sukurtas tik 1838 metais vokiečių botaniko M. Schleiden, kai šis pastebėjo augalo ląstelėse esančias krakmolo sankaupas[3]. Būtent dėl šios priežasties „amiloidas“ reiškia „panašus į krakmolą“ ir jis sudarytas iš lotynų „amylum“ ir graikų „amylon“ kalbų žodžių[4,5]. Visgi žmogaus atveju amiloido terminas buvo pavartotas tik 1854 metais vokiečių patologo Rudolf Virchow. Šis skrodimo metu organuose aptiko baltymų sankaupas, kurios nusidažė jodu ir klaidingai palaikė jas krakmolu[4]. Praėjus vos 5 metams Friedreich ir Kekule įrodė, kad šios sankaupos skyrėsi nuo krakmolo ar celiuliozės ir buvo panašios į baltymus[6].

Nepaisant ankstesnių amiloidų aprašymo atvejų, pirmoji išsamiai aprašyta amiloidozė yra Scrapie liga[7,8]. Šios ligos pavadinimas kilo nuo žodžio kasytis (angl. scrape), nes Anglijoje kilus ligos proveržiui tarp avių, pirmiausia buvo pastebėtas neįprastas jų elgesys[7]. Šios ligos sukelėjas nebuvo nustatytas iki pat 1967 metų, kol Griffith iškėlė hipotezę, kad tai gali būti baltymas[9,10]. Iki tol buvo manoma, kad šią amiloidozę sukelia parazitai, bakterijos ar virusai[9,11]. Vis dėlto tik praėjus 15 metų po „tik baltymo“ (angl. „protein only“) hipotezės paskelbimo, Prusiner kartu su kolegomis įrodė, kad iš infekuoto žiurkėno smegenų yra išskirtos būtent baltyminės kilmės agregatų sankaupos, kurias vėliau pavadino prionais[9,12].

Po to kai buvo pastebėta, jog agregatų sankaupos gali būti nudažomos jodu kaip ir krakmolas, toliau buvo siekiama rasti alternatyvius analizės metodus[4]. 1922 metais Bennhold pastebėjo, kad amiloidai taip pat gali jungti ir Kongo raudonąjį dažą. Ilgą laiką būtent šis dažas buvo naudojamas diagnozuoti amiloidozes[13]. Kadangi skirtingi amiloidai sugebėjo jungti tuos pačius dažus, buvo manoma, kad jie gali pasižymėti struktūriniais panašumais. Šią hipotezę 1959 metais, naudojant elektroninę mikroskopiją, patvirtino Cohen ir Calkins. Jie pastebėjo, kad agregatų mėginiai išgauti iš įvairių audinių ar organų yra sudaryti iš filamentų ar fibrilių[15]. Praėjus beveik 10 metų tyrėjai naudodami rentgeno spindulių difrakciją išanalizavo agregatų antrinę struktūrą ir pastebėjo, kad skirtingoms amiloidinėms fibrilėms yra būdingi kryžminių beta-klosčių struktūros elementai[16]. 1982 metais Prusiner su kolegomis taip pat pastebėjo, kad amiloidiniai agregatai pasižymi atsparumu proteazėms[21].

Pastaraisiais metais amiloidogeniniai baltymai ir jų agregacijos procesas susilaukė daug mokslininkų dėmesio. 2006 metais paruošta Chiti ir Dobson apžvalga parodė, kad skirtingų amiloidinių baltymų agregacijos procesai pasižymi bendru mechanizmu[22]. Praėjus trims metams po šių mokslininkų įžvalgų, 2009 metais Knowles su kolegomis pasiūlė teorinį šio proceso apibūdinimą, kuris susideda iš nukleacijos, elongacijos ir antrinės nukleacijos/fragmentacijos etapų[23]. Dar vienas svarbus įvykis buvo 2010 metais, kuomet amiloidinių fibrilių aukštos rezoliucijos struktūros nustatymui buvo panaudota kriogeninė elektronų mikroskopija, kuri suteikė naudingų įžvalgų apie fibrilių struktūrinius skirtumus[24,25]. Be viso to 2018 metais buvo pastebėta, kad kai kurie su amiloidozėmis siejami baltymai yra linkę sudaryti baltyminius lašelius skysčio-skysčio fazių atsiskyrimo metu ir šis procesas gali būti susijęs su jų agregacija[28].

Nepaisant to, kad iki šiol buvo nustatyta daug įvairių faktorių, kurie skatina agregacijos procesą, būdų kaip identifikuoti agregatus, tačiau efektyvių vaistų ar gydymo būdų rasta vos keli. Vis dėlto nors daugeliui junginių vis dar nepavyksta pereiti visų klinikinių tyrimų etapų, 2019 metais JAV maisto ir vaistų administracija patvirtinto vaistą „Tafamidis“, skirtą gydyti su transtiretinu susijusias kardiomiopatijas, bei 2021 metais „Aducanumab“ – monokloninį antikūną, skirtą Alzheimerio ligos gydymui[30–32]. Mažamolekulinis junginys „Tafamidis“ veikia kaip transtiretino stabilizatorius. Jis sąveikauja su transtiretino tetramero T4 jungimosi vieta, taip stabdydamas tetramero disociaciją ir tokiu būdu užkirsdamas kelią tolimesniam agregacijos procesui[33]. Priešingai nei anksčiau minėto vaisto, monokloninio antikūno „Aducanumab“ taikinys yra amiloido-beta agreguota forma[34]. Vis dėlto pastarojo gamyba buvo sustabdyta 2024 metais dėl sukeliamų šalutinių efektų.

Amiloidinės ligos

Amiloidozės yra ligų grupė, kurią sukelia baltymų konformaciniai pokyčiai ir tolimesnis agregacijos procesas. Jo metu susidaro netirpūs fibriliniai agregatai, kurie kaupiasi ir pažeidžia ląsteles, dėl ko galiausiai sutrinka įvairių organų veikla[41]. Amiloidozės yra klasifikuojamos pagal kelis aspektus. Vienas iš jų yra agregatų kaupimosi vieta. Pagal šį bruožą amiloidozės gali būti lokalizuotos (agregatai kaupiasi tik viename organe arba kūno vietoje) arba sisteminės (išplitę keliuose organuose arba audiniuose)[42]. Dar vienas skirstymo būdas yra pagal ligos atsiradimo principą. Šios ligos gali būti sporadinės (atsirandančios dėl atsitiktinių genų mutacijų ar kitų nežinomų faktorių), įgyjamos (išsivysto dėl užsikrėtimo per užterštus paviršius, kraujo perpylimą, organų transplantaciją) ar paveldimos (genų mutacijos, nulėmusios ligos atsiradimą, yra perduodamos tolimesnėms kartoms)[42]. Galiausiai amiloidozes taip pat galima klasifikuoti pagal baltymą, kurio agregacija

inicijuoja ligos vystymąsi[41]. Nepaisant šių faktorių vienos amiloidozės yra greitai progresuojančios ir sukelia mirtinas pasekmes (Creutzfield-Jacob liga), kitos pasireiškia tik vėlyvame amžiuje (Alzheimerio liga)[43]. Taip pat pasitaiko ir tokių sutrikimų, kurie nesukelia jokių mirtinų pasekmių ir su jomis žmonės gali išgyventi daug metų (lokali injekcinė amiloidozė)[44]. Šiuo metu 42 skirtingi amiloidogeniniai baltymai yra siejami su įvairiomis žmonių ligomis.

Agregacijos mechanizmas

Kad baltymas funkcionuotų tinkamai, dauguma susintetintų polipeptidinių grandinių turi įgyti tam tikrą natyvią struktūrą. Pats susilankstymas yra sudėtingas, stochastiškas procesas, kurio metu susidaro tam tikros tarpinės formos, mažiau stabilios nei galutinė natyvi forma[46]. Vis dėlto kai kuriais atvejais baltymai susilanksto neteisingai, pradeda asocijuoti ir galiausiai sudaro amiloidines fibriles, kurios yra stabilesnės už baltymo natyvią formą. Baltymų amiloidinė agregacija yra nuo nukleacijos priklausoma polimerizacijos reakcija. Šis procesas susideda iš kelių etapų, įskaitant nukleaciją, elongaciją ir antrines reakcijas (1 pav.).

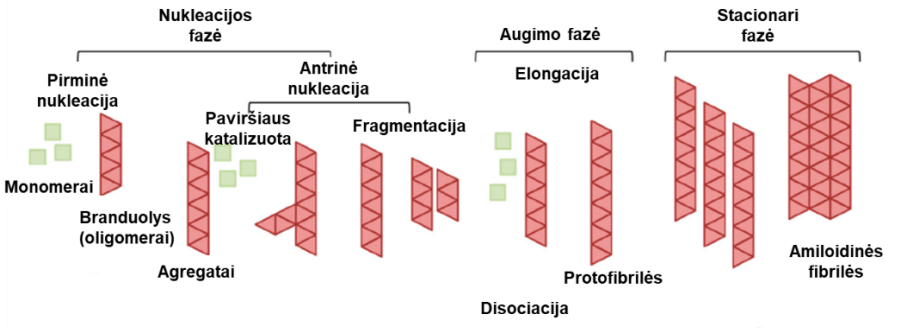

1 pav. Amiloidinių fibrilių susidarymo mechanizmo schema[48].

Spontaninės agregacijos atveju reakcija prasideda nuo pirminės nukleacijos, dar vadinamos branduolių susidarymo arba lag faze[47]. Jos metu vyksta natyvaus monomerinio baltymo konformaciniai pokyčiai, susidaro oligomerinis branduolys, prie kurio toliau jungiasi monomerai. Būtent šis etapas yra visos reakcijos greitį limituojanti stadija, nes baltymo konformaciniai struktūros pokyčiai yra nepalanki reakcija[50]. Vis dėlto susidaręs agregacijos branduolys yra pakankamai stabilus, kad baltymas nesugrįžtų į savo natyvią konformaciją. Šiuos baltymo struktūrinius pokyčius gali inicijuoti atsitiktinės mutacijos, post-transliacinės modifikacijos, ląstelinis stresas ar baltymų kokybės kontrolės disfunkcija[51,52]. Taip pat siekiant pagreitinti procesą *in vitro* baltymas destabilizuojamas, padidinant temperatūrą, pakeičiant tirpalo pH ar panaudojant denatūrantus[53]. Pagreitinti branduolių susidarymą galima ir paskatinant baltymo molekulių sąveikas

(padidinant baltymo koncentraciją), pakeičiant tirpalo joninę jėgą ar panaudojant mėginių maišymą[53]. Pradinis agregacijos branduolys įprastai veikia kaip šablonas, kuris nulemia susidarančių fibrilių struktūrą. Vis dėlto pasitaiko ir tokių atvejų, kai tas pats baltymas skirtingomis ar net identiškomis sąlygomis gali sudaryti kelias skirtingas agregatų struktūras (fibrilių kamienus). Šis reiškinys yra vadinamas polimorfizmu[55].

Kai susidaro stabilus kritinio dydžio agregacijos branduolys, toliau seka elongacijos fazė. Jos metu monomerinės baltymo molekulės jungiasi prie susidariusių branduolių, taip inicijuojant molekulių restruktūrizaciją ir įgyjant branduolio izoformą[66]. Fibrilių kamienai geba save replikuoti, išlaikant fizikines, struktūrines savybes ir perduodant šią „konformacinę atmintį“ prisijungiančiam monomerui[57]. Nepaisant to, kad šis etapas vyksta žymiai greičiau nei pirmoji branduolių susidarymo stadija, jį galima dar pagreitinti. Tai yra pasiekiama padidinant molekulių sąveikų skaičių arba skatinant monomerinio baltymo išsilankstymą[53].

Vis dėlto elongacijos etapo metu vyksta ne tik monomerinio baltymo jungimasis prie fibrilių galų, bet ir antriniai procesai – fibrilių fragmentacija ir paviršiaus inicijuota agregacija[47]. Reakcijos metu kai susidarančios fibrilės pasiekia kritinį ilgį, jos linkusios skilti, tokiu būdu atsiranda daugiau galų, prie kurių gali prisijungti ir pakeisti konformaciją naujos monomerinės molekulės[12]. Šis procesas žymiai padidina agregacijos greitį. Dar vienas antrinis procesas – paviršiaus inicijuota agregacija. Jos metu kitų fibrilių paviršius yra naudojamas kaip naujų agregacijos branduolių susidarymo katalizatorius[61]. Monomeriniai baltymai jungiasi prie hidrofobinio fibrilių paviršiaus, keičia savo konformaciją ir sudaro branduolį, kuris vėliau atskyla nuo agregaciją iniciavusios fibrilės ir veikia kaip papildomas agregacijos centras[62].

Agregacijos sekimas

Šiuo metu yra atrasti keli būdai sekti baltymų agregaciją *in vitro*. Pirmasis dažas, naudojamas sekti amiloidinių baltymų agregacijos procesą buvo Kongo raudonasis. Jį 1884 metais išrado vokiečių chemikas P. Bottiger[63]. O 1922 metais vokiečių gydytojas Bennhold pirmasis panaudojo Kongo raudonąjį diagnozuoti amiloidozes[13]. Šis dažas turi hidrofobinį centrą, kuris susideda iš dviejų fenilo žiedų, o molekulės galiniuose regionuose yra sulfono rūgšties ir amino grupės. Šiam dažui prisijungus prie amiloidinių agregatų yra stebimas sugerties piko poslinkis nuo 490 nm iki 512 nm, bei naujo piko atsiradimas 540 nm bangos ilgyje[65]. Be to poliarizuotoje šviesoje yra matomas agregatų optinės anizotropijos padidėjimas (angl. apple green birefringence)[66]. Vis dėlto šio dažo panaudojimas sumažėjo dėl savo nespecifiškumo, nes jis jungiasi ir prie kitų baltymų, tokių kaip kolagenas, elastinas[67].

Vienas dažniausiai agregacijai stebėti naudojamų junginių yra tioflavinas-T. Šis dažas yra gana specifiškas amiloidiniams agregatams ir manoma, kad su natyvios, dalinai ar pilnai išsilanksčiusios formos baltymais beveik nesąveikauja[69]. Šios molekulės panaudojimo galimybes, analizuojant susidarančius amiloidinius agregatus, 1959 metais pristatė Vassar ir Culling. Tioflavinas-T susideda iš dimetilinto benzotiazolo žiedo per bendrą jungtį sujungto su dimetilamino benzilo žiedu[70]. Vandeniniuose tirpaluose abu žiedai vienas kito atžvilgiu laisvai sukasi ir energija yra panaudojama būtent šiam procesui. Šis rotacinis judėjimas agregacijos metu yra imobilizuojamas susidarančių agregatų beta-klosčių grioveliuose. Tokiu būdu yra matomas fluorescencijos kvantinės išeigos padidėjimas[49]. Sekant spontaninės agregacijos procesą yra stebimas sigmoidės formos fluorescencijos intensyvumo pokytis nuo laiko (2 pav. raudona kreivė)[49]. Savireplikacijos metu, kuomet reakcijos mišinyje pridedama jau suformuotų agregatų, lag fazė yra žymiai sutrumpinama ir agregacija dažnai pasižymi fluorescencijos eksponentine kreivės forma (2 pav. mėlyna kreivė)[53].

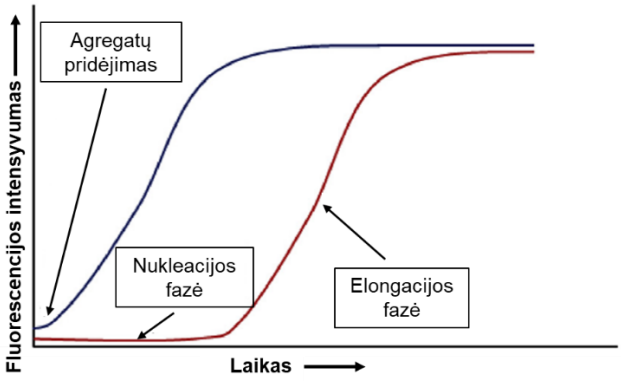

2 pav. Fluorescencijos priklausomybė nuo laiko spontaninės agregacijos (raudona kreivė) ir savireplikacijos (mėlyna kreivė) metu[50].

Fibrilių antrinė struktūra ir morfologija

Vienas pagrindinių ir pirminių amiloidinių fibrilių struktūrinių požymių yra dominuojanti beta-klosčių struktūra. Kadangi agregacijos metu keičiasi šių antrinės struktūros elementų kiekis, dažnai tyrimuose naudojami CD, FTIR ir Ramano spektroskopijos metodai[53]. Nors beta-klosčių struktūra yra būdinga skirtingų baltymų amiloidinėms fibrilėms, tačiau šių klosčių ilgis ir pasiskirstymas fibrilių struktūroje varijuoja, priklausomai nuo baltymo[48]. Beta-klostės gali sudaryti kelių tipų ketvirtines struktūras, kurios yra sutinkamos amiloidinėse fibrilėse.

Viena iš tokių struktūrų yra beta-sumuštinio (angl. beta-sandwich). Joje dvi beta-klostės išsidėsto atsisukus viena į kitą ir dažnai yra atskirtos kilpa[80]. Tyrimai rodo, kad yra galimas ir tolimesnis tokių struktūrų išsidėstymas, vadinamas superklostuota (angl. superpleated) beta-klosčių struktūra. Šiuo atveju kelios beta-klostės suformuoja struktūrą sulygiuotą viena kryptimi[81]. Dar viena beta-klosčių struktūra, randama amiloidinėse fibrilėse – beta-solenoidas. Šioje struktūroje polipeptidinė grandinė sudaro vieną fibrilės sluoksnį, apsisuka per kilpą ir toliau sudaro antrąjį[80]. Toks skirtingas antrinės struktūros motyvų pasiskirstymo variabilumas parodo dažnai pasitaikantį amiloidinių agregatų polimorfizmą[55].

Subrendusios fibrilės pasižymi periodiška struktūra, kuri priklauso nuo protofilamentų susisukimo tarpusavyje. Kadangi protofilamentai gali sudaryti skirtingas 3D struktūras, priklausomai kaip jie susirenka tarpusavyje, susidaro agregatai pasižymintys skirtinga morfologija (skirtingų fibrilių morfologijų pavyzdžiai pavaizduoti 3 pav.). Šie fibrilių kamienai gali būti skirstomi pagal fibrilės sukimosi laipsnį, jų diametrą, ar iš kiek protofilamentų yra sudaryta fibrilė[48,84]. Taip pat agregatai būna linkę asocijuoti lateraliai ar sudaryti didelius klasterius[53]. Dažniausiai siekiant išskirti morfologines izoformas yra panaudojamos atominės jėgos, kriogeninės-elektronų arba transmisijos elektronų mikroskopijos metodikos[85–87]. Agregatų polimorfizmas yra pastebimas ir neurodegeneracinių sutrikimų atvejais, kas gali paveikti ligų tipą ir progresiją[88]. Tyrimai *in vitro* rodo, kad amiloidinių agregatų, pasižyminčių skirtinga struktūra ar morfologija, susidarymas gali priklausyti ne tik nuo aplinkos faktorių, tačiau tam tikrais atvejais yra pastebimas net identiškomis sąlygomis[121].

3 pav. AJM paveikslai (A) ir atitinkami β-laktoglobulino fibrilių, pasižyminčių skirtingais periodiškumais, modeliai (B)[90].

Fibrilių stabilumas

Agregacijos tyrimuose dažnai siekiant paskatinti šį procesą yra naudojamos aplinkos sąlygos, kurios destabilizuoja baltymą. Todėl yra naudojama aukštesnė temperatūra, didelės druskų koncentracijos, denatūrantai ar keičiamas tirpalo pH. Taip pat šios sąlygos turi įtakos ir jau susidariusių

amiloidinių fibrilių stabilumui[91]. Tai yra dar viena savybė, kuri tyrimuose naudojama nustatyti skirtingų tipų agregatus. Fibrilių stabilumas dažnai priklauso nuo kelių struktūrinių parametrų. Vienas iš jų - kryžminis beta-klosčių struktūrinis motyvas, kuris priklausomai nuo sudarytų vandenilinių jungčių skaičiaus, yra vienas svarbiausių fibrilių struktūrą stabilizuojančių faktorių[92]. Jis taip pat yra atsakingas ir už fibrilių dalinį atsparumą proteazėms[18]. Kitas faktorius, kuris yra atsakingas už stabilumą, yra Van der Waals sąveikų skaičiaus padidėjimas, bei kontakto su tirpikliu sumažėjimas[93].

Nors ir agregatų stabilumo tyrimai *in vivo* nėra galimi, tačiau ši savybė suteikia daug įžvalgų apie organizme susidarančias fibriles. Atlikus iš sergančio žmogaus išskirtų agregatų stabilumo denatūruojančiomis sąlygomis tyrimą, buvo pastebėta, kad esama koreliacijos tarp fibrilių stabilumo ir prioninių ligų inkubacinių periodų trukmės[94]. Rezultatai parodė, kad prionai, kurie buvo aptinkami trumpo inkubacinio ligos periodo atveju, buvo mažiau stabilūs denatūruojančiomis sąlygomis[95].

Šiame darbe naudoti amiloidiniai baltymai

Insulinas

Insulinas yra hormonas, kuris organizme pagrinde yra atsakingas už cukraus kiekį kraujyje bei karbohidratų, baltymų, riebalų metabolizmo reguliavimą[97]. Šį hormoną į kraują sekretuoja kasos Langerhanso salelės beta-ląstelės. Insulinas susideda iš dviejų polipeptidinių grandinių, kurių antrinėje struktūroje, esant natyvios būsenos, dominuoja alfa-spiralės. Vieną grandinę sudaro 21 aminorūgštis, o antrąją – 30. Šios grandinės tarpusavyje yra sujungtos dviem disulfidiniais tilteliais, o kitas tiltelis jungia dvi aminorūgštis trumpojoje grandinėje[100]. 1921 metais mokslininkai iš Kanados – F. Banting, C. Best, J. Macleod, J. Collip sėkmingai išskyrė insuliną iš kraujo ir parodė jo funkciją organizme, o 1969 metais D. C. Hodgkin nustatė šio baltymo kristalinę struktūrą ir už tai vėliau buvo apdovanotas Nobelio premija chemijos srityje[98,101].

Vis dėlto tam tikromis sąlygomis šis globulinis baltymas yra linkęs keisti savo natyvią konformaciją ir sudaryti amiloidines fibriles. Jo agregacijos procesą analizuoti paskatino tai, kad I ir II tipo diabetu sergantiems žmonėms atliekant insulino injekcijas buvo pastebėta, kad aplink dūrio vietą susidaro netirpios agregatų sankaupos[102]. Šis sutrikimas buvo pavadintas neletalia lokalia injekcine amiloidoze[44]. 1940 metais Waugh pirmasis aprašė šio baltymo agregacijos etapus ir susidariusias amiloidines fibriles[103]. Nepaisant didelės aplinkos sąlygų įvairovės, naudojamos *in vitro* agregacijos tyrimuose, dažniausiai šio baltymo agregacija yra vykdoma žemame arba neutraliame pH, esant aukštesnei temperatūrai. Taip pat siekiant pagreitinti procesą dažnai

naudojamas purtymas[104]. Dėl sąlyginai žemos kainos ir paprasto agregacijos protokolo, šis baltymas yra dažnai naudojamas kaip modelis analizuojant fibrilių susidarymo procesą. Kadangi yra žinoma, kad insulino agregacijai būdingas susidariusių fibrilių polimorfizmas, o insulino agregacijos tyrimai dažniausiai yra atliekami žemame pH, naudojant skirtingus pagrindinius tirpalo komponentus, būtent šis baltymas buvo pasirinktas analizuoti trijų aplinkos faktorių - pH, joninės jėgos ir pagrindinio tirpalo cheminio komponento - kompleksinį poveikį agregacijos procesui (Publikacija 4).

Lizocimas

Lizocimas yra globulinis baltymas, organizme veikiantis kaip fermentas. 1922 metais A. Flemingas pirmasis iš žmogaus nosies gleivinės išskyrė šį baltymą, bei nustatė jo antibakterinę funkciją[105]. Šis baltymas yra randamas ne tik gleivinėje, bet ir seilėse, ašarose ar kraujo serume[105]. Lizocimas hidrolizuoja gram neigiamų bakterijų ląstelės sienelėje esančio peptidoglikano β-1,4 glikozidinį ryšį tarp N-acetilmuramo rūgšties ir N-acetilgliukozamino, tokiu būdu suardant sienelės integralumą[106]. Atliekant tyrimus buvo pastebėta, kad mutacija šį baltymą koduojančiame gene ir baltymo agregacija, sukelia paveldimą sisteminę lizocimo amiloidozę[107]. Progresuojant šiai ligai lizocimo agregatų sankaupos pažeidžia įvairius organus ir sukelia jų disfunkciją[108].

Vištos kiaušinio baltymo lizocimą, kuris buvo naudojamas šiame darbe, sudaro viena polipeptidinė grandinė, susidedanti iš 129 aminorūgščių[109]. Būtent šio baltymo kristalinė struktūra buvo nustatyta 1965 metais[106]. Lizocimas yra dalinamas į du domenus (alfa ir beta), kurie yra sujungti keturiais disulfidiniais tilteliais. Jie skiriasi savo antrine struktūra – alfa domeną sudaro keturios alfa-spiralės, o beta – antiparalelinės beta-klostės[110].

Kadangi vištos kiaušinio baltymo lizocimas yra žmogaus baltymo variantų, susijusių su amiloidozėmis ortologas, pasižymintis panašia seka, o jo gamyba sąlyginai pigi, jis yra naudojamas agregacijos tyrimams *in vitro*. Tyrimai rodo, kad šis baltymas yra linkęs lengvai sudaryti fibriles esant žemam pH ar aukštesnei temperatūrai[106,110]. Taip pat siekiant paskatinti agregacijos procesą yra naudojami denatūrantai (pvz. guanidino hidrochloridas) arba organiniai tirpikliai (pvz. etanolis), bei intensyvus mėginių purtymas[111]. Kadangi yra žinoma, kad lizocimo agregacijai yra būdingas susidariusių fibrilių polimorfizmas, o natyvaus baltymo lydymosi temperatūra labai priklauso nuo tirpalo pH, lizocimas šiame darbe buvo pasirinktas analizuoti pradinės baltymo susilankstymo būsenos, esant skirtingiems tirpalo pH, įtaką susidariusių agregatų struktūriniam ir morfologiniam kintamumui (Publikacija 1 ir 2).

Prioniniai baltymai

Ląsteliniai prioniniai baltymai yra membranos glikoproteinai, kurie prisijungia prie lipidinio bisluoksnio naudojant glikozilfosfatidilinozitolio inkarą[112]. Prioniniai baltymai po transliacijos yra modifikuojami, pašalinimos signalinės sekos, prikabinamas GPI inkaras, sudaromi disulfidiniai tilteliai ar glikozilinamas N- galas[113]. Didžiausi kiekiai šio baltymo yra sintetinami būtent centrinėje nervų sistemoje, bet taip pat randami ir kituose organuose[114]. Manoma, kad natyvios formos prioniniai baltymai dalyvauja oksidacinio streso valdyme, signalinių kelių moduliavime, jonų jungimosi procesuose[115]. Žinduolių prioniniai baltymai yra sudaryti iš maždaug 250 aminorūgščių, kur C- ir N- gale yra signalinės sekos. Natyvios formos prioninis baltymas sudarytas iš dviejų regionų – N- galo nestruktūrizuotos srities ir C- galo globulinio domeno. N- galo regionas taip pat dalinamas į dvi hidrofilines sritis ir vieną pasikartojančio oktapeptido sritį[116–118].

Prioninio baltymo konformaciniai pokyčiai į infektyvią formą yra susiję su neurodegeneracinėmis ligomis, vadinamomis transmisinėmis spongiforminėmis encefalopatijomis. Tokių sutrikimų pavyzdžiai yra Creutzfield-Jacob liga, Gersmann-Straussler-Scheinker sindromas, fatalinė šeimyninė nemiga, Kuru liga[114]. *In vitro* tyrimuose paskatinti šio baltymo agregacijos procesą reikalingos didelės denatūranto koncentracijos, aukštesnė temperatūra, bei intensyvus mėginio maišymas[120]. Šis konformacinis variabilumas ir didelis baltymo jautrumas aplinkos veiksniams buvo pagrindinė priežastis, kodėl jis buvo pasirinktas baltymo-baltymo tarpusavio sąveikos tyrimams šiame darbe (Publikacija 6 ir 7).

Alfa-sinukleinas

Alfa-sinukleinas yra baltymas, sudarytas iš 140 aminorūgščių liekanų[57]. Jis priklauso sinukleino baltymų šeimai, kuri yra randama stuburiniuose gyvūnuose[128]. Pirmą kartą šį baltymą 1988 metais atrado prancūzų mokslininkas Maroteaux, kuris tyrė žuvų cholinerginių neuronų branduolius ir sinapsines pūsleles[57]. Būtent dėl savo buvimo vietos, šis baltymas įgavo savo pavadinimą - „syn“ – nuo žodžio sinapsė ir „nuclein“ – branduolys[129]. Vis dėlto daugiausiai mokslininkų dėmesio šis baltymas sulaukė, kai buvo pastebėta, kad jis yra pagrindinis Lewy kūnelių ir neuritų komponentas, kurie laikomi kaip Parkinsono ligos ar demencijos su Lewy kūneliais žymenimis[130].

Pagrinde Asyn yra sintetinamas smegenyse, tačiau mažesniais kiekiais galima aptikti ir kituose organuose[131]. N- baltymo gale yra konservatyvios aminorūgščių sekos pasikartojimai. Toliau seka hidrofobiškas centrinis domenas, kuris agregacijos metu metu linkęs sudaryti β-klostes. O baltymo lanksčiame C- gale dominuoja neigiamai įkrautos aminorūgščių liekanos, bei prolinas[132]. Nors tiksli alfa-sinukleino fiziologinė funkcija nėra aiški,

manoma, kad jis yra atsakingas už sinapsinių pūslelių judėjimą sinapsiniame plyšyje[134,135].

Alfa-sinukleinas fiziologiniame pH yra nestruktūrizuotos formos, tačiau inkubuojant šį baltymą ilgesnį laiką, jis linkęs agreguoti amiloidinių fibrilių forma[136]. Tyrimai rodo, kad alfa-sinukleinas linkęs sudaryti struktūriškai skirtingus fibrilių kamienus, kurių formavimasis priklauso nuo eksperimentinių sąlygų ar reakcijoje naudojamų papildomų molekulių[137,138]. Be to taip buvo pastebėta, kad šis baltymas geba sudaryti struktūriškai skirtingas amiloidines fibriles net identiškomis sąlygomis[128]. Dėl šios priežasties šiame darbe buvo pasirinktas alfa-sinukleinas, siekiant ištirti, kaip susidarančių fibrilių struktūros yra paveikiamos aplinkos sąlygų pokyčių arba reakcijoje dalyvaujančių potencialių inhibitorių molekulių (Publikacija 3 ir 5).

S100A9

S100 baltymai yra kalcį surišančių baltymų šeima, randama tik žinduolių organizmuose[139]. 1965 metais B. W. Moore pirmasis išgrynino S100 baltymą iš jaučio smegenų. Jis būtent ir suteikė šiai šeimai S100 pavadinimą, nes šis baltymas neutraliame pH buvo tirpus 100% sočiame amonio sulfato tirpale[140]. Šiuo metu yra nustatyti 25 S100 baltymų šeimos nariai[141]. Jie dalyvauja įvairiuose tarpląsteliniuose ir viduląsteliniuose reguliaciniuose procesuose, kaip apoptozė, diferenciacija, proliferacija, kalcio homeostazė ir pan[140]. Vienas iš labiausiai ištirtų šios šeimos narių, S100A9, yra prouždegiminis baltymas, taip pat žinomas kaip kalgranulinas B arba su migraciją slopinančiu faktoriumi susijęs baltymas 14 (MRP-14). Šis baltymas daugiausia gaminamas neutrofiluose, bet mažesniais kiekiais – neuronuose ir mikroglijose[142]. Antrinei S100A9 struktūrai būdingas ilgas nestruktūrizuotas C- galas ir keturios alfa spiralės, kurios sudaro du spiralės-kilpos-spiralės motyvus, taip pat žinomus kaip EF-rankos. Šių motyvų galai yra asocijuoti su hidrofobiniais baltymo regionais, o prie pačių EF-rankų jungiasi du kalcio jonai[143]. Būtent prisijungus juos, yra inicijuojami konformaciniai pokyčiai, kai tirpalui atidengiami baltymo hidrofobiniai regionai ir taip palengvinama organizme S100A9 sąveika su kitais baltymais[139]. *In vivo* S100A9 dažniausiai randamas heterodimero pavidalu su S100A8 (kalgranulinas A arba MRP-8). Nors šių baltymų homodimerai taip pat randami mažesniais kiekiais, jie yra mažiau stabilūs nei heterodimerai[72].

In vitro S100A9 linkęs lengvai agreguoti, taip prarandant signalinę funkciją bei tampant citotoksišku[142]. Taip pat tyrimai rodo, kad būtent sąveikaujant su kitais baltymais S100A9 reguliuoja jų polinkį agreguoti[144,145]. Šis baltymas geba sudaryti amiloidines fibriles fiziologinėmis sąlygomis, reakcijoje nedalyvaujant kalcio jonams[142]. Dėl šios priežasties S100A9 buvo pasirinktas

tirti jo tarpusavio sąveiką su anksčiau minėtu prioninio baltymo fragmentu (Publikacija 7).

Superoksido dismutazė-1 (SOD1)

Superoksido dismutazė-1 (SOD1) yra labai konservatyvus metalofermentas, randamas mitochondrijų citozolyje, išorinėje membranoje ir tarpmembraninėje erdvėje[146]. Šis baltymas dalyvauja nukenksminant superoksido radikalus, kuriuos mitochondrijos išskiria kaip šalutinius redokso reakcijos produktus. Juos fermentas paverčia vandenilio peroksidu ir deguonimi. Tai yra viena pagrindinių šio baltymo funkcijų organizme[147]. Be viso to manoma, kad SOD1 veikia kaip RNR jungiantis baltymas arba transkripcijos faktorių aktyvatorius[148]. SOD1 yra 32 kDa homodimerinis baltymas, sintetinamas įvairiuose žinduolių audiniuose. Didžiausias SOD1 kiekis randamas centrinėje nervų sistemoje ir kepenyse[146]. Abu šio baltymo monomerai turi po vieną cinko ir vieną vario joną, taip pat tarpmolekulinę disulfidinę jungtį, kuri stabilizuoja homodimero struktūrą, o subvienetus laiko vandeniliniai ryšiai ir hidrofobinė sąveika[147].

Neteisingas šio baltymo susilankstymas ir agregacija yra susiję su amiotrofinės lateralinės sklerozės (ALS) išsivystymu. ALS yra gyvybei pavojingas neurodegeneracinis sutrikimas, kurio metu žūsta motoriniai neuronai, o tai sukelia raumenų atrofiją, paralyžių ir galiausiai kvėpavimo sutrikimą[149]. Tyrimai rodo, kad ALS būdinga daugiau nei 200 skirtingų mutacijų, kurios destabilizuoja homodimerinę baltymo struktūrą ir taip skatina agregaciją[151]. Nepaisant mutacijų, SOD1 agregaciją galima paskatinti pašalinant baltymo struktūrą stabilizuojančius metalo jonus arba nutraukiant disulfidinį tiltelį[147]. Tyrimų su SOD1 metu buvo pastebėta, kad jis gali pakeisti kitų amiloidogeninių baltymų agregatų susidarymo procesą. Dėl šios priežasties, panašiai kaip ir S100A9, jis buvo pasirinktas tirti jo tarpusavio sąveiką su anksčiau minėtu prioninio baltymo fragmentu (Publikacija 6).

Aplinkos faktoriai

Temperatūra ir purtymas

Temperatūra yra vienas iš dažniausiai keičiamų faktorių atliekant baltymų agregacijos tyrimus. Temperatūros pakėlimas dažniausiai yra naudojamas siekiant pagreitinti šį procesą. Kinetikos atveju didesnė temperatūra pagreitina nukleacijos procesą (lag laikas sutrumpėja), nes aukštesnėje temperatūroje didesnė dalis baltymo molekulių yra dalinai arba pilnai išsilanksčiusios būsenos, kas paskatina konformacinius pokyčius ir agregacijos branduolių susidarymą[14]. Visgi kartais yra stebimas ir žemesnės temperatūros poveikis baltymams ir jų agregacijai, vadinamas šalčio denatūracija, kas taip pat paskatina nukleaciją[152].

Šis eksperimentinis faktorius taip pat paveikia ir kitą agregacijos etapą - elongacijos fazę. Aukštesnėje temperatūroje pagreitėja molekulių judėjimas, įvyksta daugiau molekulių susidūrimų tirpale ir hidrofobinių sąveikų, todėl reakcijos greitis padidėja[46]. Vis dėlto šis aplinkos veiksnys veikia ne tik pirminius, bet ir antrinius procesus kaip fragmentacija[60]. Be įtakos agregacijos kinetiniams parametrams, temperatūra gali paveikti ir susidarančių fibrilių struktūrą. Tyrimai rodo, kad aukštesnėje temperatūroje gali būti pastebimas didesnis susidariusių fibrilių struktūrų variabilumas[89]. Be to priklausomai nuo temperatūros, susidariusios fibrilės gali skirstis savo stabilumu, toksiškumu ląstelėms, savireplikacijos efektyvumu, morfologija ar protofilamentų skaičiumi[46].

Nors tyrimuose agregacijos procesui pagreitinti dažnai naudojama aukštesnė temperatūra, literatūroje dažniausiai aprašomi kinetikos pokyčiai (branduolių susidarymo laikas, greičio konstanta), nenurodant kaip dėl to keičiasi agregacijos mechanizmas. Tačiau svarbu suprasti, kaip subtilus pradinės baltymų susilankstymo pusiausvyros pokytis lemia vėlesnį fibrilių struktūrinį variabilumą. Šio parametro įtakos agregatų polimorfizmui nustatymas galėtų suteikti svarbių įžvalgų apie skirtingų ligų fenotipų atsiradimą (pvz., prionopatijų atveju), agregatų toksiškumo skirtumus ir jų plitimą ligos metu. Dėl šios priežasties dalis mano darbo buvo skirta nustatyti ryšį tarp pradinės baltymų susilankstymo būsenos reakcijos pradžioje ir susidariusių agregatų polimorfizmo. Ryšys tarp šių dviejų parametrų mano darbe buvo nustatytas atsižvelgiant į lizocimo lydymosi temperatūrą, kartu keičiant ir kitą aplinkos veiksnį – tirpalo pH (Publikacija 1 ir 2).

Kitas svarbus aspektas, apie kurį trūksta informacijos, yra temperatūros poveikis jau susiformavusiems agregatams. Tyrimuose dažnai nustatomi struktūriškai skirtingi agregatų kamienai, kurie lyginami ne tik pagal jų struktūrinius ir morfologinius parametrus, bet stabilumą denatūruojančiomis sąlygomis ar atsparumą proteazėms, tačiau temperatūros pokyčių poveikis struktūriniam fibrilių integralumui lieka nenustatytas. Nepaisant galimybių identifikuoti skirtingus kamienus, šioje srityje lieka daug neatsakytų klausimų, ypač susijusių su agregatų dinaminiu stabilumu. Dėl šios priežasties dalis šio darbo taip pat buvo skirta analizuoti, kaip inkubacija aukštesnėje temperatūroje veikia skirtingus alfa-sinukleino iš anksto suformuotus agregatų kamienus (Publikacija 3).

Dažnai pagreitinti ir paskatinti baltymų agregacijos procesą *in vitro* tyrimuose yra pasitelkiamas mėginių purtymas. Purtymo būdų, naudojamų agregacijos skatinimui yra bent keli – vartymas, purtymas, maišymas[14]. Agregaciją skatinantys veiksniai, atsirandantys dėl įvairių maišymo formų, yra šie: papildomos skysčio ir paviršiaus arba skysčio ir oro sąveikos (baltymų

neteisingas lankstymasis sandūroje), mėginių maišymas (didesnis molekulių susidūrimų dažnis)[46].

pH ir joninė jėga

Dar vienas faktorius, kuris kinta atliekant agregacijos tyrimus *in vitro* yra tirpalo pH. Pirmiausia, kalbant apie įtaką agregacijos kinetiniams parametrams, agregacijos procesas gali skatinamas arba lėtinamas[46]. Agregacija gali būti skatinama tokiais pH-pokyčių nulemtais faktoriais: baltymo krūvio pokyčiai (esant arčiau pI vertės, baltymai lengviau sąveikauja, pagreitinami nukleacijos ir elongacijos etapai), stabilumo sumažėjimas (nutraukiami vandeniliniai arba nekovalentiniai ryšiai, padidėja hidrofobinių regionų sąveika su tirpikliu, tokiu būdu paskatinami konformaciniai pasikeitimai)[14]. Tačiau agregacija taip pat gali būti slopinama pH labiau nukrypstant nuo baltymo pI, tokiu būdu didėjant baltymo paviršiaus krūviui. Šio krūvio padidėjimas lėtina agregacijos procesą (nukleaciją, elongaciją) dėl padidėjusios elektrostatinės stūmos tarp labiau įkrautų baltymų molekulių[153]. Be įtakos kinetiniams parametrams, pH gali paveikti ir susidarančių fibrilių struktūrą. Tyrimai rodo, kad kai kuriais atvejais tirpalo pH turi įtakos susidariusių fibrilių struktūriniam variabilumui[154]. Be to fibrilės susidariusios žemesniame pH kartais būna plonesnės, labiau fragmentuotos, pasižymi mažesniu stabilumu, nei susidariusios neutraliame[155].

Agregacijos tyrimuose tirpalo joninė jėga gali paveikti tarp baltymo molekulių vykstančias elektrostatines sąveikas, dėl to šis parametras taip pat yra svarbus analizuojant šį procesą. Pagrindinis faktorius nulemiantis agregacijos procesą keičiant tirpalo joninę jėgą yra baltymo paviršiaus krūvis[46]. Didesnė joninė jėga sumažina elektrostatinį atstūmimą tarp panašiai įkrautų baltymo molekulių, mažina baltymo stabilumą, bei padidina hidrofobines sąveikas, dėl ko agregacijos procesas yra pagreitinamas[14]. Vis dėlto anijonai ir katijonai paveikia baltymo agregaciją skirtingai. Būtent šis efektas labai priklauso nuo tirpalo pH[156]. Kaip ir anksčiau aptartu atveju joninė jėga gali paveikti ir susidarančių fibrilių struktūrinius ir morfologinius parametrus, joms yra būdingas variabilumas. Tyrimai rodo, kad kartais didesnės joninės jėgos atveju susidarančioms fibrilės yra labiau tiesios[157]. Taip pat joninė jėga gali turėti įtakos susidarančių fibrilių stabilumui, citotoksiškumui bei savireplikacijos savybėms[14].

pH ir joninės jėgos įtaka baltymų amiloidinei agregacijai yra išsamiai aprašyta. Literatūroje teigiama, kad šių dviejų aplinkos veiksnių poveikis labai priklauso vienas nuo kito. Tačiau pagrindinė tyrimų problema išlieka ta, kad šie parametrai paprastai vertinami atskirai, o jų bendras sinerginis poveikis nenustatomas. Dėl šios priežasties dalis mano darbo buvo skirta išanalizuoti, kaip nedideli pH, joninės jėgos ar tirpalo pagrindinio cheminio komponento

pokyčiai gali paveikti susidariusių insulino agregatų struktūrinį ir morfologinį variabilumą (Publikacija 4).

Kiti baltymai

Kiti baltymai – ar tai būtų specifiškai sąveikaujantys, šaperonai ar atsitiktiniai – gali smarkiai pakeisti baltymų agregacijos kinetiką. Vieni iš tokių baltymų – molekuliniai šaperonai, tokie kaip Hsp70, Hsp90, jungiasi prie neteisingai susilanksčiusių baltymų ar agreguoti linkusių regionų[158,159]. Sąveikaudami su amiloidiniais baltymais jie gali lėtinti nukleacijos arba elongacijos etapus arba juos visai sustabdyti. Šie baltymai veikia dažniausiai stabilizuodami monomerinį baltymą arba išardydami jau susidariusias oligomerines formas[160]. Taip pat kai kurie baltymai gali sąveikaudami tarpusavyje sulėtinti agregacijos procesą. Viena iš tokios sąveikos pavyzdžių yra tarp S100A9 ir alfa-sinukleino. Ankstesni tyrimai parodė, kad alfa-sinukleino agregacija yra lėtinama reakcijoje dalyvaujant S100A9 baltymui, kuris sąveikauja su pastarojo N- galu[144]. Taip pat buvo aprašyta ir sąveika tarp amilodo-beta ir alfa-sinukleino. Šiuo atveju tyrimai parodė, kad buvo paskatintas tirpių, bet toksiškų, daug beta-klosčių struktūroje turinčių hetero-oligomerų susidarymas, tačiau sulėtintas tolimesnis amiloido-beta fibrilizacijos procesas[161,162]. Vis dėlto kai kuriais atvejais kiti baltymai ar jų agregatai gali veikti kaip paviršius ir paskatinti paviršiaus inicijuotą nukleacijos procesą. Vienas iš tokių pavyzdžių yra tarp amiloido-beta ir prioninio baltymo. *In vitro* tyrimai parodė, kad amiloidas-beta paskatina prioninio baltymo agregaciją net esant mikromolinėms koncentracijoms[163]. Tokios sąveikos yra nustatomos ir *in vivo*. Tai buvo stebima amiloido-beta fibrilių atveju, kurios paskatino tau baltymo agregaciją *in vivo*[164]. Be to kiti baltymai kai kuriais atvejais gali veikti kaip molekuliniai reakcijos apkrovos (angl. crowding) agentai, dėl ko susidaro didelės koncentracijos baltyminiai lašeliai ir taip paskatinama agregacija[165]. Visos šios sąveikos gali paveikti ir susidarančių agregatų struktūrinius, morfologinius parametrus, tokiu būdu susidarant naujo tipo agregatams ar stabilizuojant tam tikrą kamieną.

Nors daugelyje tyrimų daugiausia dėmesio skiriama agregacijos kinetiką moduliuojančių molekulių nustatymui, tyrimai paprastai remiasi supaprastintu mechanizmu, ieškant junginių, kurie tik sulėtina agregacijos procesą (pvz., didina agregacijos puslaikį). Šis metodas neatsižvelgia į esminę agregacijos mechanizmo detalę – inhibitoriaus poveikį susidariusių agregatų struktūrinėms savybėms. Dėl šios priežasties didelė mano darbo dalis buvo skirta nustatyti, kaip mažamolekuliniai junginiai (imidaziotiazino dariniai) arba baltymai, dalyvaujantys reakcijoje, esant natyvios arba fibrilinės formos, gali paveikti ne tik agregacijos kinetiką, bet ir susidariusių fibrilių struktūrinius ar morfologinius parametrus, bei jų kamienų variabilumą (Publikacija 5, 6, 7).

METODŲ APŽVALGA

Baltymų gryninimas

Siekiant atlikti agregacijos tyrimus pirmiausia reikėjo išsigryninti įvairius rekombinantinius baltymus. Visi šiame darbe naudojami baltymai buvo įsigyti iš komercinių įmonių (žmogaus rekombinantinis insulinas, vištos kiaušinio baltymo lizocimas) arba susintetinti *E. coli* BL21 (DE3) ląstelėse (pelės prioninio baltymo fragmentas 89-230, žmogaus alfa-sinukleinas, žmogaus SOD1, žmogaus S100A9). Pirmiausia ląstelės buvo transformuojamos naudojant karščio šoką ir auginamos autoinduktyvioje ZYM 5052 arba LB terpėje, indukuojant sintezę su IPTG. Kadangi prioninis baltymas ir S100A9 turėjo histidino žymenį, jie buvo gryninami naudojant imobilizuotų nikelio jonų afininę chromatografiją ir atplaunami nuo sorbento, naudojant buferinius tirpalus su imidazolu[72,166]. Kiti baltymai (SOD1 ir alfa-sinukleinas) buvo gryninami naudojant jonų mainų chromatografiją[167,168]. Siekiant gauti mažiau priemaišų turintį baltymą, papildomai buvo naudojama gelfiltracijos chromatografija[167]. Baltymai (alfa-sinukleinas, SOD1) po gryninimo buvo liofilizuojami ir laikomi -20°C temperatūroje. Prieš naudojimą baltymų milteliai buvo tirpinami tyrimui reikalingame buferiniame tirpale. Kitais atvejais baltymai (MoPrP89-230, S100A9) buvo sukoncentruoti ir užšaldyti -20°C temperatūroje. Šis metodas buvo naudojamas visose į disertaciją įtrauktose publikacijose.

Fibrilių susidarymo skatinimas

Siekiant paskatinti baltymo agregaciją ir kad jis pakeistų savo konformaciją, pirmiausia reikia, kad baltymas būtų destabilizuojamas. Temperatūros pakėlimas atsižvelgiant į baltymo lydymosi temperatūrą sukelia jo dalinį arba pilną išsilankstymą[169,170]. Panašiai staigus pH pakeitimas, priklausomai nuo baltymo pI, pakeičia krūvių pasiskirstymą baltymo paviršiuje, dėl ko sutrinka elektrostatinės sąveikos[14]. Taip pat dažnai šiam procesui yra naudojami denatūrantai, tokie kaip guanidino hidrochloridas ar urėja. Be šių būdų, taip pat naudojamas oksidacinis stresas, didelės druskų koncentracijos ar metalo jonų sukeliama agregacija[171].

Visgi kiekvienam baltymui reikia optimizuoti agregacijos sąlygas. Tyrimai rodo, kad insulino atveju dažnai agregacija yra atliekama žemame pH[172]. Lizocimui ir prioniniams baltymams naudojamos daugiausiai arčiau neutralaus pH vertės, tačiau būtinos denatūruojančios sąlygos. Be to šiems baltymams greičiau agreguoti naudojama aukštesnė temperatūra[121,173]. Alfa-sinukleinas ir S100A9, priešingai nei anksčiau įvardinti baltymai, geba agreguoti spontaniškai be denatūrantų įsikišimo, neutraliame pH ir fiziologinėje temperatūroje[72,137]. Papildomai, kad paskatinti ir pagreitinti

agregacijos procesą, tam yra naudojamas purtymas, kuris suskaldo susidarančias fibriles, tokiu būdu atsirandant daugiau fibrilių galų monomerinio baltymo prisijungimui[14]. Šis metodas buvo naudojamas visose į disertaciją įtrauktose publikacijose.

Agregacijos sekimas

Dažniausiai agregacijai sekti yra naudojamas fluorescencinis dažas tioflavinas-T. Naudojamo dažo koncentracijos agregacijos tyrimuose varijuoja priklausomai nuo reakcijoje dalyvaujančio baltymo koncentracijos (10-100 μM). Vis dėlto šis dažas yra hidroksilinamas benzotiazolo žiede ilgesnį laiko tarpą inkubuojant jį neutraliame ar šarminiame pH ir aukštesnėje temperatūroje, tokiu būdu paveikiant jo sugertį ir emisiją[175]. Didžiausia ThT fluorescencija dažniausiai pasiekiama sužadinant 440 nm bangos ilgyje, o maksimali emisija matuojama 480 nm bangos ilgyje[70]. Agregacijos metu didėjant dažui specifiškų struktūrų kiekiui stebimas fluorescencijos intensyvumo pokytis. Šis metodas buvo naudojamas visose į disertaciją įtrauktose publikacijose.

Kitas dažas 1-anilinonaftalen-8-sulfonatas dažnai yra naudojamas ne tik sekti agregacijos procesą, bet atliekant baltymo lydymosi tyrimą. Ši molekulė sąveikauja su hidrofobinėmis baltymo sritimis, tokiu būdu atsirandant maksimalios sugerties piko pasislinkimui link mėlynosios šviesos ir fluorescencijos padidėjimui[176,177]. Be šių dažniausiai naudojamų molekulių agregacijos procesą galima stebėti ir sekant optinio tankio pokyčius[178]. Šis metodas buvo naudojamas 1, 2 ir 7 publikacijose.

Kinetikos duomenų analizė

Agregacija dažniausiai analizuojama lyginant pagrindinius tris faktorius – lag laiką, puslaikį, greičio konstantą. Norint nustatyti šiuos parametrus pirmiausia reikia atlikti duomenų apdorojimą ir gluodinimą. Spontaninės agregacijos atveju, kuriam yra būdingos sigmoidinės kreivės, duomenų gluodinimui yra naudojama Boltzmann sigmoidinė funkcija. Savireplikacijos kinetikos atveju, kuriai būdinga eksponentinė kreivė, yra naudojamas linijinis gluodinimas, išvedant liestinę tarp 40 ir 60% fluorescencijos intensyvumo taškų, prieš tai atlikus duomenų normalizavimą ir galiausiai yra nustatomas agregacijos puslaikis. Šis metodas buvo naudojamas visose į disertaciją įtrauktose publikacijose.

Furje-transformacijos infraraudonųjų spindulių spektroskopija (FTIR)

Norint įvertinti susidariusių agregatų struktūrinius skirtumus, tam dažnai yra pasitelkiama Furje-transformacijos infraraudonųjų spindulių spektroskopija. Šis metodas leidžia nustatyti susidariusių agregatų antrinę struktūrą, nepaisant

baltymo fizinės formos, kaip pvz. baltymo tirpalai, plėvelės, kristalai, hidrogeliai ir pan[180]. Ši metodika paremta specifinėmis sugerties spektro pozicijomis, susijusiomis su baltymo peptidinių jungčių vibracija[181]. Analizuojant agregatų antrinę struktūrą daugiausia dėmesio skiriama amido I regionui (1700-1600 cm^{-1}). Amido I regione spektrams yra būdingi maksimumai, susiję su įvairiais antrinės struktūros elementais, tokiais kaip alfa-spiralės, beta-klostės, nestruktūrizuota dalis, kilpos[182]. Prieš skanuojant FTIR spektrus, agregatų mėginiai yra kelis kartus resuspenduojami į deuterio oksidą, siekiant išvengti su vandeniu susijusių signalų ir gauti geros kokybės spektrą. Analizuojant gautus duomenis pirmiausia spektrai yra apdorojami atimant deuterio oksido ir vandens garų spektrus. Pašalinus su šiais elementais susijusius intensyvumus, toliau koreguojama spektrų bazinė linija ir jie integruojami. Tai yra atliekama, kad būtų galima palyginti struktūros elementų kiekių skirtumus tarp mėginių, nepaisant fibrilių koncentracijos. Šis metodas buvo naudojamas visose į disertaciją įtrauktose publikacijose.

Apskritiminio dichroizmo spektroskopija (AD)

Dar vienas metodas nustatyti baltymo struktūrą yra apskritiminio dichroizmo spektroskopija. Šio tyrimo metu yra nustatomi baltymo antrinės ir tretinės struktūros pokyčiai, baltymo susilankstymo/išsilankstymo dinamika, jungimosi charakteristikos[50,183]. Ši metodika yra paremta diferencine apskritiminės poliarizuotos šviesos sugertimi. Molekulės sugeria kairio arba dešinio sukimo apskritiminę poliarizuotą šviesą, priklausomai nuo molekulės chiralinio centro arba 3D struktūros[46,184]. Šio metodo pliusas, kad yra gaunama informacija apie baltymo struktūrą, naudojant mažą baltymo koncentraciją, tirpaluose, kurie atitinka eksperimentines sąlygas, per gana trumpą laiko tarpą[184]. Tiriant amiloidinių baltymų konformacinius pokyčius yra analizuojami AD signalai tolimajame UV bangų ilgio regione (240-190 nm ruožas)[183]. Šis metodas buvo naudojamas 3 publikacijoje.

Atominės jėgos mikroskopija (AJM)

Norint įvertinti fibrilių morfologiją, dažnai naudojama yra AJM. Šis metodas leidžia sudaryti agregatų, padengusių žėručio paviršių, 3D žemėlapius[53]. Tai pasiekiama nustatant mėginio padėtį adatos atžvilgiu, įrašant zondo aukštį ir šiuos duomenis paverčiant trimačiu vaizdu, dažniausiai atvaizduojant spalvine schema, parodančia aukščio skirtumus[50]. Tokiu būdu galima įvertinti susidariusių fibrilių, kurios padengusios žėručio paviršių, morfologinius parametrus, tokius kaip aukštis, plotis, periodiškumas[86]. Be visa to galima pamatyti ar mėginyje yra susidariusių fibrilių ar amorfinių agregatų mišinys. Taip pat šis metodas leidžia įvertinti ar susidariusios fibrilės yra linkusios asocijuoti lateraliai, į didelius klasterius ar išlikti pavienės. Kadangi ne visada fibrilės linkusios prikibti prie žėručio paviršiaus dėl fibrilių krūvio, prieš

mėginio aplikaciją, pirmiausia žėrutis yra apdorojamas APTES siekiant pagerinti prikibimą. Šis metodas buvo naudojamas 1-4, 6 ir 7 publikacijose.

Transmisijos elektronų mikroskopija (TEM)

Dar vienas būdas įvertinti susidariusių agregatų morfologinius parametrus yra naudojant TEM. Šis metodas yra puikus įrankis, kuris leidžia susidariusių agregatų aukštos rezoliucijos vizualizavimą[87]. TEM yra paremta didelės energijos elektronų spindulio perėjimu per mėginį. Kadangi dalis elektronų sąveikauja su mėginiu, o kita dalis pereina per ploną paviršių, gaunamas vaizdas, kuriame naudojant kontrastą atkuriami agregatai[53]. Ši metodika leidžia nustatyti susidariusių agregatų dydį, formą ir jų pasiskirstymą, tačiau priešingai nei AJM neleidžia įvertinti aukščio ir topografinės informacijos. Siekiant gauti gerą kontrastą, mėginys yra neigiamai dažomas, naudojant metalų druskas, tokias kaip uranilo acetatas ar fosfotungstinė rūgštis[87]. Dar vienas šios metodikos privalumas, lyginant su AJM, yra didesnio ploto tuo pačiu metu fiksavimas, kuris leidžia nustatyti susidariusių agregatų homogeniškumą. Šis metodas buvo naudojamas 5 publikacijoje.

Fluorescencijos ir sugerties spektroskopija

Kad įvertinti susidariusių agregatų variabilumą dažnai yra matuojamos mėginio sužadinimo-emisijos matricos[186,187]. Kadangi sužadinimo ir emisijos pozicijos, kuriose stebimas fluorescencijos maksimumas, gali skirtis priklausomai nuo dažo jungimosi būdo ir atitinkamai struktūriškai skirtingo agregatų kamieno, šis metodas leidžia išskirti mėginius, kurie galimai skiriasi savo struktūra[187]. Siekiant nustatyti maksimumo pozicijas, pirmiausia yra skanuojamas fluorescencijos intensyvumas esant sužadinimo bangų ilgių ruožui, o emisija matuojama viename taške ir atvirkščiai. Gaunamas fluorescencijos intensyvumo 3D žemėlapis. Pirmiausia apdorojant šiuos duomenis reikia atsižvelgti į galimą vidinio filtro efektą, kuris sukelia fluorescencijos sumažėjimą dėl mėginio sugerties. Šis parametras priklauso nuo šviesos kelio, kurį ji turi praeiti per mėginį iki pasiekiant detektorių. Pašalinus šį efektą, galima apskaičiuoti kiekvienam mėginiui būdingas pozicijas, kuriose matomas fluorescencijos maksimumas. Šis metodas buvo naudojamas 1, 2 ir 3 publikacijose.

Dažo jungimąsi galima vertinti ir naudojant sugerties spektroskopiją. Skanuojant sugerties spektrus mėginių su fibrilėmis ir jų supernatantus, galima apskaičiuoti prijungto dažo koncentraciją[186]. Taip pat atsirandantys sugerties maksimumo pozicijos poslinkiai gali reikšti skirtingą dažo jungimosi būdą[188]. Šis metodas buvo naudojamas 2, 3 ir 4 publikacijose.

Fibrilių stabilumas denatūruojančiomis sąlygomis

Kaip dar vienas iš požymių, kuriuo tarpusavyje gali skirtis įvairių kamienų fibrilės yra stabilumas denatūruojančiomis sąlygomis. Tam baltymo agregatai yra sumaišomi su denatūranto skirtingų koncentracijų tirpalais. Mėginiai kurį laiką inkubuojami ir tuomet yra matuojamas mėginių optinis tankis. Dažniausiai tyrimo metu stebimas optinio tankio sumažėjimas sigmoidės forma didėjant denatūranto koncentracijai. Atlikus šių duomenų gluodinimą, naudojant Boltzmann sigmoidinę funkciją, gaunama denatūranto koncentracija, kurioje pusė agregatų yra disocijavę, o kita pusė išlieka stabili[91]. Pagal šią vertę, galima nustatyti ar susidarę agregatai yra labiau/mažiau atsparūs denatūranto įtakai. Šis metodas buvo naudojamas 2, 4, 6 ir 7 publikacijose.

Toksiškumas ląstelėms

Dar viena dažnai analizuojama amiloidinių fibrilių savybė yra jų toksiškumas ląstelėms. Tam dažniausiai yra pasitelkiami du būdai. Vienas iš jų yra MTT tyrimas. Jo metu yra vertinimas mitochondrijų aktyvumas ir jis pritaikomas gyvų ląstelių skaičiaus nustatymui. Ši metodika yra paremta spalvos pasikeitimu, kurį galima įvertinti panaudojant sugerties spektroskopiją ir apskaičiuoti gyvybingų ląstelių skaičių[189]. Tyrimo metu ląstelės yra inkubuojamos su geltonos spalvos 3-(4,5-dimetiltiazol-2-yl)-2,5-difeniltetrazolo bromidu (MTT), kurį aktyvi mitochondrijų sukcinato dehidrogenazė paverčia mėlynai violetinės spalvos produktu – formazanu[190]. Nors šis metodas dažnai taikomas siekiant nustatyti toksiškumą ląstelėms, vis dėlto jis turi ir trūkumų. Ląstelių gyvybingumas tyrimo metu yra nustatomas netiesiogiai, o perskaičiuojamas atsižvelgiant į mitochondrijų fermento aktyvumą ir ląstelių metabolizmą. Dėl šios priežasties būtina įvertinti ar eksperimentinės sąlygos nepakeičia šio proceso[189].

Dar vienas naudojamas metodas yra LDH išskyrimo tyrimas. Ši metodika kaip ir prieš tai minėtas MTT tyrimas, yra paremta išskiriamo produkto nustatymu, naudojant sugerties spektroskopiją. Visgi šis metodas padeda nustatyti ląstelės mirtį, remiantis jos membranos integralumo praradimu[191]. Ląstelės pažeidimo metu į terpę yra išskiriama laktato dehidrogenazė, kuri laktatą verčia piruvatu, o šis sąveikauja su jodo nitrotetrazolo chloridu, tokiu būdu susidarant formazanui. Šio tyrimo metu susidaręs formazano kiekis yra tiesiogiai susijęs su ląstelių gyvybingumu[192]. Šie metodai taip pat gali būti naudojami analizuojant potencialių anti-amiloidinių junginių citotoksiškumą. Visi šiame darbe toksiškumo tyrimai buvo atliekami naudojant SH-SY5Y neuroblastomos ląsteles. Visi ląstelių toksiškumo darbai buvo atlikti R. Sniečkutės. Šis metodas buvo naudojamas 5 ir 7 publikacijose.

Dinaminė šviesos sklaida

Viena dažniausiai naudojamų technikų nustatyti dalelių dydį (hidrodinaminį spindulį arba skersmenį) yra dinaminės šviesos sklaidos spektroskopija. Tai yra santykinai greitas metodas, nereikalaujantis sudėtingo mėginio paruošimo. Vienintelis svarbus mėginio aspektas yra maža dalelių koncentracija[193]. Kai monochromatinės šviesos spindulys susiduria su tirpale esančiomis makromolekulėmis, šviesa yra išsklaidoma visomis kryptimis, priklausomai nuo molekulių dydžio ir formos. Būtent šis sklaidos intensyvumas yra matuojamas detektoriumi, o skaitmeninio autokoreliatoriaus pagalba yra nustatoma kaip greitai šviesos išsklaidymo intensyvumas svyruoja[194]. Kadangi intensyvumo svyravimai atsiranda dėl makromolekulių Brauno judėjimo tirpale, analizuojant gautus duomenis galima nustatyti difuzijos koeficientą, kuris yra susijęs su molekulės hidrodinaminiu dydžiu[195]. Naudojant šį metodą yra nustatomas ne tik dalelių dydis homogeniškos populiacijos atveju, bet ir dalelių polidispersiškumas, kuris pateikiamas kaip standartinis nuokrypis[194]. Analizuojant baltymus šis metodas dažnai taikomas nustatyti baltymo oligomerizacijos laipsnį bei agregaciją. Vis dėlto naudojant šį metodą dalelių dydžio nustatymui yra būtina atsižvelgti į eksperimentines sąlygas, kaip temperatūra ar tirpiklio klampa, nes šie parametrai gali paveikti molekulių judėjimą ir galiausiai nustatomą jų dydį. Šis metodas buvo naudojamas 4 publikacijoje.

REZULTATŲ APŽVALGA

Publikacija 1

Lizocimo amiloidinių fibrilių struktūrinio variabilumo priklausomybė nuo pradinės baltymo susilankstymo būsenos

Tyrimo tikslas – nustatyti temperatūros ir lizocimo susilankstymo būsenos įtaką jo amiloidinių fibrilių polimorfizmui.

Rezultatai – remiantis lizocimo lydymosi temperatūra (2M GuHCl, 1x PBS pH 7.4), tolesniems tyrimams buvo pasirinktos 4 temperatūros vertės: kai dauguma baltymų molekulių buvo daugiausia susilanksčiusios arba išsilanksčiusios (50 °C, 65 °C), ir tarpinės (55 °C, 60 °C) su abiejų baltymų formų mišiniais.

Analizuojant lizocimo agregacijos kinetinius parametrus, pastebėta, kad didėjant temperatūrai, lag laikas trumpėjo, o greičio konstanta – padidėjo. Lag laiko priklausomybė nuo temperatūros turėjo lūžio tašką ties 57 °C, atitinkančiu lizocimo lydymosi temperatūrą. Greičio konstantos atveju šis taškas buvo šiek tiek žemiau lizocimo lydymosi temperatūros – 55 °C.

Siekiant nustatyti gautų fibrilių struktūrinį kintamumą, buvo nuskaitytos ir išanalizuotos sužadinimo-emisijos matricos. Šis tyrimas parodė, kad esant žemesnei nei baltymų lydymosi temperatūrai, maksimalaus ThT intensyvumo sužadinimo ir emisijos pozicijos buvo panašios ir sutelktos viename regione. Tačiau aukštesnėje temperatūroje pastebėtas žymiai didesnis pozicijų išsibarstymas su papildomo klasterio atsiradimu 65 °C sąlygomis.

Taip pat buvo nustatyti mėginių FTIR spektrai. Kai didžioji dalis lizocimo buvo sulankstytoje būsenoje, mėginių FTIR spektrai buvo labai panašūs. Tačiau aukštesnės temperatūros lėmė skirtingos formos FTIR spektrų atsiradimą ir didesnį struktūrinį kintamumą. Remiantis visų mėginių FTIR spektrais, buvo identifikuoti 3 agregatų tipai, kur žemesnės temperatūros mėginiai turėjo didžiausią santykinį beta-klosčių kiekį. AJM analizė parodė, kad 1 tipo fibrilės buvo ilgos ir nebuvo linkusios tarpusavyje asocijuoti, 2 tipo fibrilės buvo daugiausia trumpos ir susitelkusios į tinklus, o 3 tipo atveju daugiausia buvo trumpi agregatai, kurie sudarė didelius amorfinius klasterius.

Išvados – lizocimo išsilankstymas paskatina didesnį fibrilių antrinių struktūrų variabilumą ir morfologijos pasikeitimus.

Publikacija 2

Lizocimo amiloidinių fibrilių susidarymo ir struktūrinio variabilumo priklausomybės nuo pradinės susilankstymo būsenos tyrimas skirtingomis pH sąlygomis

Tyrimo tikslas – nustatyti tirpalo pH ir pradinės lizocimo susilankstymo būsenos įtaką agregacijos procesui ir susidariusių fibrilių kintamumui.

Rezultatai – ankstesnio tyrimo metu buvo pastebėta, kad temperatūra ir lizocimo susilankstymo būsena keičia jo agregacijos procesą. Kadangi pH taip pat gali turėti įtakos baltymo stabilumui, lizocimo agregacija buvo tirta esant skirtingoms pH sąlygoms (2,0–7,0). Panašiai kaip ir ankstesniame tyrime, lizocimo lydymosi temperatūrai kiekvienomis sąlygomis nustatyti buvo naudojamas terminio stabilumo tyrimas. Lizocimo agregacija buvo atlikta kiekvieno pH atveju esant temperatūroms, kuriose pradinis baltymas yra arba sulankstytas, arba išlankstytas.

Siekiant įvertinti šių veiksnių įtaką agregacijos procesui, pirmiausia buvo nustatyti tokie kinetiniai parametrai kaip lag laikas ir greičio konstanta. Visais atvejais pradinė baltymo susilankstymo būsena turėjo statistiškai reikšmingą įtaką abiem kinetiniams parametrams. Tačiau baltymo susilankstymo būsenos įtaka lag laikui priklausė nuo tirpalo pH vertės, o jos įtaka greičio konstantai išliko panaši visame pH ruože.

Toliau, siekiant įvertinti šių dviejų veiksnių įtaką susidariusių fibrilių struktūriniams parametrams, buvo naudojama FTIR spektroskopija. Rezultatai parodė, kad FTIR spektrų kintamumas priklausė tiek nuo temperatūros, tiek nuo pH. Spektrai labiau varijavo, kai lizocimo agregacija vyko aukštesnėje nei lydymosi temperatūra ir esant ribinėms pH vertėms (2,0 ir 7,0). Analizuojant mėginių FTIR spektrus, iš viso buvo identifikuoti 6 skirtingi fibrilių tipai, o jų pasiskirstymas priklausė tiek nuo pH, tiek nuo pradinės baltymo būsenos. Remiantis mėginių AJM analize, visų mėginių fibrilių morfologija buvo panaši. Tačiau agregatų tipai pasižymėjo skirtingu stabilumu denatūruojančiomis sąlygomis, taip pat ThT jungimosi savybėmis.

Išvados – lizocimo agregacijos kinetika ir susidariusių fibrilių struktūrinis kintamumas priklauso nuo tirpalo pH ir pradinės baltymo susilankstymo būsenos. Mažiausias struktūrinis kintamumas buvo pastebėtas pH 5 ir 6 atvejais, susidarant vienam agregatų tipui, nepaisant lizocimo pradinės susilankstymo būsenos.

Publikacija 3

Greita skirtingų alfa-sinukleino amiloidinių fibrilių kamienų restruktūrizacija aukštoje temperatūroje

Tyrimo tikslas – nustatyti, ar iš anksto susiformavusios alfa-sinukleino fibrilės išlieka struktūriškai stabilios, inkubuojant jas aukštesnėje temperatūroje nei susidarė.

Rezultatai – siekiant įvertinti aukštesnės temperatūros poveikį fibrilėms, buvo išanalizuotas didelis kiekis alfa-sinukleino mėginių. Remiantis EEM ir FTIR spektrais, buvo identifikuoti 4 fibrilių tipai, kurie toliau buvo panaudoti aukštesnės temperatūros poveikiui tirti. Tuo tikslu skirtingų tipų fibrilių mėginiai buvo laikomi kambario temperatūroje (kontrolė) arba 60 °C temperatūroje 24/48 val.

Analizuojant FTIR spektrus, pastebėta, kad visi keturi fibrilių mėginiai pakito inkubacijos metu, jų spektrai galiausiai sutapo, o tai rodo, kad buvo stabilizuotas vienas fibrilių tipas. Siekiant išsiaiškinti, ar šie spektriniai pokyčiai buvo susiję su alfa-sinukleino restruktūrizacija ar kitais galimais veiksniais (fibrilių lateraline asociacija, amorfinių struktūrų susidarymu), inkubuoti mėginiai buvo pakartotinai savireplikuojami pradinėje paruošimo temperatūroje. Šis tyrimas parodė, kad inkubuotų fibrilių antrinė struktūra išliko stabili, o replikuoti agregatai negrįžo į pradinę konformaciją.

Galiausiai, inkubacijos metu buvo nustatytas mėginio EEM maksimalių pozicijų poslinkis, kuris buvo didžiausias per pirmąsias 4 valandas, o vėliau palaipsniui judėjo į vieną tašką. Šie rezultatai rodo, kad alfa-sinukleino fibrilių restruktūrizacija aukštoje temperatūroje greičiausiai vyksta per trumpą laiką.

Išvados – alfa-sinukleino fibrilių restruktūrizacija aukštoje temperatūroje yra greitas procesas, kurio metu yra stabilizuojama viena fibrilių antrinė struktūra. Tačiau šis procesas neturi pastebimo poveikio agregatų morfologijai ar ThT jungimuisi.

Publikacija 4

Insulino agregacijos ir susidariusių fibrilių struktūros tyrimas skirtingomis aplinkos sąlygomis

Tyrimo tikslas – nustatyti tirpalo komponentų, pH ir joninės jėgos įtaką insulino agregacijai ir susidarančiai fibrilių struktūrai.

Rezultatai – naudojant natrio fosfatą, acto arba druskos rūgštį kaip pagrindinius tirpalo komponentus, buvo paruošti skirtingo pH ir joninės jėgos reakcijos tirpalai. Tuomet insulinas buvo ištirpintas šiame skirtingų reakcijos mišinių diapazone ir analizuojama jo agregacijos kinetika. Dauguma kinetinių kreivių pasižymėjo sigmoidės formos fluorescencijos intensyvumo pasikeitimu nuo laiko. Tačiau kai kuriais atvejais buvo stebimos dvigubos sigmoidės arba kreivės su nesibaigiančia stacionaria faze.

Natrio fosfato tirpalo atveju visos joninės jėgos sąlygos lėmė panašią lag laiko priklausomybę nuo tirpalo pH. Mažesnio pH sąlygos lėmė trumpesnį lag laiką, o didesnio pH – žymiai ilgesnes lag fazes, ypač esant didesnei joninei jėgai. Ac sąlygomis didėjanti joninė jėga lėmė lag fazės sumažėjimą. Priešingai, joninė jėga beveik neturėjo jokios įtakos insulino agregacijai HCl sąlygomis. Agregacijos greičio konstantos daugumoje išbandytų sąlygų nesilaikė aiškios tendencijos.

Gauti mėginiai buvo analizuojami naudojant FTIR spektroskopiją. Fosfato tirpalo atveju buvo identifikuotos trijų tipų antrinės struktūros. Acto rūgšties sąlygos lėmė dviejų papildomų antrinių struktūrų susidarymą. Įdomu tai, kad HCl reakcijos tirpalai skatino visų trijų tipų insulino fibrilių susidarymą, kurios buvo aptiktos fosfato tirpale. Skirtingos antrinės struktūros mėginiai buvo toliau analizuojami naudojant AJM. Fosfato tirpalo atveju buvo stebimas trijų tipų fibrilių pasiskirstymas: 1) ilgų susipynusių fibrilių tinklai, 2) lateraliai asocijuotos arba 3) kelios matomos atskiros trumpos fibrilės. Acto rūgšties agregatų ilgis ir asociacija priklausė nuo NaCl koncentracijos. HCl atveju susidariusios fibrilės turėjo panašias morfologines tendencijas kaip ir fosfato tirpaluose.

Išvados – insulino agregacija yra labai jautri įvairiems aplinkos veiksniams. Insulino agregacija fosfato ir HCl tirpaluose skatina fibrilių, pasižyminčių panašia antrine struktūra ir morfologija, susidarymą. Tačiau Ac tirpaluose susidaro kito tipo kamienai.

Publikacija 5

Imidazo[2,1-b][1,3]tiazino dariniai potencialūs alfa-sinukleino amiloidinės agregacijos moduliatoriai

Tyrimo tikslas – nustatyti mažų molekulinių junginių, priklausančių imidazotiazinų grupei, potencialą moduliuoti alfa-sinukleino agregaciją.

Rezultatai – tam buvo pasirinktas 21 mažamolekulinis junginys. Analizuojant, kaip keičiasi santykinis agregacijos puslaikis, pastebėta, kad daugelis junginių (10 iš 21) neturėjo jokio poveikio šiam parametrui, lyginant su kontroliniais mėginiais. Tačiau kiti 10 imidazotiazino darinių sulėtino alfa-sinukleino agregaciją. Kai kurie iš jų lėmė net 3 kartus didesnį agregacijos puslaikį. Be neutralių ir agregaciją slopinančių junginių, vienu atveju taip pat buvo pastebėtas agregaciją skatinantis poveikis.

Siekiant įvertinti šių junginių poveikį fibrilių struktūrinėms charakteristikoms, mėginiai toliau buvo analizuojami, naudojant FTIR spektroskopiją. Iš viso buvo identifikuoti 7 skirtingi spektrų tipai. Kontroliniai mėginiai pasižymėjo 3 skirtingais spektrais. Didžiausias struktūrų kintamumas pastebėtas 5d junginio atveju, kur buvo identifikuoti 5 skirtingi spektrų tipai. Mažiausias struktūrų kintamumas pastebėtas 2c, 2e ir 2j junginių atveju, kur buvo nustatytas tik vienas kamienas. Įdomu tai, kad taip pat buvo pastebėta koreliacija tarp junginių slopinamojo poveikio ir susidariusio fibrilių tipo.

Be antrinių struktūrų pokyčių, TEM metodu taip pat buvo analizuojami morfologiniai skirtumai tarp fibrilių tipų. I, II, III ir VI tipų fibrilių atveju pastebėta aiški agregatų tendencija jungtis į didelius klasterius. Be didelių klasterių, II tipo mėginiuose taip pat buvo matomos trumpos fibrilės. VII tipo mėginiuose pastebėtas nedidelis kiekis trumpų fibrilių, tačiau aptikta ir nemažai mažų amorfinių agregatų bei oligomerinių darinių.

Išvados – mažos molekulinės masės imidazotiazino dariniai pasižymi gebėjimu slopinti alfa-sinukleino amiloidinę agregaciją ir nukreipti reakciją kita linkme, todėl susidaro fibrilės su skirtingomis antrinėmis struktūromis ir morfologijomis.

Publikacija 6

Superoksido dismutazė-1 keičia prioninio baltymo fragmento 89-230 agregacijos greitį ir susidarančių fibrilių variabilumą

Tyrimo tikslas – nustatyti, ar superoksido dismutazė-1 keičia prioninio baltymo agregacijos procesą, bei susidariusių agregatų variabilumą.

Rezultatai – siekiant įvertinti, kaip natyvi superoksido dismutazė-1 gali paveikti prioninio baltymo agregaciją, kai jie yra kartu tirpale, buvo parinktos eksperimentinės sąlygos, kurios skatina PrP fibrilių susidarymą. Analizuojant šio proceso kinetinius parametrus, nustatyta, kad didesnės SOD1 koncentracijos lėmė ilgesnį prioninio baltymo agregacijos lag laiką ir mažesnę greičio konstantą.

Gauti prioninio baltymo agregatų mėginiai toliau buvo analizuojami naudojant FTIR spektroskopiją. Remiantis gautais FTIR spektrais, buvo nustatytos keturios agregatų grupės. Pastebėta, kad kai prioninis baltymas agregavo be SOD1, buvo nustatyti trijų tipų spektrai. Kai reakcijos tirpale buvo 25 μM SOD1, buvo stebima skirtinga FTIR spektrų įvairovė. Įdomu tai, kad esant dar didesnėms SOD1 koncentracijoms, struktūrų kintamumas išnyko ir visus spektrus buvo galima priskirti vienai grupei.

Morfologinė mėginių analizė naudojant AJM parodė, kad visų tipų agregatai turėjo tendenciją suformuoti didelius klasterius, tačiau fibrilės skyrėsi viena nuo kitos savo morfologiniais parametrais, tokiais kaip aukštis ir plotis.

Išvados – superoksido dismutazė-1 ne tik slopina prioninio baltymo branduolių susidarymą, bet ir veikia susidariusių agregatų konformaciją, priklausomai nuo SOD1 koncentracijos.

Publikacija 7

S100A9 slopina prioninio baltymo 89-230 fragmento amiloidinę agregaciją

Tyrimo tikslas – nustatyti uždegimą skatinančio S100A9 baltymo įtaką pelės prioninio baltymo 89-230 fragmento agregacijai.

Rezultatai – norint įvertinti galimą S100A9 įtaką pelės prioninio baltymo agregacijai, pirmiausia reikėjo parinkti tinkamas eksperimentines sąlygas. Reikėjo sukurti aplinką, kuri skatintų greitą prioninio baltymo agregaciją, sulėtintų S100A9 baltymo agregaciją, bei išlaikytų iš anksto suformuotų S100A9 fibrilių stabilumą. Optimizavimo procedūros metu nustatyta, kad optimali denatūranto koncentracija, naudojama tolimesniems tyrimams, yra 1,5 M GuHCl.

Prioninio baltymo agregacija buvo analizuojama esant skirtingoms (0–50 μM) neagreguoto S100A9 arba jo iš anksto suformuotų fibrilių koncentracijoms. Neagreguoto S100A9 atveju PrP agregacijos lag laikas didėjo priklausomai nuo S100A9 koncentracijos. Priešingai, S100A9 fibrilės neturėjo reikšmingos įtakos šiam parametrui.

S100A9 įtaka prioninio baltymo agregatų antrinei struktūrai buvo analizuojama, naudojant FTIR spektroskopiją. FTIR spektrų analizė parodė, kad mažos S100A9 koncentracijos (tiek neagreguoto, tiek fibrilių) radikaliai nepakeitė PrP fibrilių struktūros ir sukėlė tik nedidelį pagrindinio maksimumo pozicijos poslinkį. Tačiau 50 μM abiejų S100A9 formų įtaka buvo daug didesnė, skatinanti kitokio tipo PrP fibrilių susidarymą.

Išvados – tiek fibrilinės, tiek neagreguotos S100A9 formos veikia prioninio baltymo fragmento agregacijos procesą, keisdamos susidariusią fibrilių antrinę struktūrą ir stabilizuodamos specifinį agregato tipą. Be to, neagreguotas S100A9 slopina PrP nukleaciją.

DISKUSIJA

Temperatūros ir baltymų susilankstymo būsenos vaidmuo amiloidinėje agregacijoje

Agregacijos tyrimų *in vitro* metu temperatūra dažnai keičiama, siekiant pagreitinti fibrilių susidarymo procesą, kuris fiziologinėmis sąlygomis paprastai vyksta labai lėtai. Tačiau tokie sąlygų pakeitimai dažnai atliekami neatsižvelgiant į jų įtaką reakcijos mechanizmui. Kai kuriais atvejais net ir nedideli temperatūros skirtumai gali sukelti reikšmingus agregacijos kinetikos ir susidariusių fibrilių struktūrinius nukrypimus[196,197].

Pirmas temperatūros aspektas, į kurį turime atsižvelgti, yra baltymo susilankstymo būsenos pokytis. Pradinė sulankstymo būsena gali reikšmingai paveikti agregacijos kinetinius parametrus tiek spontaninės, tiek savireplikacijos reakcijose. Tokio tipo įtaka buvo pastebėta šiame darbe, tiriant lizocimo agregaciją keturiose skirtingose temperatūrose. Lizocimo tyrimo metu buvo pastebėta, kad baltymų molekulių išsilankstymas skatina amiloidinių branduolių susidarymą, taip pat ir greičio konstantą. Panašūs rezultatai buvo gauti Andlinger tiriant žmogaus mielomos antikūnų lengvosios grandinės agregaciją aukštoje temperatūroje. Šio tyrimo metu buvo pastebėta, kad baltymų išsivyniojimas pagreitina agregacijos procesą, ir tiek išsivyniojimo, tiek agregacijos procesai yra stipriai kinetiškai susiję[198]. Be to, Simmons su kolegomis analizuojant miofibrilinio baltymo agregaciją, pastebėjo, kad visiškas išsivyniojimas (apimantis ir galvos, ir uodegos sritis) drastiškai padidino agregacijos greitį[199]. Nenuostabu, kad temperatūros didinimas turi įtakos agregacijos kinetiniams parametrams, nes daugeliu atvejų to ir siekiama. Tačiau dažniausiai neatsižvelgiama į tai, ar tokie temperatūros pokyčiai taip pat paveiks susidariusių fibrilių struktūrą.

Tiriant lizocimo agregacijos priklausomybę nuo baltymų susilankstymo pusiausvyros, buvo pastebėtas agregatų antrinės struktūros poslinkis. Rezultatų analizė parodė, kad žemoje temperatūroje susidariusių fibrilių struktūroje buvo daugiau beta-klosčių nei agregatų, gautų aukštoje temperatūroje. Kitame Cao ir jo kolegų tyrime buvo nustatyta lizocimo sulankstymo būsenos svarba agregacijos metu susidarančių fibrilių struktūrai. Autoriai parodė, kad visiškas arba dalinis baltymų išsilankstymas gali sukelti dviejų skirtingų fibrilių tipų (grįžtamųjų / negrįžtamųjų) susidarymą, kuriems būdingos skirtingos paralelinių ir antiparalelinių beta-klosčių proporcijos[200]. Įdomu tai, kad mūsų tyrime tarp techninių pakartojimų tomis pačiomis temperatūros sąlygomis taip pat buvo pastebėti skirtingi fibrilių tipai, kurie pasižymėjo skirtingomis FTIR spektrų maksimaliomis pozicijomis. Ankstesniuose tyrimuose buvo parodytas panašus reiškinys analizuojant prioninio baltymo agregaciją, o tai rodo, kad toks struktūrinis kintamumas

identiškomis sąlygomis gali būti bendras amiloidinių agregatų bruožas[121]. Šio darbo rezultatai rodo, kad kai lizocimas yra iš dalies/visiškai susilankstęs, jis gali sudaryti vieną dominuojantį fibrilių kamieną kartu su nedideliu kiekiu kitų struktūrų, o baltymų susilankstymas gali lemti žymiai didesnį struktūrinį variabilumą.

Ankstesniuose tyrimuose buvo pastebėta, kad tioflavino-T prisijungimo būdas ir jo fluorescencijos kvantinė išeiga gali priklausyti nuo amiloidinių agregatų struktūrinių parametrų[187]. Toks efektas buvo nustatytas ir lizocimo atveju. Kadangi susidariusių agregatų struktūra priklausė nuo pradinės baltymo susilankstymo būsenos, žemos temperatūros sąlygomis susidarę agregatai pasižymėjo 10 kartų didesniu prijungto ThT fluorescencijos intensyvumu, palyginti su aukštesnės temperatūros sąlygomis susidarančiais agregatais. Be to, sužadinimo-emisijos matricų maksimalios fluorescencijos pozicijos taip pat skyrėsi. Toks mažesnis fluorescencijos intensyvumas gali būti dėl sumažėjusio beta-klosčių kiekio aukštesnės temperatūros fibrilėse, kuris buvo nustatytas analizuojant FTIR spektrus. Tačiau fluorescencijos intensyvumo pokytis ne visada tiesiogiai susijęs su beta-klosčių kiekiu. Tokio reiškinio pavyzdys buvo pateiktas Cao analizuojant skirtingų alfa-sinukleino agregatų izoformų ThT prisijungimo vietas. Šis tyrimas atskleidė, kad skirtingos alfa-sinukleino fibrilių izoformos pasižymėjo skirtingu ThT fluorescencijos intensyvumu, nepaisant panašaus β-klosčių kiekio[200]. Šį skirtumą mūsų darbe taip pat galima paaiškinti dideliu kiekiu kitų neamiloidinių struktūrų susidarymu mėginiuose, kuris buvo pastebėtas AJM vaizduose. Tai gali būti siejama su ThT specifiškumu amiloidiniams agregatams, nes jo sąveika su globuliniais baltymais arba amorfiniais agregatais dažnai laikoma nereikšminga, palyginti su jo afiniškumu amiloidinėms fibrilėms[201].

Galiausiai, pradinė baltymų susilankstymo būsena taip pat paveikė agregatų savireplikaciją. Lizocimo atveju pastebėta, kad žemos temperatūros kamienas sugebėjo sėkmingai atkartoti savo struktūrą ir suformuoti ilgas fibriles net ir esant aukštesnei temperatūrai. Tačiau aukštos temperatūros kamienų atveju pastebėtas kitoks vaizdas. Šie agregatai sugebėjo sėkmingai replikuotis pradinėmis fibrilių formavimosi sąlygomis, bet ne esant visiškai susilanksčiusiam lizocimui žemesnėje temperatūroje. Šį efektą galima paaiškinti tuo, kad fibrilių galai gali prisijungti tik iš dalies arba visiškai susilanksčiusias baltymų molekules. Ankstesni tyrimai taip pat parodė, kad aukštesnė temperatūra ir baltymų išsilankstymas skatina elongacijos procesą[166,202]. Anksčiau minėtas didelis neamiloidinių struktūrų kiekis mėginiuose taip pat galėjo prisidėti prie prasto savireplikacijos lygio. Tai patvirtintų anksčiau pateikti įrodymai, kad amorfiniai agregatai yra galutinė būsena, negalinti savęs replikuoti[203].

Kaip minėta anksčiau, konformacinė dinamika vaidina svarbų vaidmenį lizocimo, kaip ir kitų amiloidogeninių baltymų, agregacijos procese. Todėl labai svarbu nustatyti ryšį tarp baltymo susilankstymo būsenos ir susidariusių fibrilių struktūros bei morfologijos. Šis parametras gali reikšmingai pakeisti ne tik agregacijos kinetikos parametrus, bet ir susidariusių struktūrų kintamumą, dažų surišimo ir savireplikacijos savybes.

Šie rezultatai parodė, kad net ir nedideli temperatūros svyravimai agregacijos pradžioje ir jos metu gali paveikti visą procesą. Tačiau šis parametras taip pat labai svarbus jau susiformavusioms struktūroms. Ankstesniuose tyrimuose buvo parodyta, kad sumažėjusi aplinkos temperatūra gali destabilizuoti susidariusius amorfinius agregatus arba fibriles[204,205]. Priešingai, aukšta temperatūra kai kuriais atvejais gali paveikti fibrilių brendimą. Fiziologinėmis sąlygomis šis procesas yra labai lėtas ir kai kuriais atvejais gali užtrukti kelias dienas ar net mėnesius[206]. Bocharova tyrimai rodo, kad aukšta temperatūra gali sukelti prioninio baltymo fibrilių persitvarkymą, dėl ko susidaro didesnė, proteinazei K atspari šerdis[207].

Šiame darbe fibrilių brendimo reiškinys buvo tirtas naudojant keturis struktūriškai skirtingus alfa-sinukleino fibrilių mėginius. Pakėlus temperatūrą iki 60 °C, skirtingų alfa-sinukleino kamienų restruktūrizacija įvyko labai greitai, o reikšmingi antrinės struktūros pokyčiai buvo pastebėti per 24 valandas. Įdomu tai, kad inkubacijos metu visų keturių skirtingų tipų fibrilės persitvarkė į vieną bendrą kamieną. Mėginių CD spektrų analizė inkubacijos metu parodė, kad beta-klosčių kiekis reikšmingai nepadidėjo, tačiau esami struktūriniai elementai persitvarkė. Tai galima paaiškinti galimu 37 °C temperatūroje susidariusių fibrilių metastabilumu. Šių kamienų egzistavimą žemesnėje temperatūroje palengvina tik didelis energijos barjeras, kurį reikia įveikti, kad agregatai pereitų į stabilesnę formą. Kitame tyrime buvo tiriamas vištos kiaušinio baltymo lizocimo oligomerinės formos metastabilumas, atsižvelgiant į druskos ir baltymo koncentracijų pokyčius. Autoriai išaiškino dviejų tipų amiloidinių fibrilių susidarymo mechanizmus ir parodė, kaip šių sąlygų pokyčiai gali lemti oligomerų perėjimą į stabilesnę būseną[208]. Šią hipotezę taip pat patvirtina tai, kad inkubuotų ir iš pradžių 60 °C temperatūroje susidariusių agregatų FTIR spektrai yra panašūs. Tokie rezultatai dar kartą patvirtina, kad temperatūros poveikis yra labai svarbus ne tik pradinei agregacijos reakcijai, bet ir iš anksto susidariusių agregatų stabilumui.

pH ir susilankstymo būsenos koreliacija

Baltymų stabilumas yra nuo pH priklausomas parametras. Šis parametras turi įtakos baltymo krūviui, kuris savo ruožtu gali paveikti tolesnį fibrilių formavimąsi[209]. Šios makromolekulės dažnai yra labai jautrios net ir mažiems pH pokyčiams, todėl buvo svarbu įvertinti, kaip šis parametras gali paveikti jų

amiloidinę agregaciją. Kai lizocimas buvo sulankstytoje būsenoje, visų tirtų pH sąlygų atvejais buvo nustatyti labai išsibarstę lag laikai. Nesusilanksčiusioje būsenoje amiloidinė agregacija vyko esant žymiai trumpesnėms lag fazėms (maždaug 3–4 kartus trumpesni vidutiniai lag laikai), išskyrus pH 3. Įdomu tai, kad greičio konstantų santykis išliko panašus visomis pH sąlygomis, o tai rodo, kad pH 3 turi didelę įtaką pradiniam branduolių susidarymui, bet ne fibrilių ilgėjimui. Šį poveikį galima paaiškinti lizocimo nukrypimu nuo dviejų būsenų modelio šiomis specifinėmis sąlygomis[210]. Empirinis šio modelio pritaikymas parodė, kad skirtumas tarp T_{lyd} ir $T_{pradžios}$ (temperatūra, kurioje baltymas pradeda agreguoti) yra didesnis būtent rūgštinėmis sąlygomis (pH 2 ir 3), palyginti su kitomis. Be to, tai reiškia, kad mūsų pasirinkimas šiame tyrime naudoti 5 °C aukštesnę arba žemesnę nei lydymosi temperatūrą gali lemti skirtingą sulankstyto/išlankstyto lizocimo pusiausvyros pasiskirstymą tarp neutralios ir rūgštinės aplinkos. Tačiau tai nepaaiškino, kodėl lag laiko santykis buvo didelis tik esant pH 3,0, o ne esant pH 2,0. Tolimesnė mėginių analizė parodė, kad esant pH 3,0, agreguoto lizocimo koncentracija žemesnės ir aukštesnės temperatūros sąlygomis labai skyrėsi. Tai reiškia, kad stebėtas reiškinys esant pH 3,0 gali būti susijęs ne tik su skirtumais tarp T_{lyd} ir $T_{pradžios}$, bet ir su eksperimentinėms sąlygoms būdinga pusiausvyra tarp natūralios ir agreguotos baltymo būsenos.

pH ir temperatūros derinys gali paveikti ne tik agregacijos kinetiką, bet ir gautų fibrilių struktūrą bei morfologiją. Šio lizocimo tyrimo metu nustatytas didelis struktūrų kintamumas, priklausantis nuo tirpalo pH ir jo susilankstymo būsenos. pH įtaka fibrilių polimorfizmui buvo pastebėta ir kitiems baltymams. Pavyzdžiui, nustatyta, kad tirpalo pH pokyčiai fiziologiniame 5,8–7,4 diapazone sukelia skirtingas fibrilių struktūras ir skirtingus struktūrinio heterogeniškumo lygius alfa-sinukleino atveju[211]. Panašus atvejis aprašytas ir amiloido-beta šerdies fragmentui, kai pH ir temperatūros pokyčiai turėjo įtakos peptido oligomerizacijai ir galiausiai susidariusių fibrilių struktūrai bei morfologijai[212]. Nors morfologiniai parametrai mūsų darbe daugeliu atvejų reikšmingai nesiskyrė, vienam agregatų tipui buvo būdingos trumpos fibrilės ir didelis amorfinių darinių kiekis. Toks tipas buvo būdingas tik pH 7,0 sąlygoms ir tik aukštesnei nei baltymo lydymosi temperatūrai. Šiomis sąlygomis taip pat buvo nustatytas didžiausias FTIR spektrų kintamumas tarp visų mėginių, greičiausiai dėl minėtų amorfinių struktūrų susidarymo. Šie rezultatai taip pat atitinka mūsų ankstesnius pastebėjimus, kai lizocimo agregacija PBS pH 7,4 ir esant aukštesnei nei lydymosi temperatūrai, lėmė darinių, struktūroje turinčių mažesnį beta-klosčių kiekį, susidarymą.

Nepriklausomai nuo pH ir temperatūros, vienas lizocimo agregatų tipas atrodė dominuojantis tarp visų sąlygų. Esant pH 5 ir pH 6, šis kamienas buvo vienintelis, kuris susiformavo, nepaisant baltymo susilankstymo būsenos. Jam

buvo būdingas didžiausias santykinis stabilumas denatūruojančiomis sąlygomis ir jos struktūroje buvo tik vieno tipo beta-klosčių vandeniliniai ryšiai. Panašūs rezultatai buvo gauti Ziaunys alfa-sinukleino tyrime, kur fibrilių variabilumas priklausė nuo tirpalo joninės jėgos ir baltymo koncentracijos. To tyrimo metu pastebėta, kad tam tikromis sąlygomis vienas fibrilių kamienas buvo stabilizuotas[137]. Atsižvelgiant į visus šiuos stebėjimus, rūgštinio pH arba pH 7,4 sąlygos, kurios dažniausiai naudojamos lizocimo agregacijos tyrimuose, pasižymi dideliu agregatų struktūriniu kintamumu ir gali lemti klaidingas išvadas. Priešingai, pH 6 sąlygos pasižymėjo mažiausiu stochastiškumu tiek kinetikos, tiek struktūros atvejais ir lėmė vieną, labai stabilų fibrilių kamieną.

Insulino agregacijos priklausomybė nuo reakcijos sąlygų

Dažnai atliekant insulino agregacijos tyrimus, reakcija vykdoma rūgštinėje aplinkoje, neatsižvelgiant į tikslų tirpalo pH ar joninę jėgą. Daugeliu atvejų reakcijos mechanizmai arba potencialūs antiamiloidiniai junginiai yra atrenkami ir tiesiogiai palyginami tarp tyrimų grupių, neatsižvelgiant į minėtus parametrus. Anksčiau aptarti tyrimai rodo, kad šie aplinkos veiksniai gali turėti didžiulę įtaką baltymų agregacijos procesui, paveikdami ne tik kinetinius parametrus, bet ir susidariusių fibrilių struktūrą ar kitas savybes[154,213]. Todėl buvo svarbu atidžiai išanalizuoti, kaip kiekvienas sąlygų derinys veikia insulino agregacijos procesą. Siekiant to, šiame darbe insulino amiloidinė agregacija buvo tiriama naudojant įvairias pH vertes (1,0–3,0), skirtingos joninės jėgos tirpalus (100 mM–500 mM), taip pat tris tirpalo komponentus (acto rūgštį, druskos rūgštį ir natrio fosfatą).

Visomis minėtomis sąlygomis buvo atlikta insulino agregacija, siekiant įvertinti jų įtaką fibrilių susidarymo kinetikai. Esant žemam pH natrio fosfato tirpaluose, reakcijos kinetiniai parametrai buvo gana panašūs visose joninės jėgos sąlygose. Tačiau didžiausios išbandytos pH sąlygos (2,5–3,0) lėmė drastišką proceso lag laiko padidėjimą. Tokie rezultatai gali būti susiję su insulino oligomerine būsena ir tirpumu. Šiomis sąlygomis insulino tirpumas buvo mažas, o nustatytas hidrodinaminis skersmuo buvo didelis, o tai galėtų paaiškinti lėtą branduolių susidarymo procesą. Tačiau druskos rūgšties atveju didžiausios joninės jėgos sąlygos davė palyginti didelį insulino hidrodinaminį skersmenį, o ryškaus poveikio lag laikui nepastebėta. Šie rezultatai rodo, kad insulino oligomerinė būsena yra tik vienas iš komponentų, lemiančių jo polinkį amiloidinei agregacijai. Oligomerinės būsenos įtaką taip pat patvirtina ankstesni tyrimai. Pastebėta, kad kai kuriais atvejais amiloidogeninio pirmtako disociacija iš oligomerinės būsenos į monomerinę yra greitį ribojanti reakcija ir ji vyksta lėčiau nei branduolio susidarymas[216].

Šio tyrimo metu taip pat buvo pastebėtas įdomus reiškinys. Tam tikromis sąlygomis, priklausomai nuo pH arba joninės jėgos, surišto ThT signalo intensyvumo pokytis neatitiko įprastos sigmoidės formos kinetikos. Vietoj to, buvo aptikta arba dviguba sigmoidinė kinetika, arba be galo didėjantis fluorescencijos intensyvumas. Analizuojant gautus rezultatus, nustatyta, kad šios kreivės atsirado tik esant kelioms specifinėms sąlygoms. Esant žemam pH, dažniau buvo stebimos nuolat didėjančios fluorescencijos kreivės, o dvigubos sigmoidinės – esant tarpiniam pH ir mažos joninės jėgos sąlygoms. Dviguba sigmoidinė kinetika anksčiau literatūroje buvo aprašyta kaip teigiamu-ThT pasižyminčių tarpinių agregacijos produktų rezultatas, o nuolat didėjanti fluorescencija gali būti susijusi su fibrilių brendimu arba klasterių susidarymu[71,206,217].

Nors analizuojant kinetinius duomenis įvairiomis sąlygomis buvo įmanoma nustatyti tam tikras tendencijas, lyginant agregatų antrines struktūras, padėtis buvo daug sudėtingesnė. Tarp visų sąlygų pastebėtas didelis FTIR spektrų variabilumas ir nebuvo aiškios nuo sąlygų priklausančios tendencijos, priešingai nei analizuojant agregatų morfologiją. Esant žemam pH ir joninei jėgos, AJM metodu buvo aptiktos ilgos, susipynusios struktūros, kurių aukštis buvo santykinai mažas. Didesnė joninė jėga ir pH buvo palankūs trumpų fibrilių ir didelio skaičiaus amorfinių agregatų susidarymui. Acto rūgšties sąlygos ir didelės NaCl koncentracijos sudarė didžiausias struktūras, kurias suformavo daug ilgų, lateraliai asocijuotų filamentų. Visų šių fibrilių struktūrų dydis taip pat buvo tiesiogiai susijęs su jų stabilumu denatūruojančiomis sąlygomis. Toks pats joninės jėgos poveikis insulino fibrilių šoninei asociacijai acto rūgštyje buvo pastebėtas ir kitame tyrime. To tyrimo autoriai mano, kad šis poveikis susijęs su insulino oligomerine būsena[218].

Alfa-sinukleino agregacijos slopinimas imidazotiazino dariniais

Šiuo metu bandant surasti vaistus įvairių su amiloidine baltymų agregacija susijusių neurodegeneracinių sutrikimų gydymui, mokslininkams vis dar iškyla labai daug problemų. Dažnai yra siekiama susintetinti mažamolekulinį junginį, kuris galėtų pereiti kraujo-smegenų barjerą ir sustabdyti baltymų agregacijos procesą. Nepaisant to, kad nemažai junginių dažnai parodo inhibicijos potencialą pradiniuose agregacijos slopiklių atrankos etapuose, tačiau tik ne daugelis būna patvirtinti tolimesnėse fazėse, todėl svarbu nustatyti kas lemia šias nesėkmes. Analizuojant insulino agregaciją skirtingų cheminių junginių kaip pagrindinių tirpalo komponentų sąlygomis buvo pastebėta, kad šis faktorius pakeičia ne tik agregacijos kinetinius parametrus, bet ir nulemia susidarančių fibrilių antrinės struktūros, bei morfologijos skirtumus. Todėl toliau buvo siekiama išsiaiškinti ar potencialiai slopinantys mažamolekuliniai junginiai gali pakeisti alfa-sinukleino agregacijos procesą.

Analizuojant agregacijos slopinimo-junginio struktūros santykį, buvo pastebėta, kad svarbiausią vaidmenį šiame procese atliko tiazino žiedas. Junginiai, kurie neturėjo šio struktūros elemento, nepakeitė nei agregacijos puslaikio, nei fluorescencijos intensyvumo galutinio taško lyginant su kontroliniais mėginiais. Neskaitant savo slopinimo efektyvumo, daugeliu atveju alfa-sinukleinui agreguojant su imidazotiazinais, mėginiai pasižymėjo padidėjusiu fluorescencijos intensyvumu, nors patys junginiai tokiame sužadinimo-emisijos ruože nefluorescavo. Tokį efektą galima būtų paaiškinti dviem būdais – arba dalyvaujant junginiui pusiausvyra tarp agreguoto ir natyvaus alfa-sinukleino buvo pastumta fibrilių susidarymo kryptimi, arba agregacijos metu susidarė agregatai, pasižymintys skirtingu ThT jungimosi būdu[134,137,219]. Ankstesniuose tyrimuose buvo pastebėta, kad inhibitoriai gali pakeisti alfa-sinukleino agregacijos procesą susidarant skirtingo tipo fibrilėms[138].

Ši galimybė toliau buvo patvirtinta analizuojant susidariusių agregatų FTIR spektrus. Kontrolinių mėginių atveju buvo išskirti trys tipai spektrų. Toks alfa-sinukleino agregatų polimorfizmas buvo pastebėtas anksčiau panašiomis sąlygomis Toleikis ir jo kolegų tyrime[220]. Mūsų darbe alfa-sinukleinui agreguojant kartu su imidazotiazino dariniais, buvo nustatyti keturi papildomi FTIR spektrai. Įdomu tai, kad junginių, kurie padidino agregacijos puslaikį ir/arba fluorescencijos intensyvumą, atvejais dažniausiai susidarė agregatai, kurių FTIR spektrai buvo nebūdingi kontroliniams mėginiams. Tokie rezultatai aprodo galimą koreliaciją tarp junginio slopinimo efektyvumo, susidarančių fibrilių antrinių struktūrų tipo, bei ThT jungimo savybių.

Nors šie junginiai pasižymi stipriu anti-amiloidiniu aktyvumu, tačiau svarbu atsižvelgti ir į jų citotoksiškumą. Atlikus MTT tyrimą buvo pastebėta, kad visi atrinkti junginiai statistiškai reikšmingai sumažino SH-SY5Y neuroblastomos ląstelių gyvybingumą. Vis dėlto analizuojant ląstelių gyvybingumą mėginyje esant junginiui kartu su alfa-sinukleino fibrilėmis, buvo pastebėta, kad kai kuriais atvejais toksiškumas ląstelėms sumažėjo. Tokie rezultatai rodo galimą dvigubą naudą – junginys slopina alfa-sinukleino agregaciją ir tuo pačiu mažina susidariusių fibrilių žalingą poveikį. Panašūs rezultatai buvo pastebėti Seidler tyrimo metu, kai tau baltymo fibriles painkubavus su mažamolekuliniu junginiu EGCG, jų citotoksiškumas sumažėjo lyginant su kontrole[221]. Vis dėlto mūsų tyrimo rezultatai parodo, kad kuriant naujus potencialius anti-amiloidinius junginius yra būtina atsižvelgti ne tik kaip jie slopina baltymų amiloidinę agregaciją, tačiau ir kaip paveikia agregacijos mechanizmą, bei ląsteles *in vivo*.

Baltymo-baltymo sąveika

Amiloidinių baltymų agregacija fiziologinėmis sąlygomis vyksta aplinkoje, kurioje gausu įvairių makromolekulių, įskaitant kitus baltymus. Dažnai mechanistiniai *in vitro* agregacijos tyrimai atliekami naudojant tik vieno tipo amiloidinį baltymą ir neatsižvelgiama į tai, kaip kitos molekulės gali paveikti šį procesą. Ankstesniuose tyrimuose buvo parodyta, kad amiloidinėse plokštelėse gali būti randama daug skirtingų amiloidogeninių baltymų, taip pat jie gali paveikti vienas kito agregacijos kinetiką[163,222]. Todėl yra svarbu toliau tirti, kaip baltymo-baltymo sąveika gali paveikti amiloidinių fibrilių susidarymo procesą.

Visų pirma, toks procesas gali pakeisti agregacijos kinetiką. Tai buvo pastebėta ir šiame darbe, tiriant prioninio baltymo ir SOD1 sąveiką. Kai prioninis baltymas agregavo esant SOD1, branduolių susidarymo procesas buvo slopinamas, o reakcijos lag laikas pailgėjo. Panašus poveikis anksčiau buvo pastebėtas *in vivo* – kai SOD1 trūkumas pagreitino prioninio baltymo agregaciją[223]. Šiame darbe poveikis PrP agregacijos kinetikai taip pat priklausė nuo SOD1 koncentracijos. Pastebėta, kad esant ekvimolinėms koncentracijoms, padidėjo tik lag laikas, tačiau didesnės šio baltymo koncentracijos taip pat sumažino rezultatų stochastiškumą ir greičio konstantą. Šiuos skirtumus būtų galima paaiškinti įmanoma SOD1 sąveika su prioniniu baltymu branduolių susidarymo fazės metu, kuri veikia susidariusių fibrilių antrinę struktūrą ir morfologiją. Tačiau šis poveikis nebūdingas visoms baltymų sąveikoms. Kitame Honda tyrime pastebėta, kad amiloidas-beta pagreitina prioninio baltymo amiloidinę agregaciją esant mikromolinėms koncentracijoms[163].

Šiame darbe, analizuodami prioninio baltymo ir S100A9 sąveiką, stebėjome tokį patį poveikį branduolių susidarymo procesui. Natyvi S100A9 forma slopino prioninio baltymo branduolių susidarymą, o agreguota forma neturėjo jokio pastebimo poveikio šiam procesui. Šie rezultatai patvirtina hipotezę, kad ir šiuo atveju natyvi S100A9 baltymo forma gali sutrikdyti PrP branduolių susidarymo procesą, sąveikaudama su monomeriniu PrP arba jo prefibriline forma. Tačiau S100A9 agregatai padidino prioninio baltymo agregacijos greičio konstantą. Tai greičiausiai lemia hidrofobinis S100A9 fibrilių paviršius, kuris veikia kaip katalizatorius paviršiaus inicijuojamai antrinei nukleacijai[224].

Kadangi žinoma, kad S100A9 fiziologinėmis sąlygomis gali savaime agreguoti, tikėtina, kad šio baltymo agregacija bent iš dalies susijusi su prioninių ligų išsivystymu[225,226]. Šie du baltymai randami kartu smegenų žievėje ir skystyje, todėl įmanoma, kad S100A9 turi dvejopą poveikį, pagrįstą savo būsena[225–227]. Natyvi S100A9 forma slopina prioninio baltymo

branduolių susidarymą, o agreguota būsena tarnauja kaip paviršius naujiems PrP branduoliams.

Kitas svarbus aspektas yra poveikis fibrilių struktūrai. Kadangi kito baltymo dalyvavimas natyvia arba agreguota forma stipriai veikia agregacijos mechanizmą, jis paprastai taip pat sukelia struktūrinius pokyčius. Šiame PrP ir SOD1 sąveikos tyrime buvo nustatytas poveikis PrP amiloidinių struktūrų kintamumui. Kai reakcijoje nedalyvavo SOD1, FTIR analizė parodė, kad prioninis baltymas suformavo trijų skirtingų tipų fibriles. Esant ekvimolinei SOD1 koncentracijai, agregatų pasiskirstymas pasikeitė ir susidarė nauja izoforma. Kai SOD1 koncentracija dar labiau padidėjo, konformacinis variabilumas išnyko ir dauguma FTIR spektrų buvo identiški. Panašus sąveikos poveikis vieno tipo agregatų stabilizavimui buvo pastebėtas Toleikis ir jo kolegų darbe analizuojant S100A9 sąveiką su alfa-sinukleinu[220].

Jei darytume prielaidą, kad PrP fibrilų kamienas priklauso nuo pradinių branduolių konformacijos, tai reikštų, kad pradinių agregacijos branduolių susidarymo procesas yra tiesiogiai paveiktas dėl galimos šių dviejų baltymų sąveikos. Tikėtina, kad SOD1 sutrikdo tam tikrų PrP branduolių susidarymą, taip pakeisdamas reakciją link specifinės konformacijos. Šis procesas taip pat gali būti susijęs su uždelsta lag faze, kai SOD1 tik pailgina bet kokios konformacijos nukleacijos laiką, taip sudarydamas galimybę atsirasti kamienams, kuriems susidaryti ir tapti dominuojančiu tipu reikia ilgesnio laiko. Įdomu tai, kad identiškos SOD1 ir S100A9 koncentracijos neskatino to pačio PrP fibrilių kamieno susidarymo. Tai rodo, kad poveikis amiloidinės agregacijos procesui gali priklausyti nuo papildomai reakcijoje dalyvaujančio baltymo. Tokie rezultatai patvirtina, kad atliekant baltymų agregacijos tyrimus labai svarbu atsižvelgti į kitų makromolekulių dalyvavimą šioje reakcijoje, siekiant kuo labiau priartėti prie procesų, vykstančių fiziologinėmis sąlygomis.

IŠVADOS

1. Lizocimo išsivyniojimas pagreitina tiek nukleacijos procesą, tiek padidina agregacijos greičio konstantą. Žemesnėje nei lydymosi temperatūroje lizocimas sudaro beta-klostėmis praturtintas fibriles, linkusias į šoninę asociaciją.
2. Lizocimo agregatų struktūrinis kintamumas priklauso tiek nuo pH, tiek nuo dominuojančios baltymo susilankstymo būsenos agregacijos metu. Mažiausias struktūrinis variabilumas pastebėtas esant pH 5 ir 6, nepriklausomai nuo baltymo susilankstymo būsenos.
3. Struktūriškai skirtingų alfa-sinukleino agregatų inkubavimas aukštesnėje temperatūroje sukelia restruktūrizacijos procesą, dėl kurio susidaro identiška antrinė struktūra.
4. Insulino agregacija pasižymi savitomis tendencijomis, kurioms įtakos turi pH, joninė jėga ir pagrindinis tirpalo cheminis komponentas, o kinetinės kreivės kartais būna netaisyklingos formos (dviguba sigmoidė, nuolat kylanti fluorescencija). Be to tiek antrinė struktūra, tiek morfologija labai priklauso nuo aplinkos sąlygų.
5. Imidazotiazino dariniai daro įtaką tiek agregacijos puslaikiui, tiek susidariusių agregatų struktūriniam variabilumui. Taip pat nustatyta koreliacija tarp junginio slopinamojo poveikio ir susidariusių fibrilių tipo.
6. Baltymo-baltymo tarpusavio sąveika, ypač prioninio baltymo su SOD1 arba S100A9, gali slopinti branduolių susidarymo procesą, o S100A9 fibrilės taip pat gali veikti kaip paviršius prioninio baltymo paviršiaus inicijuotam branduolių susidarymui. Abiem atvejais ši tarpusavio sąveika stabilizavo vieną agregatų kamieną.

Apibendrinus, šie tyrimai analizuojant įvairių aplinkos veiksnių poveikį skirtingų amiloidogeninių baltymų agregacijos procesams parodo sudėtingą agregacijos aplinkos sąlygų ir susidarančių amiloidinių fibrilių struktūrų sąryšį.

REFERENCES/LITERATŪROS ŠALTINIAI

1. Thomas, R. H. Historical review. *Ger. Life Lett.* **5**, 66–68 (1951).
2. Ke, P. C. *et al.* Half a century of amyloids: past, present and future. *Chem. Soc. Rev.* **49**, 5473–5509 (2020).
3. Buxbaum, J. N. & Linke, R. P. A Molecular History of the Amyloidoses. *J. Mol. Biol.* **421**, 142–159 (2012).
4. Iadanza, M. G., Jackson, M. P., Hewitt, E. W., Ranson, N. A. & Radford, S. E. A new era for understanding amyloid structures and disease. *Nat. Rev. Mol. Cell Biol.* **19**, 755–773 (2018).
5. Yakupova, E. I., Bobyleva, L. G., Shumeyko, S. A., Vikhlyantsev, I. M. & Bobylev, A. G. Amyloids: The History of Toxicity and Functionality. *Biology (Basel).* **10**, 394 (2021).
6. Nizhnikov, A. A., Antonets, K. S. & Inge-Vechtomov, S. G. Amyloids: from pathogenesis to function. *Biochem.* **80**, 1127–1144 (2015).
7. Sola, D. *et al.* Diagnosis in Scrapie: Conventional Methods and New Biomarkers. *Pathogens* **12**, 1399 (2023).
8. Chiti, F. & Dobson, C. M. Protein Misfolding, Amyloid Formation, and Human Disease: A Summary of Progress Over the Last Decade. *Annu. Rev. Biochem.* **86**, 27–68 (2017).
9. Atkinson, C. J., Zhang, K., Munn, A. L., Wiegmans, A. & Wei, M. Q. Prion protein scrapie and the normal cellular prion protein. *Prion* **10**, 63–82 (2016).
10. Das, A. S. & Zou, W.-Q. Prions: Beyond a Single Protein. *Clin. Microbiol. Rev.* **29**, 633–658 (2016).
11. Sipe, J. D. & Cohen, A. S. Review: History of the Amyloid Fibril. *J. Struct. Biol.* **130**, 88–98 (2000).
12. Harrison, R. S., Sharpe, P. C., Singh, Y. & Fairlie, D. P. Amyloid peptides and proteins in review. in *Reviews of Physiology, Biochemistry and Pharmacology* **159**, 1–77 (Springer Berlin Heidelberg, 2007).
13. Yakupova, E. I., Bobyleva, L. G., Vikhlyantsev, I. M. & Bobylev, A. G. Congo Red and amyloids: history and relationship. *Biosci. Rep.* **39**, (2019).
14. Wang, W. & Roberts, C. J. Protein aggregation – Mechanisms, detection, and control. *Int. J. Pharm.* **550**, 251–268 (2018).

15. Chuang, E., Hori, A. M., Hesketh, C. D. & Shorter, J. Amyloid assembly and disassembly. *J. Cell Sci.* **131**, jcs189928 (2018).

16. Bourdenx, M. *et al.* Protein aggregation and neurodegeneration in prototypical neurodegenerative diseases: Examples of amyloidopathies, tauopathies and synucleinopathies. *Prog. Neurobiol.* **155**, 171–193 (2017).

17. Jahn, T. R. *et al.* The Common Architecture of Cross-β Amyloid. *J. Mol. Biol.* **395**, 717–727 (2010).

18. Sabaté, R. & Ventura, S. Cross-β-sheet supersecondary structure in amyloid folds: Techniques for detection and characterization. *Methods Mol. Biol.* **932**, 237–257 (2013).

19. Glenner, G. G., Terry, W., Harada, M., Isersky, C. & Page, D. Amyloid Fibril Proteins: Proof of Homology with Immunoglobulin Light Chains by Sequence Analyses. *Science (80-.).* **172**, 1150–1151 (1971).

20. Benditt, E. P., Eriksen, N., Hermodson, M. A. & Ericsson, L. H. The major proteins of human and monkey amyloid substance: Common properties including unusual N-terminal amino acid sequences. *FEBS Lett.* **19**, 169–173 (1971).

21. Prusiner, S. B. Novel Proteinaceous Infectious Particles Cause Scrapie. *Science (80-.).* **216**, 136–144 (1982).

22. Chiti, F. & Dobson, C. M. Protein Misfolding, Functional Amyloid, and Human Disease. *Annu. Rev. Biochem.* **75**, 333–366 (2006).

23. Knowles, T. P. J. *et al.* An Analytical Solution to the Kinetics of Breakable Filament Assembly. *Science (80-.).* **326**, 1533–1537 (2009).

24. Burton-Smith, R. N. *et al.* Elucidating the Unique J-Shaped Protomer Structure of Amyloid-β(1-40) Fibril with Cryo-Electron Microscopy. *Int. J. Mol. Sci.* **26**, 1179 (2025).

25. Sachse, C., Grigorieff, N. & Fändrich, M. Nanoscale Flexibility Parameters of Alzheimer Amyloid Fibrils Determined by Electron Cryo-Microscopy. *Angew. Chemie Int. Ed.* **49**, 1321–1323 (2010).

26. Fitzpatrick, A. W. & Saibil, H. R. Cryo-EM of amyloid fibrils and cellular aggregates. *Curr. Opin. Struct. Biol.* **58**, 34–42 (2019).

27. Ceska, T., Chung, C., Cooke, R., Phillips, C. & Williams, P. A. Cryo-EM in drug discovery. *Biochem. Soc. Trans.* **47**, 281–293 (2019).

28. Wegmann, S. *et al.* Tau protein liquid–liquid phase separation can

initiate tau aggregation. *EMBO J.* **37**, 1–21 (2018).

29. Lu, X. *et al.* The Role of Liquid-Liquid Phase Separation in the Accumulation of Pathological Proteins: New Perspectives on the Mechanism of Neurodegenerative Diseases. *Aging Dis.* **16**, 769 (2025).

30. Park, J. *et al.* Tafamidis: A First-in-Class Transthyretin Stabilizer for Transthyretin Amyloid Cardiomyopathy. *Ann. Pharmacother.* **54**, 470–477 (2020).

31. Abyadeh, M. *et al.* Comparative Analysis of Aducanumab, Zagotenemab and Pioglitazone as Targeted Treatment Strategies for Alzheimer's Disease. *Aging Dis.* **12**, 1964 (2021).

32. Vergaro, G. *et al.* Current and emerging treatment options for transthyretin amyloid cardiomyopathy. *Heart* heartjnl-2024-325184 (2025). doi:10.1136/heartjnl-2024-325184

33. Fontana, M. *et al.* Transthyretin amyloid cardiomyopathy: from cause to novel treatments. *Eur. Heart J.* 1–10 (2025). doi:10.1093/eurheartj/ehaf667

34. Elamin, S. A. *et al.* Anti-amyloid monoclonal antibody therapies in Alzheimer's disease – a scoping review. *Neuroscience* **589**, 50–61 (2025).

35. Bregman, N. *et al.* Lecanemab in clinical practice: real-world outcomes in early Alzheimer's disease. *Alzheimers. Res. Ther.* **17**, 119 (2025).

36. Siebrand, C. J., Bergo, N. J., Lee, S., Andersen, J. K. & Walton, C. C. Chimeric antigen receptors discriminate between tau and distinct amyloid-beta species. *J. Transl. Med.* **23**, 605 (2025).

37. Wu, C.-K. & Fuh, J.-L. A 2025 update on treatment strategies for the Alzheimer's disease spectrum. *J. Chinese Med. Assoc.* 1–29 (2025). doi:10.1097/JCMA.0000000000001252

38. Chowdhury, S. Monoclonal Antibody Treatments for Alzheimer's Disease: Aducanumab and Lecanemab. *Discoveries* **11**, e173 (2023).

39. Saido, T. C. & Iwata, N. The tale of donanemab: God is in the details. *J. Alzheimer's Dis.* **107**, 1364–1373 (2025).

40. Buxbaum, J. N. *et al.* Amyloid nomenclature 2024: update, novel proteins, and recommendations by the International Society of Amyloidosis (ISA) Nomenclature Committee. *Amyloid* **31**, 249–256 (2024).

41. Picken, M. M. The Pathology of Amyloidosis in Classification: A Review. *Acta Haematol.* **143**, 322–334 (2020).

42. Hazenberg, B. P. C. Amyloidosis. *Rheum. Dis. Clin. North Am.* **39**, 323–345 (2013).

43. Karatzetzou, S. *et al.* Iatrogenic Dementia: Providing Insight into Transmissible Subtype of Alzheimer's Disease, Creutzfeldt–Jakob Disease and Cerebral Amyloid Angiopathy. *Biomolecules* **15**, 522 (2025).

44. Gupta, Y., Singla, G. & Singla, R. Insulin-derived amyloidosis. *Indian J. Endocrinol. Metab.* **19**, 174 (2015).

45. Mehta, D., Jackson, R., Paul, G., Shi, J. & Sabbagh, M. Why do trials for Alzheimer's disease drugs keep failing? A discontinued drug perspective for 2010-2015. *Expert Opin. Investig. Drugs* **26**, 735–739 (2017).

46. Rajan, R. *et al.* Review of the current state of protein aggregation inhibition from a materials chemistry perspective: special focus on polymeric materials. *Mater. Adv.* **2**, 1139–1176 (2021).

47. Knowles, T. P. J., Vendruscolo, M. & Dobson, C. M. The amyloid state and its association with protein misfolding diseases. *Nat. Rev. Mol. Cell Biol.* **15**, 384–396 (2014).

48. Almeida, Z. L. & Brito, R. M. M. Structure and Aggregation Mechanisms in Amyloids. *Molecules* **25**, 1195 (2020).

49. Gade Malmos, K. *et al.* ThT 101: a primer on the use of thioflavin T to investigate amyloid formation. *Amyloid* **24**, 1–16 (2017).

50. Chaturvedi, S. K., Siddiqi, M. K., Alam, P. & Khan, R. H. Protein misfolding and aggregation: Mechanism, factors and detection. *Process Biochem.* **51**, 1183–1192 (2016).

51. Li, W., Li, H.-L., Wang, J.-Z., Liu, R. & Wang, X. Abnormal protein post-translational modifications induces aggregation and abnormal deposition of protein, mediating neurodegenerative diseases. *Cell Biosci.* **14**, 22 (2024).

52. Pounot, K. *et al.* Mutations in Tau Protein Promote Aggregation by Favoring Extended Conformations. *JACS Au* **4**, 92–100 (2024).

53. Housmans, J. A. J., Wu, G., Schymkowitz, J. & Rousseau, F. A guide to studying protein aggregation. *FEBS J.* **290**, 554–583 (2023).

54. Deva, T. *et al.* Off-pathway aggregation can inhibit fibrillation at high protein concentrations. *Biochim. Biophys. Acta - Proteins*

Proteomics **1834**, 677–687 (2013).

55. Adamcik, J. & Mezzenga, R. Amyloid Polymorphism in the Protein Folding and Aggregation Energy Landscape. *Angew. Chemie Int. Ed.* **57**, 8370–8382 (2018).

56. Whidden, M., Ho, A., Ivanova, M. I. & Schnell, S. Competitive inhibition reaction mechanisms for the two-step model of protein aggregation. *Biophys. Chem.* **193**–**194**, 9–19 (2014).

57. Tian, Y., Meng, L. & Zhang, Z. What is strain in neurodegenerative diseases? *Cell. Mol. Life Sci.* **77**, 665–676 (2020).

58. Christensen, C. S., Wang, S., Li, W., Yu, D. & Li, H. J. Structural Variations of Prions and Prion-like Proteins Associated with Neurodegeneration. *Curr. Issues Mol. Biol.* **46**, 6423–6439 (2024).

59. Furukawa, Y., Kaneko, K., Watanabe, S., Yamanaka, K. & Nukina, N. Intracellular seeded aggregation of mutant Cu,Zn-superoxide dismutase associated with amyotrophic lateral sclerosis. *FEBS Lett.* **587**, 2500–2505 (2013).

60. Hackert, M. L. & Riggs, A. F. When Size Matters. *Structure* **14**, 1094–1096 (2006).

61. Thacker, D., Barghouth, M., Bless, M., Zhang, E. & Linse, S. Direct observation of secondary nucleation along the fibril surface of the amyloid β 42 peptide. *Proc. Natl. Acad. Sci.* **120**, 1–9 (2023).

62. Kozell, A. *et al.* Sound-mediated nucleation and growth of amyloid fibrils. *Proc. Natl. Acad. Sci.* **121**, 9759–9770 (2024).

63. Howie, A. J. & Brewer, D. B. Optical properties of amyloid stained by Congo red: History and mechanisms. *Micron* **40**, 285–301 (2009).

64. Dapson, R. W. Amyloid from a histochemical perspective. A review of the structure, properties and types of amyloid, and a proposed staining mechanism for Congo red staining. *Biotech. Histochem.* **93**, 543–556 (2018).

65. Inouye, H. & Kirschner, D. A. Alzheimer's β-Amyloid: Insights into Fibril Formation and Structure from Congo Red Binding. in *Alzheimer's Disease* 203–224 (Springer US, 2014). doi:10.1007/0-387-23226-5_10

66. Frid, P., Anisimov, S. V. & Popovic, N. Congo red and protein aggregation in neurodegenerative diseases. *Brain Res. Rev.* **53**, 135–160 (2007).

67. Fernandez-Flores, A. A review of amyloid staining: methods and

artifacts. *Biotech. Histochem.* **86**, 293–301 (2011).

68. Siddiqui, S. I. *et al.* Investigation of Congo Red Toxicity towards Different Living Organisms: A Review. *Processes* **11**, 807 (2023).

69. Lindberg, D. J. *et al.* Binding of Thioflavin-T to Amyloid Fibrils Leads to Fluorescence Self-Quenching and Fibril Compaction. *Biochemistry* **56**, 2170–2174 (2017).

70. Biancalana, M. & Koide, S. Molecular mechanism of Thioflavin-T binding to amyloid fibrils. *Biochim. Biophys. Acta - Proteins Proteomics* **1804**, 1405–1412 (2010).

71. Ziaunys, M., Sakalauskas, A., Mikalauskaite, K. & Smirnovas, V. Exploring the occurrence of thioflavin-T-positive insulin amyloid aggregation intermediates. *PeerJ* **9**, e10918 (2021).

72. Baronaitė, I., Šulskis, D., Kopūstas, A., Tutkus, M. & Smirnovas, V. Formation of Calprotectin Inhibits Amyloid Aggregation of S100A8 and S100A9 Proteins. *ACS Chem. Neurosci.* **15**, 1915–1925 (2024).

73. Pretorius, E. *et al.* Both lipopolysaccharide and lipoteichoic acids potently induce anomalous fibrin amyloid formation: assessment with novel Amytracker™ stains. *J. R. Soc. Interface* **15**, 20170941 (2018).

74. Morten, M. J. *et al.* Quantitative super-resolution imaging of pathological aggregates reveals distinct toxicity profiles in different synucleinopathies. *Proc. Natl. Acad. Sci.* **119**, 1–12 (2022).

75. Li, D., Yang, Y., Li, C. & Liu, Y. The influence of hydrogen bonds on NIAD-4 for use in the optical imaging of amyloid fibrils. *Phys. Chem. Chem. Phys.* **19**, 15849–15855 (2017).

76. Peccati, F., Hernando, J., Blancafort, L., Solans-Monfort, X. & Sodupe, M. Disaggregation-induced fluorescence enhancement of NIAD-4 for the optical imaging of amyloid-β fibrils. *Phys. Chem. Chem. Phys.* **17**, 19718–19725 (2015).

77. Li, Y. *et al.* Fluorescence-Based Monitoring of Early-Stage Aggregation of Amyloid-β, Amylin Peptide, Tau, and α-Synuclein Proteins. *ACS Chem. Neurosci.* **15**, 3113–3123 (2024).

78. Bouzón-Arnáiz, I. *et al.* YAT2150 is irresistible in Plasmodium falciparum and active against Plasmodium vivax and Leishmania clinical isolates. *Sci. Rep.* **15**, 2941 (2025).

79. Owyong, T. C. *et al.* Development of NIAD-4 derivatives for fluorescence-based detection of protein aggregates. *Sensors & Diagnostics* **4**, 55–62 (2025).

80. Kajava, A. V. & Steven, A. C. β-Rolls, β-Helices, and Other β-Solenoid Proteins. in *Advances in Protein Chemistry* **73**, 55–96 (2006).

81. Kajava, A. V., Aebi, U. & Steven, A. C. The Parallel Superpleated Beta-structure as a Model for Amyloid Fibrils of Human Amylin. *J. Mol. Biol.* **348**, 247–252 (2005).

82. Vance, T. D. R., Ye, Q., Conroy, B. & Davies, P. L. Essential role of calcium in extending RTX adhesins to their target. *J. Struct. Biol. X* **4**, 100036 (2020).

83. Pedersen, J. S., Andersen, C. B. & Otzen, D. E. Amyloid structure – one but not the same: the many levels of fibrillar polymorphism. *FEBS J.* **277**, 4591–4601 (2010).

84. Makowski, L. The Structural Basis of Amyloid Strains in Alzheimer's Disease. *ACS Biomater. Sci. Eng.* **6**, 2498–2505 (2020).

85. Sharma, K. *et al.* Cryo-EM observation of the amyloid key structure of polymorphic TDP-43 amyloid fibrils. *Nat. Commun.* **15**, 486 (2024).

86. Simone Ruggeri, F., Habchi, J., Cerreta, A. & Dietler, G. AFM-Based Single Molecule Techniques: Unraveling the Amyloid Pathogenic Species. *Curr. Pharm. Des.* **22**, 3950–3970 (2016).

87. Gras, S. L., Waddington, L. J. & Goldie, K. N. Transmission Electron Microscopy of Amyloid Fibrils. in *Methods in Molecular Biology* **752**, 197–214 (2011).

88. Li, D. & Liu, C. Molecular rules governing the structural polymorphism of amyloid fibrils in neurodegenerative diseases. *Structure* **31**, 1335–1347 (2023).

89. Ziaunys, M., Sakalauskas, A., Mikalauskaite, K., Snieckute, R. & Smirnovas, V. Temperature-Dependent Structural Variability of Prion Protein Amyloid Fibrils. *Int. J. Mol. Sci.* **22**, 5075 (2021).

90. Adamcik, J. *et al.* Understanding amyloid aggregation by statistical analysis of atomic force microscopy images. *Nat. Nanotechnol.* **5**, 423–428 (2010).

91. Masson, P. & Lushchekina, S. Conformational Stability and Denaturation Processes of Proteins Investigated by Electrophoresis under Extreme Conditions. *Molecules* **27**, 6861 (2022).

92. Tycko, R. Amyloid Polymorphism: Structural Basis and Neurobiological Relevance. *Neuron* **86**, 632–645 (2015).

93. Sawaya, M. R., Hughes, M. P., Rodriguez, J. A., Riek, R. & Eisenberg, D. S. The expanding amyloid family: Structure, stability, function, and pathogenesis. *Cell* **184**, 4857–4873 (2021).

94. Ayers, J. I. *et al.* The Strain-Encoded Relationship between PrPSc Replication, Stability and Processing in Neurons is Predictive of the Incubation Period of Disease. *PLoS Pathog.* **7**, e1001317 (2011).

95. Bett, C. *et al.* Defining the Conformational Features of Anchorless, Poorly Neuroinvasive Prions. *PLoS Pathog.* **9**, e1003280 (2013).

96. Van der Kant, R., Louros, N., Schymkowitz, J. & Rousseau, F. Thermodynamic analysis of amyloid fibril structures reveals a common framework for stability in amyloid polymorphs. *Structure* **30**, 1178-1189.e3 (2022).

97. Ziaunys, M., Sneideris, T. & Smirnovas, V. Self-inhibition of insulin amyloid-like aggregation. *Phys. Chem. Chem. Phys.* **20**, 27638–27645 (2018).

98. Selivanova, O., Suvorina, M., Surin, A., Dovidchenko, N. & Galzitskaya, O. Insulin and Lispro Insulin: What is Common and Different in their Behavior? *Curr. Protein Pept. Sci.* **18**, 57–64 (2016).

99. Antolíková, E. *et al.* Non-equivalent Role of Inter- and Intramolecular Hydrogen Bonds in the Insulin Dimer Interface. *J. Biol. Chem.* **286**, 36968–36977 (2011).

100. Brange, J., Andersen, L., Laursen, E. D., Meyn, G. & Rasmussen, E. Toward Understanding Insulin Fibrillation. *J. Pharm. Sci.* **86**, 517–525 (1997).

101. Lambert, C. & Delgado, E. 100 Years since the Discovery of Insulin, from Its Discovery to the Insulins of the Future. *Biomedicines* **12**, 533 (2024).

102. Gancar, M. *et al.* Amyloid Aggregation of Insulin: An Interaction Study of Green Tea Constituents. *Sci. Rep.* **10**, 9115 (2020).

103. Dische, F. E. *et al.* Insulin as an amyloid-fibril protein at sites of repeated insulin injections in a diabetic patient. *Diabetologia* **31**, 158–161 (1988).

104. Nielsen, L. *et al.* Effect of Environmental Factors on the Kinetics of Insulin Fibril Formation: Elucidation of the Molecular Mechanism. *Biochemistry* **40**, 6036–6046 (2001).

105. Fleming, A. & B, P. R. S. L. On a remarkable bacteriolytic element found in tissues and secretions. *Proc. R. Soc. London. Ser. B,*

Contain. Pap. a Biol. Character **93**, 306–317 (1922).

106. Dolui, S. *et al.* Order, Disorder, and Reorder State of Lysozyme: Aggregation Mechanism by Raman Spectroscopy. *J. Phys. Chem. B* **124**, 50–60 (2020).

107. Hill, S. E., Robinson, J., Matthews, G. & Muschol, M. Amyloid Protofibrils of Lysozyme Nucleate and Grow Via Oligomer Fusion. *Biophys. J.* **96**, 3781–3790 (2009).

108. Frare, E. *et al.* Characterization of Oligomeric Species on the Aggregation Pathway of Human Lysozyme. *J. Mol. Biol.* **387**, 17–27 (2009).

109. How, S.-C. *et al.* Exploring the effects of methylene blue on amyloid fibrillogenesis of lysozyme. *Int. J. Biol. Macromol.* **119**, 1059–1067 (2018).

110. Al Adem, K., Lukman, S., Kim, T.-Y. & Lee, S. Inhibition of lysozyme aggregation and cellular toxicity by organic acids at acidic and physiological pH conditions. *Int. J. Biol. Macromol.* **149**, 921–930 (2020).

111. Perez, C. *et al.* Mechanism of Fibril and Soluble Oligomer Formation in Amyloid Beta and Hen Egg White Lysozyme Proteins. *J. Phys. Chem. B* **123**, 5678–5689 (2019).

112. Nelson, R. & Eisenberg, D. Structural Models of Amyloid-Like Fibrils. in *Advances in Protein Chemistry* **73**, 235–282 (2006).

113. Castle, A. R. & Gill, A. C. Physiological Functions of the Cellular Prion Protein. *Front. Mol. Biosci.* **4**, 1–25 (2017).

114. Sassa, Y., Kataoka, N., Inoshima, Y. & Ishiguro, N. Anti-PrP antibodies detected at terminal stage of prion-affected mouse. *Cell. Immunol.* **263**, 212–218 (2010).

115. Norrby, E. Prions and protein-folding diseases. *J. Intern. Med.* **270**, 1–14 (2011).

116. Kretzschmar, H. A. *et al.* Molecular Cloning of a Human Prion Protein cDNA. *DNA* **5**, 315–324 (1986).

117. Christen, B., Damberger, F. F., Pérez, D. R., Hornemann, S. & Wüthrich, K. Structural plasticity of the cellular prion protein and implications in health and disease. *Proc. Natl. Acad. Sci.* **110**, 8549–8554 (2013).

118. Aguzzi, A. & Lakkaraju, A. K. K. Cell Biology of Prions and Prionoids: A Status Report. *Trends Cell Biol.* **26**, 40–51 (2016).

119. Prusiner, S. B. Prions. *Proc. Natl. Acad. Sci.* **95**, 13363–13383 (1998).

120. Makarava, N., Savtchenko, R. & Baskakov, I. V. Purification and Fibrillation of Full-Length Recombinant PrP. in *Journal of Health and Social Behavior* **56**, 3–22 (2017).

121. Ziaunys, M., Sneideris, T. & Smirnovas, V. Formation of distinct prion protein amyloid fibrils under identical experimental conditions. *Sci. Rep.* **10**, 4572 (2020).

122. Race, B., Phillips, K., Meade-White, K., Striebel, J. & Chesebro, B. Increased Infectivity of Anchorless Mouse Scrapie Prions in Transgenic Mice Overexpressing Human Prion Protein. *J. Virol.* **89**, 6022–6032 (2015).

123. Riek, R. *et al.* NMR structure of the mouse prion protein domain PrP(121–231). *Nature* **382**, 180–182 (1996).

124. Apostol, M. I., Wiltzius, J. J. W., Sawaya, M. R., Cascio, D. & Eisenberg, D. Atomic Structures Suggest Determinants of Transmission Barriers in Mammalian Prion Disease. *Biochemistry* **50**, 2456–2463 (2011).

125. Bocharova, O. V., Breydo, L., Salnikov, V. V., Gill, A. C. & Baskakov, I. V. Synthetic prions generated in vitro are similar to a newly identified subpopulation of PrP Sc from sporadic Creutzfeldt-Jakob Disease. *Protein Sci.* **14**, 1222–1232 (2005).

126. Billeter, M. *et al.* Prion protein NMR structure and species barrier for prion diseases. *Proc. Natl. Acad. Sci.* **94**, 7281–7285 (1997).

127. Chatterjee, B. *et al.* Amyloid Core Formed of Full-Length Recombinant Mouse Prion Protein Involves Sequence 127–143 but Not Sequence 107–126. *PLoS One* **8**, e67967 (2013).

128. Shahnawaz, M. *et al.* Discriminating α-synuclein strains in Parkinson's disease and multiple system atrophy. *Nature* **578**, 273–277 (2020).

129. Maroteaux, L., Campanelli, J. & Scheller, R. Synuclein: a neuron-specific protein localized to the nucleus and presynaptic nerve terminal. *J. Neurosci.* **8**, 2804–2815 (1988).

130. Villar-Piqué, A., Lopes da Fonseca, T. & Outeiro, T. F. Structure, function and toxicity of alpha-synuclein: the Bermuda triangle in synucleinopathies. *J. Neurochem.* **139**, 240–255 (2016).

131. Ghosh, D., Mehra, S., Sahay, S., Singh, P. K. & Maji, S. K. α-synuclein aggregation and its modulation. *Int. J. Biol. Macromol.*

100, 37–54 (2017).

132. Wu, K.-P., Kim, S., Fela, D. A. & Baum, J. Characterization of Conformational and Dynamic Properties of Natively Unfolded Human and Mouse α-Synuclein Ensembles by NMR: Implication for Aggregation. *J. Mol. Biol.* **378**, 1104–1115 (2008).

133. Burré, J., Sharma, M. & Südhof, T. C. Cell Biology and Pathophysiology of α-Synuclein. *Cold Spring Harb. Perspect. Med.* **8**, a024091 (2018).

134. Sulatskaya, A. I. *et al.* Investigation of α-Synuclein Amyloid Fibrils Using the Fluorescent Probe Thioflavin T. *Int. J. Mol. Sci.* **19**, 2486 (2018).

135. Greten-Harrison, B. *et al.* αβγ-Synuclein triple knockout mice reveal age-dependent neuronal dysfunction. *Proc. Natl. Acad. Sci.* **107**, 19573–19578 (2010).

136. Buell, A. K. *et al.* Solution conditions determine the relative importance of nucleation and growth processes in α-synuclein aggregation. *Proc. Natl. Acad. Sci.* **111**, 7671–7676 (2014).

137. Ziaunys, M., Sakalauskas, A., Mikalauskaite, K. & Smirnovas, V. Polymorphism of Alpha-Synuclein Amyloid Fibrils Depends on Ionic Strength and Protein Concentration. *Int. J. Mol. Sci.* **22**, 12382 (2021).

138. Ziaunys, M., Mikalauskaite, K., Sakalauskas, A. & Smirnovas, V. Interplay between epigallocatechin-3-gallate and ionic strength during amyloid aggregation. *PeerJ* **9**, e12381 (2021).

139. Sanders, E. *et al.* The Stabilization of S100A9 Structure by Calcium Inhibits the Formation of Amyloid Fibrils. *Int. J. Mol. Sci.* **24**, 13200 (2023).

140. Xu, J. *et al.* S100A9 in sepsis: A biomarker for inflammation and a mediator of organ damage. *Biochem. Biophys. Res. Commun.* **752**, 151484 (2025).

141. Wang, C. *et al.* The role of pro-inflammatory S100A9 in Alzheimer's disease amyloid-neuroinflammatory cascade. *Acta Neuropathol.* **127**, 507–522 (2014).

142. Carapeto, A. P., Marcuello, C., Faísca, P. F. N. & Rodrigues, M. S. Morphological and Biophysical Study of S100A9 Protein Fibrils by Atomic Force Microscopy Imaging and Nanomechanical Analysis. *Biomolecules* **14**, 1091 (2024).

143. Gonzalez, L. L., Garrie, K. & Turner, M. D. Role of S100 proteins in

health and disease. *Biochim. Biophys. Acta - Mol. Cell Res.* **1867**, 118677 (2020).

144. Toleikis, Z. *et al.* Interactions between S100A9 and Alpha-Synuclein: Insight from NMR Spectroscopy. *Int. J. Mol. Sci.* **23**, 6781 (2022).

145. Horvath, I. *et al.* Co-aggregation of pro-inflammatory S100A9 with α-synuclein in Parkinson's disease: ex vivo and in vitro studies. *J. Neuroinflammation* **15**, 172 (2018).

146. Monteiro Neto, J. R. *et al.* SOD1, A Crucial Protein for Neural Biochemistry: Dysfunction and Risk of Amyotrophic Lateral Sclerosis. *Mol. Neurobiol.* (2025). doi:10.1007/s12035-025-05067-1

147. Tomar, V. R., Sharma, S., Siddhanta, S. & Deep, S. Biophysical and spectroscopical insights into structural modulation of species in the aggregation pathway of superoxide dismutase 1. *Commun. Chem.* **8**, 22 (2025).

148. Bedja-Iacona, L. *et al.* Post-Translational Variants of Major Proteins in Amyotrophic Lateral Sclerosis Provide New Insights into the Pathophysiology of the Disease. *Int. J. Mol. Sci.* **25**, 8664 (2024).

149. Moriyama, H. & Yokota, T. Recent Progress of Antisense Oligonucleotide Therapy for Superoxide-Dismutase-1-Mutated Amyotrophic Lateral Sclerosis: Focus on Tofersen. *Genes (Basel).* **15**, 1342 (2024).

150. Berdyński, M. *et al.* SOD1 mutations associated with amyotrophic lateral sclerosis analysis of variant severity. *Sci. Rep.* **12**, 103 (2022).

151. Huang, M., Liu, Y. U., Yao, X., Qin, D. & Su, H. Variability in SOD1-associated amyotrophic lateral sclerosis: geographic patterns, clinical heterogeneity, molecular alterations, and therapeutic implications. *Transl. Neurodegener.* **13**, 28 (2024).

152. Jonas, J. Cold Denaturation of Proteins. in *ACS Symposium Series* **676**, 310–323 (1997).

153. Takano, K., Tsuchimori, K., Yamagata, Y. & Yutani, K. Contribution of Salt Bridges near the Surface of a Protein to the Conformational Stability ,. *Biochemistry* **39**, 12375–12381 (2000).

154. Sneideris, T. *et al.* pH-Driven Polymorphism of Insulin Amyloid-Like Fibrils. *PLoS One* **10**, e0136602 (2015).

155. Lundberg, E., Olofsson, A., Westermark, G. T. & Sauer-Eriksson, A. E. Stability and fibril formation properties of human and fish transthyretin, and of the Escherichia coli transthyretin-related protein. *FEBS J.* **276**, 1999–2011 (2009).

156. Dill, K. A. Dominant forces in protein folding. *Biochemistry* **29**, 7133–7155 (1990).

157. Feng, Y., Taraban, M. & Yu, Y. B. The effect of ionic strength on the mechanical, structural and transport properties of peptide hydrogels. *Soft Matter* **8**, 11723 (2012).

158. Webster, J. M., Darling, A. L., Uversky, V. N. & Blair, L. J. Small Heat Shock Proteins, Big Impact on Protein Aggregation in Neurodegenerative Disease. *Front. Pharmacol.* **10**, 1–18 (2019).

159. Rutledge, B. S., Choy, W.-Y. & Duennwald, M. L. Folding or holding?—Hsp70 and Hsp90 chaperoning of misfolded proteins in neurodegenerative disease. *J. Biol. Chem.* **298**, 101905 (2022).

160. Sharma, S. K. & Priya, S. Expanding role of molecular chaperones in regulating α-synuclein misfolding; implications in Parkinson's disease. *Cell. Mol. Life Sci.* **74**, 617–629 (2017).

161. Ono, K., Takahashi, R., Ikeda, T. & Yamada, M. Cross-seeding effects of amyloid β-protein and α-synuclein. *J. Neurochem.* **122**, 883–890 (2012).

162. Huang, F. *et al.* Co-aggregation of α-synuclein with amyloid-β stabilizes β-sheet-rich oligomers and enhances the formation of β-barrels. *Phys. Chem. Chem. Phys.* **25**, 31604–31614 (2023).

163. Honda, R. Amyloid-β Peptide Induces Prion Protein Amyloid Formation: Evidence for Its Widespread Amyloidogenic Effect. *Angew. Chemie Int. Ed.* **57**, 6086–6089 (2018).

164. Vasconcelos, B. *et al.* Heterotypic seeding of Tau fibrillization by pre-aggregated Abeta provides potent seeds for prion-like seeding and propagation of Tau-pathology in vivo. *Acta Neuropathol.* **131**, 549–569 (2016).

165. Kuznetsova, I., Turoverov, K. & Uversky, V. What Macromolecular Crowding Can Do to a Protein. *Int. J. Mol. Sci.* **15**, 23090–23140 (2014).

166. Milto, K., Michailova, K. & Smirnovas, V. Elongation of Mouse Prion Protein Amyloid-Like Fibrils: Effect of Temperature and Denaturant Concentration. *PLoS One* **9**, e94469 (2014).

167. Šneideris, T. *et al.* Looking for a generic inhibitor of amyloid-like fibril formation among flavone derivatives. *PeerJ* **3**, e1271 (2015).

168. Musteikyte, G., Ziaunys, M. & Smirnovas, V. Methylene blue inhibits nucleation and elongation of SOD1 amyloid fibrils. *PeerJ* **8**, e9719 (2020).

169. Feng, Z., Li, Y. & Bai, Y. Elevated temperatures accelerate the formation of toxic amyloid fibrils of hen egg-white lysozyme. *Vet. Med. Sci.* **7**, 1938–1947 (2021).

170. Lapidus, L. J. Protein unfolding mechanisms and their effects on folding experiments. *F1000Research* **6**, 1723 (2017).

171. Weiffert, T. *et al.* Influence of denaturants on amyloid β42 aggregation kinetics. *Front. Neurosci.* **16**, 1–20 (2022).

172. Thorlaksen, C. *et al.* Subtle pH variation around pH 4.0 affects aggregation kinetics and aggregate characteristics of recombinant human insulin. *Eur. J. Pharm. Biopharm.* **179**, 166–172 (2022).

173. Sarimov, R. M., Binhi, V. N., Matveeva, T. A., Penkov, N. V. & Gudkov, S. V. Unfolding and Aggregation of Lysozyme under the Combined Action of Dithiothreitol and Guanidine Hydrochloride: Optical Studies. *Int. J. Mol. Sci.* **22**, 2710 (2021).

174. Gade Malmos, K. *et al.* ThT 101: a primer on the use of thioflavin T to investigate amyloid formation. *Amyloid* **24**, 1–16 (2017).

175. Foderà, V. *et al.* Thioflavin T Hydroxylation at Basic pH and Its Effect on Amyloid Fibril Detection. *J. Phys. Chem. B* **112**, 15174–15181 (2008).

176. Guliyeva, A. J. & Gasymov, O. K. ANS fluorescence: Potential to discriminate hydrophobic sites of proteins in solid states. *Biochem. Biophys. Reports* **24**, 100843 (2020).

177. Younan, N. D. & Viles, J. H. A Comparison of Three Fluorophores for the Detection of Amyloid Fibers and Prefibrillar Oligomeric Assemblies. ThT (Thioflavin T); ANS (1-Anilinonaphthalene-8-sulfonic Acid); and bisANS (4,4′-Dianilino-1,1′-binaphthyl-5,5′-disulfonic Acid). *Biochemistry* **54**, 4297–4306 (2015).

178. Van Hee, P. *et al.* Selective recovery of micrometer particles from mixtures using a combination of selective aggregation and dissolved-air flotation. *Colloids Surfaces A Physicochem. Eng. Asp.* **280**, 216–231 (2006).

179. Meisl, G. *et al.* Molecular mechanisms of protein aggregation from global fitting of kinetic models. *Nat. Protoc.* **11**, 252–272 (2016).

180. Natalello, A. & Doglia, S. M. Insoluble Protein Assemblies Characterized by Fourier Transform Infrared Spectroscopy. in *Methods in Molecular Biology* **1258**, 347–369 (2015).

181. Kurouski, D., Van Duyne, R. P. & Lednev, I. K. Exploring the structure and formation mechanism of amyloid fibrils by Raman

spectroscopy: a review. *Analyst* **140**, 4967–4980 (2015).

182. Watson, M. D. & Lee, J. C. Coupling chemical biology and vibrational spectroscopy for studies of amyloids in vitro and in cells. *Curr. Opin. Chem. Biol.* **64**, 90–97 (2021).

183. Bashir, S. *et al.* Probing protein aggregation through spectroscopic insights and multimodal approaches: A comprehensive review for counteracting neurodegenerative disorders. *Heliyon* **10**, e27949 (2024).

184. Miles, A. J. & Wallace, B. A. Circular dichroism spectroscopy of membrane proteins. *Chem. Soc. Rev.* **45**, 4859–4872 (2016).

185. Micsonai, A., Bulyáki, É. & Kardos, J. BeStSel: From Secondary Structure Analysis to Protein Fold Prediction by Circular Dichroism Spectroscopy. in *Methods in Molecular Biology* **2199**, 175–189 (2021).

186. Ziaunys, M., Mikalauskaite, K. & Smirnovas, V. Amyloidophilic Molecule Interactions on the Surface of Insulin Fibrils: Cooperative Binding and Fluorescence Quenching. *Sci. Rep.* **9**, 20303 (2019).

187. Ziaunys, M., Sakalauskas, A. & Smirnovas, V. Identifying Insulin Fibril Conformational Differences by Thioflavin-T Binding Characteristics. *Biomacromolecules* **21**, 4989–4997 (2020).

188. Girych, M. *et al.* Combined thioflavin T-Congo red fluorescence assay for amyloid fibril detection. *Methods Appl. Fluoresc.* **4**, 34010 (2016).

189. Goodwin, A. M. In vitro assays of angiogenesis for assessment of angiogenic and anti-angiogenic agents. *Microvasc. Res.* **74**, 172–183 (2007).

190. Gutiérrez, L. *et al.* Nanotechnology in Drug Discovery and Development. in *Comprehensive Medicinal Chemistry III* **1**–**8**, 264–295 (Elsevier, 2017).

191. Kaja, S., Payne, A. J., Naumchuk, Y. & Koulen, P. Quantification of Lactate Dehydrogenase for Cell Viability Testing Using Cell Lines and Primary Cultured Astrocytes. *Curr. Protoc. Toxicol.* **72**, 814–818 (2017).

192. Cox, M. C. *et al.* Application of LDH assay for therapeutic efficacy evaluation of ex vivo tumor models. *Sci. Rep.* **11**, 18571 (2021).

193. Lorber, B., Fischer, F., Bailly, M., Roy, H. & Kern, D. Protein analysis by dynamic light scattering: Methods and techniques for students. *Biochem. Mol. Biol. Educ.* **40**, 372–382 (2012).

194. Han, Q. *et al.* Scattering approaches to unravel protein solution behaviors in ionic liquids and deep eutectic solvents: From basic principles to recent developments. *Adv. Colloid Interface Sci.* **331**, 103242 (2024).

195. Rubin, J., San Miguel, A., Bommarius, A. S. & Behrens, S. H. Correlating Aggregation Kinetics and Stationary Diffusion in Protein−Sodium Salt Systems Observed with Dynamic Light Scattering. *J. Phys. Chem. B* **114**, 4383–4387 (2010).

196. Andlinger, D. J., Schrempel, U., Hengst, C. & Kulozik, U. Heat-induced aggregation kinetics of potato protein – Investigated by chromatography, calorimetry, and light scattering. *Food Chem.* **389**, 133114 (2022).

197. Simmons, M. J. H., Jayaraman, P. & Fryer, P. J. The effect of temperature and shear rate upon the aggregation of whey protein and its implications for milk fouling. *J. Food Eng.* **79**, 517–528 (2007).

198. Džupponová, V., Huntošová, V. & Žoldák, G. A kinetic coupling between protein unfolding and aggregation controls time-dependent solubility of the human myeloma antibody light chain. *Protein Sci.* **29**, 2408–2421 (2020).

199. Chai, J., Zhao, X., Xu, Y. & Xu, X. An unfolding/aggregation kinetic instructed rational design towards improving graft degree of glycation for myofibrillar protein. *Food Chem.* **446**, 138876 (2024).

200. Cao, Y., Adamcik, J., Diener, M., Kumita, J. R. & Mezzenga, R. Different Folding States from the Same Protein Sequence Determine Reversible vs Irreversible Amyloid Fate. *J. Am. Chem. Soc.* **143**, 11473–11481 (2021).

201. Rovnyagina, N. R. *et al.* Binding of thioflavin T by albumins: An underestimated role of protein oligomeric heterogeneity. *Int. J. Biol. Macromol.* **108**, 284–290 (2018).

202. Sedov, I. & Khaibrakhmanova, D. Molecular Mechanisms of Inhibition of Protein Amyloid Fibril Formation: Evidence and Perspectives Based on Kinetic Models. *Int. J. Mol. Sci.* **23**, (2022).

203. Basha, S., Mukunda, D. C., Pai, A. R. & Mahato, K. K. Assessing amyloid fibrils and amorphous aggregates: A review. *Int. J. Biol. Macromol.* **311**, 143725 (2025).

204. Ikenoue, T. *et al.* Cold Denaturation of α-Synuclein Amyloid Fibrils. *Angew. Chemie Int. Ed.* **53**, 7799–7804 (2014).

205. Ziaunys, M. *et al.* Liquid–liquid phase separation of alpha-synuclein

increases the structural variability of fibrils formed during amyloid aggregation. *FEBS J.* **291**, 4522–4538 (2024).

206. Sidhu, A., Segers-Nolten, I., Raussens, V., Claessens, M. M. A. E. & Subramaniam, V. Distinct Mechanisms Determine α-Synuclein Fibril Morphology during Growth and Maturation. *ACS Chem. Neurosci.* **8**, 538–547 (2017).

207. Bocharova, O. V. *et al.* Annealing Prion Protein Amyloid Fibrils at High Temperature Results in Extension of a Proteinase K-resistant Core. *J. Biol. Chem.* **281**, 2373–2379 (2006).

208. Miti, T., Mulaj, M., Schmit, J. D. & Muschol, M. Stable, Metastable, and Kinetically Trapped Amyloid Aggregate Phases. *Biomacromolecules* **16**, 326–335 (2015).

209. Schmittschmitt, J. P. & Scholtz, J. M. The role of protein stability, solubility, and net charge in amyloid fibril formation. *Protein Sci.* **12**, 2374–2378 (2003).

210. Haezebrouck, P. *et al.* An Equilibrium Partially Folded State of Human Lysozyme at Low pH. *J. Mol. Biol.* **246**, 382–387 (1995).

211. Frey, L. *et al.* On the pH-dependence of α-synuclein amyloid polymorphism and the role of secondary nucleation in seed-based amyloid propagation. *Elife* **12**, 1–29 (2024).

212. Xu, W., Zhang, C., Morozova-Roche, L., Zhang, J. Z. H. & Mu, Y. pH-Dependent Conformational Ensemble and Polymorphism of Amyloid-β Core Fragment. *J. Phys. Chem. B* **117**, 8392–8399 (2013).

213. Marek, P. J., Patsalo, V., Green, D. F. & Raleigh, D. P. Ionic Strength Effects on Amyloid Formation by Amylin Are a Complicated Interplay among Debye Screening, Ion Selectivity, and Hofmeister Effects. *Biochemistry* **51**, 8478–8490 (2012).

214. Nettleton, E. J. *et al.* Characterization of the oligomeric states of insulin in self-assembly and amyloid fibril formation by mass spectrometry. *Biophys. J.* **79**, 1053–1065 (2000).

215. Zazeri, G., Povinelli, A. P. R., Pavan, N. M., Jones, A. M. & Ximenes, V. F. Solvent-Induced Lag Phase during the Formation of Lysozyme Amyloid Fibrils Triggered by Sodium Dodecyl Sulfate: Biophysical Experimental and In Silico Study of Solvent Effects. *Molecules* **28**, 6891 (2023).

216. Ecroyd, H. *et al.* Dissociation from the Oligomeric State Is the Rate-limiting Step in Fibril Formation by κ-Casein. *J. Biol. Chem.* **283**, 9012–9022 (2008).

217. Grudzielanek, S., Smirnovas, V. & Winter, R. Solvation-assisted pressure tuning of insulin fibrillation: From novel aggregation pathways to biotechnological applications. *J. Mol. Biol.* **356**, 497–509 (2006).

218. Thorlaksen, C. *et al.* Morphological integrity of insulin amyloid-like aggregates depends on preparation methods and post-production treatments. *Eur. J. Pharm. Biopharm.* **179**, 147–155 (2022).

219. Sidhu, A., Vaneyck, J., Blum, C., Segers-Nolten, I. & Subramaniam, V. Polymorph-specific distribution of binding sites determines thioflavin-T fluorescence intensity in α-synuclein fibrils. *Amyloid* **25**, 189–196 (2018).

220. Toleikis, Z. *et al.* S100A9 Alters the Pathway of Alpha-Synuclein Amyloid Aggregation. *Int. J. Mol. Sci.* **22**, 7972 (2021).

221. Seidler, P. M. *et al.* Structure-based discovery of small molecules that disaggregate Alzheimer's disease tissue derived tau fibrils in vitro. *Nat. Commun.* **13**, 5451 (2022).

222. Guo, J. L. *et al.* Distinct α-Synuclein Strains Differentially Promote Tau Inclusions in Neurons. *Cell* **154**, 103–117 (2013).

223. Akhtar, S. *et al.* Sod1 Deficiency Reduces Incubation Time in Mouse Models of Prion Disease. *PLoS One* **8**, e54454 (2013).

224. Koloteva-Levine, N. *et al.* Amyloid particles facilitate surface-catalyzed cross-seeding by acting as promiscuous nanoparticles. *Proc. Natl. Acad. Sci.* **118**, 1–12 (2021).

225. Kim, M.-S. *et al.* A draft map of the human proteome. *Nature* **509**, 575–581 (2014).

226. Guldbrandsen, A. *et al.* In-depth Characterization of the Cerebrospinal Fluid (CSF) Proteome Displayed Through the CSF Proteome Resource (CSF-PR). *Mol. Cell. Proteomics* **13**, 3152–3163 (2014).

227. Bauernfeind, A. L. *et al.* High spatial resolution proteomic comparison of the brain in humans and chimpanzees. *J. Comp. Neurol.* **523**, 2043–2061 (2015).

CURRICULUM VITAE

EDUCATION:

2015 - 2019: Bachelor's degree in Biochemistry, Vilnius University, Vilnius, Lithuania.
2019 - 2021: Master's degree in Pharmaceutical Chemistry, Vilnius University, Vilnius, Lithuania.
2021 - 2025: PhD studies in Chemical Engineering, Vilnius University, Vilnius, Lithuania

WORK EXPERIENCE:

2018 – 2020: Intern at Amyloid Research Group, Institute of Biotechnology, Vilnius University, Vilnius, Lithuania.
2020 – 2023: Project technician at Amyloid Research Sector, Institute of Biotechnology, Vilnius University, Vilnius, Lithuania.
2021 – current: Junior researcher at Amyloid Research Sector, Institute of Biotechnology, Vilnius University, Vilnius, Lithuania.
2022 – current: Occupational Health and Safety Specialist in the Amyloid Research Sector.

PARTICIPATION IN PROJECTS

1. European Social Fund project operated by Central Project Management Agency „Exploring drug candidates for cancer and neurodegenerative diseases“ (01.2.2-CPVA-K-703-03-0006) 2020-2023;
2. Lithuanian researcher group project P-MIP-22-115 "Cross-interactions in amyloid fibril formation: the role of pro-inflammatory S100A9 protein" 2022-2025
3. National researcher group project S-MIP-24-52 "Cross-interaction between pro-inflammatory "S100A9 and neurodegenerative disease-related proteins during liquid-liquid phase separation". 2024-2027
4. Lithuanian-Latvian-Taiwan joint project Nr. TAP LLT-24-14 "Structure determination of transthyretin amyloid fibrils" 2024 – 2026.

Science promotion activities
One of the practical part presenters in an event organized by The COINS "Scientific article writing ABC"

LIST OF PUBLICATIONS/PUBLIKACIJŲ SĄRAŠAS

Publications included in the dissertation/Publikacijos įtrauktos į disertaciją

1. Ziaunys, M., **Mikalauskaite, K.**, Veiveris, D., Sakalauskas, A., Smirnovas, V. Superoxide dismutase-1 alters the rate of prion protein aggregation and resulting fibril conformation. Arch. Biochem. Biophys. 715, 109096 (2022). Contribution: I conceptualized part of the research plan, purified prion protein and performed FTIR measurements, as well as data analysis. I also contributed to the initial manuscript preparation and further modifications during the review process.
2. **Mikalauskaite, K.**, Ziaunys, M., Smirnovas, V. Lysozyme Amyloid Fibril Structural Variability Dependence on Initial Protein Folding State. Int. J. Mol. Sci. 23, 5421 (2022). Contribution: I conceptualized part of the research plan, performed FTIR, EEM and AFM measurements, as well as data analysis. I also contributed to the initial manuscript preparation and figure preparation, as well as further modifications during the review process.
3. Ziaunys, M., Sakalauskas, A., **Mikalauskaite, K.**, Smirnovas, V. Rapid restructurization of conformationally-distinct alpha-synuclein amyloid fibrils at an elevated temperature. PeerJ 10, e14137 (2022). Contribution: I conceptualized part of the research plan, purified alpha-synuclein and performed FTIR, CD measurements, as well as data analysis. I also contributed to the initial manuscript preparation, figure preparation and further modifications during the review process.
4. Ziaunys, M., **Mikalauskaite, K.**, Sakalauskas, A., Smirnovas, V. Investigating lysozyme amyloid fibril formation and structural variability dependence on its initial folding state under different pH conditions. Protein Sci. 33, 0–2 (2024). Contribution: I conceptualized part of the research plan, performed lysozyme aggregation kinetic assay, FTIR, stability under denaturing conditions measurements, as well as data analysis. I also contributed to the initial manuscript preparation and further modifications during the review process.
5. Ziaunys, M., **Mikalauskaite, K.**, Sakalauskas, A., Smirnovas, V. Study of Insulin Aggregation and Fibril Structure under Different Environmental Conditions. Int. J. Mol. Sci. 25, 9406 (2024). Contribution: I conceptualized part of the research plan, performed aggregation kinetic assay, DLS, FTIR, stability under denaturing conditions measurements, as well as data analysis. I also contributed

to the initial manuscript preparation and further modifications during the review process.

6. Misiūnaitė, I., **Mikalauskaite, K.**, Paulauskaite, M., Snieckute, R., Smirnovas, V., Brukstus, A., Ziaunys, M., Zutaute, I. Imidazo[2,1- b][1,3]thiazine Derivatives as Potential Modulators of Alpha-Synuclein Amyloid Aggregation. ACS Chem. Neurosci. 15, 4418–4430 (2024). Contribution: I conceptualized part of the research plan, purified alpha-synuclein, performed aggregation kinetic assays, FTIR, TEM measurements, as well as data analysis. I also strongly contributed to the initial manuscript and figure preparation, as well as further modifications during the review process.
7. Ziaunys, M, Sulskis, D., **Mikalauskaite, K.**, Sakalauskas, A., Snieckute, R., Smirnovas, V. S100A9 inhibits and redirects prion protein 89-230 fragment amyloid aggregation. Arch. Biochem. Biophys. 758, 110087 (2024). Contribution: I conceptualized part of the research plan, purified prion protein and performed kinetic, FTIR measurements, as well as data analysis. I also contributed to the initial manuscript preparation and further modifications during the review process.

Publications not included in the dissertation/Publikacijos neįtrauktos į disertaciją

1. Ziaunys, M., **Mikalauskaite, K.**, Sakalauskas, A., Smirnovas, V. Interplay between epigallocatechin-3-gallate and ionic strength during amyloid aggregation. PeerJ 9, e12381 (2021).
2. Ziaunys, M., Sakalauskas, A., **Mikalauskaite, K.**, Smirnovas, V. Polymorphism of Alpha-Synuclein Amyloid Fibrils Depends on Ionic Strength and Protein Concentration. Int. J. Mol. Sci. 22, 12382 (2021).
3. Sakalauskas, A., Janoniene, A., Zvinys, G., **Mikalauskaite, K.**, Ziaunys, M., Smirnovas, V. Exploring the Formation of Polymers with Anti-Amyloid Properties within the 2′3′-Dihydroxyflavone Autoxidation Process. Antioxidants 11, 1711 (2022).
4. Ziaunys, M., **Mikalauskaite, K.**, Krasauskas, L., Smirnovas, V. Conformation-Specific Association of Prion Protein Amyloid Aggregates with Tau Protein Monomers. Int. J. Mol. Sci. 24, 9277 (2023).
5. Ziaunys, M., Sulskis, D., Veiveris, D., Kopustas, A., Snieckute, R., **Mikalauskaite, K.**, Sakalauskas, A., Tutkus, M., Smirnovas, V. Liquid–liquid phase separation of alpha-synuclein increases the structural variability of fibrils formed during amyloid aggregation. FEBS J. 291, 4522–4538 (2024).

6. Ziaunys, M., Sulskis, D., Veiveris, D., Sakalauskas, A., **Mikalauskaite, K.**, Smirnovas, V. Diverse effects of fluorescent labels on alpha-synuclein condensate formation during liquid-liquid phase separation. Int. J. Biol. Macromol. 283, 137688 (2024).
7. Veiveris, D., Kopustas, A., Sulskis, D., **Mikalauskaite, K.**, Alsamsam, M., Tutkus, M., Smirnovas, V., Ziaunys, M. Heterotypic Droplet Formation by Pro-Inflammatory S100A9 and Neurodegenerative Disease-Related α-Synuclein. Biomacromolecules 26, 3525–3537 (2025).

LIST OF SCIENTIFIC EVENTS/KONFERENCIJŲ SĄRAŠAS

1. **K. Mikalauskaite**, M. Ziaunys, A. Sakalauskas, V. Smirnovas. “Using lysozyme amyloid fibrils as a means of scavenging aggregation-inhibiting compounds”, 22nd International Conference on Alzheimer's Drug Discovery. Online conference
2. **K. Mikalauskaite**, M. Ziaunys, A. Sakalauskas, V. Smirnovas. “Baltymų agregaciją slopinančių junginių atskyrimas naudojant lizocimo amiloidines fibriles”, Bioateitis - gamtos ir gyvybės mokslų perspektyvos. Lithuania
3. **K. Mikalauskaite**, M. Ziaunys, A. Sakalauskas, V. Smirnovas. “Interplay between epigallocatechin-3-gallate and ionic strength during amyloid aggregation”, Coins 2022. Lithuania
4. **K. Mikalauskaite**, M. Ziaunys, A. Sakalauskas, V. Smirnovas. “Interplay between epigallocatechin-3-gallate and ionic strength during amyloid aggregation”, Open Readings 2022. Lithuania
5. **K. Mikalauskaite**, M. Ziaunys, A. Sakalauskas, V. Smirnovas. “Interplay between epigallocatechin-3-gallate and ionic strength during amyloid aggregation”, Healthy aging from a multidisciplinary perspective 2022. Lithuania
6. **K. Mikalauskaite**, M. Ziaunys, D. Veiveris, A. Sakalauskas, V. Smirnovas. “Superoxide Dismutase-1 Alters the Rate of Prion Protein Aggregation and Resulting Fibril Conformation”, The Leuven Protein Aggregation Meeting 2022. Belgium
7. **K. Mikalauskaite**, M. Ziaunys, V. Smirnovas. “Exploring the Effect of Amyloid-Specific Molecules on Protein Aggregation”, 3rd Baltic Biophysics Conference 2022. Lithuania
8. **K. Mikalauskaite**, M. Ziaunys, D. Veiveris, A. Sakalauskas, V. Smirnovas. “Superoxide Dismutase-1 Alters the Rate of Prion Protein Aggregation and Resulting Fibril Conformation”, Conference Jacques Monod "Protein phase transitions in ageing and age-related diseases: from atomic resolution to cellular solutions" 2022. France
9. **K. Mikalauskaite**, M. Ziaunys, D. Veiveris, A. Sakalauskas, V. Smirnovas. “Superoxide Dismutase-1 Alters the Rate of Prion Protein Aggregation and Resulting Fibril Conformation” 2022, 9th Scandinavian and Baltic Conference, Amyloid Diseases and Amyloid Mechanisms (ADAM 9) 2022. Latvia
10. **K. Mikalauskaite**, M. Ziaunys, D. Veiveris, A. Sakalauskas, V. Smirnovas. “Superoxide Dismutase-1 Alters the Rate of Prion Protein Aggregation and Resulting Fibril Conformation” 2022, 33rd International Symposium on ALS/MND 2022. Online conference

11. **K. Mikalauskaite**, M. Ziaunys, A. Sakalauskas, V. Smirnovas. “Lysozyme amyloid fibril structural variability dependence on initial protein folding state” 2023, Open Readings 2023. Lithuania
12. **K. Mikalauskaite**, M. Ziaunys, A. Sakalauskas, V. Smirnovas. “Lysozyme amyloid fibril structural variability dependence on initial protein folding state” 2023, Jędrzej Sniadecki Memorial Conference “Frontiers in Molecular Life Sciences”. Lithuania
13. **K. Mikalauskaite**, M. Ziaunys, A. Sakalauskas, V. Smirnovas. “Polymorphism of alpha-synuclein amyloid fibrils depends on ionic stength and protein concentration” 2023, 1st ML4NGP Meeting on Machine Learning and Non-Globular Proteins 2023. Slovakia
14. **K. Mikalauskaite**, M. Ziaunys, A. Sakalauskas, V. Smirnovas. “Polymorphism of alpha-synuclein amyloid fibrils depends on ionic stength and protein concentration” 2023, III PHASAGE international conference “A multiscale understanding of protein aggregation and phase separation: from molecules to the brain”. Portugal
15. **K. Mikalauskaite**, M. Ziaunys, D. Sulskis, D. Veiveris, A. Kopustas, R. Snieckute, A. Sakalauskas, M. Tutkus, V. Smirnovas. “Influence of liquid-liquid phase separation on amyloid fibril structural variability” 2024, Latvia-Lithuania-Taiwan Trilateral Joint Symposium on TTR Amyloidosis. Taiwan
16. **K. Mikalauskaitė**, M. Žiaunys, D. Šulskis, D. Veiveris, A. Kopūstas, R. Sniečkutė, A. Sakalauskas, M. Tutkus, V. Smirnovas. “Influence of liquid-liquid phase separation on amyloid fibril structural variability” 2024, the 16th International Conference of the Lithuanian Neuroscience Association. Lithuania
17. **K. Mikalauskaite**, M. Ziaunys, D. Sulskis, D. Veiveris, A. Kopustas, R. Snieckute, A. Sakalauskas, M. Tutkus, V. Smirnovas. “Influence of liquid-liquid phase separation on amyloid fibril structural variability” 2025, 10th Scandinavian and Baltic Conference, Amyloid Diseases and Amyloid Mechanisms (ADAM 10) 2025. Sweden
18. **K. Mikalauskaite**, M. Ziaunys, D. Sulskis, D. Veiveris, A. Kopustas, R. Snieckute, A. Sakalauskas, M. Tutkus, V. Smirnovas. “Influence of liquid-liquid phase separation on amyloid fibril structural variability” 2025, 3rd ML4NGP Meeting on Machine Learning and Non-Globular Proteins 2025. Lithuania

COPIES OF PUBLICATIONS/PUBLIKACIJŲ KOPIJOS

International Journal of
Molecular Sciences

MDPI

Article

Lysozyme Amyloid Fibril Structural Variability Dependence on Initial Protein Folding State

Kamile Mikalauskaite, Mantas Ziaunys and Vytautas Smirnovas *

Institute of Biotechnology, Life Sciences Center, Vilnius University, LT-10257 Vilnius, Lithuania; kamile.mikalauskaite@gmc.vu.lt (K.M.); mantas.ziaunys@gmc.vu.lt (M.Z.)
* Correspondence: vytautas.smirnovas@bti.vu.lt

Abstract: Amyloid fibril formation is associated with several amyloidoses, including neurodegenerative Alzheimer's or Parkinson's diseases. The process of such fibrillar structure formation is still not fully understood, with new mechanistic insights appearing on a regular basis. This, in turn, has limited the development of potential anti-amyloid compounds, with only a handful of effective cures or treatment modalities available. One of the multiple amyloid aggregation factors that requires further examination is the ability of proteins to form multiple, structurally distinct aggregates, based on the environmental conditions. In this work, we examine how the initial folding state affects the fibrilization of lysozyme—an amyloidogenic protein, often used in protein aggregation studies. We show that there is a correlation between the initial state of the protein and the aggregate formation lag time, rate of elongation, resulting aggregate structural variability and dye-binding properties, as well as formation lag time and rate of elongation.

Keywords: amyloid; protein aggregation; lysozyme; fibril

Citation: Mikalauskaite, K.; Ziaunys, M.; Smirnovas, V. Lysozyme Amyloid Fibril Structural Variability Dependence on Initial Protein Folding State. *Int. J. Mol. Sci.* **2022**, *23*, 5421. https://doi.org/10.3390/ijms23105421

Academic Editor: Holger Wille

Received: 3 May 2022
Accepted: 11 May 2022
Published: 12 May 2022

1. Introduction

Protein aggregation in the form of amyloid fibrils is linked with the onset and progression of several amyloidoses [1], including neurodegenerative Alzheimer's or Parkinson's disease [2]. Despite decades of intense research and countless studies [3], a full understanding of such aggregate formation remains elusive [4]. This, in turn, has significantly complicated the search for potential anti-amyloid compounds and there are currently very few drugs or treatment modalities available [5,6]. The constantly increasing number of affected individuals and projected further growth in cases [7,8] make it vitally important to obtain a better understanding of the amyloid fibril formation process.

In general, the mechanism of protein aggregation can be broken down into multiple basic parts. First, proteins have to undergo a misfolding event, during which they form the initial amyloid nuclei (primary nucleation) [9,10]. These nuclei then grow by incorporating other homologous protein molecules into their structure, forming elongated aggregates—fibrils [11–13]. Once sufficiently sized aggregates form, secondary processes can also occur during the elongation phase, which include fibril fragmentation [14] and surface-mediated nucleation (fibril surface acts as a catalyst for new nuclei formation) [15–17]. Apart from this general mechanism, there are also multiple additional events proposed, such as fibril maturation over a long time period [18], as well as lateral association and aggregate cluster formation [19].

The structure of amyloid fibrils has been studied using a wide range of techniques. These include solid state nuclear magnetic resonance (ssNMR), cryo-electron microscopy (cryo-EM), atomic force microscopy (AFM), Fourier-transform infrared spectroscopy (FTIR), as well as small-angle X-ray scattering (SAXS). These methods have also been utilized to track and analyse the formation of amyloid fibrils and to determine the various types of intermediate species present during the aggregation reaction [20–23]. While most protein

aggregation events follow a similar mechanism, there is a wide variety of structurally and morphologically distinct fibrils formed, depending on the initial protein and the reaction conditions, such as ionic strength, pH, temperature or protein concentration [24–28]. It was even shown that amyloid-beta (which is associated with Alzheimer's disease) [29], alpha-synuclein (Parkinson's disease) [18], prion proteins (prionopathies) [30] and Tau proteins (tauopathies) [31] can aggregate into multiple distinct structures under the same environmental conditions. Structural polymorphism is considered to be related to fibril toxicity, replication rates and could explain the onset of different diseases, originating from the same precursor protein [32]. While the ability of identical proteins to form conformationally distinct amyloid fibrils is an interesting phenomenon, it significantly complicates the search for potential anti-amyloid compounds or treatments.

We recently observed that prion protein polymorphism depends on the folding state of the initial protein, with distinct types of fibril structures being formed above and below the melting temperature [30]. Similarly, the formation of aggregates with higher cytotoxic properties at higher temperatures [33] was reported for lysozyme—a model amyloidogenic protein, commonly used in aggregation studies [34]. Considering that temperature is often modulated to alter the rate of protein aggregation in vitro [35,36] and that lysozyme amyloid formation is known to have a condition–structure relationship [37,38], it was important to examine the phenomenon in greater detail. In this work, large sets of identical hen egg-white lysozyme samples were aggregated under a range of temperatures, from lower, where most protein molecules were folded, to higher, where they were fully unfolded. The generated aggregates were then examined and compared based on their secondary structure and dye-binding properties. We show that lysozyme amyloid fibril polymorphism exists both below and above the melting temperature and that there is a significant shift in the variability of structures associated with the folding state of the initial, non-aggregated protein.

2. Results

All details regarding sample preparation, experiments and data analysis are reported at the end of the article. In order to determine the melting point of lysozyme under the selected experimental conditions (phosphate-buffered saline (PBS) solution, containing 2 M guanidine hydrochloride, pH 7.4) and select a range of temperatures for the aggregation experiments, an 8-anilinonaphthalene-1-sulfonic acid (ANS) protein melt assay was carried out (Figure 1A). Up to 50 °C, it was observed that the dye signal intensity gradually decreased due to a temperature-related reduction in fluorescence quantum yield. After this point, the ANS emission intensity began rising to a maximum point at 65 °C, after which it rapidly decreased. These results show that the majority of lysozyme was folded up to 50 °C and it is fully unfolded at 65 °C (T_m = (57 ± 1) °C). Based on this information, four different temperature conditions were chosen for further examination (marked with colour-coded dashed lines in Figure 1A).

For each temperature, full 96-well plates of identical lysozyme samples were incubated under constant agitation (as described in the Materials and Methods section) and their fibrillization reactions were tracked by measuring the fluorescence emission intensity of fibril-bound thioflavin-T (ThT) (examples of aggregation reaction kinetic curves are shown in Appendix A Figure A1). At 50 °C, the aggregation lag time (t_{lag}) had an average value of ~1300 min (Figure 1B), and a temperature increase of 5 °C caused a 3-fold decrease in t_{lag} to ~400 min. Further changes to the reaction temperature had a less significant effect on the t_{lag} value (~190 min at 60 °C and ~160 min at 65 °C), with a point of discontinuity detected between 55 °C and 60 °C, which was similar to the T_m value of lysozyme under these experimental conditions. The apparent rate constant of aggregation had the most significant change between the two lowest tested temperatures (2-fold increase from ~0.01 to ~0.02), while the values between 55 °C and 65 °C followed a linear trend in a semi-logarithmic plot (Figure 1C). Similar to the lag time values, there was also a point of discontinuity; however, in this case, it was detected closer to 55 °C (slightly below the T_m value). Despite

the massive differences in both t_{lag} and apparent rate constant values in this temperature range, there were no detectable sub-groups of samples with specific aggregation kinetic parameters and all data followed a normal distribution.

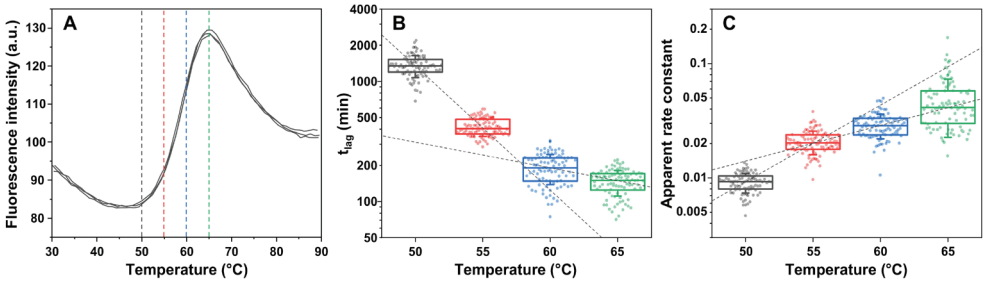

Figure 1. Lysozyme aggregation kinetic parameters depended on folding state. 8-anilinonaphthalene-1-sulfonic acid (ANS) signal intensity under a range of temperatures and in the presence of 200 µM lysozyme in PBS with 2 M guanidine hydrochloride (GuHCl) (pH 7.4). (**A**) Colour-coded dashed lines indicate temperatures chosen for further analysis. Lysozyme aggregation reaction t_{lag} (**B**) and apparent rate constant (**C**) values under the four selected temperature conditions (all data are colour-coded). Panel B and C box plots indicate the interquartile range and error bars are one standard deviation (n = 96). ANS protein melt and aggregation assay procedures are described in the Materials and Methods section. Raw data are available as Supplementary Materials.

During the aggregation assay, a substantial difference between the end-point ThT fluorescence emission intensity values of samples generated at low and high-temperature conditions was observed. There was also a significant variation in these values between samples from the same aggregation conditions. Such distinct bound-ThT fluorescence intensities can be associated with the existence of fibrils with different secondary structures or morphologies [30,39]. These ThT-binding modes are usually accompanied by specific maximum excitation and emission wavelength positions, which can be used to differentiate between fibril types [40].

Each sample's excitation/emission matrix (EEM) was scanned and their "center of mass" positions, as well as their correlation to the signal intensity, were compared. In the case of lysozyme aggregates prepared at 50 °C and 55 °C, the EEM maxima positions were clustered at a specific area (449–451 nm excitation and 480–483 nm emission wavelengths), with only a small amount of samples deviating from this position (Figure 2A,B). When the aggregation temperature increased past the T_m value, a sizeable portion of sample EEM maxima positions deviated from the main cluster, with certain positions being located as far as 5 nm from the cluster excitation or emission wavelength values (Figure 2C). Matters became even more interesting when the majority of initial lysozyme monomers were in their unfolded state during aggregation. In this case, a new main cluster formed at 444–446 nm excitation and 481–483 nm emission wavelengths, with the large dispersion of positions persisting (Figure 2D), as was the case for the 60 °C samples (Figure 2C).

When examining the correlation between sample EEM positions and fluorescence intensity (Figure 2E), the high-intensity samples appeared near the lower-temperature cluster position (observed in Figure 2A,B), while the lower-intensity samples gathered around the higher-temperature cluster position (observed in Figure 2D). There was also a clear dependence between the distribution of sample fluorescence intensity values and the temperature used in their preparation (Figure 2F). When most lysozyme monomers were folded, the resulting ThT fluorescence intensity had an average value of ~440 a.u. with a relatively small dispersion. At 55 °C, the average value decreased to ~360 a.u. and there was a significant increase in the signal intensity deviation. When the aggregation temperature passed the T_m value, there was a substantial reduction in average signal intensity (~110 a.u.),

while the high level of dispersion persisted. At the highest tested temperature, where most lysozyme monomers were unfolded, the average fluorescence intensity was even lower (~40 a.u.) and the value dispersion mirrored the 50 °C condition samples.

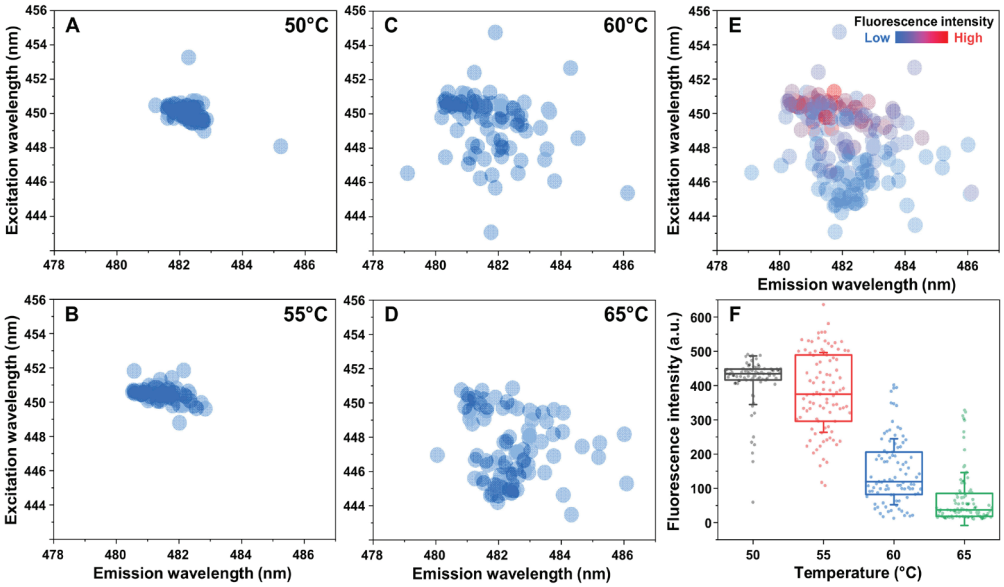

Figure 2. Correlation between sample fluorescence parameters and lysozyme aggregation temperatures. Bound ThT excitation-emission matrix (EEM) "center of mass" positions of samples prepared under 50 °C (**A**), 55 °C (**B**), 60 °C (**C**) and 65 °C (**D**) conditions. EEM position and signal intensity correlation of 50 °C and 65 °C samples (**E**). Fluorescence intensity value distribution of samples prepared under different aggregation conditions (**F**). Box plots indicate the interquartile range and error bars are for one standard deviation. All data acquisition and analysis procedures are described in the Materials and Methods section. Raw data are available in the Supplementary Materials.

Interestingly, conditions below the T_m value did not result in a single EEM position located at the high-temperature cluster, while 60 °C and 65 °C led to samples with positions at both cluster areas. This suggests that specific aggregate structures or morphologies require the initial protein to be unfolded. The fluorescence intensity distributions displayed that all temperature conditions caused the formation of samples with significant deviation from the average values (low-intensity samples at low temperatures and large-intensity samples at high temperatures). This hints at a possibility of mixtures, composed of different types of aggregates, which have specific ThT-binding parameters.

Since the EEM data suggested a possible high variety of lysozyme aggregate structures, each sample was replicated and examined using Fourier-transform infrared spectroscopy (FTIR). In the case of 50 °C (Figure 3A) and 55 °C (Figure 3B) samples, the FTIR spectra shared similarities, between both different temperature conditions as well as between each other. At 60 °C (Figure 3C), there appeared to be a mixture of distinct secondary structures, with some spectra being similar to those observed at lower temperatures. At the highest temperature (Figure 3D), the variability decreased and most samples had FTIR spectra dissimilar to ones that were present at lower temperatures.

Peak fitting for the FTIR spectra revealed that there were three dominant secondary structures (Figure 3E–J), with distinct peak maxima positions and areas. The Type 1 aggregates were the main structure at 50 °C and 55 °C, while making up only a fraction

of 60 °C samples and being nearly non-existent at 65 °C. Conversely, the Type 2 and 3 aggregates were only present at 60 °C and 65 °C temperature conditions. Comparing the peak maxima positions and areas revealed that all three fibril types had similar maximum position peaks at 1614–1615 cm^{-1} (associated with strong hydrogen bonding in the beta-sheet structure [41]) and 1627 cm^{-1} (associated with weaker hydrogen bonding). While the 1614–1615 cm^{-1} position peaks had similar areas among all aggregate types, the 1627 cm^{-1} peaks were significantly smaller in the case of Type 2 and 3 aggregates. Overall, Type 1 had the highest percentage of cross-beta structures, Type 2 had less and Type 3, a minimum amount of such beta sheets. A small peak at 1637 cm^{-1} in the FTIR spectrum of Type 2 aggregates can be attributed to the weak hydrogen bonding of beta sheets, while significant peaks at 1642–1643 cm^{-1} in Type 1 and 3 sample FTIR spectra and at 1648 cm^{-1} in the case of Type 2 aggregates is associated with the presence of unstructured regions. The rest of the peaks in all spectra most probably arise from different turn/loop motifs, though there is a possibility that peaks at the highest wavenumbers could mean the presence of some antiparallel beta sheets.

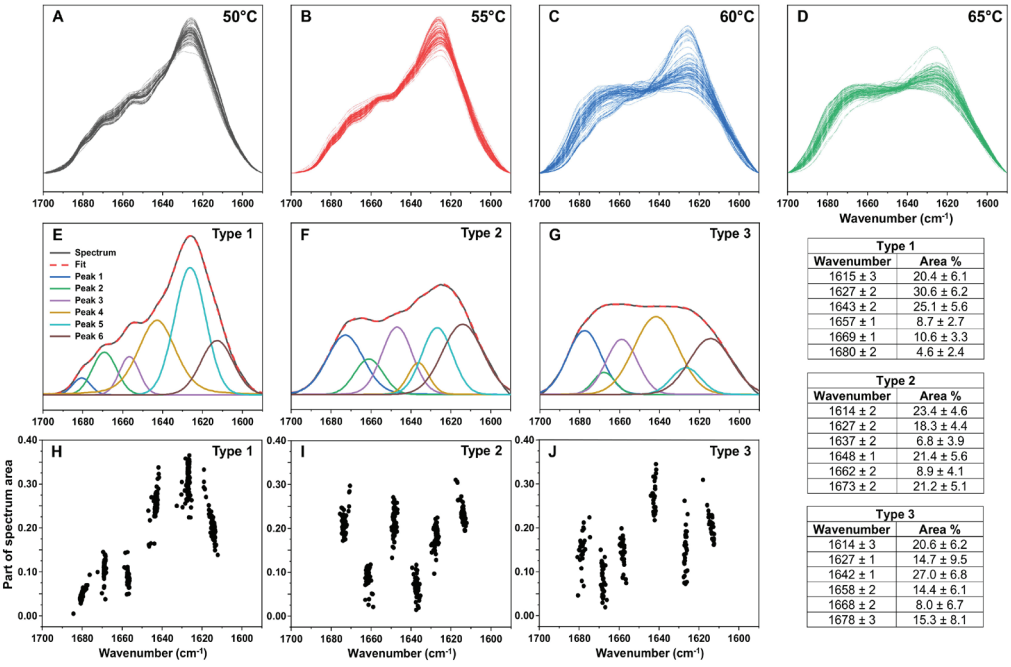

Type 1	
Wavenumber	Area %
1615 ± 3	20.4 ± 6.1
1627 ± 2	30.6 ± 6.2
1643 ± 2	25.1 ± 5.6
1657 ± 1	8.7 ± 2.7
1669 ± 1	10.6 ± 3.3
1680 ± 2	4.6 ± 2.4

Type 2	
Wavenumber	Area %
1614 ± 2	23.4 ± 4.6
1627 ± 2	18.3 ± 4.4
1637 ± 2	6.8 ± 3.9
1648 ± 1	21.4 ± 5.6
1662 ± 2	8.9 ± 4.1
1673 ± 2	21.2 ± 5.1

Type 3	
Wavenumber	Area %
1614 ± 3	20.6 ± 6.2
1627 ± 1	14.7 ± 9.5
1642 ± 1	27.0 ± 6.8
1658 ± 2	14.4 ± 6.1
1668 ± 2	8.0 ± 6.7
1678 ± 3	15.3 ± 8.1

Figure 3. Fourier-transform infrared (FTIR) spectra of lysozyme aggregates prepared under different temperature conditions. Spectra of lysozyme aggregates prepared at 50 °C (**A**), 55 °C (**B**), 60 °C (**C**) and 65 °C (**D**), with all sample ($n = 96$) spectra superimposed and colour-coded. Peak-fit of Type 1 (**E**), Type 2 (**F**) and Type 3 (**G**) aggregate spectra and peak position/area distributions (**H**–**J**). The peak-fitting procedure was performed on 50 °C and 65 °C condition spectra. Table inserts display the peak positions and areas of all three aggregate-type FTIR spectra. Raw data are available in the Supplementary Materials.

Since the higher-temperature aggregate FTIR spectra displayed smaller peaks, associated with beta-sheet hydrogen bonding and more unstructured regions, their ability to form fibrillar structures was examined using atomic force microscopy (AFM). In order to facilitate the formation of elongated structures, the samples were reseeded under quies-

cent conditions at their respective temperatures. For all three aggregate types, the ThT fluorescence intensity signal growth proceeded with no lag phase (Figure 4), indicating aggregation self-replication. In the case of Type 2 and Type 3 aggregates (Figure 4B,C), the end-point fluorescence intensity was significantly lower than Type 1 (Figure 4A), as was observed with the initial samples.

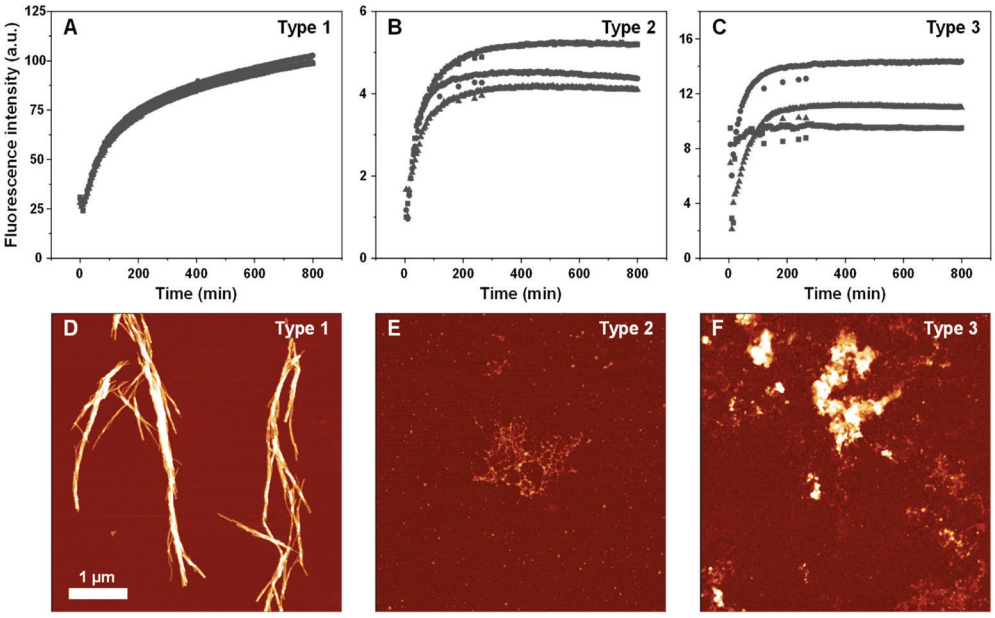

Figure 4. Self-replication kinetics (**A**–**C**) and atomic force microscopy images (**D**–**F**) of three types of lysozyme aggregates. Kinetic curves are from three repeats (different symbols represent separate samples). Self-replication and AFM imaging procedures are described in the Materials and Methods section. Raw data are available in the Supplementary Material.

The Type 1 AFM image displayed long (3–5 μm) fibrillar structures, with an average cross-sectional height of 10 nm (Figure 4D). The Type 2 aggregates were significantly shorter (~0.3 μm), with a lower average height of 2 nm and they were associated into web-like systems (Figure 4E). This sample also contained a number of small, round structures, which may be short lysozyme oligomers or amorphous aggregates. Unlike the previous two cases, the Type 3 sample contained mostly short aggregates (Figure 4F), which associated into larger clusters and very few elongated structures were observed. These images suggest that the higher temperature resulted in lysozyme aggregates, which had lower stability and likely formed a considerable number of amorphous structures, coinciding with the significantly reduced beta-sheet-related peaks in their respective FTIR spectra.

In order to determine whether the lower-temperature fibrils were capable of replicating their structure at higher temperatures and vice versa, a reseeding experiment was carried out, as described in the Materials and Methods section. When the Type 1 fibrils were reseeded at 65 °C, the resulting aggregate FTIR spectra was nearly identical to the original (Figure 5A), showing that the fibrils were capable of replicating their structure and that the increased temperature had no effect on them. Conversely, when the Type 2 and 3 aggregates were reseeded at 50 °C, there was a significant change in their FTIR spectra (Figure 5B,C). In both cases, the resulting spectra became similar to the Type 1 aggregates and to one another.

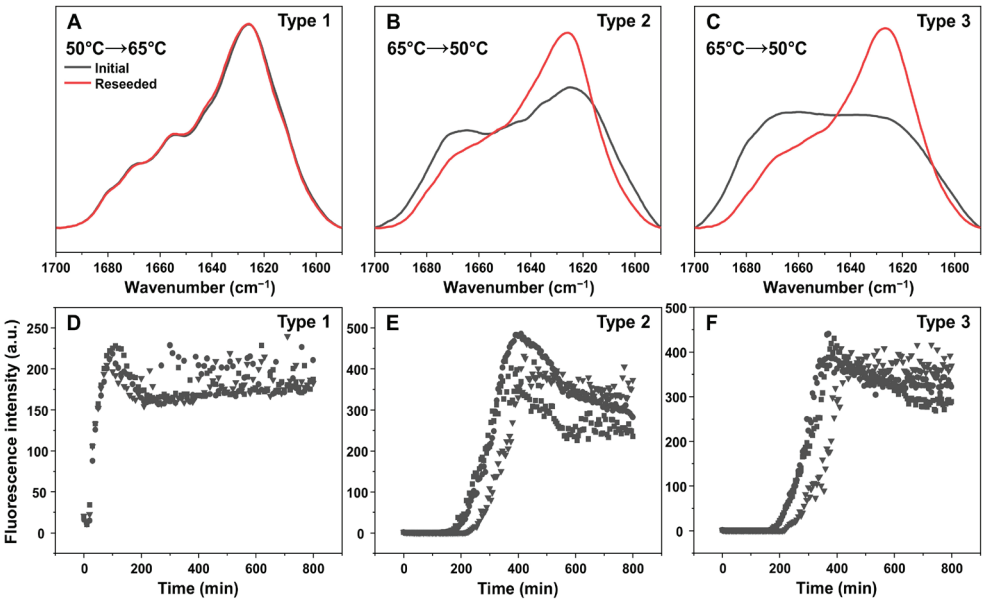

Figure 5. Fourier-transform infrared (FTIR) spectra of Type 1 (**A**), Type 2 (**B**) and Type 3 (**C**) lysozyme aggregates before and after the reseeding reaction and their respective aggregation kinetic curves (**D**–**F**). The reseeding procedure is described in the Materials and Methods section. Kinetic curves are from three repeats (different symbols represent separate samples). Raw data are available in the Supplementary Materials.

Based on the aggregation kinetic data, the Type 1 fibril reseeding reaction had practically no lag time and proceeded immediately (Figure 5D). This was not the case for both Type 2 and 3 aggregates (Figure 5E,F), where a considerable lag period was observed. Despite the aggregates causing a significant reduction in lag time (~200 min, as opposed to ~1500 min during spontaneous reaction), the change in FTIR spectra suggested that they were not efficient at replicating their structure at 50 °C. This reduced lag time may be due to the Type 2 and 3 aggregates acting as a surface for secondary nucleation, which would explain the formed aggregate FTIR spectra similarity to Type 1 fibrils.

3. Discussion

Based on the results from this study, it is clear that the initial folding state of lysozyme is an important factor for multiple amyloid aggregation aspects, including lag time, resulting structural variability, bound-ThT fluorescence intensity and self-replication. In all cases, a discontinuity of kinetic or structural parameters was observed to occur in the relatively small gap between temperatures where lysozyme transitioned from folded to unfolded states. The complex effect of this transition has to be taken into account during studies of lysozyme amyloid aggregation.

The first notable aspect was the significant temperature-related shift in aggregate secondary structure. At lower temperatures, the sample FTIR spectra displayed a considerably larger content of beta-sheet structures, when compared to the two different aggregate types formed above the melting temperature. This transition, however, did not occur instantly, as we observed Type 1 fibrils present at higher-temperature conditions as well, with their number decreasing significantly when lysozyme was unfolded. Interestingly, there was a minor level of structural variability, even under identical conditions, most visible based

on the FTIR spectra peak area value deviations (Figure 3H–J). Such variability was also previously observed for prion protein amyloid fibrils [30]. These results suggest that when lysozyme is (partially) folded, it can only transition to one dominant amyloid aggregate (Type 1, Figure 3E), with a minor level of structural variability. However, once lysozyme becomes unfolded, it can form up to three different aggregate types with characteristic peak positions/areas.

Another point worth noting is the self-replication properties of the three different structures. In the case of aggregates formed under conditions where lysozyme was predominantly folded, they were able to easily replicate their structure at the highest tested temperature (Figure 5A,D). They also formed long fibrils when replicated under quiescent conditions (Figure 4D). This suggests that they could incorporate lysozyme monomers, regardless of their folding state. Conversely, this was not the case for the aggregate types that were formed at higher temperatures. While they appeared to be able to self-replicate under their initial preparation conditions (Figure 4B,C), they were unable to do so under a temperature, where lysozyme was folded. One possibility is that such aggregate types are only capable of incorporating partially or fully unfolded protein molecules. Another likely explanation is that the higher temperature samples contained a significant number of non-amyloid structures, as seen in Type 2 and especially Type 3 AFM images (Figure 4E,F).

The final significant observation from this study is the remarkably high correlation between the structure of lysozyme aggregates and their ThT-binding characteristics. The transition from Type 1 (at 50 °C) to Type 2 and 3 (at 65 °C) structures caused a 10-fold decrease in the average fluorescence intensity values (Figure 2F). This was also followed by a shift in the bound-ThT EEM maxima positions, which signifies a different dye binding mode (Figure 2A–D) [40]. Such a massive decrease in signal value may be related to the reduction in the aggregate beta-sheet content, which was evident based on the sample FTIR spectra (Figure 3A–D) or the formation of non-amyloid structures (Figure 4E,F). The intermediate temperature aggregates also had a very large ThT fluorescence intensity value deviation, with a several-fold difference between samples from identical conditions. Taking into consideration that ThT fluorescence intensity is often used as a parameter of the relative abundance of amyloid aggregates, such variations can have drastic effects on the conclusions drawn from experimental data.

Overall, these results highlight the importance of the folding state of lysozyme on its amyloid aggregation kinetic and structural parameters, as well as their variability. Taking into account that a similar relationship exists for the neurodegenerative-disease-related prion protein, it suggests that this is a significant influencing factor for amyloid fibril formation and should be taken into account during protein aggregation studies.

4. Materials and Methods

4.1. Lysozyme Aggregation Kinetics

Hen egg-white lysozyme powder (Sigma-Aldrich, St. Louis, MO, USA, cat. No. L6876) was dissolved in 1 × PBS buffer (pH 7.4) containing 2 M guanidine hydrochloride (GuHCl) to a protein concentration of 300 μM (ε_{280} = 37,970 $M^{-1}cm^{-1}$). Thioflavin-T (ThT) powder (Sigma-Aldrich, St. Louis, MO, USA, cat. No. T3516) was dissolved in MilliQ H_2O to a concentration of ~11 mM and filtered through a 0.22 μm pore size syringe filter. The concentration of the ThT solution was determined by diluting an aliquot of the dye solution 100 times with H_2O and scanning its absorbance at 412 nm (ε_{412} = 23,250 $M^{-1}cm^{-1}$). The final ThT stock solution concentration was then set to 10 mM. The lysozyme, ThT and reaction buffer (1 × PBS (pH 7.4) with 2 M GuHCl) were combined to result in a solution with 200 μM lysozyme and 100 μM ThT. In order to avoid batch-to-batch variability, 80 mL of this solution was divided into 20 mL portions and frozen at −20 °C prior to use in kinetic experiments.

To measure lysozyme aggregation kinetics, 20 mL of frozen reaction solution was thawed at room temperature and distributed to a 96-well plate (200 μL final volume, each well contained one 3 mm glass bead), after which it was sealed with Nunc-sealing tape. Ag-

gregation kinetics were monitored in a ClarioStar Plus (BMG Labtech, Ortenberg, Germany) plate reader by measuring sample fluorescence emission intensity (excitation wavelength—440 nm, emission—480 nm) every 5 min, with constant 600 RPM orbital shaking between measurements. The experiment was conducted under four different temperatures based on the lysozyme melt assay (from 50 °C to 65 °C). Reaction lag times, rates and end-point fluorescence values were determined as shown previously [27]. All data processing was done using Origin (OriginLab Corporation, Northampton, MA, USA) software.

4.2. Lysozyme Melt Assay

8-anilinonaphthalene-1-sulfonic acid (ANS) powder (Sigma-Aldrich, St. Louis, MO, USA, cat. No. A1028) was dissolved in MilliQ H_2O at room temperature under dark conditions. The solution was then filtered through a 0.22 μm pore size syringe filter. The concentration of the ANS solution was determined by diluting an aliquot of the dye solution 100 times with H_2O and scanning its absorbance at 351 nm (ε_{351} = 5100 $M^{-1}cm^{-1}$). The final ANS stock solution concentration was then set to 10 mM and stored at 4 °C under dark conditions prior to use. For the melt assay, lysozyme was prepared as described in the aggregation kinetics method section with ANS added instead of ThT. The lysozyme samples were then placed in 3 mm pathlength cuvettes (200 μL volume each) and sealed with plug caps.

The melt assay was conducted by placing the cuvettes in a Varian Cary Eclipse (Agilent, Santa Clara, CA, USA) spectrofluorometer and measuring sample fluorescence intensity (excitation wavelength—370 nm, emission—470 nm) under a range of temperatures (starting temperature—25 °C, end temperature—90 °C, incubation at starting temperature—5 min, temperature change rate—2 °C/min, measurements every 30 s).

4.3. Excitation–Emission Matrices

After aggregation reaction kinetic measurements, the 96-well plates were cooled down to 25 °C. In order to account for ThT hydroxylation under neutral pH and elevated temperatures, each well was supplemented with 1 μL of the ThT stock solution (additional 50 μM ThT in each sample). The plates were then placed in the plate reader and incubated at 25 °C for 10 min under constant 600 RPM shaking. Immediately after agitation, each well's ThT excitation–emission matrix (EEM) was scanned. This was done by measuring sample fluorescence at a constant 485 nm emission wavelength under a range of excitation wavelengths (from 430 nm to 460 nm) and measuring sample fluorescence under a range of emission wavelengths (from 470 nm to 500 nm) at a constant 445 nm excitation wavelength. The data were then combined into an EEM using the ClarioStar MARS 3D spectra function. Each EEM maximum intensity position was determined by calculating the "center of mass" of the highest 10% intensity value positions as described previously [27].

4.4. Fourier-Transform Infrared Spectroscopy

An aliquot (100 μL) from each aggregation reaction kinetics plate well was removed and combined with 900 μL of initial reaction solution (prepared as described in the aggregation kinetics method section) and placed in a 1.5 mL test tube. Each test tube contained two 3 mm glass beads and was sealed with parafilm. The test tubes were then incubated in a dry-bath incubator under constant 600 RPM agitation at their respective temperature (based on initial sample preparation temperature). After 24 h of incubation, the samples were cooled down to room temperature and centrifuged at 12 500 RPM for 15 min. After this, the supernatant was removed and the aggregate pellets were resuspended into 500 μL of D_2O, containing 400 mM NaCl (replacement of H_2O with D_2O helps to avoid H-O-H bands, which overlap with the Amide I region and the addition of NaCl improves fibril sedimentation [39]). The samples were then mixed, centrifuged, and resuspended into 200 μL D_2O with 400 mM NaCl. The centrifugation and resuspension procedure were repeated 4 times in total. After the final supernatant removal, the fibril pellets were resuspended into 50 μL of D_2O with 400 mM NaCl.

Samples were placed between two CaF_2 transmission windows separated by a 0.05 mm teflon spacer. FTIR spectra were scanned using a Bruker Invenio S FTIR spectrometer, equipped with a liquid-nitrogen-cooled mercury cadmium telluride detector, at room temperature and constant dry-air purging. For every sample, 256 interferograms were recorded at 2 cm^{-1} resolution and averaged. D_2O and water vapour spectra were subtracted from the sample spectra, which were then baseline corrected and normalised to the same band area in a range between 1700 cm^{-1} and 1590 cm^{-1}. Spectra decomposition was done by using a Peak Fitting function (mixed Gaussian-Lorentzian) in a range between 1590 cm^{-1} and 1700 cm^{-1}. For each spectrum, the maximum peak number was set to 6 and RMS Noise was set to 0.04 when applying the fit. Peak parameter (maximum position and area) correlation graphs were then plotted for each sample and superimposed for comparison. All data processing was done using GRAMS software.

4.5. Aggregate Reseeding

Based on the results of the FTIR measurements, three distinct secondary structure samples were chosen for reseeding under different temperatures. Aliquots of lysozyme aggregate samples (80 µL) were combined with the initial reaction solution (720 µL) and incubated as described in the lysozyme aggregation kinetics section (200 µL final volume with a 3 mm glass bead in each well). Seeds prepared at 50 °C were incubated at 65 °C and samples prepared at 65 °C were incubated at 50 °C. After aggregation had occurred, the samples were cooled down to 25 °C and their FTIR spectra were measured as described previously. For sample reseeding under their respective initial preparation temperatures under quiescent conditions, the procedure was done without agitation or the addition of glass beads.

4.6. Atomic Force Microscopy

Aliquots of samples from the reseeding experiment (30 µL, after 800 min of quiescent incubation at their respective temperatures) were gently mixed by repetitive pipetting, placed on freshly cleaved mica and left to adsorb for 3 min. The samples were then gently washed with 3 mL of H_2O and dried using airflow. Further, 1024 × 1024 pixel three-dimensional images were obtained using a Dimension Icon atomic force microscope (Bruker, Billerica, MA, USA) as described previously [40]. Aggregate cross-sectional heights were determined by tracing line profiles perpendicular to the fibril axes. All data processing was done using Gwyddion software.

Supplementary Materials: The following supporting information can be downloaded at: https://www.mdpi.com/article/10.3390/ijms23105421/s1. The supplementary material includes raw data of lysozyme aggregation kinetics, ANS protein melt assay, fibril FTIR spectra, EEM spectra and different fibril type AFM images.

Author Contributions: Conceptualization, V.S. and M.Z.; investigation, K.M. and M.Z.; resources, V.S.; data analysis, V.S., K.M. and M.Z.; writing—original draft preparation, M.Z.; writing—review and editing, V.S., K.M. and M.Z. All authors have read and agreed to the published version of the manuscript.

Funding: This research received no external funding.

Institutional Review Board Statement: Not applicable.

Informed Consent Statement: Not applicable.

Data Availability Statement: All data are available in the Supplementary Materials.

Conflicts of Interest: The authors declare no conflict of interest.

Appendix A

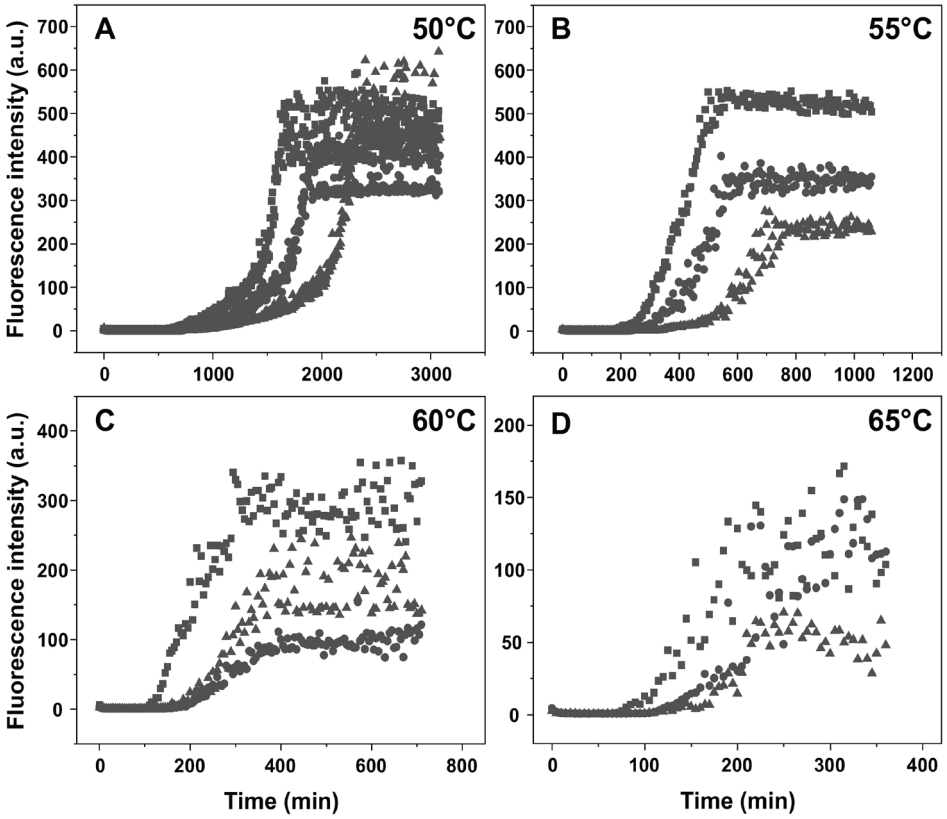

Figure A1. Examples of lysozyme aggregation kinetic curves at 50 °C (**A**), 55 °C (**B**), 60 °C (**C**) and 65 °C (**D**). Kinetic curves are from three repeats (different symbols represent separate samples).

References

1. Baker, K.R.; Rice, L. The Amyloidoses: Clinical Features, Diagnosis and Treatment. *Methodist Debakey Cardiovasc. J.* **2012**, *8*, 3–7. [CrossRef] [PubMed]
2. Knowles, T.P.J.; Vendruscolo, M.; Dobson, C.M. The amyloid state and its association with protein misfolding diseases. *Nat. Rev. Mol. Cell Biol.* **2014**, *15*, 384–396. [CrossRef] [PubMed]
3. Cummings, J.; Lee, G.; Zhong, K.; Fonseca, J.; Taghva, K. Alzheimer's disease drug development pipeline: 2021. *Alzheimer's Dement. Transl. Res. Clin. Interv.* **2021**, *7*, e12179. [CrossRef] [PubMed]
4. Chatani, E.; Yamamoto, N. Recent progress on understanding the mechanisms of amyloid nucleation. *Biophys. Rev.* **2018**, *10*, 527–534. [CrossRef] [PubMed]
5. Mehta, D.; Jackson, R.; Paul, G.; Shi, J.; Sabbagh, M. Why do trials for Alzheimer's disease drugs keep failing? A discontinued drug perspective for 2010–2015. *Expert Opin. Investig. Drugs* **2017**, *26*, 735–739. [CrossRef]
6. Doig, A.J.; del Castillo-Frias, M.P.; Berthoumieu, O.; Tarus, B.; Nasica-Labouze, J.; Sterpone, F.; Nguyen, P.H.; Hooper, N.M.; Faller, P.; Derreumaux, P. Why Is Research on Amyloid-β Failing to Give New Drugs for Alzheimer's Disease? *ACS Chem. Neurosci.* **2017**, *8*, 1435–1437. [CrossRef]
7. Arthur, K.C.; Calvo, A.; Price, T.R.; Geiger, J.T.; Chiò, A.; Traynor, B.J. Projected increase in amyotrophic lateral sclerosis from 2015 to 2040. *Nat. Commun.* **2016**, *7*, 12408. [CrossRef]
8. Brookmeyer, R.; Gray, S.; Kawas, C. Projections of Alzheimer's disease in the United States and the public health impact of delaying disease onset. *Am. J. Public Health* **1998**, *88*, 1337–1342. [CrossRef]

9. Meisl, G.; Yang, X.; Hellstrand, E.; Frohm, B.; Kirkegaard, J.B.; Cohen, S.I.A.; Dobson, C.M.; Linse, S.; Knowles, T.P.J. Differences in nucleation behavior underlie the contrasting aggregation kinetics of the Aβ40 and Aβ42 peptides. *Proc. Natl. Acad. Sci. USA* **2014**, *111*, 9384–9389. [CrossRef]
10. Buell, A.K.; Galvagnion, C.; Gaspar, R.; Sparr, E.; Vendruscolo, M.; Knowles, T.P.J.; Linse, S.; Dobson, C.M. Solution conditions determine the relative importance of nucleation and growth processes in α-synuclein aggregation. *Proc. Natl. Acad. Sci. USA* **2014**, *111*, 7671–7676. [CrossRef]
11. Gurry, T.; Stultz, C.M. Mechanism of amyloid-β fibril elongation. *Biochemistry* **2014**, *53*, 6981–6991. [CrossRef]
12. Milto, K.; Botyriute, A.; Smirnovas, V. Amyloid-Like Fibril Elongation Follows Michaelis-Menten Kinetics. *PLoS ONE* **2013**, *8*, e68684. [CrossRef]
13. Rodriguez, R.A.; Chen, L.Y.; Plascencia-Villa, G.; Perry, G. Thermodynamics of Amyloid-β Fibril Elongation: Atomistic Details of the Transition State. *ACS Chem. Neurosci.* **2018**, *9*, 783–789. [CrossRef] [PubMed]
14. Nicoud, L.; Lazzari, S.; Balderas Barragán, D.; Morbidelli, M. Fragmentation of Amyloid Fibrils Occurs in Preferential Positions Depending on the Environmental Conditions. *J. Phys. Chem. B* **2015**, *119*, 4644–4652. [CrossRef] [PubMed]
15. Törnquist, M.; Michaels, T.C.T.; Sanagavarapu, K.; Yang, X.; Meisl, G.; Cohen, S.I.A.; Knowles, T.P.J.; Linse, S. Secondary nucleation in amyloid formation. *Chem. Commun.* **2018**, *54*, 8667–8684. [CrossRef]
16. Foderà, V.; Librizzi, F.; Groenning, M.; Van De Weert, M.; Leone, M. Secondary nucleation and accessible surface in insulin amyloid fibril formation. *J. Phys. Chem. B* **2008**, *112*, 3853–3858. [CrossRef]
17. Gaspar, R.; Meisl, G.; Buell, A.K.; Young, L.; Kaminski, C.F.; Knowles, T.P.J.; Sparr, E.; Linse, S. Secondary nucleation of monomers on fibril surface dominates α-synuclein aggregation and provides autocatalytic amyloid amplification. *Q. Rev. Biophys.* **2017**, *50*, e6. [CrossRef]
18. Sidhu, A.; Segers-Nolten, I.; Raussens, V.; Claessens, M.M.A.E.; Subramaniam, V. Distinct Mechanisms Determine α-Synuclein Fibril Morphology during Growth and Maturation. *ACS Chem. Neurosci.* **2017**, *8*, 538–547. [CrossRef]
19. Fujiwara, S.; Matsumoto, F.; Yonezawa, Y. Effects of salt concentration on association of the amyloid protofilaments of Hen egg white lysozyme studied by time-resolved neutron scattering. *J. Mol. Biol.* **2003**, *331*, 21–28. [CrossRef]
20. Loquet, A.; El Mammeri, N.; Stanek, J.; Berbon, M.; Bardiaux, B.; Pintacuda, G.; Habenstein, B. 3D structure determination of amyloid fibrils using solid-state NMR spectroscopy. *Methods* **2018**, *138*, 26–38. [CrossRef]
21. Lattanzi, V.; André, I.; Gasser, U.; Dubackic, M.; Olsson, U.; Linse, S. Amyloid β 42 fibril structure based on small-angle scattering. *Proc. Natl. Acad. Sci. USA* **2021**, *118*, 6–11. [CrossRef] [PubMed]
22. Karamanos, T.K.; Kalverda, A.P.; Thompson, G.S.; Radford, S.E. Mechanisms of amyloid formation revealed by solution NMR. *Prog. Nucl. Magn. Reson. Spectrosc.* **2015**, *88*, 86–104. [CrossRef] [PubMed]
23. Moran, S.D.; Zanni, M.T. How to Get Insight into Amyloid Structure and Formation from Infrared Spectroscopy. *J. Phys. Chem. Lett.* **2014**, *5*, 1984–1993. [CrossRef] [PubMed]
24. Sneideris, T.; Darguzis, D.; Botyriute, A.; Grigaliunas, M.; Winter, R.; Smirnovas, V. pH-Driven Polymorphism of Insulin Amyloid-Like Fibrils. *PLoS ONE* **2015**, *10*, e0136602. [CrossRef]
25. Wawer, J.; Szociński, M.; Olszewski, M.; Piątek, R.; Naczk, M.; Krakowiak, J. Influence of the ionic strength on the amyloid fibrillogenesis of hen egg white lysozyme. *Int. J. Biol. Macromol.* **2019**, *121*, 63–70. [CrossRef]
26. Gaspar, R.; Lund, M.; Sparr, E.; Linse, S. Anomalous Salt Dependence Reveals an Interplay of Attractive and Repulsive Electrostatic Interactions in α-synuclein Fibril Formation. *QRB Discov.* **2020**, *1*, e2. [CrossRef]
27. Noormägi, A.; Valmsen, K.; Tõugu, V.; Palumaa, P. Insulin Fibrillization at Acidic and Physiological pH Values is Controlled by Different Molecular Mechanisms. *Protein J.* **2015**, *34*, 398–403. [CrossRef]
28. Sakalauskas, A.; Ziaunys, M.; Smirnovas, V. Concentration-dependent polymorphism of insulin amyloid fibrils. *PeerJ* **2019**, *7*, e8208. [CrossRef]
29. Fändrich, M.; Meinhardt, J.; Grigorieff, N. Structural polymorphism of Alzheimer Aβ and other amyloid fibrils. *Prion* **2009**, *3*, 89–93. [CrossRef]
30. Ziaunys, M.; Sakalauskas, A.; Mikalauskaite, K.; Snieckute, R.; Smirnovas, V. Temperature-dependent structural variability of prion protein amyloid fibrils. *Int. J. Mol. Sci.* **2021**, *22*, 5075. [CrossRef]
31. Zhang, W.; Falcon, B.; Murzin, A.G.; Fan, J.; Crowther, R.A.; Goedert, M.; Scheres, S.H.W. Heparin-induced tau filaments are polymorphic and differ from those in alzheimer's and pick's diseases. *eLife* **2019**, *8*, e43584. [CrossRef]
32. Collinge, J.; Clarke, A.R. A General Model of Prion Strains and Their Pathogenicity. *Science* **2007**, *318*, 930–936. [CrossRef] [PubMed]
33. Feng, Z.; Li, Y.; Bai, Y. Elevated temperatures accelerate the formation of toxic amyloid fibrils of hen egg-white lysozyme. *Vet. Med. Sci.* **2021**, *7*, 1938–1947. [CrossRef] [PubMed]
34. Swaminathan, R.; Ravi, V.K.; Kumar, S.; Kumar, M.V.S.; Chandra, N. *Lysozyme: A model protein for amyloid research. In Advances in Protein Chemistry and Structural Biology*; Elsevier: Amsterdam, The Netherlands, 2011; Volume 84, pp. 63–111. ISBN 9780123864833.
35. Ow, S.-Y.; Dunstan, D.E. The effect of concentration, temperature and stirring on hen egg white lysozyme amyloid formation. *Soft Matter* **2013**, *9*, 9692. [CrossRef] [PubMed]
36. Arnaudov, L.N.; De Vries, R. Thermally induced fibrillar aggregation of hen egg white lysozyme. *Biophys. J.* **2005**, *88*, 515–526. [CrossRef]

37. Sulatskaya, A.I.; Rodina, N.P.; Povarova, O.I.; Kuznetsova, I.M.; Turoverov, K.K. Different conditions of fibrillogenesis cause polymorphism of lysozyme amyloid fibrils. *J. Mol. Struct.* **2017**, *1140*, 52–58. [CrossRef]
38. Rahimi Araghi, L.; Dee, D.R. Cross-Species and Cross-Polymorph Seeding of Lysozyme Amyloid Reveals a Dominant Polymorph. *Front. Mol. Biosci.* **2020**, *7*, 206. [CrossRef]
39. Ziaunys, M.; Sakalauskas, A.; Mikalauskaite, K.; Smirnovas, V. Polymorphism of Alpha-Synuclein Amyloid Fibrils Depends on Ionic Strength and Protein Concentration. *Int. J. Mol. Sci.* **2021**, *22*, 12382. [CrossRef]
40. Ziaunys, M.; Sakalauskas, A.; Smirnovas, V. Identifying Insulin Fibril Conformational Differences by Thioflavin-T Binding Characteristics. *Biomacromolecules* **2020**, *21*, 4989–4997. [CrossRef]
41. Barth, A. Infrared spectroscopy of proteins. *Biochim. Biophys. Acta Bioenerg.* **2007**, *1767*, 1073–1101. [CrossRef]

Rapid restructurization of conformationally-distinct alpha-synuclein amyloid fibrils at an elevated temperature

Mantas Ziaunys, Andrius Sakalauskas, Kamile Mikalauskaite and Vytautas Smirnovas

Institute of Biotechnology, Life Sciences Center, Vilnius University, Vilnius, Lithuania

ABSTRACT

Protein aggregation in the form of amyloid fibrils is linked with the onset and progression of more than 30 amyloidoses, including multiple neurodegenerative disorders, such as Alzheimer's or Parkinson's disease. Despite countless studies and years of research, the process of such aggregate formation is still not fully understood. One peculiar aspect of amyloids is that they appear to be capable of undergoing structural rearrangements even after the fibrils have already formed. Such a phenomenon was reported to occur in the case of alpha-synuclein and amyloid beta aggregates after a long period of incubation. In this work, we examine whether incubation at an elevated temperature can induce the restructurization of four different conformation alpha-synuclein amyloid fibrils. We show that this structural alteration occurs in a relatively brief time period, when the aggregates are incubated at 60 °C. Additionally, it appears that during this process multiple conformationally-distinct alpha-synuclein fibrils all shift towards an identical secondary structure.

Subjects Biochemistry, Biophysics, Molecular Biology
Keywords Amyloid, Alpha-synuclein, Protein aggregation, Protein fibrils, Fibril structure

Submitted 2 June 2022
Accepted 6 September 2022
Published 30 September 2022

Corresponding author
Mantas Ziaunys,
mantas.ziaunys@gmail.com

Academic editor
Vladimir Uversky

Additional Information and Declarations can be found on page 13

DOI **10.7717/peerj.14137**

INTRODUCTION

Protein aggregation into highly-structured amyloid fibrils is linked with the onset and progression of over 30 amyloidoses, including neurodegenerative Alzheimer's or Parkinson's diseases (*Knowles, Vendruscolo & Dobson, 2014*; *Chiti & Dobson, 2017*). Currently, the process of fibril formation is still not completely understood (*Lee & Terentjev, 2017*; *Chaudhuri et al., 2019*), which, in turn, has resulted in very few approved drugs or treatment modalities (*Mehta et al., 2017*; *Doig et al., 2017*; *Maurer et al., 2018*; *Cummings et al., 2020*). It is projected that the already high number of patients afflicted with these disorders will continue to rise in the upcoming years (*Brookmeyer, Gray & Kawas, 1998*; *Arthur et al., 2016*). In order to prevent this and discover potential cures, a better understanding of both the formation pathways (*Brännström et al., 2018*), as well as the resulting aggregates (*Fändrich et al., 2018*) is necessary.

Protein misfolding and association into fibrillar structures proceeds through multiple stages. The first step in amyloid aggregation is primary nucleation—a process during which native protein molecules misfold and assemble into a stable, β-sheet-rich nucleus

How to cite this article Ziaunys M, Sakalauskas A, Mikalauskaite K, Smirnovas V. 2022. Rapid restructurization of conformationally-distinct alpha-synuclein amyloid fibrils at an elevated temperature. **PeerJ 10:e14137 DOI 10.7717/peerj.14137**

(*Buell et al., 2014*; *Meisl et al., 2014*). Once a stable nucleus is formed, it can then incorporate other, homologous protein molecules into its structure and elongate into a protofibrillar aggregate. The process of elongation occurs at the ends of the fibrillar structure, which act as both a catalyst and template for the conversion of native protein/peptide molecules (*Milto, Botyriute & Smirnovas, 2013*; *Gurry & Stultz, 2014*; *Rodriguez et al., 2018*). When amyloid fibrils reach a critical length, they can experience fragmentation—a process during which the aggregate breaks into two shorter fibrils, each with its own aggregation-catalyzing ends. The incidence of fragmentation depends on both the structural stability of the aggregate, as well as the environmental conditions (*Nicoud et al., 2015*). Another process, which occurs once amyloid fibrils form, is surface-mediated nucleation (also referred to as secondary nucleation) (*Foderà et al., 2008*; *Gaspar et al., 2017*; *Törnquist et al., 2018*). During this step, the surface of aggregates acts as a catalyst for the formation of new amyloid nuclei. Unlike elongation at fibril ends, this process does not template the aggregate's structure onto the nuclei, but only increase their probability of formation (*Sneideris, Milto & Smirnovas, 2015*).

It is usually considered that once the aggregation reaction uses up all or most of the available monomers, then the amyloid formation process is complete, with only certain other events occurring, such as fibril lateral association (*Fujiwara, Matsumoto & Yonezawa, 2003*) or large cluster formation (*Manno et al., 2006*). However, this may not be the case. It was shown that during a long incubation time, alpha-synuclein (*Sidhu et al., 2017*) and amyloid beta fibrils (*Ma et al., 2013*) experienced structural alterations. It was hypothesized that this type of aggregate "maturation" may also be required for fibrils to obtain a higher level of infectivity (*Yamaguchi et al., 2005*). If this restructurization occurs for other amyloids as well, then it may also have an impact on *in vitro* experiments, making incubation time (*Morel et al., 2010*) a crucial factor. Even if the exact same reaction solution and protocol is used, the aggregates may undergo structural rearrangement after their formation (*Mahdavimehr, Katebi & Meratan, 2018*). If the assay employs a set timeframe of fibrillization, then uninhibited aggregation would yield fibers sooner than in the inhibitor reaction solution and they would incubate for a relatively longer time. This could result in aggregates with seemingly different structural aspects (*Pellarin et al., 2010*) and skew the experimental data, as well as conclusions of the study.

In this work, we generated alpha-synuclein fibrils under previously reported experimental conditions, which yield multiple structurally-distinct aggregates from an identical protein solution (*Toleikis et al., 2021*). The resulting four distinct fibril solutions were then incubated at 60 °C and their structural alterations were observed using CD, infrared and UV/Vis spectroscopy, atomic force microscopy, as well as ThT-binding assays (*Hoyer et al., 2002*; *Ziaunys, Sakalauskas & Smirnovas, 2020*). We show that all four different types of fibrils rapidly converge into aggregates with similar secondary structures and that this change occurs in the matter of hours.

MATERIALS AND METHODS

Initial fibril preparation

Alpha-synuclein (α-syn) was purified as described previously (*Šneideris et al., 2015*), lyophilized, and stored at −20 °C prior to use. Further fibril preparation procedures were done under similar conditions as described previously (*Toleikis et al., 2021*). The α-syn powder was dissolved in a phosphate-buffered saline (PBS, pH 7.4) and filtered through a 0.22 μm syringe filter, after which the protein concentration was determined using a Shimadzu UV-1800 spectrophotometer (ε_{280} = 5,960 $M^{-1}cm^{-1}$). The protein solution was then combined with a 10 mM thioflavin-T (ThT) solution and PBS to result in a final protein concentration of 70 and 100 μM ThT. The solution was then distributed to 96-well half-area non-binding plates (cat. No 3881, Fisher Scientific, Hampton, NH, USA) (each well contained 100 μL of the solution and one 3 mm diameter glass-bead (cat. No 104015, Merck, Kenilworth, NJ, USA) and sealed with Nunc sealing-tape. The 96-well plates were incubated at 37 °C in a ClarioStar Plus plate reader, under constant 600 RPM agitation for 48 h, with measurements taken every 5 min (excitation wavelength was 440 nm, emission – 480 nm). For aggregation monitoring under 60 °C, all sample preparation and incubation procedures, apart from the set temperature, were identical. After aggregation, the plates were cooled down to room temperature prior to further examination. Aggregation lag time and apparent rate constants were determined as described previously (*Ziaunys et al., 2021a*).

Excitation-emission matrices (EEM)

The procedure of EEM acquisition was based on a previous study on alpha-synuclein aggregation (*Ziaunys et al., 2021a*). In short, 96-well plates containing the fibril samples were placed in a ClarioStar Plus platereader and incubated at 25 °C for 5 min. Bound-ThT excitation-emission matrices (EEM) were obtained by first scanning the sample fluorescence emission intensity at a fixed wavelength (485 nm), using a range of excitation wavelengths (430–460 nm). Afterwards, the intensity was scanned under a range of emission wavelengths (470–500 nm), using a fixed excitation wavelength (445 nm). The data was combined into an EEM by using ClarioStar MARS 3D spectrum function. EEM "centers of mass" were calculated as described previously (*Ziaunys & Smirnovas, 2019*). In short, the center of mass was calculated for the top 10% intensity values from each EEM. All the maximum position values were then plotted in a single graph for comparison. Since alpha-synuclein and other amyloid fibril ThT-binding characteristics can be related to their structure/morphology (*Sidhu et al., 2018*; *Ziaunys et al., 2021a*; *Ziaunys et al., 2021b*), eight out of the 96 samples with distinct EEM maximum positions were selected for further replication and analysis. This selection procedure was done in order to improve the likelihood of obtaining different types of alpha-synuclein fibrils, without the necessity to analyze the entirety of the large number of samples.

Fibril reseeding

In order to generate a higher quantity of aggregates, the eight selected samples (100 μL) were each combined with 400 μL of the initial reaction solution, containing 70 μM α-syn

monomers. The resulting solutions were placed in 1.5 mL test-tubes (each containing two 3 mm glass beads) and incubated at 37 °C with constants 600 RPM agitation for 24 h in a Digital Heating Shaking Dry bath (Fisher Scientific, Hampton, NH, USA). The resulting aggregate solutions were then combined with 2 mL of the initial reaction solution, divided into 1.5 mL test-tubes (500 µL each) and incubated identically for another 24 h.
The resulting 2.5 mL solutions were combined with 2.5 mL of initial reaction solutions and incubated as described previously, resulting in 5 mL volume α-syn aggregate solutions, which were then cooled down to room temperature.

Each fibril solution was then distributed to 1.5 mL test-tubes (1 mL each) and centrifuged at 10,000×*g* for 15 min, after which the supernatant (900 µL) was removed and replaced with an identical volume of the initial buffer solution, which did not contain α-syn monomers. These centrifugation and fibril pellet resuspension steps were repeated three times, in order to remove non-aggregated protein monomers. This was done in case the aggregation reactions at 37 °C did not use up all available monomers (the resulting samples may also contain a fraction of monomers due to an equilibrium between native and aggregated proteins). Afterwards the samples were combined to a final volume of 5 mL. All further experimental procedures were performed using only these replicated and resuspended samples.

Fibril incubation

Each 5 mL fibril sample was vigorously agitated for 10 s and then distributed to sets of three 1.5 mL test-tubes (1.5 mL solution volume, each test-tube contained two 3 mm glass beads). The first set was kept at room temperature, while the other two sets were incubated at 60 °C under constant 600 RPM agitation for either 24 or 48 h. During the incubation procedures, aliquots of each sample were taken for further analysis by Fourier-transform infrared (FTIR) and circular dichroism (CD) spectroscopies, atomic force microscopy (AFM) and UV/Vis spectroscopy.

To measure the changes in bound-ThT EEM positions, the selected samples were placed into 96-well half-area non-binding plates (100 µL volume, one 3 mm glass bead in each well) and incubated in a ClarioStar Plus plate reader at 60 °C under constant 600 RPM agitation. EEMs were scanned every hour. Both the scanning and analysis procedure was identical to the one described in the previous method section.

Fourier-transform infrared (FTIR) spectroscopy

For FTIR measurements, 500 µL of each aggregate sample was centrifuged at 10,000 × *g* for 15 min, after which the supernatant was removed and replaced with 500 µL D_2O (containing 400 mM NaCl in order to improve fibril sedimentation (*Mikalauskaite et al., 2020*)). The centrifugation and resuspension procedure was repeated four times. After the final step, the fibril pellet was resuspended into 50 µL D_2O and mixed vigorously for 10 s. FTIR spectra were acquired as described previously (*Mikalauskaite, Ziaunys & Smirnovas, 2022*), which were then baseline corrected and normalized to the same band area in a range between 1,700 and 1,595 cm^{-1}. All data processing was done using GRAMS software.

Circular dichroism (CD) spectroscopy

For CD spectroscopy measurements, aliquots of each fibril sample (50 µL) were taken every hour for the first 10 incubation hours, then after 24 and 48 h. The samples were cooled down to 25 °C and placed in a 0.1 mm pathlength cuvette. The CD spectra were measured between 200 and 250 nm, using a Jasco J-815 spectropolarimeter. For each sample, three spectra were recorded and averaged, after which a PBS solution spectrum was subtracted from each sample spectrum. The data was then analyzed using BeStSel Protein Circular Dichroism (*Micsonai et al., 2015*) spectra analysis software, in order to determine the content of secondary structures.

Atomic force microscopy (AFM)

AFM sample preparations and measurements were performed as described previously (*Ziaunys et al., 2021a*). Before sample deposition, freshly cleaved mica surface was modified with (3-aminopropyl) triethoxysilane (APTES). 0.5% (% v/v) APTES solution (30 µL) was spread on the surface of the mica, incubated at room temperature for 5 min, gently washed with 2 mL of H_2O and dried using airflow. 30 µL aliquots of each sample were placed on APTES-modified mica and left to adsorb for 60 s. The mica were then gently washed with 3 mL of H_2O and dried using airflow. AFM images were acquired using a Dimension Icon (Bruker) atomic force microscope and analyzed using Gwyddion 2.5.5 software as described previously (*Ziaunys et al., 2021a*).

UV/Vis spectroscopy

Each fibril sample (500 µL) was supplemented with 5 µL 10 mM ThT and vigorously agitated for 10 s. The samples were then placed in a 3 mm pathlength cuvette and sample absorbance spectra were scanned in the 200–600 nm range using a Shimadzu UV-1800 spectrophotometer (three repeats were scanned for each sample and averaged). After this, 200 µL of each sample was centrifuged at 10,000×*g* for 15 min and 100 µL of the supernatant was carefully removed. The supernatant absorbance spectra were scanned as described previously. In order to determine the absorbance spectra of bound-ThT molecules, the supernatant spectra were subtracted from the fibril-ThT spectra and baseline corrected between 300 and 550 nm using Origin 2018 software baseline subtraction function with three anchor points at each side of the peak.

RESULTS

In order to test the effect that an elevated temperature has on alpha-synuclein (α-syn) fibril structure, different conformation aggregates were first generated. Since α-syn is capable of spontaneously forming structurally distinct fibrils under identical experimental conditions (*Toleikis et al., 2021*; *Ziaunys et al., 2021a*) at random, a large number of samples (n = 96) was aggregated for an initial assessment. Potential conformationally-distinct fibrils were then identified by scanning their bound-ThT excitation-emission matrices (EEM) and selecting eight samples from the set, based on their unique EEM positions (Fig. 1A) (*Ziaunys et al., 2021a*). This was done in order to increase the likelihood of obtaining different structure samples, without the necessity to analyze the entire set. The selected

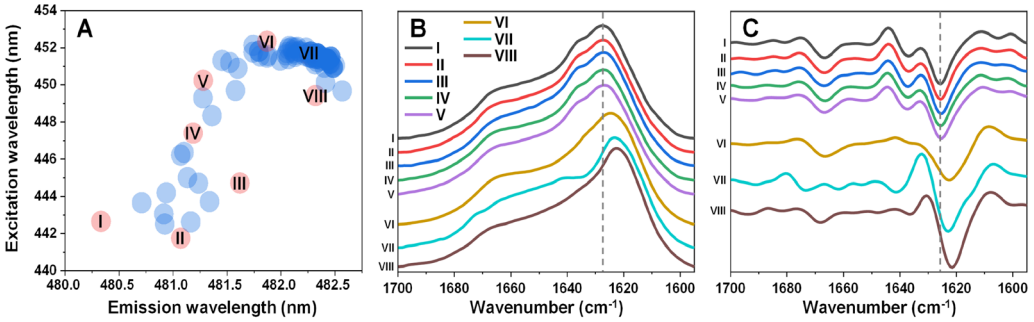

Figure 1 Excitation-emission matrix (EEM) positions of fibril-bound ThT fluorescence (A) and selected fibril sample FTIR spectra (B) and their second derivatives (C). EEM maximum positions were determined as described in the Materials and Methods section (96 samples) after sample aggregation. Red color-coded circles marked with Roman numerals represent samples chosen for further analysis.

Full-size DOI: 10.7717/peerj.14137/fig-1

samples were then replicated as described in the Materials and Methods section in order to generate a higher quantity of aggregates. To determine which of the samples contained significantly different secondary structures, an aliquot from each was scanned using Fourier-transform infrared spectroscopy (FTIR).

Five of the samples contained aggregates with similar secondary structures (Figs. 1B, 1C), with the FTIR spectrum main maximum at 1,627 cm^{-1} and a shoulder at 1,636 cm^{-1} (same position minima in the second derivatives, which are positions associated with hydrogen bonds in the beta-sheet structure (*Barth, 2007*)). They also had a minimum in the second derivative at 1,666 cm^{-1}, which is related to turn/loop motifs. Due to their similarities, these five samples were regarded as Type 1 fibrils. The VI sample shared some similarities to Type 1 aggregates in the turn/loop motif position (1,666 cm^{-1}), however, the main maximum was shifted to 1,624 cm^{-1}, suggesting a different type of hydrogen bonding in the beta-sheet structure. Since this sample FTIR spectra was different from all other seven and had a main maximum position between other two group spectra positions, it was regarded as consisting of Type 2 fibrils. The other two remaining samples (VII and VIII) shared a similar main maximum position at 1,623–1,624 cm^{-1}, with significant variation in the turn/loop motif regions (minima at 1,662 and 1,673 cm^{-1} for Type 3, 1,668 cm^{-1} for Type 4). These four replicated fibril types were then used in all further experimental procedures.

Before incubating the selected fibrils at an elevated temperature, the aggregates were first centrifuged and resuspended into their initial buffer solution, in case they contained a significant concentration of non-aggregated protein. This was done to avoid any possible additional aggregation occurring during the incubation procedure. The resuspended fibrils were then incubated at 60 °C with constant agitation for 24 or 48 h as described in the Materials and Methods section. After this step, a portion of each sample was used to scan their FTIR spectra.

In the case of Type 1 fibrils (Figs. 2A, 2E) after 24 h of incubation, there was a shift of the FTIR spectrum main maximum position towards 1,625–1,626 cm^{-1} and a reduction of the

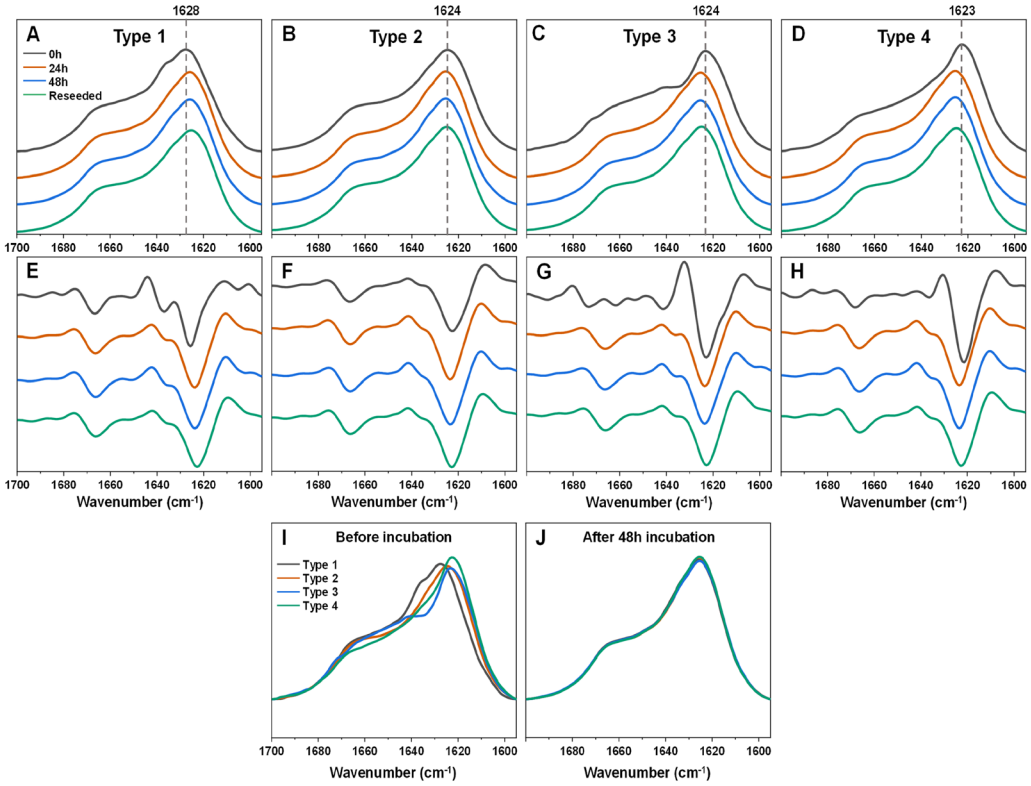

Figure 2 Fourier-transform infrared (FTIR) spectra and second derivatives of α-syn fibril samples before and after incubation at 60 °C and reseeding at 37 °C. Type 1 (A, E), Type 2 (B, F), Type 3 (C, G) and Type 4 (D, H) fibril sample FTIR spectra and second derivatives. Black lines correspond to the control samples, orange–after 24 h of incubation at 60 °C, blue–after 48 h of incubation at 60 °C and green–48 h incubation samples reseeded at 37 °C. Dotted grey lines indicate the main maximum position of the initial sample FTIR spectrum. Superimposed FTIR spectra of all four fibril types before (I) and after 48 h of incubation at 60 °C (J). Full-size DOI: 10.7717/peerj.14137/fig-2

shoulder at 1,636 cm^{-1} with minimal changes in the region associated with turn/loop motifs. This suggests that incubation at an elevated temperature resulted in the reduction of weaker hydrogen bonds and the formation of stronger ones. Further incubation at an elevated temperature did not yield any notable changes. An opposite effect was observed for the Type 3 and Type 4 samples (Figs. 2C, 2D, 2G, 2H). Here, the main maximum positions shifted towards a larger wavenumber (from 1,623–1,624 to 1,625–1,626 cm^{-1}). Surprisingly, the resulting FTIR spectra were almost completely identical to the one which formed when Type 1 fibrils were incubated (Figs. 2A, 2E). The Type 2 sample spectrum (Figs. 2B, 2F) experienced only very minor changes during incubation, which was to be expected, as it had a similar spectrum to the incubated fibril spectra, as seen for Type 1, 3 and 4 fibrils. Taken together, this indicates that the α-syn fibril polymorphism, which

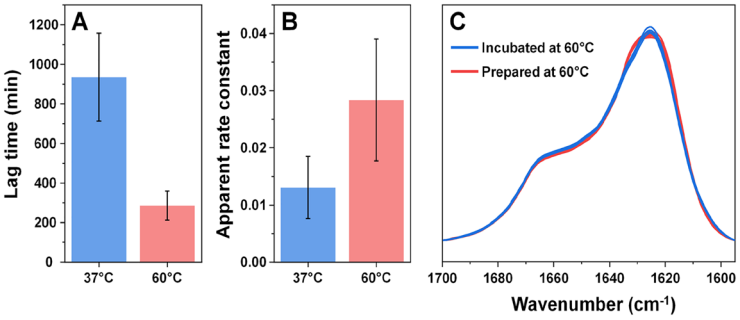

Figure 3 Comparison of alpha-synuclein aggregation kinetics and resulting structure under different temperatures. The lag time (A) and apparent rate constant of fibril elongation (B) at 37 °C and 60 °C ($n = 8$). Superimposed FTIR spectra of Type 1–4 incubated fibrils (blue color) and eight spectra of fibrils prepared at 60 °C (red color). Full-size DOI: 10.7717/peerj.14137/fig-3

existed when aggregation occurred at 37 °C, was completely negated when the fibrils were incubated at an elevated temperature.

In order to verify if this newly-formed fibril type is the result of restructurization or simply a temperature-induced association/clumping, each 48 h incubation sample was reseeded at 37 °C as described in the Materials and Methods section and the resulting aggregate FTIR spectra were scanned. Interestingly, all four of the α-syn samples retained the same identical spectra as were obtained after incubation at 60 °C. This suggests that the newly-formed fibril type is capable of templating its structure under lower temperature conditions as well and does not revert back to its original state. Comparing all four FTIR spectra before and after incubation shows how they all become practically identical and overlap with each other (Figs. 2I, 2J).

Considering that an elevated temperature resulted in the formation of aggregates with an identical secondary structure, it was interesting to compare them to fibrils which originally formed at 60 °C. Based on the kinetic data, alpha-synuclein aggregation proceeded significantly quicker when subjected to a higher temperature. The process average lag time was reduced three times (Fig. 3A) and the apparent rate constant of fibril elongation increased two times (Fig. 3B). The formed aggregate FTIR spectra were almost completely identical to the incubated fibril spectra, with the same main maximum position and overlapping spectra in the turn/loop motif region. This indicates that an elevated temperature leads to the same specific alpha-synuclein conformation, regardless if the aggregates were prepared at 37 °C or 60 °C.

Since incubation led to changes in fibril secondary structure, it was important to also analyze any possible morphological differences. Comparing the AFM images of all three fibril Types (Figs. 4A–4D, with their 48 h incubation counterparts (Figs. 4E–4H)), it can be observed that both the initial and incubated samples contained long fibers with some of them having periodicity patterns. Based on a visual inspection, it may appear that the

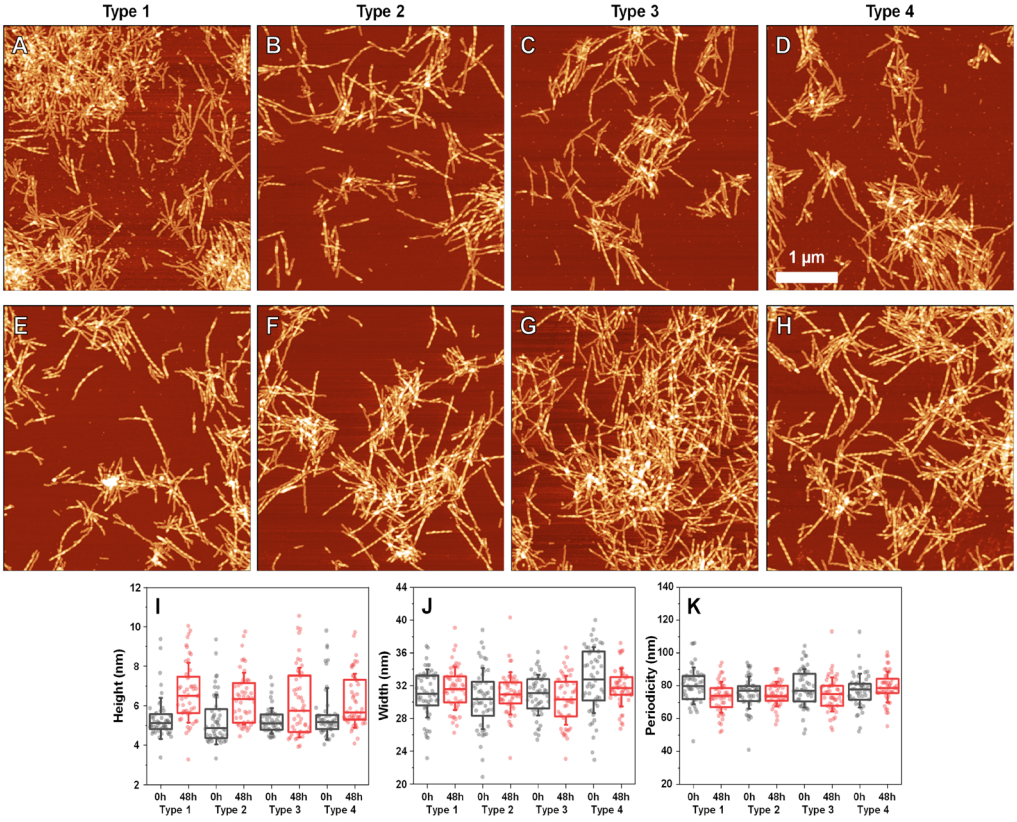

Figure 4 Atomic force microscopy (AFM) images of different fibril types before and after incubation. AFM images of Type 1 (A, E), Type 2 (B, F), Type 3 (C, G) and Type 4 (D, H) fibrils, as well as height (I), width (J) and periodicity (K) distribution before and after incubation respectively. All images are of identical 5 × 5 µm scale. Fibril height, width and periodicity were determined as described in the Materials and Methods section. Distribution box plots (n = 50) indicate the interquartile range and error bars are for one standard deviation.

Full-size DOI: 10.7717/peerj.14137/fig-4

incubated samples contained a larger number of fibrils with periodicity patterns, however, such a conclusion is difficult to make based on AFM images alone.

Comparing the heights of fibrils (Fig. 4I) revealed that in all three cases, the average values were slightly higher for incubated samples (1–2 nm difference). This could be the result of the aforementioned morphological changes or fibril lateral association, however, the small difference in average values, coupled with no differences in fibril width (Fig. 4J) led to an assumption that incubation had no substantial effect on these parameters. Interestingly, the distances between periodic repeats of fibrils also did not change upon incubation (Fig. 4K), which means that the alterations in secondary structure did not have an influence on this morphological parameter. Additionally, all four cases (control and

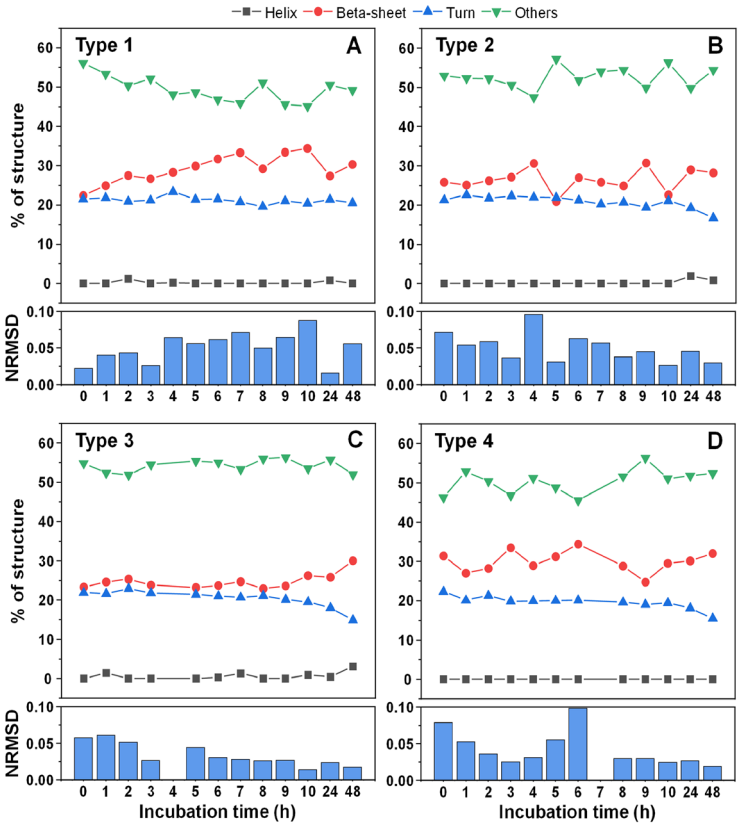

Figure 5 Alpha-synuclein fibril secondary structure element distribution during incubation at 60 °C. The secondary structures for Type 1 (A), Type 2 (B), Type 3 (C) and Type 4 (D) fibrils were determined by scanning each sample's CD spectra after different periods of incubation and fitting the data using BeStSel Protein circular dichroism spectra analysis software. The normalized root mean square deviation (NRMSD) of each sample's secondary structure element distribution is displayed under their respective distribution graphs. Full-size DOI: 10.7717/peerj.14137/fig-5

incubated), did not have a homogenous distribution, as both non-periodic and periodic fibrils could be detected in all samples. This suggests that the restructurization may not affect certain subgroups of aggregates, which may require a significantly longer time to change, as shown by *Sidhu et al. (2017)*.

Since there was a slight increase in fibril height, there existed a possibility that parts of the unstructured protein region became incorporated into the aggregate core region. In order to examine this possibility, CD spectra of all four fibril types were scanned after each hour of incubation for 10 h, as were the 24 and 48 h samples. When comparing the initial and end-point samples, for Type 1 (Fig. 5A) and Type 3 fibrils (Fig. 5C) there was a

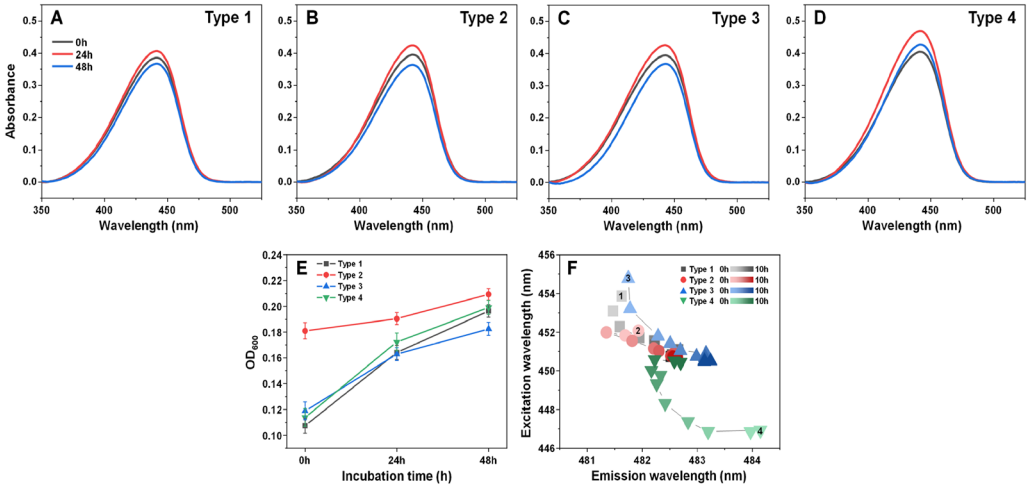

Figure 6 Absorbance and fluorescence spectra of fibril-bound ThT during incubation at 60 °C. Absorbance spectra of Type 1 (A), Type 2 (B), Type 3 (C) and Type 4 (D) fibril-bound ThT before and after incubation at 60 °C for 24 and 48 h. Optical density of all four samples before and after incubation (E), determined at 600 nm. Sample bound-ThT fluorescence EEM position changes over the course of 10 h of incubation (F). The change in EEM positions over time is represented as a color gradient in subfigure F (lighter color–shorter incubation time, darker color–longer incubation time). The initial 0 h sample EEM positions were measured after the samples reached 60 °C (the heating procedure was 10 min). Sample absorbance and fluorescence measurement procedures are described in the Materials and Methods section. Absorbance data is the average of three repeats.
Full-size DOI: 10.7717/peerj.14137/fig-6

slight increase in the fraction of beta-sheets and a reduction in either turn or unstructured regions. For the other two fibril types (Figs. 5B, 5D), there were no notable deviations observed. In all cases, however, the change was rather marginal and, due to the relatively large normalized root mean square deviation values (NRMSD) (*Micsonai et al., 2015*), could not be considered as statistically significant.

Examining the absorbance spectra of fibril-bound ThT (Figs. 6A–6D) revealed that there were no sizeable variations in either the maximum absorbance value position or the maximum absorbance itself. This indicates that the structural rearrangements did not cause significant changes to the amount of bound ThT molecules. Interestingly, the same cannot be said about the sample optical density. There was a clear disparity between the Type 2 fibril sample and the rest (Fig. 6E), where the Type 2 sample had an OD_{600} of 0.18, while for Type 1, 3 and 4 it was 0.10–0.12. After 24 h of incubation, there was only a minimal increase in OD_{600} for the Type 2 sample, while the other three aggregate samples experienced a substantial OD_{600} increase to 0.16–0.17. Additional incubation caused a further convergence of the OD_{600} values. Considering that the fibrils were resuspended into the initial reaction solution, which did not contain α-syn monomers, additional aggregation can be ruled out as a cause of such a significant increase in optical density. This leaves the possibility that aggregate structural rearrangement caused an increase in the sample light scattering properties. This is further supported by the fact that the Type 2

sample experienced the least significant change in OD_{600}, similarly to it having the least notable FTIR spectrum shift.

In order to examine whether there was also a shift in bound-ThT EEM maximum positions, the four different fibril types were incubated as described in the Materials and Methods section at 60 °C and their EEM spectra were scanned every hour. The initial scans were performed after the samples reached 60 °C (after 10 min of incubation). During the first 4 h, the EEM positions shifted significantly (Fig. 6F), suggesting a change in the ThT-binding properties of the aggregates (as a note, the 60 °C EEM positions do not correlate to the Fig. 1 positions due to the elevated sample temperature, which reduces the dye's fluorescence quantum yield and may influence the mode of binding). After 5–6 h of incubation, all four fibril type bound-ThT EEM positions converged to a similar position, which falls in line with the FTIR results. Comparing this information to the minimal change observed in ThT absorbance spectra, it appears that the structural alterations mainly affect the dye's mode of binding, rather than the quantity of surface-associated molecules. These results suggest that most major changes to the fibril structures occur during the initial 4 h of incubation.

DISCUSSION

Taking into consideration all the results presented in this work, it appears that different conformation α-syn fibrils undergo rapid restructurization at an elevated temperature. While physiological temperatures were also reported to cause aggregate maturation, the process spanned over several days or even months (*Ma et al., 2013*; *Sidhu et al., 2017*). In this case, based on changes in FTIR spectra and sample optical density, significant alterations to the secondary structure occurred in less than 24 h. If we use ThT fluorescence as an indicator of distinct structure aggregates, then the ThT excitation-emission matrix assay displays that most of the significant changes happened during the initial 4 h of incubation. If this is the case, then it is possible that α-syn fibril maturation is a condition-dependent process, which is greatly escalated at higher temperatures.

Another interesting aspect was the apparent convergence of multiple distinct conformation fibrils into one type of dominant aggregate with the increase of the solution's temperature. The four fibril types with distinct FTIR spectra all rapidly changed into one specific conformation, which was also capable of replicating its structure at the initial 37 °C temperature, similarly to the initial four aggregate types. The structural alterations also do not appear to be caused by a significant increase in the fibril beta-sheet content (as seen during CD analysis), but rather due to a restructurization of existing secondary structure elements. This hints at a possible meta-stability of the fibrils generated at 37 °C and that their existence is only facilitated by a high energy barrier needed to cross into the higher stability structure. Such a hypothesis is supported by the FTIR spectra similarity of incubated fibrils and aggregates prepared at 60 °C (Fig. 3C). However, while this may be the case for pre-existing fibril conversion, the barrier does not appear to prevent the initial formation of such aggregates (Type 2 fibrils). In the AFM images, we can observe each initial sample containing fibrils with periodicity patterns. Such fibers seem to be the

dominant type of structure after incubation and their presence in each sample suggests that they can readily form at 37 °C as well. Despite this appearance, it is difficult to quantitatively verify such an observation due to the nature of AFM imaging.

While this, in itself, is an interesting phenomenon, such a rapid aggregate restructurization may have a negative impact both during *in vitro* drug screenings and may even have certain physiological implications. If ThT fluorescence intensity or sample optical density are used as a means of identifying changes in aggregate concentration, then such restructurization events may provide false-negative or false-positive results, as seen in the OD_{600} (Fig. 6E) and ThT (Fig. 6F) assays. If experimental procedures involve the characterization of fibril structural parameters, then this type of rapid change to secondary structure may also lead to skewed experimental results and conclusions. Finally, if elevated temperatures can increase the incidence of the restructurization events, then this may be one of the many possible factors that influence the onset of neurodegenerative disorders, by stabilizing a certain fibril conformation.

CONCLUSIONS

Overall, it is apparent that an elevated temperature can not only significantly enhance the rate of alpha-synuclein fibril restructurization/maturation, but also result in the stabilization of a certain aggregate structure. This process also leads to changes in bound-ThT signal intensity and optical density, as well as alterations in fibril secondary structure, which should be taken into account during studies of both alpha-synuclein and other amyloid proteins.

ADDITIONAL INFORMATION AND DECLARATIONS

Funding

The authors received no funding for this work.

Competing Interests

The authors declare that they have no competing interests.

Author Contributions

- Mantas Ziaunys conceived and designed the experiments, performed the experiments, analyzed the data, prepared figures and/or tables, authored or reviewed drafts of the article, and approved the final draft.
- Andrius Sakalauskas performed the experiments, authored or reviewed drafts of the article, and approved the final draft.
- Kamile Mikalauskaite performed the experiments, authored or reviewed drafts of the article, and approved the final draft.
- Vytautas Smirnovas conceived and designed the experiments, analyzed the data, authored or reviewed drafts of the article, and approved the final draft.

Data Availability

The following information was supplied regarding data availability:

The raw data is available in the Supplemental Files.

Supplemental Information

Supplemental information for this article can be found online at http://dx.doi.org/10.7717/peerj.14137#supplemental-information.

REFERENCES

Arthur KC, Calvo A, Price TR, Geiger JT, Chiò A, Traynor BJ. 2016. Projected increase in amyotrophic lateral sclerosis from 2015 to 2040. *Nature Communications* **7(1)**:12408 DOI 10.1038/ncomms12408.

Barth A. 2007. Infrared spectroscopy of proteins. *Biochimica et Biophysica Acta (BBA) – Bioenergetics* **1767(9)**:1073–1101 DOI 10.1016/j.bbabio.2007.06.004.

Brookmeyer R, Gray S, Kawas C. 1998. Projections of Alzheimer's disease in the United States and the public health impact of delaying disease onset. *American Journal of Public Health* **88(9)**:1337–1342 DOI 10.2105/AJPH.88.9.1337.

Brännström K, Islam T, Gharibyan AL, Iakovleva I, Nilsson L, Lee CC, Sandblad L, Pamrén A, Olofsson A. 2018. The properties of amyloid-β fibrils are determined by their path of formation. *Journal of Molecular Biology* **430(13)**:1940–1949 DOI 10.1016/j.jmb.2018.05.001.

Buell AK, Galvagnion C, Gaspar R, Sparr E, Vendruscolo M, Knowles TPJ, Linse S, Dobson CM. 2014. Solution conditions determine the relative importance of nucleation and growth processes in -synuclein aggregation. *Proceedings of the National Academy of Sciences of The United States of America* **111(21)**:7671–7676 DOI 10.1073/pnas.1315346111.

Chaudhuri P, Prajapati KP, Anand BG, Dubey K, Kar K. 2019. Amyloid cross-seeding raises new dimensions to understanding of amyloidogenesis mechanism. *Ageing Research Reviews* **56**:100937 DOI 10.1016/j.arr.2019.100937.

Chiti F, Dobson CM. 2017. Protein misfolding, amyloid formation, and human disease: a summary of progress over the last decade. *Annual Review of Biochemistry* **86(1)**:27–68 DOI 10.1146/annurev-biochem-061516-045115.

Cummings J, Lee G, Ritter A, Sabbagh M, Zhong K. 2020. Alzheimer's disease drug development pipeline: 2020. *Alzheimer's & Dementia: Translational Research & Clinical Interventions* **6(1)**:1–29 DOI 10.1002/trc2.12050.

Doig AJ, del Castillo-Frias MP, Berthoumieu O, Tarus B, Nasica-Labouze J, Sterpone F, Nguyen PH, Hooper NM, Faller P, Derreumaux P. 2017. Why is research on amyloid-β failing to give new drugs for alzheimer's disease? *ACS Chemical Neuroscience* **8(7)**:1435–1437 DOI 10.1021/acschemneuro.7b00188.

Fändrich M, Nyström S, Nilsson KPR, Böckmann A, LeVine H, Hammarström P. 2018. Amyloid fibril polymorphism: a challenge for molecular imaging and therapy. *Journal of Internal Medicine* **283(3)**:218–237 DOI 10.1111/joim.12732.

Foderà V, Librizzi F, Groenning M, Van De Weert M, Leone M. 2008. Secondary nucleation and accessible surface in insulin amyloid fibril formation. *Journal of Physical Chemistry B* **112(12)**:3853–3858 DOI 10.1021/jp710131u.

Fujiwara S, Matsumoto F, Yonezawa Y. 2003. Effects of salt concentration on association of the amyloid protofilaments of Hen egg white lysozyme studied by time-resolved neutron scattering. *Journal of Molecular Biology* **331(1)**:21–28 DOI 10.1016/S0022-2836(03)00722-8.

Gaspar R, Meisl G, Buell AK, Young L, Kaminski CF, Knowles TPJ, Sparr E, Linse S. 2017. Secondary nucleation of monomers on fibril surface dominates α-synuclein aggregation and provides autocatalytic amyloid amplification. *Quarterly Reviews of Biophysics* **50**:359 DOI 10.1017/S0033583516000172.

Gurry T, Stultz CM. 2014. Mechanism of amyloid-β fibril elongation. *Biochemistry* **53(44)**:6981–6991 DOI 10.1021/bi500695g.

Hoyer W, Antony T, Cherny D, Heim G, Jovin TM, Subramaniam V. 2002. Dependence of α-synuclein aggregate morphology on solution conditions. *Journal of Molecular Biology* **322(2)**:383–393 DOI 10.1016/S0022-2836(02)00775-1.

Knowles TPJ, Vendruscolo M, Dobson CM. 2014. The amyloid state and its association with protein misfolding diseases. *Nature Reviews Molecular Cell Biology* **15(6)**:384–396 DOI 10.1038/nrm3810.

Lee CT, Terentjev EM. 2017. Mechanisms and rates of nucleation of amyloid fibrils. *Journal of Chemical Physics* **147(10)**:105103 DOI 10.1063/1.4995255.

Ma J, Komatsu H, Kim YS, Liu L, Hochstrasser RM, Axelsen PH. 2013. Intrinsic structural heterogeneity and long-term maturation of amyloid β peptide fibrils. *ACS Chemical Neuroscience* **4(8)**:1236–1243 DOI 10.1021/cn400092v.

Mahdavimehr M, Katebi B, Meratan AA. 2018. Effect of fibrillation conditions on the anti-amyloidogenic properties of polyphenols and their involved mechanisms. *International Journal of Biological Macromolecules* **118**:552–560 DOI 10.1016/j.ijbiomac.2018.06.109.

Manno M, Craparo EF, Martorana V, Bulone D, San Biagio PL. 2006. Kinetics of insulin aggregation: disentanglement of amyloid fibrillation from large-size cluster formation. *Biophysical Journal* **90(12)**:4585–4591 DOI 10.1529/biophysj.105.077636.

Maurer MS, Schwartz JH, Gundapaneni B, Elliott PM, Merlini G, Waddington-Cruz M, Kristen AV, Grogan M, Witteles R, Damy T, Drachman BM, Shah SJ, Hanna M, Judge DP, Barsdorf AI, Huber P, Patterson TA, Riley S, Schumacher J, Stewart M, Sultan MB, Rapezzi C. 2018. Tafamidis treatment for patients with transthyretin amyloid cardiomyopathy. *New England Journal of Medicine* **379(11)**:1007–1016 DOI 10.1056/NEJMoa1805689.

Mehta D, Jackson R, Paul G, Shi J, Sabbagh M. 2017. Why do trials for Alzheimer's disease drugs keep failing? A discontinued drug perspective for 2010–2015. *Expert Opinion on Investigational Drugs* **26(6)**:735–739 DOI 10.1080/13543784.2017.1323868.

Meisl G, Yang X, Hellstrand E, Frohm B, Kirkegaard JB, Cohen SIA, Dobson CM, Linse S, Knowles TPJ. 2014. Differences in nucleation behavior underlie the contrasting aggregation kinetics of the Aβ40 and Aβ42 peptides. *Proceedings of the National Academy of Sciences of the United States of America* **111(26)**:9384–9389 DOI 10.1073/pnas.1401564111.

Micsonai A, Wien F, Kernya L, Lee Y-H, Goto Y, Réfrégiers M, Kardos J. 2015. Accurate secondary structure prediction and fold recognition for circular dichroism spectroscopy. *Proceedings of the National Academy of Sciences of the United States of America* **112(24)**:E3095–E3103 DOI 10.1073/pnas.1500851112.

Mikalauskaite K, Ziaunys M, Smirnovas V. 2022. Lysozyme amyloid fibril structural variability dependence on initial protein folding state. *International Journal of Molecular Sciences* **23(10)**:5421 DOI 10.3390/ijms23105421.

Mikalauskaite K, Ziaunys M, Sneideris T, Smirnovas V. 2020. Effect of ionic strength on thioflavin-T Affinity to amyloid fibrils and its fluorescence intensity. *International Journal of Molecular Sciences* **21(23)**:8916 DOI 10.3390/ijms21238916.

Milto K, Botyriute A, Smirnovas V. 2013. Amyloid-like fibril elongation follows michaelis-menten kinetics. *PLOS ONE* **8(7)**:8–11 DOI 10.1371/journal.pone.0068684.

Morel B, Varela L, Azuaga AI, Conejero-Lara F. 2010. Environmental conditions affect the kinetics of nucleation of amyloid fibrils and determine their morphology. *Biophysical Journal* **99(11)**:3801–3810 DOI 10.1016/j.bpj.2010.10.039.

Nicoud L, Lazzari S, Balderas Barragán D, Morbidelli M. 2015. Fragmentation of amyloid fibrils occurs in preferential positions depending on the environmental conditions. *The Journal of Physical Chemistry B* **119(13)**:4644–4652 DOI 10.1021/acs.jpcb.5b01160.

Pellarin R, Schuetz P, Guarnera E, Caflisch A. 2010. Amyloid fibril polymorphism is under kinetic control. *Journal of the American Chemical Society* **132(42)**:14960–14970 DOI 10.1021/ja106044u.

Rodriguez RA, Chen LY, Plascencia-Villa G, Perry G. 2018. Thermodynamics of amyloid-β fibril elongation: atomistic details of the transition state. *ACS Chemical Neuroscience* **9(4)**:783–789 DOI 10.1021/acschemneuro.7b00409.

Sidhu A, Segers-Nolten I, Raussens V, Claessens MMAE, Subramaniam V. 2017. Distinct mechanisms determine α-synuclein fibril morphology during growth and maturation. *ACS Chemical Neuroscience* **8(3)**:538–547 DOI 10.1021/acschemneuro.6b00287.

Sidhu A, Vaneyck J, Blum C, Segers-Nolten I, Subramaniam V. 2018. Polymorph-specific distribution of binding sites determines thioflavin-T fluorescence intensity in α-synuclein fibrils. *Amyloid-International Journal of Experimental and Clinical Investigation* **25(3)**:189–196 DOI 10.1080/13506129.2018.1517736.

Šneideris T, Baranauskienė L, Cannon JG, Rutkienė R, Meškys R, Smirnovas V. 2015. Looking for a generic inhibitor of amyloid-like fibril formation among flavone derivatives. *PeerJ* **3**:e1271 DOI 10.7717/peerj.1271.

Sneideris T, Milto K, Smirnovas V. 2015. Polymorphism of amyloid-like fibrils can be defined by the concentration of seeds. *PeerJ* **3**:e1207 DOI 10.7717/peerj.1207.

Toleikis Z, Ziaunys M, Baranauskiene L, Petrauskas V, Jaudzems K, Smirnovas V. 2021. S100A9 alters the pathway of alpha-synuclein amyloid aggregation. *International Journal of Molecular Sciences* **22(15)**:7972 DOI 10.3390/ijms22157972.

Törnquist M, Michaels TCT, Sanagavarapu K, Yang X, Meisl G, Cohen SIA, Knowles TPJ, Linse S. 2018. Secondary nucleation in amyloid formation. *Chemical Communications* **54(63)**:8667–8684 DOI 10.1039/C8CC02204F.

Yamaguchi KI, Takahashi S, Kawai T, Naiki H, Goto Y. 2005. Seeding-dependent propagation and maturation of amyloid fibril conformation. *Journal of Molecular Biology* **352(4)**:952–960 DOI 10.1016/j.jmb.2005.07.061.

Ziaunys M, Sakalauskas A, Mikalauskaite K, Smirnovas V. 2021a. Polymorphism of alpha-synuclein amyloid fibrils depends on ionic strength and protein concentration. *International Journal of Molecular Sciences* **22(22)**:12382 DOI 10.3390/ijms222212382.

Ziaunys M, Sakalauskas A, Mikalauskaite K, Snieckute R, Smirnovas V. 2021b. Temperature-dependent structural variability of prion protein amyloid fibrils. *International Journal of Molecular Sciences* **22(10)**:5075 DOI 10.3390/ijms22105075.

Ziaunys M, Sakalauskas A, Smirnovas V. 2020. Identifying insulin fibril conformational differences by thioflavin-T binding characteristics. *Biomacromolecules* **21(12)**:4989–4997 DOI 10.1021/acs.biomac.0c01178.

Ziaunys M, Smirnovas V. 2019. Additional thioflavin-T binding mode in insulin fibril inner core region. *The Journal of Physical Chemistry B* **123(41)**:8727–8732 DOI 10.1021/acs.jpcb.9b08652.

International Journal of
Molecular Sciences

MDPI

Article

Study of Insulin Aggregation and Fibril Structure under Different Environmental Conditions

Mantas Ziaunys, Kamile Mikalauskaite, Andrius Sakalauskas and Vytautas Smirnovas *

Institute of Biotechnology, Life Sciences Center, Vilnius University, LT-10257 Vilnius, Lithuania; mantas.ziaunys@gmc.vu.lt (M.Z.); kamile.mikalauskaite@gmc.vu.lt (K.M.); andrius.sakalauskas@gmc.vu.lt (A.S.)
* Correspondence: vytautas.smirnovas@bti.vu.lt

Abstract: Protein amyloid aggregation is linked with widespread and fatal neurodegenerative disorders as well as several amyloidoses. Insulin, a small polypeptide hormone, is associated with injection-site amyloidosis and is a popular model protein for in vitro studies of amyloid aggregation processes as well as in the search for potential anti-amyloid compounds. Despite hundreds of studies conducted with this specific protein, the procedures used have employed a vast array of different means of achieving fibril formation. These conditions include the use of different solution components, pH values, ionic strengths, and other additives. In turn, this variety of conditions results in the generation of fibrils with different structures, morphologies and stabilities, which severely limits the possibility of cross-study comparisons as well as result interpretations. In this work, we examine the condition–structure relationship of insulin amyloid aggregation under a range of commonly used pH and ionic strength conditions as well as solution components. We demonstrate the correlation between the reaction solution properties and the resulting aggregation kinetic parameters, aggregate secondary structures, morphologies, stabilities and dye-binding modes.

Keywords: amyloids; environmental conditions; fibril structure; insulin; protein aggregation

Citation: Ziaunys, M.; Mikalauskaite, K.; Sakalauskas, A.; Smirnovas, V. Study of Insulin Aggregation and Fibril Structure under Different Environmental Conditions. *Int. J. Mol. Sci.* **2024**, *25*, 9406. https://doi.org/10.3390/ijms25179406

Academic Editor: Konstantin K. Turoverov

Received: 7 August 2024
Revised: 27 August 2024
Accepted: 28 August 2024
Published: 29 August 2024

1. Introduction

Protein aggregation into amyloid fibrils is associated with the onset and progression of several amyloidoses, including the neurodegenerative Alzheimer's or Parkinson's diseases [1]. Despite various anti-amyloid compound screenings and a plethora of studies, there are still only a handful of anti-amyloid compounds available for a limited number of disease-associated proteins [2]. Considering that the incidence of amyloid-related disorders is still rising [3,4], there is a need for a better understanding of the protein aggregation process, which would reduce the number of failed clinical trials conducted on seemingly effective drug molecules [5].

One of the few possible reasons for the lack of effective treatment modalities is the high level of structural variety of the formed amyloid fibrils, which persists both in vivo and in vitro [6–8]. It has been observed that amyloid-beta variants [8], Tau protein [9], prion proteins [10] and alpha-synuclein [11], as well as insulin [12], lysozyme [13] and, likely, many other proteins [14] can form fibrils with distinct secondary structures and morphologies. Interestingly, these structural aspects can influence their affinity towards amyloid-specific molecules [12], including aggregation inhibitors [15]. This suggests that structural variability may be an important factor in determining the effectiveness of the tested drug molecules, and it may also explain the high number of failed clinical trials.

In vitro studies of amyloidogenic protein aggregation have demonstrated that environmental conditions have a profound effect on not only the rate of amyloid fibril formation but also their resulting secondary structure and morphology. Since mimicking in vivo conditions would result in unreasonably long protein aggregation times, alterations are often made that greatly accelerate the process [16]. These include changes in protein concentration [17], solution ionic strength [18] and pH values [19], the addition of denaturants,

the inclusion of agitation [20] and above-physiological temperatures [21]. In some cases, these differences in conditions are quite extreme, such as prion protein fibrillisation under high concentrations of denaturants [22] or insulin aggregation in acidic solutions [23,24]. Despite being advantageous for quick screening procedures, there is still a lack of information regarding the relation between the various deviations from physiological conditions and the resulting aggregate types.

The aforementioned insulin is a small polypeptide hormone that acts as a regulator of carbohydrate, fat and protein metabolism [25]. Its aggregation into amyloid fibrils is associated with localised amyloidosis at sites of repeat injections [26]. Despite being the cause of a relatively rare disorder, it is often used in protein aggregation studies, especially when analysing amyloid aggregation mechanisms [27,28] and screening for potential anti-amyloid compounds [29–31]. While most of these studies are conducted under acidic conditions, a wide variety of different low-pH reaction solutions have been used. These range from simple diluted acids (hydrochloric acid [32,33], acetic acid [34,35]) to buffered solutions (sodium phosphate [36,37], sodium acetate [38,39]). The ionic strength of the reaction solutions also differs significantly between each study, where the addition of sodium chloride is often used to enhance the rate of fibril formation [40,41]. In addition, insulin aggregation studies are often conducted in the presence of various additives, such as nanoparticles [42], lipids [43], organic solvents [44], surfactants [45] and many other compounds [46]. Considering that insulin is known to form multiple distinct fibril types under different conditions [12] and that even relatively small changes in pH [19] or ionic strength [47] can influence their structural variability, this may pose an issue when analysing and comparing data obtained from different studies.

In this work, we examined insulin aggregation under a range of different low-pH conditions and conducted an in-depth analysis of both the fibrillisation process and the resulting fibril structures. The results revealed that there was a highly complex relationship between the reaction solution conditions and the aggregation kinetic parameters as well as with fibril secondary structures and morphologies. These findings highlight the importance of insulin aggregation condition selection and the high level of variability stemming from even small changes in a solution's ionic strength or pH value.

2. Results

The insulin samples prepared under various conditions were first examined using dynamic light scattering (DLS) to determine their dominant oligomeric state. In the case of sodium phosphate solutions with the lowest total ionic strength (Figure 1A), the pH value had minimal effect on the oligomeric state of insulin, and the particle diameter was within the margin of error throughout the entire range (3.2–3.7 nm, comprising monomeric/dimeric insulin [48]). At 300 mM total ionic strength, all the samples had significantly higher particle diameter values compared with using 100 mM NaCl ($p < 0.01$, n = 12), and the solution's pH value played a more prominent role (Figure 1B). In this case, the pH 2.0-condition insulin particles had the lowest average hydrodynamic diameter (4.0 nm), while this was significantly higher under pH 1.0 (4.4 nm) and pH 3.0 (5.0 nm) conditions. At this ionic strength, the samples were likely composed of dimeric/tetrameric insulin [48]. At 500 mM ionic strength (Figure 1C), the average particle diameter was even higher, with pH 1.0–2.0 having a comparable average value of 4.7–4.9 nm, pH 2.5 having an average of 5.4 nm and pH 3.0 having an average of 5.7 nm. In this case, the largest average-particle-diameter samples likely contained even higher oligomeric states of insulin, such as tetramers or hexamers [48].

Under 20% acetic acid conditions (Ac; Figure 1D) and 25 mM HCl conditions (HCl; Figure 1E), there was also a NaCl-concentration-induced increase in particle diameter. In the case of Ac, the difference was less notable, with the average value ranging from 3.6 nm (100 mM NaCl) to 4.3 nm (500 mM NaCl). Interestingly, despite the pH-meter readout of ~1.8 for Ac conditions, the particle diameter was higher than both pH 1.5 and pH 2.0 sodium phosphate conditions at 100 mM and lower at 500 mM. For HCl, the difference

in particle size was considerably more substantial: from 3.5 nm (100 mM NaCl) to 4.8 nm (500 mM NaCl). Unlike Ac conditions, all three ionic strength conditions (with a measured pH value for the HCl solutions of ~1.5) resulted in comparable diameters to the sodium phosphate samples at pH 1.5. This suggests that the presence of 20% acetic acid plays a role in determining the oligomeric state of insulin in solution. A previous study on lysozyme aggregation with high concentrations of organic solvents also displayed its possible role in determining the oligomeric state by affecting the protein's solvation [44].

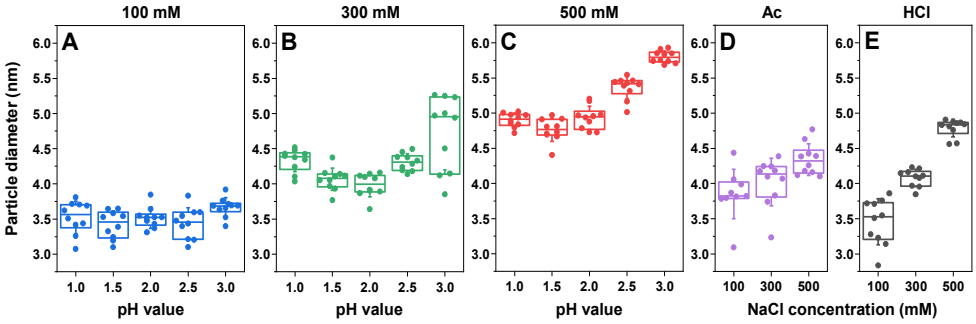

Figure 1. Insulin sample dynamic light scattering (DLS) measurements. The dependence of the insulin hydrodynamic diameter on the sample pH value in sodium phosphate solutions of 100 mM (**A**), 300 mM (**B**) and 500 mM (**C**) total ionic strength. Dependence of the insulin hydrodynamic diameter on the sample ionic strength in 20% acetic acid (**D**) and 25 mM HCl (**E**) solutions. Box plots indicate the interquartile range, and the error bars represent one standard deviation (n = 10).

Another interesting aspect was that the diameter of insulin had a significant dependence on the solution's pH value, with the 500 mM ionic strength pH 3.0 sample having the highest particle diameter out of all the conditions. Coincidentally, the solubility of insulin during sample preparation was also noticeably lower under these conditions when compared with other pH values or ionic strengths.

The aggregation of all the different insulin samples was conducted identically as described in the Section 4. During the analysis of kinetic data, it was observed that, despite the majority of aggregation curves possessing a typical sigmoidal shape with a lag phase, exponential signal increase and a plateau (60.5% of a total of 828 curves), there were two different types of curves present (Figure A1). The first type of irregular kinetics had a characteristic double-sigmoidal shape (13.4%), which can be attributed to the formation of ThT-positive insulin aggregation intermediates [49]. The second type of irregular kinetic curves had a gradual and seemingly unending signal increase after the exponential growth phase (26.1%). Such changes in fluorescence intensity could be related to multiple factors, including amyloid fibril maturation [11] (resulting in different ThT binding characteristics), aggregate lateral association and clumping into clusters (ThT entrapment in the structures) or the dissociation of amorphous, ThT-negative structures and their incorporation into amyloid fibrils.

Due to the relatively large number of such irregular curves (39.5%), it was not possible to fit all the data using a standard sigmoidal function. For this reason, the lag time of insulin aggregation was deemed as the time between the start of the reaction and the first notable increase in signal intensity (four times higher signal than the average baseline value). For all three different total ionic strength sodium phosphate solutions (Figure 2A–C), the lag times only experienced minor variations in the majority of samples with pH values from 1.0 to 2.3–2.5, after which they were all considerably higher. Comparing 100 mM (Figure 2A) and 300 mM conditions (Figure 2B), the lag time values overlapped, and the only notable difference was the seemingly higher stochasticity of the 100 mM condition

value distribution. Unlike both of these conditions, a total ionic strength of 500 mM resulted in a significantly (n = 12, $p < 0.05$) higher pH 3.0-condition average lag time when compared with lower ionic strength values (Figure 2C). These conditions also had the highest particle hydrodynamic diameters at higher pH values (Figure 1), suggesting a possible correlation between insulin oligomeric states and their lag times in sodium phosphate solutions. In the case of Ac (Figure 2D), higher NaCl concentration conditions resulted in considerably shorter lag time values (300 mM NaCl—70 min; 500 mM NaCl—60 min), when compared with the 100 mM NaCl conditions (130 min). In contrast, under HCl conditions (Figure 2E), the different ionic strengths had the least notable effect, with no significant differences observed between all three NaCl concentrations.

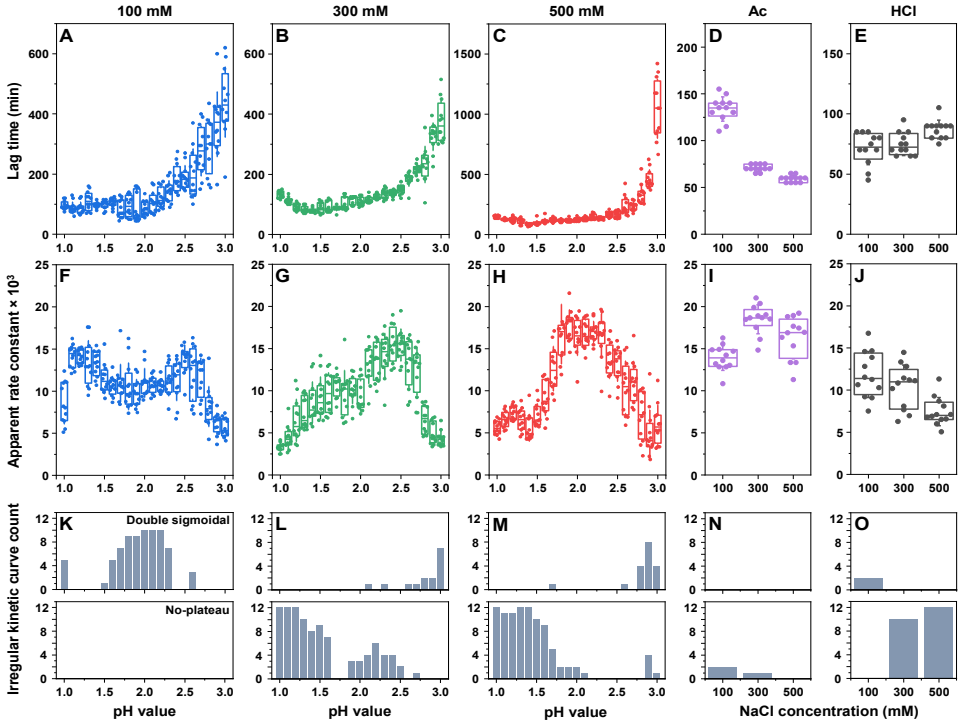

Figure 2. Insulin aggregation kinetic parameters and curve types. The lag time and apparent rate of insulin aggregation under different pH conditions in sodium phosphate solutions of 100 mM (**A**,**F**), 300 mM (**B**,**G**) and 500 mM (**C**,**H**) total ionic strength. The lag time and apparent rate of insulin aggregation under different NaCl concentrations in 20% acetic acid (**D**,**I**) and 25 mM HCl (**E**,**J**) solutions. The distribution of double-sigmoidal (upper panel) and unending signal increase (lower panel) curves for 100 mM (**K**), 300 mM (**L**), 500 mM (**M**) total ionic strength sodium phosphate solutions, as well as for 20% acetic acid (**N**) and 25 mM HCl (**O**) solutions. Box plots indicate the interquartile range, and the error bars represent one standard deviation (n = 12).

Examination of the apparent rate constants displayed a far more complicated picture, with each set of conditions showing different changes in this parameter. In the case of the 100 mM total ionic strength sodium phosphate solution (Figure 2F), there was a significant

increase between the pH 1.0 and pH 1.1 conditions, a gradual decrease between pH 1.1 and pH 1.8, an increase between pH 1.8 and pH 2.6 and a sharp drop between pH 2.6 and pH 3.0. For this ionic strength condition, the apparent rate constant and, to a certain extent, the lag time values at pH 1.0 and from 1.5 to 2.5 could have been influenced by the presence of double-sigmoidal aggregation kinetics (Figure 2K). At a 300 mM ionic strength (Figure 2G), the apparent rate constant gradually increased between the pH 1.0 and pH 2.4 conditions, followed by a sharp decrease between pH 2.4 and pH 3.0. Under these conditions, while the prevalence of double-sigmoidal kinetics was quite low, there was an abundant amount of the second type of irregular curves with an unending signal growth phase (Figure 2L). This phenomenon was highly prevalent at the lowest pH conditions (pH 1.0–1.3) and relatively small at the other marked conditions (Figure 2L), which may explain the low apparent rate constants of these samples. At 500 mM NaCl (Figure 2G), the pH 1.0–1.5 conditions all suffered from a high number of the aforementioned irregular curves (Figure 2M), resulting in a low calculated apparent rate constant. Under higher pH-value conditions (pH 2.0–3.0), the constant had comparable values to the 300 mM NaCl conditions.

Conditions with acetic acid (Figure 2I) had a relatively low number of irregular curves, with the occasional unending plateau at 100 mM and 300 mM NaCl (Figure 2N). The apparent rate constant at 300 mM NaCl was roughly 25% higher than at 100 mM and was within the margin of error for the 500 mM NaCl conditions. The HCl conditions (Figure 2J) resulted in a couple of double-sigmoidal curves at the lowest ionic strength and an abundance of unending plateau kinetics at 300 mM and 500 mM NaCl (Figure 2O). The apparent rate constant under these conditions was lower at higher NaCl concentrations, a factor which may also be linked with the presence of the aforementioned irregular curves. Interestingly, only a few out of all the tested conditions resulted in all twelve aggregation curves having a regular sigmoidal shape. While this does not appear to cause significant variations in the process lag time values, it is very prevalent when determining the apparent rate constants.

In order to determine the condition–structure relationship of insulin amyloid fibrils, the sample FTIR spectra were acquired. To account for possible structural variability among the repeats, all twelve samples from each of the selected conditions were replicated and analysed. The dominant FTIR spectra from each condition were chosen and displayed in Figure 3. The spectra were then compared against each other, and the ones that shared similarities were assigned into variant groups (Figure 3; lowercase letters indicate the group). The five variant FTIR spectra and their second derivative minima positions are displayed in Figure A2.

Under 100 mM total ionic strength conditions, the main maximum position in the insulin FTIR spectra was at 1628 cm^{-1} (related to beta-sheet hydrogen bonding [50]) throughout the entire pH range (Figure 3A). However, between the pH 1.0 and pH 3.0 conditions, the bands at 1659 cm^{-1} and 1640 cm^{-1} became more expressed, which was also visible in the spectra's second derivatives (Figure 3E). The latter FTIR spectra were nearly identical to previous reports of insulin fibrils generated under pH 2.0 [19]. When the aggregation was conducted under a 300 mM total ionic strength, there was a significantly higher level of variation in the dominant fibril secondary structure (Figure 3B,F). Unlike the 100 mM conditions, the main maximum position ranged from 1628 cm^{-1} to 1632 cm^{-1} at different pH conditions. The pH 1.5 spectrum was identical to the lower-pH-value 100 mM condition spectra, while pH 3.0 spectrum had similarities to the higher-pH-value 100 mM condition spectra, albeit with a higher level of unstructured regions (possibly related to the presence of amorphous aggregates at 1650 cm^{-1} [50]). The remaining 300 mM-condition spectra were different from the 100 mM conditions, while possessing a high level of similarity among each other. This third variant was previously observed when aggregation was conducted under conditions of 100 mM sodium phosphate supplemented with 100 mM NaCl (pH 2.4) [12]. In the case of a 500 mM total ionic strength (Figure 3C,G), the pH 1.0–2.5-condition spectra all shared similarities with minor variations in the main

maximum position. The FTIR spectrum of the pH 3.0 sample was comparable to the 300 mM pH 3.0-condition spectrum, with a considerably higher level of noise and more amorphous structures (relatively lower peak in the region associated with beta-sheet hydrogen bonding).

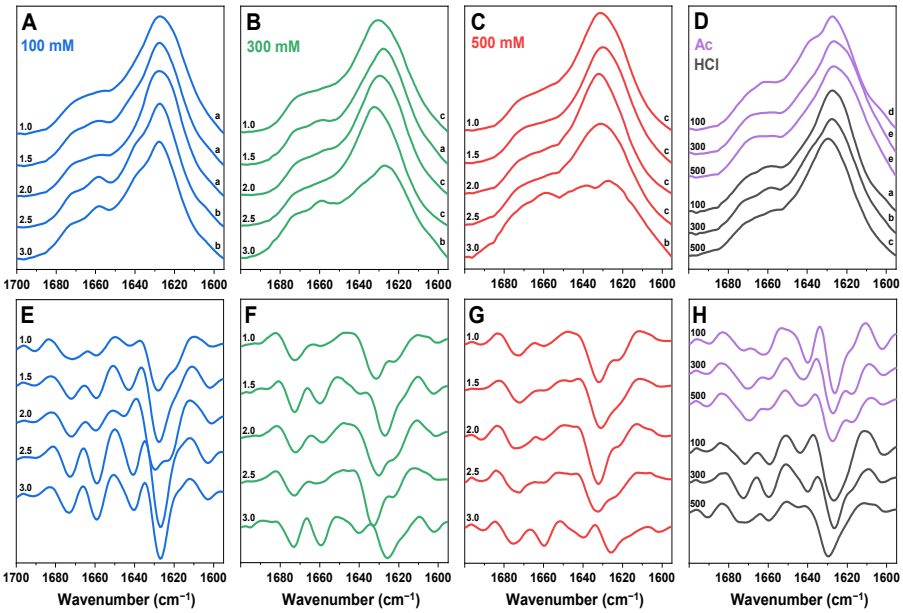

Figure 3. Comparison of insulin aggregate secondary structures. FTIR spectra of insulin aggregates formed in sodium phosphate solutions of 100 mM (**A**), 300 mM (**B**) and 500 mM (**C**) total ionic strength (pH values are indicated on the left sides of the spectra). FTIR spectra of aggregates formed in Ac and HCl conditions (**D**; ionic strengths are indicated on the left side of the spectra). Second derivatives of the FTIR spectra (**E**–**H**) are colour-coded and displayed below their respective FTIR spectra. FTIR spectra variants are indicated by lowercase letters on the right side of the spectra.

For Ac conditions (Figure 3D,H), the lowest NaCl concentration spectrum shared some similarities to the 100 mM pH 2.5 and 3.0 spectra, with a notable difference in the region associated with turns/loops (second derivative minima at 1663 cm^{-1}, as opposed to 1659 cm^{-1}). At higher NaCl concentrations, the fibril FTIR spectra had a reduced band at 1641 cm^{-1} and an increase in the 1620 cm^{-1} position. We have previously reported a nearly identical shift in a study that demonstrated a protein-concentration-dependent change in the insulin fibril secondary structure [51]. Here, an increase in NaCl concentration, accompanied by a change in particle hydrodynamic diameter, resulted in the same effect on aggregation as a higher concentration of the protein. Finally, in the case of HCl (Figure 3D,H), the three different NaCl concentration conditions yielded three distinct FTIR spectra, which shared similarities to the spectra of the 100 mM pH 1.0, 100 mM pH 3.0 and 300 mM pH 1.0 fibrils, respectively.

Analysis of insulin aggregate sample atomic force microscopy images (AFM, Figure 4A) revealed that there were three types of fibril distributions in the sodium phosphate solutions of varying ionic strength and pH values. At 100 mM pH 1.5 and pH 2.0, as well as in the 300 mM pH 1.0 conditions, the fibrils formed long intertwined networks, and there was minimal lateral association or aggregate clumping. In contrast, at 300 mM pH 3.0 and 500 mM pH 3.0, very few aggregates could be detected during the AFM scanning procedure.

Combined with the FTIR results of these two conditions, it appears that insulin may have formed either amorphous (multiple large clusters were observed on the mica) or unstable aggregates, which would explain the lack of fibrillar structures in the AFM images. Finally, all other conditions resulted in a similar aggregate distribution, with 3–4 µm length fibrils forming lateral associations rather than intertwined networks.

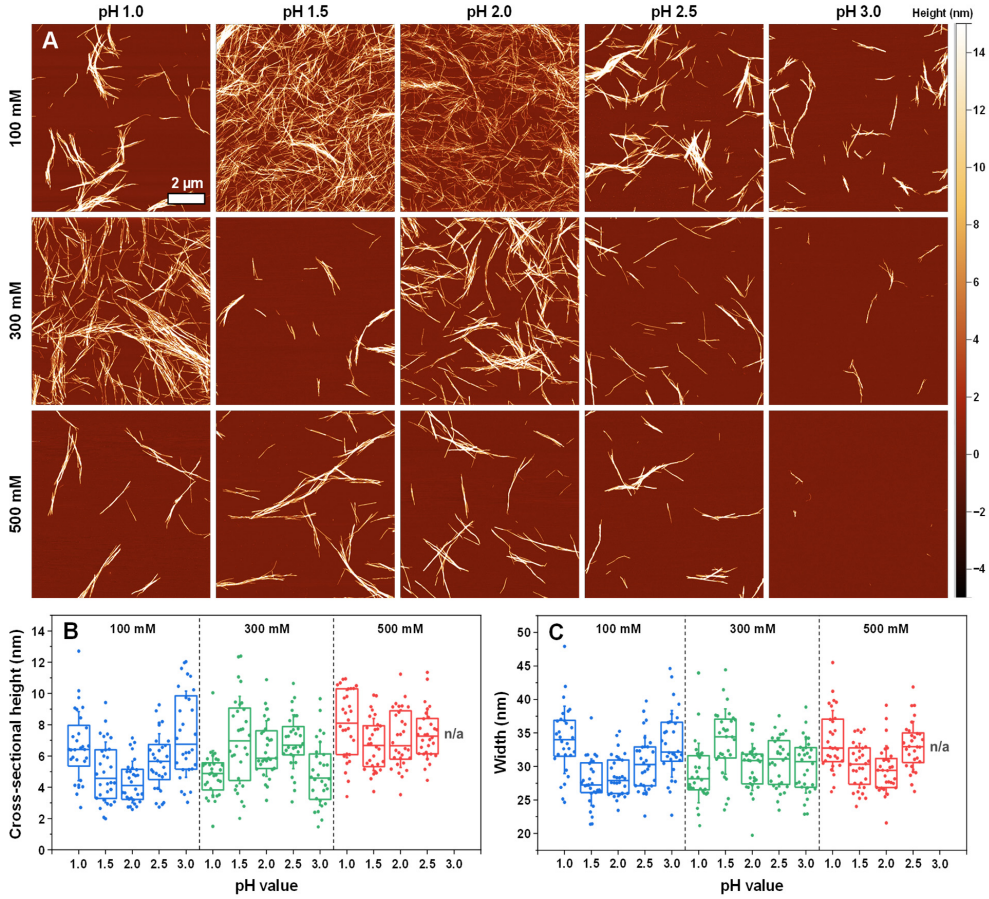

Figure 4. Morphology of insulin aggregates prepared in sodium phosphate solutions. The atomic force microscopy (AFM) images of different condition insulin aggregates (**A**) and their cross-sectional heights (**B**) and widths (**C**). For each condition, 30 traces were taken to determine the height and width values. Box plots indicate the interquartile range, and the error bars represent one standard deviation.

Examining the cross-sectional height (Figure 4B) and width (Figure 4C) distribution of the formed fibrils revealed that the average height varied between 4 nm and 8 nm, while their width ranged from 26 nm to 34 nm. The lowest cross-sectional heights were measured for the 100 mM pH 1.5 and 2.0 and the 300 mM pH 1.0 and pH 3.0 conditions. Three out of these four lowest-height fibrils were also the ones that formed the previously mentioned intertwined networks. The largest average height was determined as belonging to the 500 mM pH 1.0 fibrils, with all other conditions falling in between the two fringe values. The average cross-sectional width was highest for the 100 mM pH 1.0 and 300 mM pH 1.5

conditions and lowest for the 100 mM pH 1.5 and pH 2.0 and 300 mM pH 1.0 conditions, with all other fibrils having intermediate widths.

In the case of insulin fibrils prepared under acetic acid conditions (Figure 5A), the solution ionic strength played a role in determining their morphology. Under 100 mM NaCl conditions, the fibrils were relatively short and laterally associated, while under 300 mM and 500 mM NaCl, they were long and formed intertwined networks. This difference was also evident based on the significantly higher cross-sectional heights (Figure 5B) and widths (Figure 5C) of the Ac-condition aggregates. In contrast, a change in NaCl concentration did not have any significant effect on either the height or width of the insulin fibrils when they were aggregated under HCl conditions, and the morphologies shared similarities to the majority of fibrils under sodium phosphate conditions.

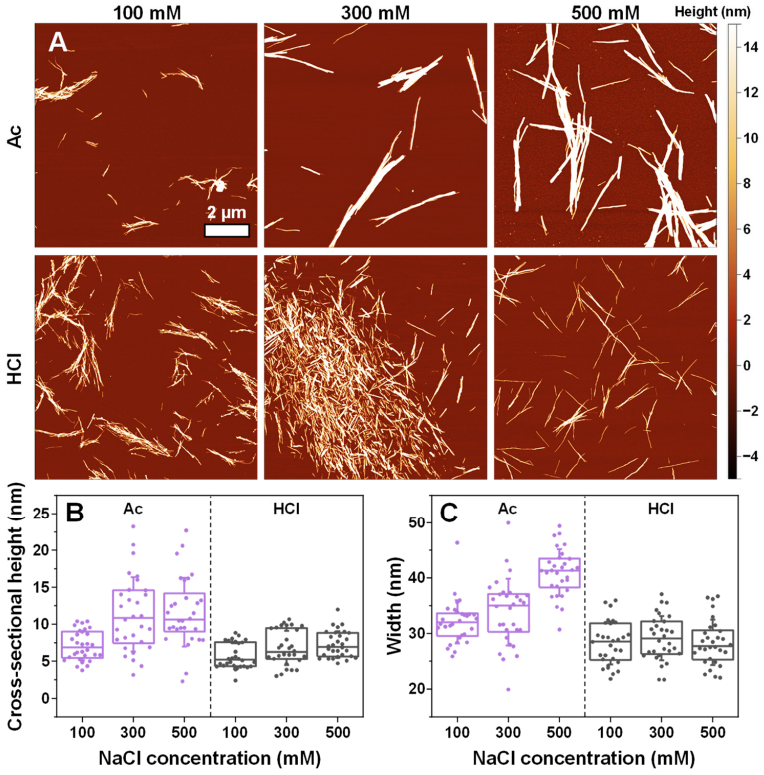

Figure 5. Morphology of insulin aggregates prepared in 20% acetic acid (Ac) and 25 mM hydrochloric acid (HCl) solutions. The atomic force microscopy (AFM) images of insulin aggregates under different conditions (**A**) and their cross-sectional heights (**B**) and widths (**C**). For each condition, 30 traces were taken to determine the height and width values. Box plots indicate the interquartile range, and the error bars represent one standard deviation (n = 30).

Since the generated fibrils differed in both their secondary structure and morphology, further investigation was dedicated to determining if they also had distinct structural stabilities or dye-binding properties. Analysis of the aggregate stability against denaturation by guanidinium thiocyanate (GuSCN) revealed that most of the aggregates had a similar 1.9–2.1 M denaturation midpoint (Figure 6A–E), with some outliers. The highest stability was observed in the case of the Ac 300 mM and 500 mM NaCl conditions, which corre-

sponded with them having the largest morphological structures. The lowest stabilities were determined for the higher pH and ionic strength conditions, especially for the pH 2.5 and pH 3.0 sodium phosphate solutions. For the 500 mM pH 3.0 condition, it was not possible to calculate the dissociation midpoint due to a very low concentration of stable aggregates.

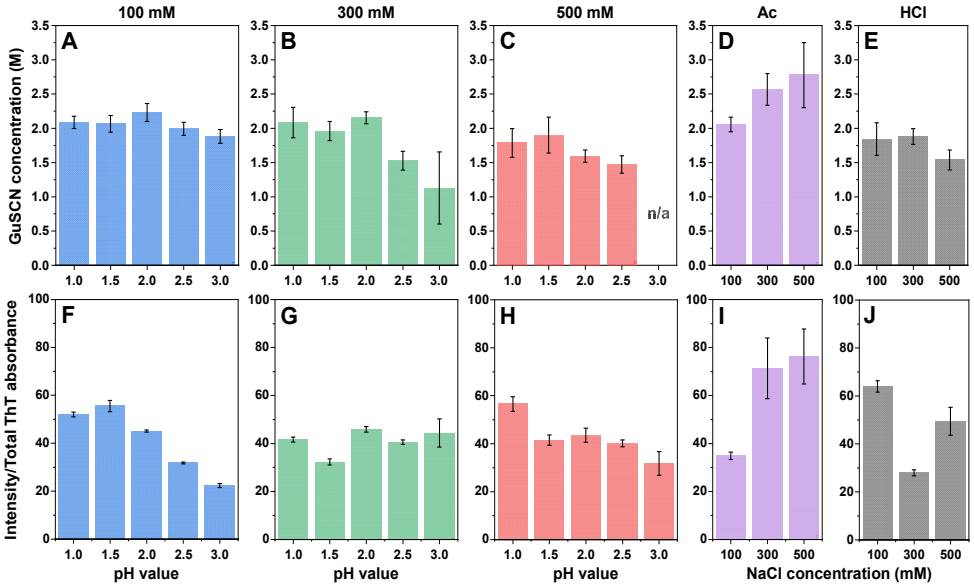

Figure 6. Insulin aggregate stability and bound-ThT fluorescence quantum yield. The midpoint of the aggregate denaturation curves of insulin aggregate samples prepared under 100 mM (**A**), 300 mM (**B**), 500 mM (**C**) total ionic strength sodium phosphate conditions, as well as under acetic acid (**D**) and hydrochloric acid (**E**) conditions. The average bound-ThT fluorescence quantum yield of insulin aggregate samples prepared under 100 mM (**F**), 300 mM (**G**), 500 mM (**H**) total ionic strength sodium phosphate conditions, as well as under acetic acid (**I**) and hydrochloric acid (**J**) conditions. For each condition, three measurements were taken and averaged. The error bars represent one standard deviation (n = 3).

The dye binding/fluorescence properties (Figure 6F–J) were much more varied, with the highest average quantum yield observed in the case of the Ac 300 mM and 500 mM NaCl conditions (similarly to them having the highest structural stability and fibril size), as well as for the HCl 100 mM NaCl conditions. The lowest average quantum yields of ThT fluorescence were determined for the 100 mM pH 3.0, 300 mM pH 1.5, 500 mM pH 3.0, Ac 100 mM NaCl and HCl 300 mM NaCl conditions, with all other conditions having intermediate values. Considering that there was no clear trend observed under any of the conditions, it is likely that the dye-binding properties of the generated aggregates were structure-specific, as was shown previously [12].

3. Discussion

In most insulin aggregation studies, the process of fibril formation is carried out under acidic conditions, with limited regard to the solution's exact pH or ionic strength values. In this work, we have conducted an examination of insulin amyloid aggregation under a range of different solutions, which encompass most of the commonly used conditions. The results demonstrate that small changes in pH, ionic strength or the solution component type strongly influence the aggregation kinetics, resulting altered fibril secondary structure,

morphology, stability and dye-binding properties. These observations exemplify the importance of environmental conditions on in vitro insulin fibrillisation and how the conclusions drawn from the aggregation assays may be influenced by small variations in the chosen reaction solutions.

The first notable aspect is the influence of the reaction solution on the oligomeric state of insulin. Previous reports have demonstrated that insulin may exist in various oligomeric states based on either the solution's pH or ionic strength conditions [24]. In this study, we observe that both of these factors, as well as the type of the solution's components, all play a mutual role in determining the association of insulin molecules. While the solution's ionic strength had a similar influence in increasing the protein's oligomeric state under all of the chosen pH (1.0–3.0) and solution component (sodium phosphate, acetic acid, hydrochloric acid) conditions, matters were more complex in the case of the other two parameters. Changes in pH values had no effect at low ionic strength conditions, while they had a profound influence under both the 300 mM and 500 mM conditions. The solution components also played a role in determining how the ionic strength can change insulin's oligomeric state, which is best exemplified in the Ac and HCl solutions. Under hydrochloric acid conditions, the particle hydrodynamic diameter was significantly different among all three NaCl concentrations, while the difference was only minor in the case of acetic acid conditions.

The aggregation kinetics of insulin were also heavily influenced by the type of reaction solution. While the lag times were similar at lower pH conditions, in the case of sodium phosphate solutions, at higher pH conditions, they were significantly longer. Under all three ionic strength conditions, pH 3.0 reaction solutions yielded lag times that were 6 to 10 times larger than their lower-pH-condition counterparts. This may be related to the oligomeric state of insulin and its solubility. During the preparation of the initial samples, it was observed that insulin solubility was particularly low under pH 3.0 conditions. Coupled with the relatively high particle hydrodynamic diameter under these conditions, it may explain why the primary nucleation reactions proceeded at such a slow rate. However, the HCl solutions with 500 mM NaCl displayed similar insulin hydrodynamic diameters without having such a profound effect on lag times, suggesting that the oligomeric state of the protein may not be the most important aspect in this matter.

Another highly peculiar aspect of insulin aggregation was also observed when conducting this large fibrillisation condition screening assay. Under certain sets of pH and ionic strength values, the aggregation reactions resulted in irregular kinetic curves, which were either double-sigmoidal or had gradual unending signal intensity increases after the exponential growth phase. Such irregularities were previously reported for certain specific types of aggregation conditions [49,52]. In this case, we observed that the irregular curves were highly condition-dependent, such as endless plateaus at low pH values and double-sigmoidal curves at intermediate pH values and low ionic strengths. While the double-sigmoidal kinetics can be easily explained by the presence of ThT-positive aggregation intermediates [52], the unending plateau ones can be caused by a number of different factors ranging from fibril maturation to aggregate cluster formation. The relatively high abundance of such irregular curves may influence the aggregation kinetic parameters derived from the data, as there is no definitive way to fit all three curve types using the same kinetic model or function.

Exploring the correlation between aggregation conditions and the secondary structure of insulin aggregates revealed that there were no clearly defined "borders" between aggregate types, with gradual structure–condition changes observed throughout the range of reaction solutions. Analysis of all the dominant secondary structures showed that each one was similar to one of the few previously described structures, with moderate variability in band positions/intensities. The most peculiar FTIR spectra were obtained under pH 3.0 conditions, where the signal to noise ratio was relatively high, and the beta-sheet hydrogen bonding peaks were relatively small, suggesting the presence of a high number of amorphous aggregates. This conclusion was also supported by other assays, including AFM

images and the stability assay. It is also worth noting that not a single condition yielded completely identical FTIR spectra and there was a similar level of variability in each case.

Morphological analysis of all the dominant secondary structures indicated that there were, in general, four different classes of morphologies. In most cases, insulin aggregates formed 2–3 μm length structures with a moderate level of lateral association. Fibrils under lower pH and ionic strength conditions assembled into long intertwined structures and had relatively low cross-sectional heights. The largest structures, composed of multiple laterally associated long filaments, formed under higher ionic strength acetic acid conditions. Finally, higher ionic strength and pH conditions yielded low amounts of short fibrils, with most of the aggregates assembling into amorphous structures, as observed in other assays and as indicated by the comparatively low number of structures visible in the AFM images.

The two other aggregate parameters, namely stability against denaturation and dye-binding properties, were closely related to either their structure or morphology. Fibrils that formed larger structures had significantly higher stability against denaturation (best exemplified in the case of Ac 300 mM and 500 mM conditions), while the stability of aggregates formed under higher pH and ionic strength sodium phosphate conditions was either very low or impossible to determine accurately. The average bound-ThT fluorescence quantum yield did not display any clear tendencies with either increasing pH or ionic strength, leading to the conclusion that this parameter was highly dependent on the fibril surface type and ThT binding modes resulting from their distinct secondary structures [12].

In conclusion, this study demonstrates the high level of insulin amyloid aggregation variability and highlights the condition–structure relationships of the resulting fibrils. It shows that even minor alterations throughout the entire tested pH and ionic strength range, as well as the solution component type, can modulate the aggregation kinetic curve type, lag time and apparent rate constant, as well as the resulting aggregate secondary structure, morphology, stability and dye-binding properties. This work encompasses many of the most commonly used insulin aggregation conditions and fills in the gaps between them to create a clearer picture of insulin amyloid formation.

4. Materials and Methods

4.1. Reaction Solution Preparation

To prepare low-pH-value thermodynamically corrected buffer solutions with identical ionic strengths, the recipes were based on Professor Robert J Beynon's on-line buffer calculator (http://phbuffers.org/BuffferCalc/Buffer.html (accessed on 25 March 2023)). Phosphoric acid and sodium phosphate (final concentration—100 mM), as well as sodium chloride (final concentrations were determined from the online calculation tool) were dissolved in MilliQ H_2O at 22 °C. The pH of the solution was determined using a ThermoFisher (Waltham, MA, USA) pH meter (Orion 9110DJWP), and corrections were made using concentrated hydrochloric acid or sodium hydroxide. The solutions were then filtered through 0.22 μm pore-size syringe filters and stored at 4 °C (for up to 24 h before use). The resulting buffer solutions had pH values in the range from 1.0 to 3.0 in 0.1 increments and total calculated ionic strengths of 100 mM, 300 mM and 500 mM.

The other two types of reaction solutions used in this work were 20% acetic acid and 25 mM HCl solutions with different NaCl concentrations. The appropriate volume of 99.5% acetic acid was diluted to 20% using MilliQ H_2O. Concentrated HCl (25%) was diluted to 25 mM using MilliQ H_2O. Both solutions were supplemented with either 100 mM, 300 mM or 500 mM NaCl. The solutions were then filtered through 0.22 μm pore-size syringe filters and stored at 4 °C (for up to 24 h before use).

4.2. Insulin Aggregation

Human recombinant insulin powder (Sigma-Aldrich, St. Louis, MO, USA, cat. No. 91077C) was dissolved in the previously prepared reaction solutions to a final protein concentration of ~300 μM. The solutions were then filtered using 0.22 μm pore-size syringe filters and the protein concentration was determined by scanning the sample absorbance at 280 nm

(ε_{280} = 6335 $M^{-1}cm^{-1}$) using a Shimadzu (Kyoto, Japan) UV-1800 spectrophotometer in 3 mm pathlength cuvettes. Thioflavin-T powder (ThT, Sigma-Aldrich, cat. No. T3516) was dissolved in Milli-Q H_2O to a concentration of ~11 mM, filtered through a 0.22 µm pore-size syringe filter, diluted to 10 mM (ε_{412} = 23,250 $M^{-1}cm^{-1}$) and stored at −20 °C under dark conditions. The insulin solutions were then combined with ThT and their respective reaction solutions to result in mixtures with 100 µM ThT and 200 µM insulin. To prevent batch-to-batch variability, all protein solutions were prepared simultaneously using the same insulin powder batch. The solutions were then frozen at −80 °C and thawed prior to the aggregation experiments.

The insulin reaction solutions were distributed into 96-well plates (Greiner, Kremsmunster, Austria, cat. No. 11877192; final volume in each well—200 µL) in an alternating placement and avoiding corner wells to account for the plate-edge-effect during the aggregation process [53] (an example is shown in Figure A3). The plates were then sealed using Nunc sealing tape (ThermoFisher, Waltham, MA, USA, cat. No. 10265411) and incubated in a ClarioStar Plus plate reader (BMG Labtech, Ortenberg, Germany) with a constant 60 °C temperature and no agitation. Sample measurements were taken every 5 min using 440 nm excitation and 480 nm emission wavelengths (0.1 s settling time, 50 flashes per sample). For each condition, a total of 12 samples were aggregated (4 samples per run). After aggregation, the plates were cooled down to room temperature prior to further use. Due to the sample incubation being at an elevated temperature, small deviations from the initial reaction conditions (pH, ionic strength and protein concentration) may have occurred during the procedure.

4.3. Dynamic Light Scattering

The non-aggregated insulin samples (200 µM protein concentration, 20 µL volume) were placed in 1 mm pathlength quartz cuvettes and covered with plug caps. The protein hydrodynamic diameter was then measured using a Malvern Panalytical (Malvern, UK) Zetasizer µV light-scattering detector at a constant 22 °C temperature. For each sample, ten technical replicates (each composed of ten scans over the span of 1 min) were measured. The thermal equilibration time was set to 1 min, and the total scan time was 10 min.

4.4. Kinetic Data Analysis

Under multiple conditions, the aggregation kinetic data could not be fit using standard sigmoidal curves, due to either requiring double-sigmoidal kinetic curves or there being a gradual shift in the signal intensity after the main exponential growth phase. For this reason, the extent of the lag phase was determined as the time period, during which the sample signal intensity remained below a set intensity value for each sample (average value of the initial baseline (10 points) multiplied by 4 (to exclude random signal variations)). An example of the lag time determination is show in Figure A4. To obtain the maximum apparent rate constants, first-order derivatives were calculated for each reaction curve as described previously [52]. The maximum point value from each derivative was then divided by the signal intensity at the end of the reaction (the end-point fluorescence intensity was determined at the same time for each set of conditions; an example is shown in Figure A4).

4.5. Fourier-Transform Infrared Spectroscopy (FTIR)

Aliquots of 100 µL were taken from each sample and centrifuged at 10,000 RPM (Fisherbrand™ High-Speed Mini-Centrifuge, ThermoFisher, Waltham, MA, USA, cat. no 12972041) for 15 min. The supernatants were then removed, and the aggregate pellets were resuspended into 200 µL D_2O with 400 mM NaCl (addition of NaCl improves insulin fibril sedimentation [54]). The centrifugation and resuspension procedures were repeated an additional two times. After the final centrifugation, the aggregate pellets were resuspended into 40 µL D_2O with 400 mM NaCl, resulting in a final protein concentration of ~500 µM (assuming the majority of insulin was in its aggregated state). The sample FTIR spectra

were acquired and analysed as described previously [55]. In short, the fibril FTIR spectra were scanned using an Invenio S infrared spectrometer (Bruker, Billerica, MA, USA). For every sample, 256 interferograms were recorded at a 2 cm^{-1} resolution and averaged. The D_2O and water vapour spectra were then subtracted from the sample spectra, which were then baseline-corrected and normalised to the same Amide I/I′ band area (1700–1595 cm^{-1}). Data analysis was performed using the GRAMS software Version 9.3 SP1, (ThermoFisher, Waltham, MA, USA).

4.6. ThT-Binding Assay

Samples from each set of conditions were chosen based on which FTIR spectra were the most common among the 12 repeats. The samples (100 µL) were then combined with their initial reaction solutions (900 µL) and incubated at 60 °C for 24 h in non-binding 2.0 mL volume test-tubes to increase the number of fibrils for further experimental procedures. To mitigate the effect of solution pH and ionic strength on the dye-binding parameters, the samples were centrifuged as described previously, and the aggregates were resuspended into an equivalent volume of 100 mM sodium phosphate (pH 2.0, adjusted to a total ionic strength of 300 mM using NaCl).

Aliquots of 200 µL of each sample were supplemented with 2 µL of a 10 mM ThT stock solution, mixed and incubated at 22 °C for 1 h. The samples were then centrifuged at 10,000 RPM for 10 min and resuspended into 200 µL of the pH 2.0 buffer solution, which did not contain ThT. This centrifugation and resuspension procedure was repeated 3 times to remove non-bound ThT molecules from the solution. After the final resuspension step, the aggregate samples were placed in 3 mm cuvettes, and their absorbance spectra were scanned using a Shimadzu UV-1800 spectrophotometer (200–600 nm range, 1 nm steps). The fluorescence of bound-ThT molecules was scanned using a Varian CaryEclipse spectrofluorometer (Agilent Technologies, Santa Clara, CA, USA, 440 nm excitation, 480 nm emission wavelengths, 2.5 s signal averaging time). For each sample, three technical replicates were scanned, and the spectra were averaged.

The absorbance spectra were baseline-corrected between 300 nm and 600 nm using the Origin Software 2018 (OriginLab, Northampton, MA, USA). Baseline correction function (B-spline with 4 anchor points at each end of the spectrum). The spectra were then integrated between 340 nm and 520 nm to obtain the areas of the bound-ThT absorbance spectra. ThT fluorescence intensities were corrected for the inner filter effect using their respective absorbance values at 440 nm and 480 nm as described previously [56].

4.7. Atomic Force Microscopy (AFM)

Aliquots of each sample were diluted to a 40 µM protein concentration, placed on freshly cleaved mica and incubated at room temperature for 5 min. The micas were then gently washed with 2 mL of H_2O and dried using airflow. The AFM image acquisition procedure was performed as described previously [55] using a Dimension Icon atomic force microscope (Bruker, Billerica, MA, USA). The AFM images were analysed using the Gwyddion 2.57 software (http://gwyddion.net, accessed on 28 December 2020). From each image, 30 fibril cross-sectional heights and widths were determined by tracing lines perpendicular to the fibril axes. The lines were only traced on fibril ends, which were not part of aggregate clusters, to reduce the effect of lateral association on the calculated height and width parameters. Data were compared using one-way ANOVA Bonferroni means comparison ($p < 0.01$, n = 30).

4.8. Aggregate Denaturation Assay

Aliquots of each sample (46 × 10 µL) were combined with a range of guanidinium thiocyanate (GuSCN) solutions of different concentrations (90 µL of pH 2.0, 100 mM sodium phosphate; total ionic strength without GuSCN was adjusted to 300 mM using NaCl). The final sample GuSCN concentrations ranged from 0 to 4.5 M in 0.1 M increments. The prepared solutions were then incubated at 22 °C for 24 h, after which they were placed

into 96-well non-binding plates (cat. No 3881, Fisher Scientific, Hampton, NH, USA, final volume was 100 µL in each well). The sample optical densities at 600 nm were scanned using a ClarioStar Plus plate reader (BMG Labtech, Ortenberg, Germany) with 0.1 s settling time and 50 flashes per sample. Each sample was scanned three times and the plates agitated for short periods in between (10 s, 600 RPM orbital agitation). The data was fitted using a Boltzmann sigmoidal equation to determine the mid-point of insulin aggregate denaturation (Figure A5).

Supplementary Materials: The following supporting information can be downloaded at: https://www.mdpi.com/article/10.3390/ijms25179406/s1.

Author Contributions: Conceptualisation, V.S. and M.Z.; investigation, K.M., A.S. and M.Z.; resources, V.S.; data analysis, V.S. and M.Z.; writing—original draft preparation, M.Z.; writing—review and editing, V.S., K.M., A.S. and M.Z. All authors have read and agreed to the published version of the manuscript.

Funding: This research received no external funding.

Institutional Review Board Statement: Not applicable.

Informed Consent Statement: Not applicable.

Data Availability Statement: All data are available in the Supplementary Materials.

Conflicts of Interest: The authors declare no conflicts of interest.

Appendix A

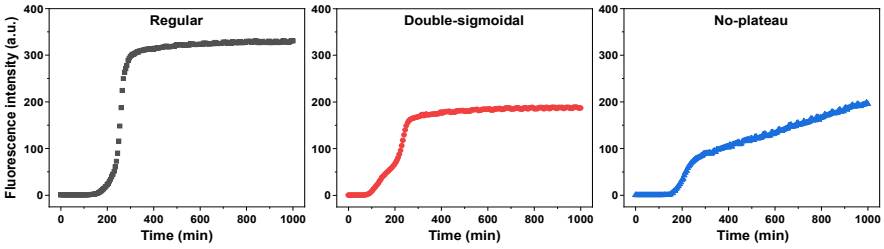

Figure A1. Examples of regular, double-sigmoidal and no-plateau insulin aggregation kinetic curves.

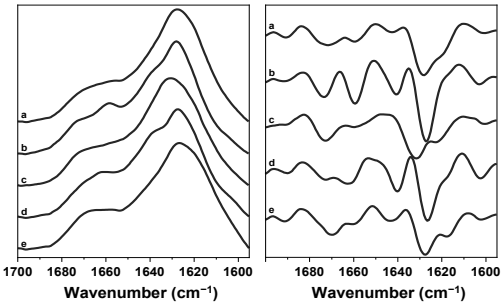

Variant	Beta-sheets (cm^{-1})	Turn/loop
a	1628/1642	1659/1671
b	1627/1641	1659/1673
c	1623/1631	1660/1673
d	1626/1640	1662/1672
e	1617/1627/1642	1660/1671

Figure A2. Different insulin fibril FTIR spectra variants, their second derivatives, second-derivative minima positions and their relation to beta-sheets and turns/loops.

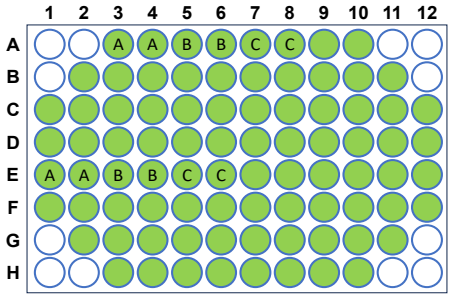

Figure A3. Insulin reaction solution placement in the 96-well plate. Green-coloured wells indicate where the insulin reaction solutions were placed during aggregation. The marked wells provide an example of the sample placement (samples A, B and C).

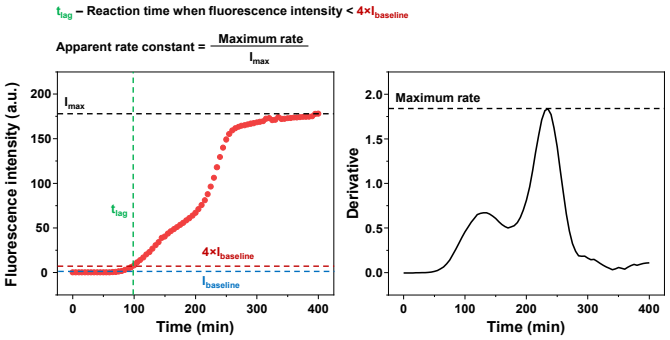

Figure A4. Example of the aggregation reaction lag time and apparent rate constant calculation. Dashed lines are color-coded to their specific parameters.

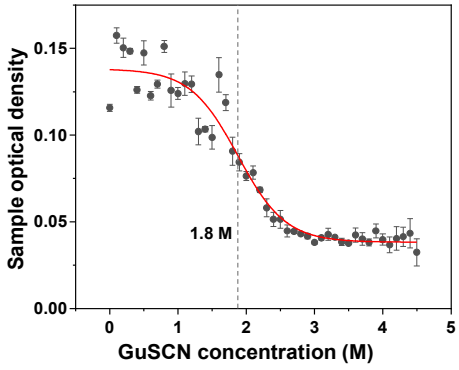

Figure A5. Example of the insulin fibril denaturation midpoint determination.

References

1. Knowles, T.P.J.; Vendruscolo, M.; Dobson, C.M. The amyloid state and its association with protein misfolding diseases. *Nat. Rev. Mol. Cell Biol.* **2014**, *15*, 384–396. [CrossRef] [PubMed]
2. Cummings, J.; Lee, G.; Nahed, P.; Kambar, M.E.Z.N.; Zhong, K.; Fonseca, J.; Taghva, K. Alzheimer's disease drug development pipeline: 2022. *Alzheimer's Dement. Transl. Res. Clin. Interv.* **2022**, *8*, e12295. [CrossRef]
3. Arthur, K.C.; Calvo, A.; Price, T.R.; Geiger, J.T.; Chiò, A.; Traynor, B.J. Projected increase in amyotrophic lateral sclerosis from 2015 to 2040. *Nat. Commun.* **2016**, *7*, 12408. [CrossRef]
4. Brookmeyer, R.; Gray, S.; Kawas, C. Projections of Alzheimer's disease in the United States and the public health impact of delaying disease onset. *Am. J. Public Health* **1998**, *88*, 1337–1342. [CrossRef]
5. Chatani, E.; Yamamoto, N. Recent progress on understanding the mechanisms of amyloid nucleation. *Biophys. Rev.* **2018**, *10*, 527–534. [CrossRef] [PubMed]
6. Bousset, L.; Pieri, L.; Ruiz-Arlandis, G.; Gath, J.; Jensen, P.H.; Habenstein, B.; Madiona, K.; Olieric, V.; Böckmann, A.; Meier, B.H.; et al. Structural and functional characterization of two alpha-synuclein strains. *Nat. Commun.* **2013**, *4*, 2575. [CrossRef] [PubMed]
7. Yang, S.; Thackray, A.M.; Hopkins, L.; Monie, T.P.; Burke, D.F.; Bujdoso, R. Polymorphisms at amino acid residues 141 and 154 influence conformational variation in ovine PrP. *BioMed Res. Int.* **2014**, *2014*, 372491. [CrossRef]
8. Fändrich, M.; Meinhardt, J.; Grigorieff, N. Structural polymorphism of Alzheimer Aβ and other amyloid fibrils. *Prion* **2009**, *3*, 89–93. [CrossRef]
9. Zhang, W.; Falcon, B.; Murzin, A.G.; Fan, J.; Crowther, R.A.; Goedert, M.; Scheres, S.H.W. Heparin-induced tau filaments are polymorphic and differ from those in Alzheimer's and pick's diseases. *eLife* **2019**, *8*, e43584. [CrossRef]
10. Surewicz, W.K.; Apostol, M.I. Prion Protein and Its Conformational Conversion: A Structural Perspective. In *Peptide-Based Materials*; Springer: Berlin/Heidelberg, Germany, 2011; Volume 310, pp. 135–167. ISBN 978-3-540-73346-1.
11. Sidhu, A.; Segers-Nolten, I.; Raussens, V.; Claessens, M.M.A.E.; Subramaniam, V. Distinct Mechanisms Determine α-Synuclein Fibril Morphology during Growth and Maturation. *ACS Chem. Neurosci.* **2017**, *8*, 538–547. [CrossRef]
12. Ziaunys, M.; Sakalauskas, A.; Smirnovas, V. Identifying Insulin Fibril Conformational Differences by Thioflavin-T Binding Characteristics. *Biomacromolecules* **2020**, *21*, 4989–4997. [CrossRef] [PubMed]
13. Mocanu, M.-M.; Ganea, C.; Siposova, K.; Filippi, A.; Demjen, E.; Marek, J.; Bednarikova, Z.; Antosova, A.; Baran, I.; Gazova, Z. Polymorphism of hen egg white lysozyme amyloid fibrils influences the cytotoxicity in LLC-PK1 epithelial kidney cells. *Int. J. Biol. Macromol.* **2014**, *65*, 176–187. [CrossRef]
14. Tycko, R. Amyloid Polymorphism: Structural Basis and Neurobiological Relevance. *Neuron* **2015**, *86*, 632–645. [CrossRef] [PubMed]
15. Sternke-Hoffmann, R.; Peduzzo, A.; Bolakhrif, N.; Haas, R.; Buell, A.K. The aggregation conditions define whether EGCG is an inhibitor or enhancer of α-synuclein amyloid fibril formation. *Int. J. Mol. Sci.* **2020**, *21*, 1995. [CrossRef]
16. Sinnige, T. Molecular mechanisms of amyloid formation in living systems. *Chem. Sci.* **2022**, *13*, 7080–7097. [CrossRef] [PubMed]
17. Ow, S.-Y.; Dunstan, D.E. The effect of concentration, temperature and stirring on hen egg white lysozyme amyloid formation. *Soft Matter* **2013**, *9*, 9692–9701. [CrossRef]
18. Wawer, J.; Szociński, M.; Olszewski, M.; Piątek, R.; Naczk, M.; Krakowiak, J. Influence of the ionic strength on the amyloid fibrillogenesis of hen egg white lysozyme. *Int. J. Biol. Macromol.* **2019**, *121*, 63–70. [CrossRef]
19. Sneideris, T.; Darguzis, D.; Botyriute, A.; Grigaliunas, M.; Winter, R.; Smirnovas, V. pH-Driven Polymorphism of Insulin Amyloid-Like Fibrils. *PLoS ONE* **2015**, *10*, e0136602. [CrossRef]
20. Lee, C.F.; Bird, S.; Shaw, M.; Jean, L.; Vaux, D.J. Combined effects of agitation, macromolecular crowding, and interfaces on amyloidogenesis. *J. Biol. Chem.* **2012**, *287*, 38006–38019. [CrossRef]
21. Feng, Z.; Li, Y.; Bai, Y. Elevated temperatures accelerate the formation of toxic amyloid fibrils of hen egg-white lysozyme. *Vet. Med. Sci.* **2021**, *7*, 1938–1947. [CrossRef]
22. Wang, F.; Wang, X.; Orrú, C.D.; Groveman, B.R.; Surewicz, K.; Abskharon, R.; Imamura, M.; Yokoyama, T.; Kim, Y.S.; Vander Stel, K.J.; et al. Self-propagating, protease-resistant, recombinant prion protein conformers with or without in vivo pathogenicity. *PLoS Pathog.* **2017**, *13*, e1006491. [CrossRef] [PubMed]
23. Whittingham, J.L.; Scott, D.J.; Chance, K.; Wilson, A.; Finch, J.; Brange, J.; Guy Dodson, G. Insulin at pH 2: Structural analysis of the conditions promoting insulin fibre formation. *J. Mol. Biol.* **2002**, *318*, 479–490. [CrossRef] [PubMed]
24. Nettleton, E.J.; Tito, P.; Sunde, M.; Bouchard, M.; Dobson, C.M.; Robinson, C.V. Characterization of the Oligomeric States of Insulin in Self-Assembly and Amyloid Fibril Formation by Mass Spectrometry. *Biophys. J.* **2000**, *79*, 1053–1065. [CrossRef] [PubMed]
25. Tokarz, V.L.; MacDonald, P.E.; Klip, A. The cell biology of systemic insulin function. *J. Cell Biol.* **2018**, *217*, 2273–2289. [CrossRef]
26. Chiti, F.; Dobson, C.M. Protein Misfolding, Amyloid Formation, and Human Disease: A Summary of Progress over the Last Decade. *Annu. Rev. Biochem.* **2017**, *86*, 27–68. [CrossRef]
27. Foderà, V.; Librizzi, F.; Groenning, M.; Van De Weert, M.; Leone, M. Secondary nucleation and accessible surface in insulin amyloid fibril formation. *J. Phys. Chem. B* **2008**, *112*, 3853–3858. [CrossRef]
28. Noormägi, A.; Valmsen, K.; Tõugu, V.; Palumaa, P. Insulin Fibrillization at Acidic and Physiological pH Values is Controlled by Different Molecular Mechanisms. *Protein J.* **2015**, *34*, 398–403. [CrossRef]
29. Jayamani, J.; Shanmugam, G. Gallic acid, one of the components in many plant tissues, is a potential inhibitor for insulin amyloid fibril formation. *Eur. J. Med. Chem.* **2014**, *85*, 352–358. [CrossRef]

30. Nie, R.; Zhu, W.; Peng, J.; Ge, Z.; Li, C. A-type dimeric epigallocatechin-3-gallate (EGCG) is a more potent inhibitor against the formation of insulin amyloid fibril than EGCG monomer. *Biochimie* **2016**, *125*, 204–212. [CrossRef]
31. Gong, H.; He, Z.; Peng, A.; Zhang, X.; Cheng, B.; Sun, Y.; Zheng, L.; Huang, K. Effects of several quinones on insulin aggregation. *Sci. Rep.* **2015**, *4*, 5648. [CrossRef]
32. Deckert-Gaudig, T.; Deckert, V. High resolution spectroscopy reveals fibrillation inhibition pathways of insulin. *Sci. Rep.* **2016**, *6*, 39622. [CrossRef]
33. Katebi, B.; Mahdavimehr, M.; Meratan, A.A.; Ghasemi, A.; Nemat-Gorgani, M. Protective effects of silibinin on insulin amyloid fibrillation, cytotoxicity and mitochondrial membrane damage. *Arch. Biochem. Biophys.* **2018**, *659*, 22–32. [CrossRef]
34. Herranz-Trillo, F.; Groenning, M.; van Maarschalkerweerd, A.; Tauler, R.; Vestergaard, B.; Bernadó, P. Structural Analysis of Multi-Component Amyloid Systems by Chemometric SAXS Data Decomposition. *Structure* **2017**, *25*, 5–15. [CrossRef]
35. Nie, R.; Zhu, W.; Peng, J.; Ge, Z.; Li, C. Comparison of disaggregative effect of A-type EGCG dimer and EGCG monomer on the preformed bovine insulin amyloid fibrils. *Biophys. Chem.* **2017**, *230*, 1–9. [CrossRef]
36. Zheng, Q.; Lazo, N.D. Mechanistic Studies of the Inhibition of Insulin Fibril Formation by Rosmarinic Acid. *J. Phys. Chem. B* **2018**, *122*, 2323–2331. [CrossRef]
37. Nusrat, S.; Zaman, M.; Masroor, A.; Siddqi, M.K.; Zaidi, N.; Neelofar, K.; Abdelhameed, A.S.; Khan, R.H. Deciphering the enhanced inhibitory, disaggregating and cytoprotective potential of promethazine towards amyloid fibrillation. *Int. J. Biol. Macromol.* **2018**, *106*, 851–863. [CrossRef] [PubMed]
38. Yamamoto, N.; Tsuhara, S.; Tamura, A.; Chatani, E. A specific form of prefibrillar aggregates that functions as a precursor of amyloid nucleation. *Sci. Rep.* **2018**, *8*, 62. [CrossRef] [PubMed]
39. Zheng, Z.; Jing, B.; Sorci, M.; Belfort, G.; Zhu, Y. Accelerated insulin aggregation under alternating current electric fields: Relevance to amyloid kinetics. *Biomicrofluidics* **2015**, *9*, 044123. [CrossRef]
40. Saithong, T.; Thilavech, T.; Adisakwattana, S. Cyanidin-3-rutinoside reduces insulin fibrillation and attenuates insulin fibrils-induced oxidative hemolysis of human erythrocytes. *Int. J. Biol. Macromol.* **2018**, *113*, 259–268. [CrossRef]
41. Silva, A.; Sárkány, Z.; Fraga, J.S.; Taboada, P.; Macedo-Ribeiro, S.; Martins, P.M. Probing the occurrence of soluble oligomers through amyloid aggregation scaling laws. *Biomolecules* **2018**, *8*, 108. [CrossRef] [PubMed]
42. Flint, Z.; Grannemann, H.; Baffour, K.; Koti, N.; Taylor, E.; Grier, E.; Sutton, C.; Johnson, D.; Dandawate, P.; Patel, R.; et al. Mechanistic Insights Behind the Self-Assembly of Human Insulin under the Influence of Surface-Engineered Gold Nanoparticles. *ACS Chem. Neurosci.* **2024**, *15*, 2359–2371. [CrossRef]
43. Joshi, R.; Zhaliazka, K.; Holman, A.P.; Kurouski, D. Elucidation of the Role of Lipids in Late Endosomes on the Aggregation of Insulin. *ACS Chem. Neurosci.* **2023**, *14*, 3551–3559. [CrossRef] [PubMed]
44. Zazeri, G.; Povinelli, A.P.R.; Pavan, N.M.; Jones, A.M.; Ximenes, V.F. Solvent-Induced Lag Phase during the Formation of Lysozyme Amyloid Fibrils Triggered by Sodium Dodecyl Sulfate: Biophysical Experimental and In Silico Study of Solvent Effects. *Molecules* **2023**, *28*, 6891. [CrossRef] [PubMed]
45. Khan, J.M.; Malik, A.; Alresaini, S.M. Molecular mechanism of insulin aggregation in the presence of a cationic surfactant. *Int. J. Biol. Macromol.* **2023**, *230*, 123370. [CrossRef] [PubMed]
46. Das, A.; Shah, M.; Saraogi, I. Molecular Aspects of Insulin Aggregation and Various Therapeutic Interventions. *ACS Bio Med Chem Au* **2022**, *2*, 205–221. [CrossRef]
47. Ziaunys, M.; Mikalauskaite, K.; Sakalauskas, A.; Smirnovas, V. Interplay between epigallocatechin-3-gallate and ionic strength during amyloid aggregation. *PeerJ* **2021**, *9*, e12381. [CrossRef]
48. Banga, A.K. *Therapeutic Peptides and Proteins*; CRC Press: Boca Raton, FL, USA, 2015; ISBN 9780429099908.
49. Grudzielanek, S.; Smirnovas, V.; Winter, R. Solvation-assisted Pressure Tuning of Insulin Fibrillation: From Novel Aggregation Pathways to Biotechnological Applications. *J. Mol. Biol.* **2006**, *356*, 497–509. [CrossRef]
50. Barth, A. Infrared spectroscopy of proteins. *Biochim. Biophys. Acta-Bioenerg.* **2007**, *1767*, 1073–1101. [CrossRef]
51. Sakalauskas, A.; Ziaunys, M.; Smirnovas, V. Concentration-dependent polymorphism of insulin amyloid fibrils. *PeerJ* **2019**, *7*, e8208. [CrossRef]
52. Ziaunys, M.; Sakalauskas, A.; Mikalauskaite, K.; Smirnovas, V. Exploring the occurrence of thioflavin-T-positive insulin amyloid aggregation intermediates. *PeerJ* **2021**, *9*, e10918. [CrossRef]
53. Mansoury, M.; Hamed, M.; Karmustaji, R.; Al Hannan, F.; Safrany, S.T. The edge effect: A global problem. The trouble with culturing cells in 96-well plates. *Biochem. Biophys. Rep.* **2021**, *26*, 100987. [CrossRef]
54. Mikalauskaite, K.; Ziaunys, M.; Sneideris, T.; Smirnovas, V. Effect of Ionic Strength on Thioflavin-T Affinity to Amyloid Fibrils and Its Fluorescence Intensity. *Int. J. Mol. Sci.* **2020**, *21*, 8916. [CrossRef] [PubMed]
55. Mikalauskaite, K.; Ziaunys, M.; Smirnovas, V. Lysozyme Amyloid Fibril Structural Variability Dependence on Initial Protein Folding State. *Int. J. Mol. Sci.* **2022**, *23*, 5421. [CrossRef] [PubMed]
56. Ziaunys, M.; Smirnovas, V. Additional Thioflavin-T Binding Mode in Insulin Fibril Inner Core Region. *J. Phys. Chem. B* **2019**, *123*, 8727–8732. [CrossRef] [PubMed]

ACS Chemical Neuroscience

pubs.acs.org/chemneuro
Research Article

Imidazo[2,1-*b*][1,3]thiazine Derivatives as Potential Modulators of Alpha-Synuclein Amyloid Aggregation

Indrė Misiūnaitė,[#] Kamilė Mikalauskaitė,[#] Martyna Paulauskaitė, Rūta Sniečkutė, Vytautas Smirnovas, Algirdas Brukštus, Mantas Žiaunys, and Ieva Žutautė*

Cite This: https://doi.org/10.1021/acschemneuro.4c00451
Read Online

ABSTRACT: Insoluble amyloid fibrils accumulate in the intercellular spaces of organs and tissues, leading to various amyloidosis-related disorders in the human body. Specifically, Parkinson's disease is associated with the aggregation of alpha-synuclein. However, current treatments for Parkinson's primarily focus on managing motor symptoms and slowing disease progression. Efforts to prevent and halt the progression of these diseases involve the search for small molecular compounds. In this work, we synthesized imidazo[2,1-*b*][1,3]thiazines in an atom-economic way by cyclization of 2-alkynylthioimidazoles using 10% AuCl as the catalyst. We identified several compounds with specific functional groups capable of both inhibiting the aggregation of alpha-synuclein and redirecting the fibril formation pathway. The investigation into how these substances function revealed that imidazo[2,1-*b*][1,3]thiazine derivatives can influence alpha-synuclein aggregation in several ways. They not only inhibit the primary nucleation process and maintain a balance toward nonaggregated protein states but also stabilize smaller oligomeric species of alpha-synuclein and cause the formation of fibrils with unique structures and forms. These imidazo[2,1-*b*][1,3]thiazines could potentially be used in developing highly efficient, small molecular weight protein aggregation inhibitors.

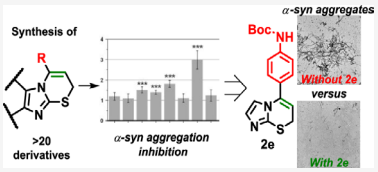

KEYWORDS: *alkynes, Au catalysis, cyclization, imidazoles, alpha-synuclein, amyloid aggregation*

INTRODUCTION

Amyloid protein aggregation in the form of insoluble fibrils is associated with multiple widespread and incurable disorders, such as Alzheimer's or Parkinson's disease.[1,2] More than 30 different proteins and peptides have been identified, whose cytotoxic aggregates accumulate in the intercellular spaces of organs and tissues.[1] Despite decades of research and enormous effort in deciphering the amyloid aggregation process, there are still very few known treatment modalities,[3,4] and the number of affected individuals is projected to increase further in the foreseeable future.[5,6] Efforts to prevent and halt the progression of these diseases involve the search for various types of inhibitors, which range from small molecular weight compounds[7] to monoclonal antibodies[8] or complex drug mixtures.[9,10]

In the case of small molecules, a number of different class compounds have been identified as having antiamyloid potential by either directly inhibiting the fibril formation process or targeting factors that create conditions suitable for amyloid aggregation. These compounds include various polyphenols (gallic acid,[11] epigallocatechin-3-gallate[12]), alkaloids (tolserine,[13] galantamine[14]), terpenoids (1.8-cineole,[15] α-pinene[16]), and polyketides (hispidin[17]). Several small molecular weight compounds have progressed to clinical trials, such as Anleb138b and NPT100-18A.[18] Anleb138b has been found to inhibit alpha-synuclein (α-syn) oligomer formation,[19] while NPT100-18A interferes with α-syn aggregation by displacing the protein from membranes.[20] Minzasolmin, currently in Phase 2 clinical trials, stands out as one of the most promising potential disease-modifying therapeutics for Parkinson's disease.[21] Biophysical evaluations revealed that this compound acts early in the aggregation process by displacing membrane-bound oligomeric α-syn and returning it to a monomeric form, thus preventing the formation of larger protein aggregates and eventually Lewy bodies.[21] However, despite hundreds of such potential antiamyloid compounds, the success rate in clinical trials remains very low, with most molecules failing at the initial phases.[22]

To expand the list of potential amyloid aggregation inhibitors, this work was dedicated to analyzing the activity of a previously unexplored small molecular weight compound group – imidazo[2,1-*b*][1,3]thiazines. These molecules are synthetically novel and have not been observed in nature, which has limited extensive investigations of their properties. Despite no prior research on their antiamyloid potential, it has

Received: July 17, 2024
Revised: November 20, 2024
Accepted: November 21, 2024

Table 1. Au(I)Cl Initiated Cyclization Reactions of Various 2-Alkynylthioimidazoles[abc]

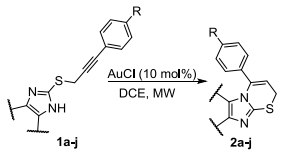

Entry	Starting Material		Temp. (°C)	Time (h)	Product	Yield (%)
1		R = 4-Me **1a**	50	2.3	**2a**	88
2		R = 4-OMe **1b**	50	2.3	**2b**	82
3		R = 4-OEt **1c**	50	2.3	**2c**	69
4		R = 4-OCH_2COOEt **1d**	50	15	**2d**	90
5		R =4-NHBoc **1e**	50	12.3	**2e**	92
6		R = 4-N(Boc)$CH_2CONHCH_2CH(CH_3)_2$ **1f**	50	2.3	**2f**	76
7		R = 4-OEt **1g**	80	2.3	**2g**	68
8		R = 4-$OCH_2CONHCH_2CH(CH_3)_2$ **1h**	80	2.3	**2h**	52
9[b]		R = 4-OEt **1i**	40	2	**2i**	69
10		R = 4-N(**Boc**)$CH_2CONHCH_2CH(CH_3)_2$ **1j**	50	2.3	**2j**	88
11[c]		R = 4-N**H**$CH_2CONHCH_2CH(CH_3)_2$ **2j**			**3**	61

[a]In an MW vial, compound **1** (from 50 mg to 200 mg, 0.17−0.45 mmol) was dissolved in 5 mL of DCE, and AuCl (10 mol %) was added under an argon atmosphere. The sealed vial was subjected to microwave irradiation until full conversion of the starting material. [b]Substrate **1i** (80 mg, 0.30 mmol) was dissolved in 5 mL of DCM, then 10 mol % of AuCl was added, and the reaction mixture was refluxed under an argon atmosphere. [c]Deprotection conditions: to the solution of **2j** (140 mg, 0,28 mmol, 1.0 equiv) in DCM (5 mL), TFA (1 mL) was added dropwise. The reaction mixture was stirred at room temperature overnight until full conversion of the starting material.

been shown that compounds bearing a 1,3-thiazine moiety exhibit a wide range of biological activities,[23] including antimicrobial, anti-inflammatory, antidiabetic, analgetic, and anticancer properties. To evaluate their possible influence on amyloid fibril formation, we synthesized 21 compounds and examined their effect on the aggregation process of α-syn − an intrinsically disordered protein related to the onset and progression of Parkinson's disease.[24]

We discovered that some of the imidazo[2,1-*b*][1,3]thiazine derivatives possessed strong antiamyloid properties, which resulted in significantly longer aggregation lag phases. The inhibitor compounds also redirected the aggregation pathway, causing the formation of fibrils with different secondary structures and morphologies. Additionally, the presence of the imidazo[2,1-*b*][1,3]thiazine framework also shifted the α-syn monomer-fibril equilibrium toward the nonaggregated state. Together with previous reports of various positive biological activities, these results indicate that imidazo[2,1-*b*][1,3]-thiazine derivatives are promising candidates for both synthetic and pharmaceutical applications.

RESULTS AND DISCUSSIONS

Compound Synthesis. The synthesis of imidazo[2,1-*b*][1,3]thiazines **2** was carried out under the conditions established in our previous work.[25] Various functionalized alkynes were selected as starting materials for the gold(I) chloride-promoted nucleophilic closure reaction in a microwave (MW) synthesizer. The synthesis of 2-alkynylthioimidazoles **1** typically began with the Sonogashira cross-coupling reaction of aryl iodides, followed by bromination of the hydroxyl group, and was concluded with nucleophilic substitution with the desired thioimidazole (see the Supporting Information). However, using 4-iodoaniline as the starting compound, the Sonogashira reaction did not proceed as expected. Therefore, a *tert*-butyloxycarbonyl (*Boc*) protective group was introduced into the molecule, allowing for selective alkylation and the Sonogashira reaction. The synthesis of imidazo[2,1-*b*][1,3]thiazines was generally carried out in a MW synthesizer at 50 °C for 140 min. Adjustments to these conditions were made, depending on the thioimidazole moiety in the starting material (Table 1). For instance, 2-alkynylthio-4,5-dimethylimidazoles **1g,h** required higher reaction temperatures to fully convert the starting materials while maintaining similar reaction time to those of compounds **1a−c,f** (Table 1, entries 1−3, 6), and the cyclization of compound **1e** (Table 1, entry 5) required a prolonged reaction time of up to 12.3 h. Compounds **2a**, **2c**, **2d**, **2g**, and **2i** (Table 1, entries 1, 3−4, 7, 9) were synthesized and isolated in our previous work.[25] To evaluate the impact of the protecting group on α-syn aggregation, the *Boc* group was removed from compound **2j** (Table 1, entry 11). The deprotection was carried out under acidic conditions using TFA in DCM, resulting in compound **3** with a 61% yield.

To broaden the scope of the compounds for investigation, ester **2d** was modified by substituting it with an amide group. This modification can be achieved from either an ester or an acid. To streamline the process and minimize the number of reaction steps, reactions involving ester **2d** were prioritized. According to the literature,[26] amides can be synthesized from esters in ethanol using an appropriate amine. However, this method yielded only 33% of the desired amide. Another method suggested that esters and amines could react in DMF at 35−40 °C;[27] however, after 5 days of heating, only a small amount of product was detected by TLC, leading to the

https://doi.org/10.1021/acschemneuro.4c00451
ACS Chem. Neurosci. XXXX, XXX, XXX−XXX

Table 2. Synthesis of Amides 5 from Ester 2d[a]

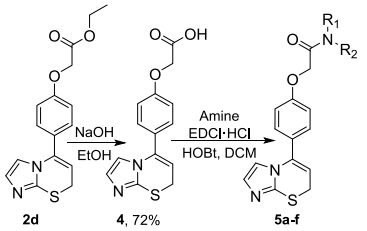

Entry	Amine (NHR_1R_2)	Product	Yield (%)
1		**5a**	47
2		**5b**	79
3		**5c**	73
4		**5d**	75
5		**5e**	73
6	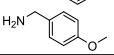	**5f**	98

[a]Reaction condition for acid **4**: into a solution of **2d** (883.2 mg, 2.79 mmol, 1.0 equiv) in 20 mL of EtOH, NaOH (111.7 mg, 2.79 mmol, 1.0 equiv) was added. The reaction mixture was stirred at room temperature overnight. Reaction conditions for amides **5**: into a solution of compound **4** (50 mg, 0.17 mmol, 1 equiv) in 5 mL of DCM, EDCI·HCl (49.9 mg, 0.26 mmol, 1.5 equiv), HOBt (35.2 mg, 0.26 mmol, 1.5 equiv), and appropriate amine (0.21 mmol, 1.2 equiv) were added. The reaction mixture was stirred at room temperature overnight.

termination of this reaction. Subsequent attempts to synthesize amides using excess amine as both a reagent and solvent also failed. Consequently, ester **2d** was hydrolyzed to its corresponding acid **4**, and a more sophisticated approach was employed using EDCI (1-ethyl-3-(3-dimethylaminopropyl)carbodiimide) and HOBt (1-hydroxybenzotriazole)[28] as coupling reagents. Although the yield of amide formation with isobutylamine was modest, superior yields exceeding 70% were achieved with the corresponding amines (Table 2). Notably, compound **2h** was synthesized from the corresponding 2-alkynylthio-4,5-dimethylimidazole. Both methods are viable, depending on whether the goal is to modify an existing compound rapidly or to obtain a specific target compound.

To investigate the necessity of the imidazothiazine ring for α-syn aggregation, it was decided to synthesize compounds **6** and **7** while retaining the imidazole ring and maintaining the same distance to the functional group as in the imidazothiazine **5a**. The mentioned compounds were obtained under classical alkylation and acylation conditions (Scheme 1). These molecules exhibit structural similarities to oxindoles, which have been studied for their effects on amyloidogenic protein aggregation by Kimura and colleagues.[29]

Alpha-Synuclein Aggregation Inhibition. The aggregation-inhibiting potential of the 18 synthesized imidazo[2,1-*b*][1,3]thiazine derivatives was determined (Figure S1) was examined by combining them with an equimolar concentration of α-syn and monitoring the formation of amyloid fibrils (Figure 1). During this research, the main attention was focused on substituents to the condensed heterocyclic system and additional functional groups in the phenyl *para* position of 5-arylimidazo[2,1-*b*][1,3]thiazines. First, the influence of substituents on the imidazole ring on α-syn aggregation was

Scheme 1. Synthesis of Compounds 6 and 7

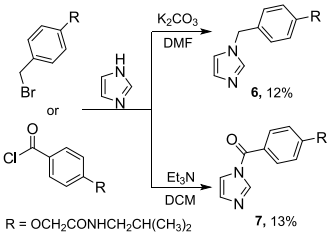

investigated. Imidazo[2,1-*b*][1,3]thiazine **2c** and benzimidazo-[2,1-*b*][1,3]thiazine **2i** resulted in aggregation curves with significantly higher t_{50} values (Bonferroni means comparison, $n = 6$, $p < 0.01$), while for 2,3-dimethylimidazo[2,1-*b*][1,3]-thiazine **2g**, the values were only slightly above the control but were not statistically significant (Figure 1A). Interestingly, all three molecules resulted in a significant increase in the sample end-point ThT fluorescence intensity values (Figure 1B), which would suggest an opposite effect to inhibition. According to the results, it was evident that the strongest aggregation reduction was achieved with compound **2c** bearing an unsubstituted imidazo[2,1-*b*][1,3]thiazine heterocyclic system. An additional comparison of compounds **2h** and **5a** confirmed the decrease in activity resulting from the introduction of methyl groups to the imidazole ring. 2,3-Dimethylimidazo[2,1-*b*][1,3]thiazine **2h** did not affect either the t_{50} values or the sample fluorescence intensity, while imidazo[2,1-*b*][1,3]thiazine **5a** displayed a significant effect on both parameters. However, it was considerably lower than that in the case of **2c**.

https://doi.org/10.1021/acschemneuro.4c00451
ACS Chem. Neurosci. XXXX, XXX, XXX−XXX

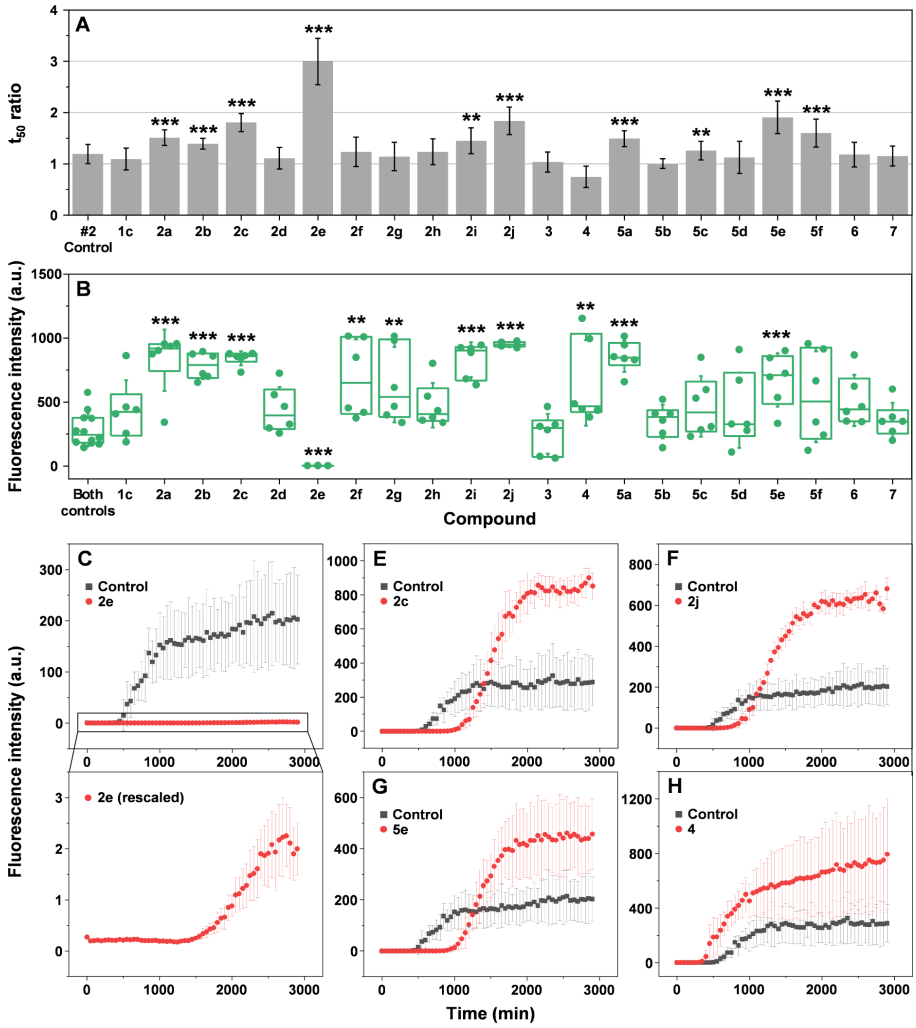

Figure 1. α-Syn aggregation kinetics in the presence of different imidazothiazine derivatives. (A) Aggregation half-time (t_{50}) ratios (sample t_{50} values divided by control t_{50} values) of α-syn samples containing equimolar concentrations of different compounds (100 μM, n = 6, error bars are combined standard deviations). (B) End-point sample ThT fluorescence intensity value distribution (n = 6, box plots indicate the interquartile range, error bars are for one standard deviation). Significant differences were determined using ANOVA Bonferroni means comparison, ** p < 0.01, *** p < 0.001. (C−H). Rescaled images of kinetics with compound **2e** are shown below in panel C. Example kinetic curves of α-syn aggregation in the presence of compounds that inhibit or enhance the reaction.

The crucial role in reducing α-syn aggregation of the thiazine ring was confirmed by tests with compounds **1c**, **6**, and **7**. All of them resulted in aggregation curves with similar t_{50} values. The 2-((3-(4-ethoxyphenyl)prop-2-yn-1-yl)thio)-1*H*-imidazole **1c**, the starting material of imidazothiazine **2c**, exhibited t_{50} values that were almost identical to the control. Compounds **6** and **7** affected α-syn aggregation significantly less than the corresponding imidazothiazine **5a** and were not significantly different from the control. Similar to the lack of influence on α-syn aggregation, these three compounds also did not cause any end-point sample fluorescence value deviations from the control samples (Figure 1B). From these results, it is evident that the imidazothiazine fragment forms an appropriate angle for the aryl substituent in the molecule and also may take part in interaction with the protein.

Next, the impact of the R group at the *para* position on the phenyl substituents in 5-arylimidazo[2,1-*b*][1,3]thiazines was examined. Even a single carbon difference had a notable

https://doi.org/10.1021/acschemneuro.4c00451
ACS Chem. Neurosci. XXXX, XXX, XXX−XXX

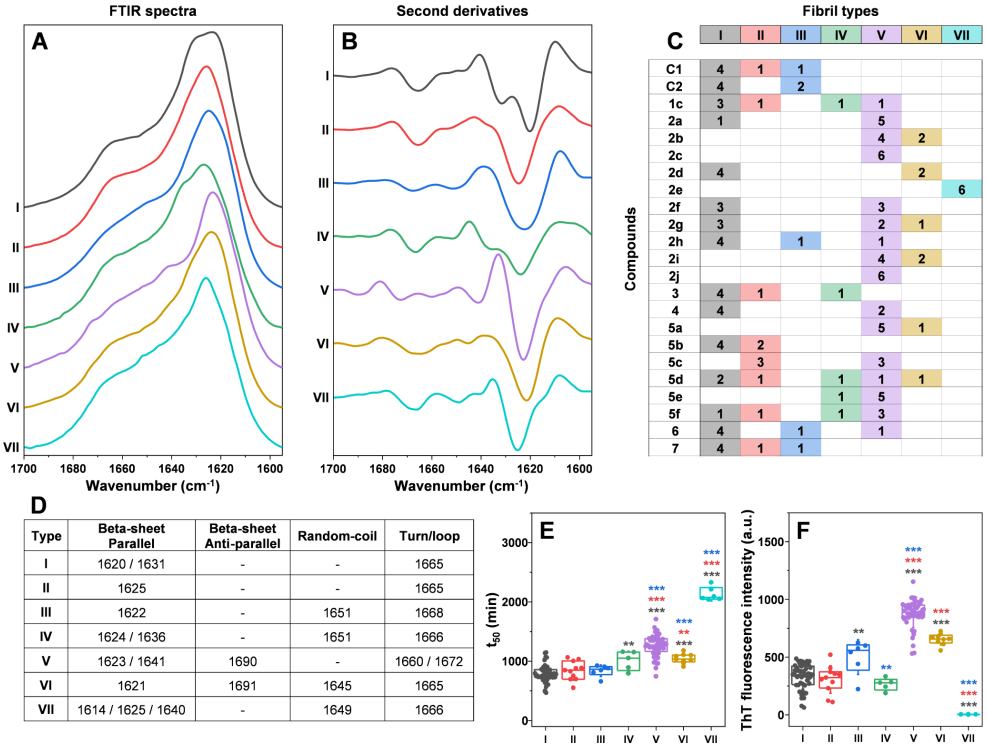

Type	Beta-sheet Parallel	Beta-sheet Anti-parallel	Random-coil	Turn/loop
I	1620 / 1631	-	-	1665
II	1625	-	-	1665
III	1622	-	1651	1668
IV	1624 / 1636	-	1651	1666
V	1623 / 1641	1690	-	1660 / 1672
VI	1621	1691	1645	1665
VII	1614 / 1625 / 1640	-	1649	1666

Figure 2. α-Syn aggregate secondary structure dependence on the presence of compounds. (A, B) Seven different α-syn fibril FTIR spectra (FTIR) and their second derivatives detected after aggregation with or without compounds. (C) Fibril type distribution in samples without (control #1, control #2) or with different compounds (color-coded boxes indicate the number of each specific type of fibril). (D) Different fibril FTIR spectra second-derivative minimum positions related to parallel beta-sheets, antiparallel beta sheets, random-coil, and turn/loop motifs. (E, F) t_{50} and end-point ThT fluorescence intensity value distribution of different fibril type aggregation curves. Significant differences were determined using ANOVA Bonferroni means comparison, ** $p < 0.01$, *** $p < 0.001$.

outcome on α-syn aggregation. Comparing compound **2c**, with an −OEt group, and compound **2b**, with an −OMe group, revealed that a shorter chain decreased the average aggregation half-time ratio from 1.75 to 1.3. Compound **2a** differed from compound **2b** only in having a −Me group instead of an −OMe. This small structural change did not significantly impact α-syn aggregation reduction as the average values were 1.5 and 1.3, respectively. Despite these differences, all three compounds (**2a**, **2b**, **2c**) resulted in a significant increase in both the reaction t_{50} values, as well as the end-point fluorescence intensities (Figure 1A,B). Additionally, the functionalization of the phenolic group with an ester moiety in compound **2d** showed minimal change in α-syn aggregation, with t_{50} and fluorescence intensity values being similar to those of the control. The corresponding acid **4** appeared to even enhance the aggregation process. However, the change was not statistically significant. Replacing the ester group with various amides (compounds **5a**, **5c**, and **5e**−**5f**) increased activity compared to compounds **2d** and **4**, while activity remained the same for compounds **5b** and **5d**. The best result was achieved with amide **5e**, which yielded an average half-time ratio of 1.8, while the introduction of an additional −OMe group in benzyl (amide **5f**) resulted in a similar activity to compound **2c**, with a half-time ratio of 1.6 (Figure 1A). Of all amides **5a**−**f**, only **5a** and **5e** caused significantly higher end-point fluorescence intensity values (Figure 1B).

Replacing the phenolic group with substituted anilines resulted in enhanced activity of the corresponding compounds. Compound **2e**, bearing only the *Boc* group on aniline, unexpectedly demonstrated the largest half-time ratio value (Figure 1A). Unlike all other inhibitors, **2e** caused a massive reduction in the sample end-point fluorescence intensity (Figure 1B). While the addition of the $-CH_2CONHCH_2CH(CH_3)_2$ group in compound **2f** did not enhance the t_{50} value as expected and even lowered it, compared to lose aniline **2e** and mimicked compound **5a**. Maintaining this additional group while changing the imidazole ring to benzimidazole **2j** resulted in an increased average half-time ratio of 1.8, similar to compounds **2c** and **5e**. The role of the protecting group in α-syn aggregation reduction was crucial, as the activity was completely diminished in the case of compound **3**.

In summary, 21 compounds were tested for their ability to inhibit α-syn aggregation. The highest half-time ratios were achieved with imidazo[2,1-*b*][1,3]thiazines **2e**, **5e**, and **2c** and

https://doi.org/10.1021/acschemneuro.4c00451
ACS Chem. Neurosci. XXXX, XXX, XXX−XXX

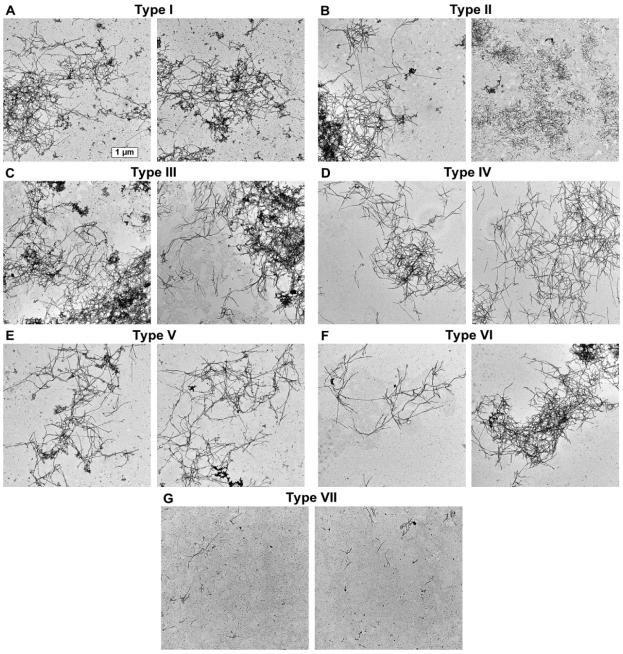

Figure 3. Electron microscopy (EM) images of α-syn aggregates with seven distinct FTIR spectra. (A–G) Two 4096 × 4096 pixel resolution representative images for each fibril type. The scale bar (presented in the top left image) is identical for all images.

benzimidazo[2,1-*b*][1,3]thiazines **2j** (Figure 1C–G), while acid **4** displayed a possible aggregation-enhancing effect (Figure 1H). The presence of the imidazo[2,1-*b*][1,3]thiazine fragment was crucial for improved protein aggregation reduction. Particularly, the best results were achieved with *Boc* protected aniline **2e**. However, the addition of extra groups to this structure led to a drastic drop in the efficiency. Nonetheless, the benzimidazole moiety helped to mitigate the impact of additional groups.

Effect on Fibril Structure and Morphology. Despite the positive antiamyloid activity of the compounds, a majority of them yielded samples with a significantly higher ThT fluorescence intensity (Figure 1B). Since none of these compounds possess an intrinsic fluorescence capacity under the ThT-specific excitation and emission wavelengths (Figure S2), the observed phenomenon had two possible explanations. Either the compounds shifted the equilibrium between the native and aggregated states of α-syn in favor of amyloid fibrils, or the resulting structures had different ThT binding modes.[30] We have previously observed a similar event, where antiamyloid compounds redirected α-syn aggregation into fibrils with different secondary structures,[31] which, in turn, can affect their dye-binding properties.[32,33]

To examine this possibility, all samples (n = 6 for each compound) were tested using Fourier-transform infrared (FTIR) spectroscopy. The resulting spectra of the amide I region and their second derivatives were compared against each other and grouped based on similarities in their peak and minima positions (Figure 2A,B). In the case of samples from both control runs, the FTIR spectra were divided into three distinct types: I, II, and III (Figure 2C). Such random polymorphism has been shown in previous studies under similar conditions.[34] Type I fibril FTIR spectra second derivatives contained two minima at 1631 and 1620 cm^{-1} (Figure 2D), associated with two different strengths of hydrogen bonding in the beta-sheet structure[35] and a minimum at 1665 cm^{-1} (turn/loop motif). Type II displayed a single minimum related to beta-sheets at 1625 cm^{-1} and a minimum identical to type I at 1665 cm^{-1}. Type III fibril FTIR derivatives had minima at 1622 cm^{-1} (beta-sheets), 1651 cm^{-1} (random-coil), and 1668 cm^{-1} (turn/loop motif).

When α-syn was aggregated in the presence of exploratory compounds, four additional types of FTIR spectra were observed. Type IV was only detected in one out of the six repeats for samples containing compounds **1c**, **3**, **5d**, **5e**, and **5f** (Figure 2C). Its second derivatives had minima at 1624 cm^{-1}, with a shoulder at 1636 cm^{-1} (two different strength hydrogen bonding types in the beta-sheet structure) and minima at 1651 cm^{-1} (random-coil), 1666 cm^{-1} (turn/loop motif). Type V, on the other hand, was the most abundant spectral type detected among all of the samples (Figure 2C). It had minima related to beta-sheets at 1641 and 1623 cm^{-1}, turn/loop motifs at 1660 and 1672 cm^{-1}, as well as a minimum associated with antiparallel beta-sheets at 1690 cm^{-1} (Figure 2B,D). Type VI fibril FTIR spectra were detected only for a small number of samples containing **2b**, **2d**, **2g**, **2i**, **5a**, and **5d** compounds (Figure 2C). Their second derivatives had minima at 1621 cm^{-1} (beta-sheets), 1645 cm^{-1} (random-coil), 1665 cm^{-1}

https://doi.org/10.1021/acschemneuro.4c00451
ACS Chem. Neurosci. XXXX, XXX, XXX−XXX

(turn/loop motif), and 1691 cm^{-1} (antiparallel beta-sheets). Finally, type VII spectra were observed only in the case of the strongest inhibitor compound **2e**. Their second derivatives had minima at 1625 cm^{-1} with a shoulder at 1614 cm^{-1} (two types of hydrogen bonding strength in the beta-sheet structure), 1640 cm^{-1} (weak beta-sheet hydrogen bonding), 1649 cm^{-1} (random-coil), and 1666 cm^{-1} (turn/loop motif).

Based on the FTIR spectral distribution, it was clear that imidazo[2,1-*b*][1,3]thiazine derivatives could influence the secondary structure of the formed aggregates. In some cases, such as with compounds **2c**, **2e**, and **2j**, the aggregation reaction was redirected to produce fibrils with a single FTIR spectrum across all six repeats. Interestingly, the compounds that increased t_{50} and/or fluorescence intensity were also, for the most part, the ones that promoted the formation of these four different secondary structures (Figures 1A and 2C). These findings suggest a possible correlation among the inhibitory effect, the resulting aggregate structures, and their ThT-binding ability.

In order to test this hypothesis, the sample aggregation t_{50} values and end-point fluorescence intensities were grouped based on their respective FTIR spectrum type. Surprisingly, the spread of data was minimal for almost all types, further supporting the aforementioned correlation. In the case of t_{50} value distributions (Figure 2E), samples resulting in type I−III FTIR spectra did not have any significant differences between them (ANOVA Bonferroni means comparison). Conversely, type V−VII samples all displayed significantly different t_{50} value distributions. The type IV sample t_{50} values were significantly different from those of only one of the three types detected in the control samples. A similar tendency was observed for the fluorescence intensity distributions (Figure 2F). Type V−VII samples were significantly different from either all or two of the three control sample types. However, unlike the t_{50} values, the three control samples also did not display nearly identical distributions, with type III having a mean value significantly higher than that of the type I samples. Finally, type IV sample fluorescence intensities were comparable to two of the three control samples and shared a dissimilarity to the type III samples.

Taken together, these data revealed that there was a strong correlation between the aggregate secondary structures and their formation time, as well as ThT-binding parameters. This could be achieved either by the compounds promoting the formation of certain fibril nuclei or by selectively inhibiting the assembly of type I−III aggregate nuclei. Considering that all samples with type IV−VII FTIR spectra had larger t_{50} values, the selective inhibition hypothesis seemed like the most likely explanation.

Since different α-syn secondary structures are often an indicator of distinct fibril morphologies, the seven fibril types were further examined using electron microscopy (EM). Based on the results, four unique morphological aspects were observed. Type I, II, III, and VI fibrils displayed a high level of self-association, yielding large aggregate clusters (Figure 3A−C and F). Type IV and V fibrils, despite possessing similar lengths to the aforementioned types, were less prone toward such clump formation and associated into intertwined networks (Figure 3D,E). Type II aggregates, along with their tendency of cluster formation, also displayed an abundance of short (<1 μm) fibrils (Figure 3B, second image). Finally, type VII samples were composed of a low concentration of fibrillar structures and a relatively high amount of small amorphous aggregates or oligomeric species (Figure 3G).

These results were correlated with the previously described sample fluorescence intensity values. The type VII samples displayed the least amount of fibrillar structures, and they also pertained the lowest fluorescence intensities. Type I, II, III, and VI fibrils formed large aggregate clusters, which likely impeded the ability of ThT to bind on some parts of the structures. Due to this reason, the type V and VI fibrils, which formed intertwined networks, were also the ones with the highest ThT fluorescence intensity. These morphological distinctions indicate that the inhibitory compounds can affect α-syn fibril self-association tendencies and length as well as the appearance of oligomeric or amorphous structures and the resulting overall sample ThT fluorescence intensity.

Mechanism of Inhibition. Despite these observations, two important questions remained: what is the mechanism of inhibition, and how do the imidazo[2,1-*b*][1,3]thiazine derivatives affect the monomer-fibril equilibrium. In order to gain deeper insight into the process and answer these questions, five compounds (**2c**, **2e**, **2j**, **4**, and **5e**) were selected for further study (Figure 4). According to the

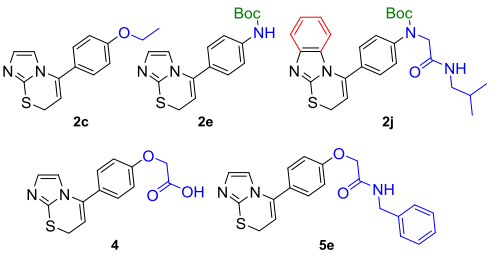

Figure 4. Structures of selected active compounds **2e**, **2c**, **2j**, **4**, and **5e**.

obtained experimental data, compound **2e** was chosen as the strongest inhibitor, and compounds **2c**, **2j**, and **5e** were selected as moderate inhibitors. Imidazothiazine **2c** represents the simplest active structure with an ethoxy substituent. Compound **2j** bears a benzimidazothiazine moiety with an amide substituent like imidazothiazine **5e**. Imidazotiazinylphenoxyacetic acid **4** was also additionally tested as the only compound that displayed a possible aggregation-enhancing activity. To determine which fibrillization step was influenced by these compounds, α-syn aggregation was carried out under different compound concentrations. The resulting aggregation curves were fit using a Boltzmann sigmoidal equation, and three parameters were calculated, which included the reaction lag time (affected by primary nucleation), apparent rate constant (affected by the rate of elongation, secondary nucleation, and fragmentation), and end-point fluorescence intensity (affected by aggregate structure and quantity).

In the case of all four inhibitors, there was an increase in reaction lag times based on the concentration of the compounds (Figure 5A, **2c**, **2e**, **2j**, and **5e**). Interestingly, each compound displayed different tendencies in how the lag times changed. In the case of compound **2c**, both 50 and 100 μM concentrations resulted in an almost identical value, while 200 μM yielded a considerably higher level of inhibition. For compound **2e**, the inhibitory effect became saturated at 100

https://doi.org/10.1021/acschemneuro.4c00451
ACS Chem. Neurosci. XXXX, XXX, XXX−XXX

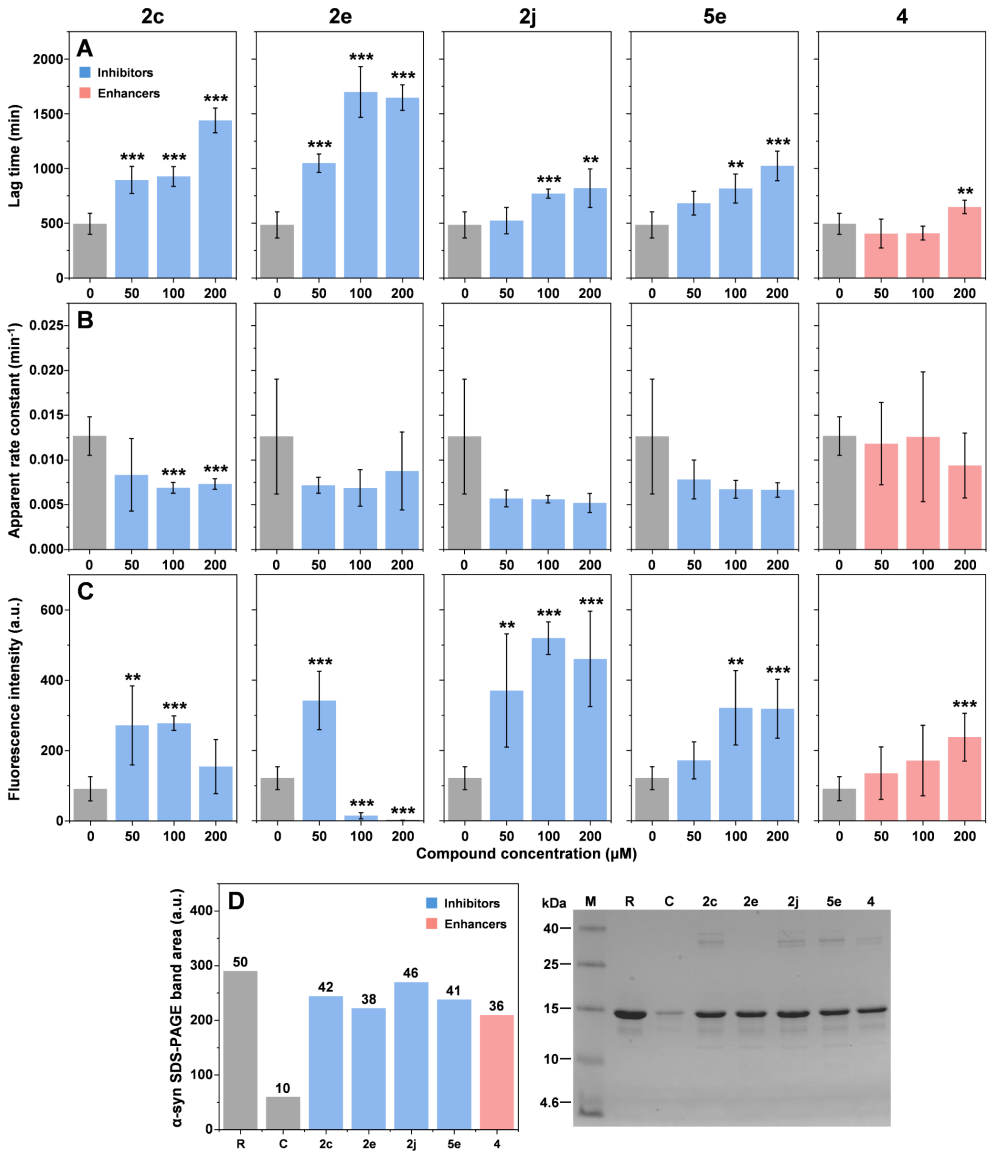

Figure 5. α-Syn aggregation kinetic parameter dependence on different concentrations of compounds. (A–C) Lag time, apparent rate constant, and fluorescence intensity value distribution of α-syn aggregation curves in the presence of different compound concentrations. Significant differences were determined using ANOVA Bonferroni means comparison, $n = 6$, ** $p < 0.01$, *** $p < 0.001$. (D) Sample supernatant SDS-PAGE gel and α-syn band area distribution, "R" – reference 50 μM monomeric α-syn sample, "C" – control fibril sample supernatant, and numbers indicate the calculated concentration of α-syn based on the reference band.

μM and a higher concentration did not result in any notable effect. Compound **2j** only displayed an inhibitory effect at 100 and 200 μM, which was also similar under both conditions. Out of the four inhibitors, **5e** demonstrated the most linear dependence between the aggregation lag time and compound concentration. The previously detected aggregation-enhancing compound **4** resulted in reduced reaction lag times under 50 and 100 μM concentrations. However, this effect was not

https://doi.org/10.1021/acschemneuro.4c00451
ACS Chem. Neurosci. XXXX, XXX, XXX–XXX

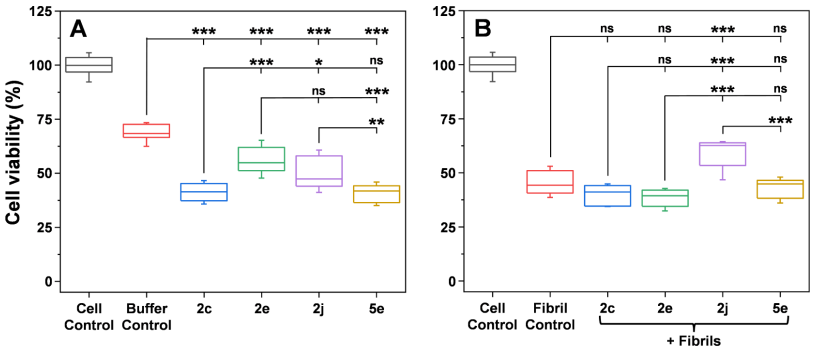

Figure 6. Effect of imidazo[2,1-*b*][1,3]thiazine derivatives on SH-SY5Y human neuroblastoma cells. MTT viability assay of the selected compounds (20 μM) in the absence (A) or presence (B) of α-syn amyloid fibrils (20 μM). For each condition, three independent assays were carried out (each with three sample repeats), and error bars represent one standard deviation (n = 9). One-way ANOVA Bonferroni means comparison was conducted to determine differences between samples (ns – not significant, * $p < 0.05$, ** $p < 0.01$, *** $p < 0.001$).

statistically significant. Interestingly, 200 μM of the compound yielded a significantly higher reaction lag time, suggesting that it may act as an enhancer or inhibitor based on its concentration.

Examination of the reaction apparent rate constants (Figure 5B) revealed that all four inhibitors (**2c**, **2e**, **2j**, **5e**) induced a concentration-dependent decrease in their average value, where the 200 μM compound concentration samples displayed a 2-fold lower rate constant than the control. In the case of the possible enhancer, the average apparent rate constant decrease was not as intense. However, due to the large stochasticity of this parameter, statistically significant differences could only be determined for compound **2c**.

The end-point fluorescence data presented an even more complicated picture (Figure 5C). Compound **2c** resulted in an arc-shaped fluorescence intensity dependence on its concentration, with 50 and 100 μM condition samples having significantly higher average values, while 200 μM condition samples were similar to the control. In the case of **2e**, the fluorescence intensity was significantly higher under conditions with 50 μM compound, while both higher concentrations yielded samples where the ThT signal was almost completely quenched. Compound **2j** produced samples with highly variable fluorescence intensities, with all condition values within the margin of error. For compound **5e**, both 100 and 200 μM conditions resulted in an almost identical and significantly higher fluorescence intensity. The enhancer compound resulted in a linear dependence between its concentration and the average sample fluorescence intensity values. However, only the 200 μM condition samples were significantly different.

A possible explanation for these highly stochastic results is the previously shown correlation between fibril types and their fluorescence intensities. If lower compound concentrations are not sufficient to redirect all nuclei formation to a certain structure, then each condition results in a different distribution of fibril types, each with its own specific fluorescence intensity. To determine if the significant differences in end-point fluorescence intensity were purely related to distinct fibril structures or a shift in monomer–aggregate equilibrium, the highest compound concentration samples were centrifuged, and their supernatants were examined with SDS-PAGE. As two reference points, a 50 μM α-syn sample (Figure 5D, marked as "R", 50 μM concentration was used to avoid signal overflow during gel analysis) and a control α-syn fibril sample supernatant (Figure 5D, marked as"C") were used. The dyed gel was imaged and analyzed by using GelAnalyzer software.

In the case of the control fibril sample, the band was almost nondetectable, indicating an efficient conversion of the majority of α-syn into its aggregated state (90 μM out of 100 μM). Surprisingly, all tested compounds resulted in a similar residual concentration of α-syn regardless of the inhibitory effect or the end-point fluorescence values. In all cases, the nonaggregated α-syn composed approximately 40% of the total protein content in the samples, which was considerably higher than under conditions with no imidazo-[2,1-*b*][1,3]thiazine derivatives. This result suggests that the fluorescence signal was almost entirely related to the types of fibrils that were formed and not due to their quantity. Another interesting aspect was the presence of bands between 25 and 40 kDa markers in samples with compounds **2c**, **2j**, **5e**, and **4**. Since this band is not observed in either the monomeric or control sample, it suggests that the compounds may have been capable of stabilizing dimeric and trimeric forms of α-syn.

Compound Toxicity. To determine whether the compounds with the highest antiaggregation effects can also counteract the cytotoxic effects of α-syn fibrils, an MTT assay was performed using SH-SY5Y human neuroblastoma cells. When 20 μM of each compound was introduced to the medium without α-syn aggregates, all of them caused a statistically significant reduction in cell viability (Figure 6A, n = 9, ANOVA Bonferroni means comparison). The chosen concentration of compounds for the cell viability assay was much higher than the concentration that would likely exist at target locations after compound administration. However, it was required to compare the relative toxicity of each compound, as lower concentrations do not significantly deviate from the buffer solution control (Figure S3).

The negative effect on cell viability was significantly greater for compounds **2c** ((41 ± 4)% cell viability) and **5e** ((41 ± 4)%) when compared to the buffer solution control ((69 ± 4)%). In contrast, the reduction in cell viability was less pronounced for compounds **2e** ((56 ± 6)%) and **2j** ((50 ± 7)%), with **2e** having the smallest impact. When the medium

https://doi.org/10.1021/acschemneuro.4c00451
ACS Chem. Neurosci. XXXX, XXX, XXX–XXX

contained both α-syn fibrils and the compounds (Figure 6B), **2j** stood out by markedly reducing aggregate-induced cytotoxicity. The effects of compounds **2c** ((40 ± 4)%), **2e** ((38 ± 4)%), and **5e** ((43 ± 4)%) were similar to the fibril control ((45 ± 5)%), while neuroblastoma cell viability in the presence of **2j** was significantly higher ((59 ± 6)%). Given the compound's **2j** dual effect in inhibiting aggregation and reducing cytotoxicity, these results suggest that this compound decreases not only the rate of aggregate formation but also the cytotoxic effects of aggregates themselves.

Considering all the aforementioned results, imidazo[2,1-*b*][1,3]thiazine derivatives appear to have multiple effects on α-syn aggregation. Not only do they inhibit primary nucleation and shift the monomer-fibril equilibrium toward the non-aggregated state, but they also can stabilize small oligomeric states of α-syn and redirect the aggregation reaction toward fibrils with distinct secondary structures and morphologies. It is important to note that the best results were achieved with imidazo[2,1-*b*][1,3]thiazines containing phenylcarbamate fragments (**2e**, **2j**). Further modification of the core structure of compound **2e**, resulting in the more substituted benzimidazo-[2,1-*b*][1,3]thiazine **2j**, led to a statistically significant reduction in the cytotoxic effects of the aggregates. However, compound **2j** still negatively affected cell viability at relatively high concentrations. Therefore, future studies should focus on further structure modifications to improve compound's antiamyloid activity and physicochemical properties as potential drug candidates while minimizing their cytotoxicity.

CONCLUSIONS

In summary, we synthesized 18 compounds containing an imidazothiazine framework (**2a**−**j**, **3**, **4**, and **5a**−**f**) under mild conditions using AuCl as a catalyst. A diversity of functional groups was obtained by modifying the formed 5-arylimidazo-[2,1-*b*][1,3]thiazines at their *para*-phenyl positions. The significance of the imidazo[2,1-*b*][1,3]thiazine framework was demonstrated through inhibition activity comparison with two synthesized model compounds, **6** and **7**. The highest half-time ratios were achieved with compounds **2e**, **2j**, **5e**, and **2c**, with the best results observed for *Boc*-protected aniline **2e**. However, further adding extra groups to the aniline or its deprotection led to a decreased efficiency. Nonetheless, the benzimidazole moiety helped mitigate the impact of additional groups. Based on the FTIR spectra distribution, it was evident that imidazo[2,1-*b*][1,3]thiazine derivatives influenced the secondary structure of the formed aggregates. The study of the inhibition mechanism revealed that imidazo[2,1-*b*][1,3]-thiazine derivatives may have multiple effects on α-syn aggregation. These compounds not only inhibit primary nucleation and shift the monomer-fibril equilibrium toward the nonaggregated state but also stabilize the oligomeric states of α-syn and redirect the aggregation reaction toward fibrils with distinct secondary structures and morphologies. Additionally, one compound (**2j**) could reduce the cytotoxic effects of α-syn fibrils. These findings suggest that compounds containing the imidazo[2,1-*b*][1,3]thiazine framework could serve as potential α-syn aggregation inhibitors.

MATERIALS AND METHODS

Compound Preparation. Detailed compound synthesis protocols and their NMR spectra are provided as Supporting Information. All reagents and solvents were dried commonly before use, according to standard procedures. Commercially available reagents were used without further purification, unless otherwise noted. Oxygen- and moisture-sensitive reactions were carried out under an argon atmosphere. ^{1}H and ^{13}C NMR spectra were recorded in deuterated solvents on a Bruker Ascened 400 MHz spectrometer. High-resolution mass spectra (HRMS) were recorded on an Agilent LC/MSD TOF mass spectrometer by electrospray ionization time-of-flight (ESI-TOF) reflection experiments. Infrared spectra were recorded on a PERKIN-ELMER 1000 FT-IR spectrometer with a UATR annex. Microwave (MW) irradiation reactions were carried out using a CEM Discover SP microwave synthesizer. Reactions were monitored by thin layer chromatography (TLC) carried out on 0.25 mm Merck silica plates (60 F_{254}), using UV light as the visualizing agent and/or vanillin and heat as a developing agent. Column chromatography was performed with Kieselgel 60 (40−63 μm) silica gel. Melting points were measured on a Student SMP10 instrument and were uncorrected. Here are the general methods of the main reactions used for the synthesis of targeted compounds.

Synthesis of Imidazo[2,1-*b*][1,3]thiazine Framework 2. The solution of 2-alkynylthioimidazole **1** (1.0 equiv) in DCE was stirred under an argon atmosphere at room temperature in a microwave vial for 15 min, then AuCl (10 mol %) was added, and the sealed vial was subjected to microwave irradiation. The reaction was carried out using a dynamic method at constant temperature (four cycles: three times for 40 min and one time for 20 min). If the reaction was not completed during this time, the cycles were repeated. After reaction completion, monitored by TLC, the solvent was evaporated under reduced pressure, and the product **2** was isolated by column chromatography.

Synthesis of Amides 5. To the solution of acetic acid **4** (1.0 equiv) in DCM, EDCI·HCl (1.5 equiv), HOBt (1.5 equiv), and appropriate amine (1.2 equiv) were added. The reaction mixture was stirred at room temperature overnight. After reaction completion, monitored by TLC, the mixture was diluted with H_2O and extracted with DCM. The combined organic layers were washed once with brine, dried with anhydrous Na_2SO_4, and concentrated under reduced pressure. The product **5** was isolated by column chromatography using the eluent $CHCl_3$:CH_3CN (4:1).

Alpha-Synuclein Aggregation Assay. Alpha-synuclein was purified based on a previously described protocol,[36] exchanged to PBS (pH 7.4), concentrated to 600 μM, and stored at −20 °C prior to use. The compounds were dissolved in 99.9% dimethyl sulfoxide (DMSO) to a final concentration of 10 mM. Thioflavin-T (ThT) powder (Sigma-Aldrich cat. no. T3516) was dissolved in Milli-Q H_2O to a concentration of ∼11 mM and filtered through a 0.22 μm pore-size syringe filter. The exact concentration of the dye was determined by diluting a small aliquot (10 μL) to 1 mL of Milli-Q H_2O and scanning its absorbance at 412 nm using a Shimadzu UV-1800 spectrophotometer. The final concentration of the ThT stock solution was then set to 10 mM. Both the compound and ThT stock solutions were used immediately after preparation, flash frozen, and stored at −20 °C under dark conditions to be used in further experimental procedures.

To conduct the aggregation assays, α-syn, compound, ThT, 10× PBS, and 1× PBS solutions were combined to result in final reaction solutions containing 100 μM α-syn, 100 μM compound, 100 μM ThT, and 1× PBS. The protein concentration of 100 μM was chosen to reduce the aggregation reaction stochasticity.[33] For the initial assessment, both the dye and compound concentrations were set to be equimolar to α-syn. Control solutions were supplemented with 99.9% DMSO instead of the compound solution. The reaction solutions were then distributed to 96-well nonbinding half-area plates (Fisher Scientific, cat. no 3881, 100 μL volume, 6 repeats for each condition, each well contained one 3 mm glass bead) in an alternating pattern to account for uneven temperature distribution.[37] The aggregation reactions were monitored by incubating the plates in a ClarioStar Plus plate reader at 37 °C with 600 rpm agitation between readings. ThT fluorescence measurements were taken every 5 min using 440 nm excitation and 480 nm emission wavelengths. For aggregation conditions with different compound concentrations, the samples were prepared as described previously. To account for the

https://doi.org/10.1021/acschemneuro.4c00451
ACS Chem. Neurosci. XXXX, XXX, XXX−XXX

different concentrations of DMSO added to the compound stock solution, all reaction solutions were supplemented with DMSO to a final concentration of 2%.

The aggregation reaction curves were fitted using a Boltzmann sigmoidal equation (Origin 2018 software). Reaction half-time (t_{50}), lag time, apparent rate constant, and end-point fluorescence intensities were determined from the fitted data as shown previously.[33] Statistical analysis of the reaction parameters was done by using a one-way ANOVA Bonferroni means comparison (Origin 2018 software).

Compound Fluorescence Assay. Each compound stock solution was diluted to 100 μM using 1× PBS. The resulting solutions were then placed in 96-well nonbinding half-area plates (Fisher Scientific, cat. no 3881, 100 μL volume, 3 repeats for each condition) and incubated at room temperature for 10 min. The sample fluorescence intensities were scanned by using 440 nm excitation and 480 nm emission wavelengths with a ClarioStar Plus plate reader. As a control, the ThT stock solution was diluted with 1× PBS and supplemented with 1% DMSO to a final dye concentration of 100 μM.

Fourier-Transform Infrared Spectroscopy (FTIR). After the aggregation assay, the 96-well plates were cooled to 22 °C and fibrils in each well were resuspended by pipetting, after which aliquots of 80 μL were recovered for the FTIR assay. To exchange H_2O for D_2O, the fibril solutions were centrifuged at 9000g for 15 min, and the pelleted aggregates were resuspended into 200 μL of D_2O, supplemented with 400 mM NaCl (to improve sedimentation[38]). The centrifugation and resuspension procedure was repeated an additional two times. After the final centrifugation step, the fibrils were resuspended in 30 μL of D_2O, supplemented with 400 mM NaCl. The sample FTIR spectra were then scanned as described previously,[39] using a Bruker Invenio S FTIR spectrometer. D_2O and water vapor spectra were subtracted from the sample spectra, which were then baseline corrected and normalized to the same area between 1700 and 1595 cm^{-1}. Data processing was performed using GRAMS software.

To determine the different types of aggregate structures present in the samples, second-order derivatives were calculated for each spectrum, which were then compared and grouped based on similarities in their minimum positions. The grouping procedure was semisubjective due to possible α-syn fibril polymorphism, with some samples containing mixtures of different secondary structure aggregates.

Transmission Electron Microscopy (TEM). The α-syn fibril samples were diluted five times using 1× PBS (final concentration 20 μM). Before sample application, 300 mesh Formvar/carbon coated copper grids (Agar Scientific, U.K.) were UV irradiated. 5 μL of diluted α-syn aggregate solutions was then placed on the grids for 1 min, followed by drying with filter paper. The grids were negatively stained with 5 μL of 2% (w/v) uranyl acetate for 1 min, after which the excess solution was dried with filter paper. Finally, the grids were washed with 5 μL of Milli-Q water, and this washing/drying procedure was repeated 3 times. All TEM images were recorded using a Talos 120C (Thermo Fisher) transmission electron microscope operating at 120 V and equipped with 4k × 4k Ceta CMOS Camera. After acquisition, images were analyzed by using ImageJ software.

Residual Monomer Quantification. α-Syn samples from the 200 μM compound concentration conditions were pooled together (6 × 100 μL) and centrifuged at 14 000g for 15 min. Part of the supernatant (100 μL) was carefully removed for analysis by SDS-PAGE electrophoresis. For control samples, the same procedure was carried out with the control fibril and 50 μM nonaggregated α-syn samples. 30 μL of aliquots of each supernatant was combined with a 4 times concentrated SDS-PAGE sample buffer solution (10 μL) and incubated at 98 °C for 10 min. The samples and a Spectra Multicolor Low Range Protein Ladder (ThermoFisher Scientific, cat. no. 26628) were then loaded on a 16% acrylamide gel (5 μL of each). The gel was stained with GelCode Blue Safe Protein Stain. The concentration of residual monomers was calculated with GelAnalyzer 23.1.1 software using the 50 μM nonaggregated α-syn sample band as a reference.

Cell Viability Assay. The MTT assay was performed as previously described.[40] In brief, SH-SY5Y cells were seeded in a 96-well plate (~15 000 cells/well) and were incubated overnight. After incubation, the medium was changed to one containing either 20 μM of each selected compound or 20 μM of α-syn fibrils (from the control aggregation samples) with 20 μM of each compound. The medium also contained 0.2% DMSO from the compound stock solutions. For the control, the medium was supplemented with an equal concentration of PBS solution with DMSO. After 48 h of incubation, 10 μM of 3-(4,5-dimethylthiazol- 2-yl)-2,5-diphenyltetrazolium bromide (MTT) reagent (12.1 mM in PBS) was added to each well, followed by 2 h of incubation. To dissolve formazan crystals, 100 μL of 10% SDS with a 0.01 N HCl solution was added to each well. After 2 h, the absorbance was measured at 570 and 690 nm (as reference wavelength) using a ClarioStar Plus plate reader. Three separately prepared sets of samples with three repeats for each condition were used. Statistical analysis of the results was conducted by using Origin 2018 software one-way analysis of variance (ANOVA) Bonferroni means comparison (n = 9).

■ ASSOCIATED CONTENT

Supporting Information

The Supporting Information is available free of charge at https://pubs.acs.org/doi/10.1021/acschemneuro.4c00451.

Additional experimental details, synthesis methods, materials, and methods, including ^1H and ^{13}C NMR spectra for all new compounds (PDF)

■ AUTHOR INFORMATION

Corresponding Author

Ieva Žutautė − *Institute of Chemistry, Faculty of Chemistry and Geosciences, Vilnius University, Vilnius LT-03225, Lithuania*; orcid.org/0000-0001-9654-3875; Email: ieva.zutaute@chgf.vu.lt

Authors

Indrė Misiūnaitė − *Institute of Chemistry, Faculty of Chemistry and Geosciences, Vilnius University, Vilnius LT-03225, Lithuania*; orcid.org/0009-0009-1846-1239

Kamilė Mikalauskaitė − *Institute of Biotechnology, Life Sciences Center, Vilnius University, Vilnius LT-10257, Lithuania*

Martyna Paulauskaitė − *Institute of Chemistry, Faculty of Chemistry and Geosciences, Vilnius University, Vilnius LT-03225, Lithuania*

Rūta Sniečkutė − *Institute of Biotechnology, Life Sciences Center, Vilnius University, Vilnius LT-10257, Lithuania*

Vytautas Smirnovas − *Institute of Biotechnology, Life Sciences Center, Vilnius University, Vilnius LT-10257, Lithuania*; orcid.org/0000-0002-1829-5455

Algirdas Brukštus − *Institute of Chemistry, Faculty of Chemistry and Geosciences, Vilnius University, Vilnius LT-03225, Lithuania*

Mantas Žiaunys − *Institute of Biotechnology, Life Sciences Center, Vilnius University, Vilnius LT-10257, Lithuania*; orcid.org/0000-0002-8368-6188

Complete contact information is available at: https://pubs.acs.org/10.1021/acschemneuro.4c00451

Author Contributions

#I.M. and K.M. contributed equally to this work. I.M.: synthesis, investigation, writing—review and editing, and visualization. K.M.: investigation, formal analysis, writing—review and editing, and visualization. M.P.: synthesis and

investigation. R.S.: investigation. A.B. and V.S.: writing—review and editing, and supervision. M.Ž.: conceptualization, formal analysis, writing—original draft, writing—review and editing, and visualization. I.Ž.: conceptualization, writing—original draft, writing—review and editing, visualization, and supervision. All authors have given approval to the final version of the manuscript.

Notes

The authors declare no competing financial interest.

■ ACKNOWLEDGMENTS

The research topic was supported by the Lithuanian Academy of Sciences Young Researcher Scholarship Programme.

■ REFERENCES

(1) Chiti, F.; Dobson, C. M. Protein Misfolding, Amyloid Formation, and Human Disease: A Summary of Progress Over the Last Decade. *Annu. Rev. Biochem.* **2017**, *86* (1), 27−68.
(2) Knowles, T. P. J.; Vendruscolo, M.; Dobson, C. M. The Amyloid State and Its Association with Protein Misfolding Diseases. *Nat. Rev. Mol. Cell Biol.* **2014**, *15* (6), 384−396.
(3) Park, J.; Egolum, U.; Parker, S.; Andrews, E.; Ombengi, D.; Ling, H. Tafamidis: A First-in-Class Transthyretin Stabilizer for Transthyretin Amyloid Cardiomyopathy. *Ann. Pharmacother.* **2020**, *54* (5), 470−477.
(4) Doig, A. J.; Del Castillo-Frias, M. P.; Berthoumieu, O.; Tarus, B.; Nasica-Labouze, J.; Sterpone, F.; Nguyen, P. H.; Hooper, N. M.; Faller, P.; Derreumaux, P. Why Is Research on Amyloid-β Failing to Give New Drugs for Alzheimer's Disease? *ACS Chem. Neurosci.* **2017**, *8* (7), 1435−1437.
(5) Arthur, K. C.; Calvo, A.; Price, T. R.; Geiger, J. T.; Chiò, A.; Traynor, B. J. Projected Increase in Amyotrophic Lateral Sclerosis from 2015 to 2040. *Nat. Commun.* **2016**, *7* (1), 12408.
(6) Brookmeyer, R.; Gray, S.; Kawas, C. Projections of Alzheimer's Disease in the United States and the Public Health Impact of Delaying Disease Onset. *Am. J. Public Health* **1998**, *88* (9), 1337−1342.
(7) Yao, W.; Yang, H.; Yang, J. Small-Molecule Drugs Development for Alzheimer's Disease. *Front. Aging Neurosci.* **2022**, *14*, 1019412.
(8) Cummings, J. Anti-Amyloid Monoclonal Antibodies Are Transformative Treatments That Redefine Alzheimer's Disease Therapeutics. *Drugs* **2023**, *83* (7), 569−576.
(9) Kabir, M. T; Uddin, M. S.; Al Mamun, A.; Jeandet, P.; Aleya, L.; Mansouri, R. A.; Md Ashraf, G.; Mathew, B.; Bin-Jumah, M. N.; Abdel-Daim, M. M. Combination Drug Therapy for the Management of Alzheimer's Disease. *Int. J. Mol. Sci.* **2020**, *21* (9), 3272.
(10) Cummings, J.; Zhou, Y.; Lee, G.; Zhong, K.; Fonseca, J.; Cheng, F. Alzheimer's Disease Drug Development Pipeline: 2023. *Alzheimer's Dementia* **2023**, *9* (2), No. e12385.
(11) Liu, Y.; Carver, J. A.; Calabrese, A. N.; Pukala, T. L. Gallic Acid Interacts with α-Synuclein to Prevent the Structural Collapse Necessary for Its Aggregation. *Biochim. Biophys. Acta, Proteins Proteomics* **2014**, *1844* (9), 1481−1485.
(12) Xu, Y.; Zhang, Y.; Quan, Z.; Wong, W.; Guo, J.; Zhang, R.; Yang, Q.; Dai, R.; McGeer, P. L.; Qing, H. Epigallocatechin Gallate (EGCG) Inhibits Alpha-Synuclein Aggregation: A Potential Agent for Parkinson's Disease. *Neurochem. Res.* **2016**, *41* (10), 2788−2796.
(13) Kamal, M. A.; Greig, N. H.; Alhomida, A. S.; Al-Jafari, A. A. Kinetics of Human Acetylcholinesterase Inhibition by the Novel Experimental Alzheimer Therapeutic Agent, Tolserine. *Biochem. Pharmacol.* **2000**, *60* (4), 561−570.
(14) Castillo, W.; Aristizabal-Pachon, A. Galantamine Protects against Beta Amyloid Peptide-Induced DNA Damage in a Model for Alzheimer's Disease. *Neural Regener. Res.* **2017**, *12* (6), 916.
(15) Khan, A.; Vaibhav, K.; Javed, H.; Tabassum, R.; Ahmed, M. E.; Khan, M. M.; Khan, M. B.; Shrivastava, P.; Islam, F.; Siddiqui, M. S.; Safhi, M. M.; Islam, F. 1,8-Cineole (Eucalyptol) Mitigates Inflammation in Amyloid Beta Toxicated PC12 Cells: Relevance to Alzheimer's Disease. *Neurochem. Res.* **2014**, *39* (2), 344−352.
(16) Khan-Mohammadi-Khorrami, M.; Asle-Rousta, M.; Rahnema, M.; Amini, R. Neuroprotective Effect of Alpha-pinene Is Mediated by Suppression of the TNF-α/NF-κB Pathway in Alzheimer's Disease Rat Model. *J. Biochem. Mol. Toxicol.* **2022**, *36* (5), No. e23006.
(17) Lai, M. C.; Liu, W. Y.; Liou, S. S.; Liu, I. M. Hispidin in the Medicinal Fungus Protects Dopaminergic Neurons from JNK Activation-Regulated Mitochondrial-Dependent Apoptosis in an MPP+-Induced In Vitro Model of Parkinson's Disease. *Nutrients* **2023**, *15* (3), 549.
(18) De Luca, L.; Vittorio, S.; Peña-Díaz, S.; Pitasi, G.; Fornt-Suñé, M.; Bucolo, F.; Ventura, S.; Gitto, R. Ligand-Based Discovery of a Small Molecule as Inhibitor of α-Synuclein Amyloid Formation. *Int. J. Mol. Sci.* **2022**, *23* (23), 14844.
(19) Heras-Garvin, A.; Weckbecker, D.; Ryazanov, S.; Leonov, A.; Griesinger, C.; Giese, A.; Wenning, G. K.; Stefanova, N. Anle138b Modulates α-Synuclein Oligomerization and Prevents Motor Decline and Neurodegeneration in a Mouse Model of Multiple System Atrophy. *Mov. Disord.* **2019**, *34* (2), 255−263.
(20) Price, D. L.; Koike, M. A.; Khan, A.; Wrasidlo, W.; Rockenstein, E.; Masliah, E.; Bonhaus, D. The Small Molecule Alpha-Synuclein Misfolding Inhibitor, NPT200−11, Produces Multiple Benefits in an Animal Model of Parkinson's Disease. *Sci. Rep.* **2018**, *8* (1), 1−12.
(21) Price, D. L.; Khan, A.; Angers, R.; Cardenas, A.; Prato, M. K.; Bani, M.; Bonhaus, D. W.; Citron, M.; Biere, A.-L. In Vivo Effects of the Alpha-Synuclein Misfolding Inhibitor Minzasolmin Supports Clinical Development in Parkinson's Disease. *npj Parkinson's Dis.* **2023**, *9* (1), 114.
(22) Mehta, D.; Jackson, R.; Paul, G.; Shi, J.; Sabbagh, M. Why Do Trials for Alzheimer's Disease Drugs Keep Failing? A Discontinued Drug Perspective for 2010−2015. *Expert Opin. Invest. Drugs* **2017**, *26* (6), 735−739.
(23) Asif, M. Chemical and Pharmacological Potential of Various Substituted Thiazine Derivatives. *J. Pharm. Appl. Chem.* **2015**, *1* (2), 1−16.
(24) Stefanis, L. A-Synuclein in Parkinson's Disease. *Cold Spring Harbor Perspect. Med.* **2012**, *2* (2), a009399−a009399.
(25) Misiūnaitė, I.; Bajarūnaitė, R.; Bukšnaitienė, R.; Brukštus, A.; Žutautė, I. Straightforward Approach to 5-Substituted 7H-Imidazo-[2,1-b] [1,3]Thiazines via Cyclization of 2-Alkynylthioimidazoles. *Synthesis* **2023**, *55* (24), 4213−4223.
(26) Jia, Y.; Guo, X.; Jia, L.; Zhao, Z.; Yang, R.; Zhang, Y.; Sun, H. Novel Asymmetrical Bis-Surfactants with Naphthalene and Two Amide Groups: Synthesis, Foamability and Foam Stability. *J. Mol. Liq.* **2021**, *329*, 115534.
(27) Gazieva, G. A.; Serkov, S. A.; Sigay, N. V.; Kostikova, N. N.; Popov, L. D.; Kravchenko, A. N. Functionally Substituted Aromatic Aldehydes as Reagents in the Synthesis of New Substituted Thioglycolurils. *Org. Chem.* **2017**, *2017* (3), 279−286.
(28) Möller, M.; Hentschel, C.; Chi, L.; Studer, A. Aggregation Behaviour of Peptide−Polymer Conjugates Containing Linear Peptide Backbones and Multiple Polymer Side Chains Prepared by Nitroxide-Mediated Radical Polymerization. *Org. Biomol. Chem.* **2011**, *9* (7), 2403.
(29) Kimura, S.; Kamishina, H.; Hirata, Y.; Furuta, K.; Furukawa, Y.; Yamato, O.; Maeda, S.; Kamatari, Y. O. Novel Oxindole Compounds Inhibit the Aggregation of Amyloidogenic Proteins Associated with Neurodegenerative Diseases. *Biochim. Biophys. Acta, Gen. Subj.* **2022**, *1866* (5), 130114.
(30) Sulatskaya, A.; Rodina, N.; Sulatsky, M.; Povarova, O.; Antifeeva, I.; Kuznetsova, I.; Turoverov, K. Investigation of α-Synuclein Amyloid Fibrils Using the Fluorescent Probe Thioflavin T. *Int. J. Mol. Sci.* **2018**, *19* (9), 2486.
(31) Ziaunys, M.; Mikalauskaite, K.; Sakalauskas, A.; Smirnovas, V. Interplay between Epigallocatechin-3-Gallate and Ionic Strength during Amyloid Aggregation. *PeerJ* **2021**, *9*, No. e12381.
(32) Sidhu, A.; Vaneyck, J.; Blum, C.; Segers-Nolten, I.; Subramaniam, V. Polymorph-Specific Distribution of Binding Sites

https://doi.org/10.1021/acschemneuro.4c00451
ACS Chem. Neurosci. XXXX, XXX, XXX−XXX

Determines Thioflavin-T Fluorescence Intensity in α-Synuclein Fibrils. *Amyloid* **2018**, *25* (3), 189−196.
(33) Ziaunys, M.; Sakalauskas, A.; Mikalauskaite, K.; Smirnovas, V. Polymorphism of Alpha-Synuclein Amyloid Fibrils Depends on Ionic Strength and Protein Concentration. *Int. J. Mol. Sci.* **2021**, *22* (22), 12382.
(34) Toleikis, Z.; Ziaunys, M.; Baranauskiene, L.; Petrauskas, V.; Jaudzems, K.; Smirnovas, V. S100A9 Alters the Pathway of Alpha-Synuclein Amyloid Aggregation. *Int. J. Mol. Sci.* **2021**, *22* (15), 7972.
(35) Barth, A. Infrared Spectroscopy of Proteins. *Biochim. Biophys. Acta, Bioenerg.* **2007**, *1767* (9), 1073−1101.
(36) Šneideris, T.; Baranauskienė, L.; Cannon, J. G.; Rutkienė, R.; Meškys, R.; Smirnovas, V. Looking for a Generic Inhibitor of Amyloid-like Fibril Formation among Flavone Derivatives. *PeerJ* **2015**, *3* (9), No. e1271.
(37) Mansoury, M.; Hamed, M.; Karmustaji, R.; Al Hannan, F.; Safrany, S. T. The Edge Effect: A Global Problem. The Trouble with Culturing Cells in 96-Well Plates. *Biochem. Biophys. Rep.* **2021**, *26* (May2020), 100987.
(38) Mikalauskaite, K.; Ziaunys, M.; Sneideris, T.; Smirnovas, V. Effect of Ionic Strength on Thioflavin-T Affinity to Amyloid Fibrils and Its Fluorescence Intensity. *Int. J. Mol. Sci.* **2020**, *21* (23), 8916.
(39) Mikalauskaite, K.; Ziaunys, M.; Smirnovas, V. Lysozyme Amyloid Fibril Structural Variability Dependence on Initial Protein Folding State. *Int. J. Mol. Sci.* **2022**, *23* (10), 5421.
(40) Sakalauskas, A.; Janoniene, A.; Zvinys, G.; Mikalauskaite, K.; Ziaunys, M.; Smirnovas, V. Exploring the Formation of Polymers with Anti-Amyloid Properties within the 2′3′-Dihydroxyflavone Autoxidation Process. *Antioxidants* **2022**, *11* (9), 1711.

https://doi.org/10.1021/acschemneuro.4c00451
ACS Chem. Neurosci. XXXX, XXX, XXX−XXX

Vilniaus universiteto leidykla
Saulėtekio al. 9, III rūmai, LT-10222 Vilnius
El. p. info@leidykla.vu.lt, www.leidykla.vu.lt
bookshop.vu.lt, journals.vu.lt
Tiražas 15 egz.